

Continuous Flow Gas-liquid Reactions in Micro-reactors and its Applications in Catalytic Synthesis

Fanfu Guan

Submitted in accordance with the requirements for the degree of Doctor of Philosophy

The University of Leeds

School of Chemistry

November 2021

Acknowledgement

Firstly, I would like to thank my parents for all the help both in terms of mentality and finance, which allowed me to take the risk for a PhD journey. Then, I would like to thank my supervisors Professor John Blacker Professor Xumu Zhang, Professor Jialin Wen and Professor Nikil Kapur for their continued intellectual and mental guidance throughout, along with all the members of the iPRD Laboratory and SUSTech. Project meetings with Professor John were both informative and comforting. His wide knowledge and big smile can always free me from anxiety. Although Professor Xumu's high taste of chemistry that pushed me for exploring new and complicated chemistry sometimes drove me crazy, his full trust and financial support are crucial for me to stick to flow chemistry. His occasional encouragement can be very warm. For example, when my paper was rejected by *Angewandte Chemie*, he told me that the most important works were always not in the top journal, and the rejection will not depreciate your work. Thanks to the presence of Professor Jialin, I was not alone in working on this brand-new direction of SUSTech. We share the irrational enthusiasm about new technologies, which makes our discussion full of nova thoughts. Without his enlightenment on chemistry, especially organometallic chemistry, I cannot finish this project. Professor Nikil Kapur broadened my horizon on reactor technology, coding, Arduino and so on. I would never expect that I had a supervisor from mechanical department. I would like to express my appreciation to Professor Karine Loubiere, my master final year project supervisor. She equipped me with a chemical engineering research methodology that benefits my PhD study.

I will not be so mentally healthy without iPRD Friday therapy activity in Library, of course, Library pub and SUSTech Taobao fruit group. I was so lucky that my good mate, Luke, learned pumps, Arduino, fReactor, matlab and all these new things together, Connor helps me a lot with DoE and coding, Rosie talked with me about chemistry and Donnie Yan, Fernando played basketball with me and so many good memories in Leeds. What a chance for a foreign guy to have such a warm team. Thank you for the accompany of Yongjie Shi, Huaxin Yang, Bijin Lin, Ting Wu, Yang Zhou and all my friends. It was them who offered me a colorful life in SUSTech. I am grateful for the funding from Southern University of Science and Technology and University of Leeds. Both universities provide great facilities of research, living and sports. This project helps me nurture complete skill for my future career, strong spirit when facing difficulties and ability to deal with different culture. I hope more students can benefit from cross-discipline and multinational jointed PhD program.

Abstract

Efficient amplification of chirality through asymmetric catalysis is one of the fundamental scientific problems. Recent developments in reactor technology, especially micro-reactors, have been creating new opportunities in reaction control. The work reported herein describes studies of (asymmetric) hydrogenation and transfer (de)hydrogenation in different kinds of continuous flow reactors.

Catalytic (enantioselective) hydrogenations have been rarely used in lab and industry-scale continuous flow reactions, and this defines much of the novelty of this work.^[1] Asymmetric hydrogenation (AH) is one of the most powerful synthetic tools to obtain chiral molecules in pharmaceutical industry.^[2] However, practical homogeneous hydrogenation with a low catalyst loading typically requires a long reaction time (more than 24 hours), which poses challenges for continuous operation.^[3] Catalyst performance can be improved by adopting high pressure and temperature flow processes.

A slug flow reactor system that can hold up to 150 bars was developed. AH of acetophenone can achieve full conversion and >99% ee with 40000 TON in 6.5 minutes residence time. The TOF can reach up to 274000 h⁻¹. Two multi-step processes of drug synthesis were developed, in which AH was the key step.

However, the slug flow reactors have several disadvantages. Firstly, the slug flow tends to be unstable with high linear velocity and gas liquid volume ratio. In addition, the thin tube in which the reactions proceed can be easily clogged. Therefore, a miniature CSTR, fReactor, was employed to overcome these problems. Such active mixing reactors can avoid blocking and decouple mixing with flow rate, which allows the reactor to operate under a wide range of gas and liquid flow rates. A horizontal fReactor system was successfully applied in heterogeneous and homogeneous hydrogenation and to elongate the residence time of reaction medium, a vertical fReactor system was designed and constructed. It is featured with decoupling gas flow rate with liquid flow rate, and was used in hydroformylation reactions. A novel reactor named flashstop reactor was designed and built to obtain kinetic data for the scenario in which ultrafast pressurized reactions such as isomerization is conducted.

A continuous reactor system was also designed to solve the problem of diastereomeric as well as enantiomeric control by integrating hydrogenation, transfer hydrogenation and transfer dehydrogenation. A single enantiomer can be selectively oxidized via asymmetric transfer dehydrogenation to produce an unsaturated intermediate. This product can be reduced via asymmetric (transfer) hydrogenation to enrich the desired enantiomer. This strategy can outperform a single reaction, such as AH or ADH, with respect to enantioselectivity, especially tackling some challenging substrates.

Contents

Chapter 1: Introduction.....	14
1.1 Homogeneous catalytic hydrogenation	14
1.2 Asymmetric hydrogenation catalysts and reactions	17
1.3 Flow chemistry and microreactor	21
1.3 Reactor designs for biphasic catalytic gas liquid reactions	23
1.4 Controlling diastereoselectivity	29
1.5 Objectives.....	37
Chapter 2: The high-pressure gas-liquid slug flow reactor and application in asymmetric hydrogenation.	38
2.1 Equipment	38
2.2 Formation of stable slug flow.....	41
2.3 Optimization of reaction conditions (Synthesis of Ezetimibe)	46
2.4 Optimization of reaction conditions (Synthesis of Eslicarbazepine)	51
2.5 Multistep continuous flow synthesis of Ezetimibe	53
2.6 Multistep continuous flow synthesis of Eslicarbazepine Acetate	56
2.7 Asymmetric synthesis of biotin in a cyclic slug flow reactor.....	62
2.8 Conclusion.....	66
Chapter 3: A horizontal micro-fluidics CSTR and its application in heterogeneous and homogeneous hydrogenation.....	67
3.1 Design of Experiment.....	67
3.2 Equipment.....	69
3.3 Gas liquid mass transfer in fReactor	74
3.4 Heterogeneous hydrogenation in fReactor system.....	76
3.5 Homogeneous asymmetric hydrogenation in fReactor system	91
3.6 Conclusion.....	97
Chapter 4: Continuous hydroformylation in microreactor.....	99
4.1 Continuous hydroformylation in slug flow reactor	100
4.2 Multi-way valve reactors for kinetic study of the pressurized gas liquid reactions	103
4.3 Kinetic studies in batch and flow reactors	105
4.4 Continuous hydroformylation in a vertical fReactor system.....	115
4.5 Conclusion.....	116
Chapter 5: Controlling diastereoselectivity: Integrating asymmetric (transfer) hydrogenation and transfer dehydrogenation.	118

5.1 Reaction modelling using matlab for controlling diastereoselectivity.....	118
5.2 Catalytic systems	122
5.3 Synthesis of substrates.....	124
5.4 Results of asymmetric transfer dehydrogenation	129
5.5 Results of asymmetric transfer hydrogenation	136
5.6 Process combining AH and ADH.....	144
5.7 Conclusion	145
Chapter 6: Conclusions and Outlook.....	146
6.1 Conclusion	146
6.2 Outlook.....	148
Chapter 7: Experimental	148
7.1 Chapter 2: High-pressure gas-liquid slug flow reactor and its application in asymmetric hydrogenation.....	148
7.2 Chapter 3: Horizontal micro-fluidics CSTR and its application in heterogeneous and homogeneous hydrogenation.....	161
7.3 Chapter 4: Continuous hydroformylation in microreactor.....	169
7.4 Chapter 5: Controlling diastereoselectivity: Integrating asymmetric (transfer) hydrogenation and transfer dehydrogenation.	173
7.5 NMR, HPLC and GC spectrum	191
7.6 Analytical protocol	231
8. References.....	237
9. Appendix	245

Abbreviation

acac: acetylacetonate

AH: asymmetric hydrogenation

a/i: ratio between aldehyde production rate and isomerized product generation rate

API: active pharmaceutical ingredient

ATH: asymmetric transfer hydrogenation

ATD: asymmetric transfer dehydrogenation

b-aldehyde: branched-aldehyde

BINAP: 2,2-bis(diphenylphosphino)-1,1-binaphthyl

BPR: back pressure regulator

COD: 1,5-cyclooctadiene

Cp*: Pentamethylcyclopentadiene

(*S, S, S*)-CsDPEN: (*1S, 2S*)-*N*-[(*1S*)-Camphorsulphonyl]-1,2-diphenylethylenediamine

CSTR: continuous stirred tank reactor

DCM: dichloromethane

de: diastereomeric excess

Diphos: ethylenebis(biphenylphosphine)

DIPAMP: ethylenebis(2-methoxyphenylphenylphosphine)

DTBM: 3,5-di-*tert*-butyl-4-methoxyphenyl

DMAP: 4-dimethylaminopyridine

DoE: Design of Experiment

d.r.: diastereomeric ratio

(*S,S*)-Methyl-Duphos: (+)-1,2-bis[(*2S,5S*)-2,5-dimethylphospholano]benzene

EA: ethyl acetate

(*R,R*)-Ethyl-DuPhos: (+)-1,2-bis[(*2R,5R*)-2,5-diisopropylphospholano]benzene

e.e. : enantiomeric excess

GC: gas chromatography

HPLC: high performance liquid chromatography

l-aldehyde: linear-aldehyde

NBD: nornornadiene

NEt₃: Triethylamine

NMR: nuclear magnetic resonance

PCy₃: tricyclohexylphosphine

PE: Petroleum ether

PPh₃: triphenylphosphine

rt: room temperature (within a range of 25 ~ 27°C)

sccm: standard cubic centimeters per minute under 273 K and 1 bar

SPY: space time yield

S/C: Ratio between Substrate and Catalyst

THF: tetrahydrofuran

TON: turnover of the catalyst

TOF: turn-over-frequency of the catalyst

TsDPEN: T-*p*-Tosyl-1,2-diphenylethylenediamine

UPLC: ultra-performance liquid chromatography

Table of Figures

Figure 1 Homogeneous hydrogenation catalysts.....	14
Figure 2 Monohydride and dihydride hydrogenation catalyst.....	15
Figure 3 Conventional mechanism for the H ₂ -hydrogenation by Ru Catalyst.....	16
Figure 4 Pioneering ligands for asymmetric hydrogenation.....	18
Figure 5 diphosphine ligands developed in Zhang's lab.....	19
Figure 6 Pioneering tridentate ligands.....	19
Figure 7 Ferrocene based tridentate ligand---f-series ligands.....	20
Figure 8 Some examples of asymmetric transfer hydrogenation catalysts.....	21
Figure 9 Microreactors adopting passive mixing (a) and active mixing (b).....	22
Figure 10 Examples of reactors used for biphasic hydrogenation reactions.....	24
Figure 11 H-cube reactor (upper left); tube-in-tube reactor (upper right); micro-structured mesh reactor (lower left); helicoidal single channel falling film micro-reactor (lower right).....	27
Figure 12 Three generations of pipe-in-series reactors.....	28
Figure 13 fReactor flow system ^[56]	29
Figure 14 APIs with multiple chiral centres ^[12-15]	30
Figure 15 Strategies for obtaining compounds with two chiral centres.....	31
Figure 16 Mechanism of hydrogenation and dehydrogenation ^[88]	33
Figure 17 Continuous reactor system to obtain diastereomers.....	34
Figure 18 HIV Protein Inhibitors with multiple chiral centres requiring diastereocontrol ^[93a]	36
Figure 19 Core molecule of HIV protein inhibitor ^[93]	36
Figure 20 Drug molecules containing building block of β -amino α -hydroxy ester.....	36
Figure 21 Kinetic profile for asymmetric hydrogenation in batch.....	38
Figure 22 Set-up for high-pressure hydrogenation combining in-situ IR analysis.....	40
Figure 23 Remote control system and inline analysis system.....	41
Figure 24 Factors related to mass transfer in Taylor Flow ^[100b]	42
Figure 25 Factors related to mass transfer in Taylor Flow ^[100c]	42
Figure 26 A universal map of gas liquid flow in a microchannel at 15 bar gas pressure.....	43
Figure 27 Uniform slug flow ($r = 1.5$; $g = 0.68$ mL/min; $l = 0.46$ mL/min).....	44
Figure 28 Slug flow with long liquid slug length ($r = 0.5$; $g = 0.38$ mL/min; $l = 0.75$ mL/min).....	44
Figure 29 Pulsed slug flow with breakage caused by pulse ($r = 3$; $g = 2.5$ mL/min; $l = 0.85$ mL/min).....	45
Figure 30 Effect of gas liquid ratio in continuous flow hydrogenation.....	48
Figure 31 Effect of pressure in continuous flow hydrogenation.....	49
Figure 32 Effect of temperature in continuous flow hydrogenation.....	49
Figure 33 Inline analysis by in-situ TFIR for the condition optimization. (Entry 10 and 11).....	52
Figure 34 Hydrogenation of Asymmetric hydrogenation of 5 (Entry 9).....	52
Figure 35 Hydrogenation of Asymmetric hydrogenation of 5 (Entry 12, 13, 14).....	53
Figure 36 Batch mode fReactor.....	55
Figure 37 Two steps process for synthesis of ezetimibe.....	56
Figure 38 Multi-step synthesis of (<i>R</i>)-eslicarbazepine acetate.....	60
Figure 39 Module 2 for synthesis of eslicarbazepine acetate.....	61
Figure 40 Module 3 for synthesis of eslicarbazepine acetate.....	61
Figure 41 Comparison of the crude product and the pure product by ¹ H NMR.....	62
Figure 42 Scale up from cyclic flow reactor to continuous production.....	65
Figure 43 A central composite design for three variables ^[112]	68

Figure 44 Parr Hydrogenator (upper left); Flask with hydrogen balloon (upper right); Gas Pumping Step of Batch Mode Reactor (lower left); Batch Mode fReactor (lower right).....	69
Figure 45 Batch mode fReactor with hydrogen syringe (upper left); Batch mode fReactor with continuous feeding of hydrogen (upper right and lower)	70
Figure 46 Frit in a ferrule	71
Figure 47 Gas-liquid Separator (vertical fReactor)	71
Figure 48 Components of a continuous fReactor hydrogenation system	73
Figure 49 Pressure pattern under different liquid flow rates.....	74
Figure 50 Left, Characterization of gas-liquid mass transfer $\ln(\alpha)$ via hydrogen uptake in batch. Right, A bar chart showing the mass transfer coefficient ($k_L a$, for calculation see appendix) under different conditions; r = volume of gas/volume of liquid.	76
Figure 51 Kinetics of hydrogenation in batch reactor	77
Figure 52 Strategies of conducting flow reaction in fReactor	77
Figure 53 Reaction pathway and intermediate involved in hydrogenation of nitrobenzene	78
Figure 54 NMR of reaction medium after hydrogenation.....	79
Figure 55 Pressure changing of a batch mode fReactor	79
Figure 56 Hydrogen uptake and yield of hydrogenation in fReactor and Parr Reactor	80
Figure 57 Effect of stirring rate	81
Figure 58 Summary of fit for screening step	83
Figure 59 Response surface plot of screening step	83
Figure 60 Coefficient plot of screening step.....	84
Figure 61 Coefficient plot of optimization step.....	86
Figure 62 Summary of fit for optimization step	86
Figure 63 Response surface plot of optimization step	86
Figure 64 Continuous hydrogenation of nitrobenzene Entry 25	88
Figure 65 Continuous hydrogenation of nitrobenzene Entry 26	89
Figure 66 Continuous hydrogenation of nitrobenzene Entry 27	89
Figure 67 Continuous hydrogenation of nitrobenzene Entry 28.....	89
Figure 68 Kinetic study of asymmetric hydrogenation by C.2	94
Figure 69 Reaction results of Entry 44.....	96
Figure 70 Flashstop reactor	104
Figure 71 Kinetic in 200 minutes	106
Figure 72 Kinetic in 60 minutes	106
Figure 73 Kinetic in combination of two sets of microreactor	107
Figure 74 Kinetic under 10 bar in the 6 m tube unit flashstop reactor	108
Figure 75 Kinetic under 15 bar in the 1 m tube unit flashstop reactor	109
Figure 76 Effect of pressure on l-aldehyde generation	111
Figure 77 Effect of pressure on isomerization.....	111
Figure 78 Effect of pressure on 1-octene consumption	112
Figure 79 Kinetic study of tetrakis ligand	113
Figure 80 Comparison between tetraphosphine and tetraphosphite ligand.....	114
Figure 81 Kinetic study of hydroformylation of 2-octene	114
Figure 82 vertical fReactor system	115
Figure 83 kinetic profile of ADH reaction	119
Figure 84 Effect of k_S/k_R ratio on reaction time to achieve 95% ee and alcohol product concentration.	119
Figure 85 Reaction progress of ADH with a racemic reducing agent in the system.....	120
Figure 86 Effect of k_S/k_R ratio on equilibrium ee with a racemic reducing agent	120

Figure 87 Reaction progress of ADH with a chiral ATH catalyst	121
Figure 88 Mechanism of dehydrogenation.....	131
Figure 89 ATH of substrate 73	143
Figure 90 Results of screening by DoE.....	164
Figure 91 Predicted kinetic profiles of the reaction constituents of $S/C = 2000$ (left) and $S/C = 200$ (right) in 4.5 bar	165
Figure 92 Results of optimization by DoE.....	165
Figure 93 Kinetic data of hydroformylation in flow under 20 bar	172
Figure 94 Kinetic data of hydroformylation in flow under 15 bar	172
Figure 95 Kinetic data of hydroformylation in flow under 5 bar	173
Figure 96 Target Peak of 6 in IR spectrum	232
Figure 97 Calibration Curve of 6	232
Figure 98 Nitrobenzene calibration curve	233
Figure 99 Aniline calibration curve	233
Figure 100 (<i>Z</i>)-methyl-3-acetamido-2-butenoate calibration curve	234
Figure 101 (<i>E</i>)-methyl-3-acetamido-2-butenoate calibration curve	234
Figure 102 racemic methyl 3-acetamidobutanoate calibration curve	235
Figure 103 Calibration curve of 1-octene with tridecane as internal standard.....	235
Figure 104 Calibration curve of aldehyde with tridecane as internal standard	236
Figure 105 Calibration curve of octane with tridecane as internal standard	236
Figure 106 Calibration curve of 2-octene with tridecane as internal standard.....	237
Figure 107 Calibration curve of 3-octene with tridecane as internal standard.....	237
Figure 108 Left (a) Adding pressure by a 5 mL syringe pump; Right (b) prediction and measured value.....	249
Figure 109 The pressure changing under different stirring rates with 1 mL MeOH ($r = 0.7$) in the reactor.....	251
Figure 110 Steps of calculation of kLa	252
Figure 111 Matlab interface of Pressure Measurement	254
Figure 112 Pressure sensor and pressure sensor holder	254

Table of Tables

Table 1	Interfacial surface areas for various reactors	22
Table 2	Examples of continuous reactors for asymmetric hydrogenation.....	26
Table 3	Examples of diphasic reactions carried out in pipe-in-series reactors.	28
Table 4	Groups adaptable to Felkin–Anh and chelated control pathway	32
Table 5	Results of asymmetric hydrogenation of acetophenone.....	46
Table 6	Asymmetric hydrogenation of 3 in batch	47
Table 7	Effect of catalyst loading in continuous flow hydrogenation.	50
Table 8	Effect of residence time in continuous flow hydrogenation	50
Table 9	Asymmetric hydrogenation of 6 in continuous flow.	51
Table 10	Optimization of debenzylation in fReactor system.....	54
Table 11	Optimization of acylation step.....	58
Table 12	Results in batch	63
Table 13	Results in cyclic flow reactor.....	64
Table 14	Results in DRAT-DM reactor	65
Table 15	Technical specifications of Parr, “balloon” reactor and fReactor	70
Table 16	Screening of reaction conditions for hydrogenation of nitrobenzene	82
Table 17	Optimization of reaction conditions	85
Table 18	Reaction conditions of heterogeneous hydrogenation in flow	87
Table 19	Results of heterogeneous hydrogenation in flow.....	90
Table 20	Comparison between fReactor and H-Cube reactor.....	91
Table 21	Hydrogenation by Ru(OAc) ₂ (BINAP).....	92
Table 22	Hydrogenation by C.2	93
Table 23	Reaction conditions of asymmetric hydrogenation in flow	95
Table 24	Reaction results of asymmetric hydrogenation in flow	95
Table 25	Comparison of asymmetric hydrogenation in different reactors	97
Table 26	The effect of pressure on continuous hydroformylation.....	101
Table 27	The effect of temperature on continuous hydroformylation	101
Table 28	The effect of catalyst loading on continuous hydroformylation.	102
Table 29	The effect of residence time on continuous hydroformylation.....	103
Table 30	Conditions of kinetic in batch	105
Table 31	The reaction rate under 10 bar in 6 m tubes unit flashstop reactor	107
Table 32	Reaction rate in a 1 m tube unit flash stop reactor	108
Table 33	Kinetic constants of l-aldehyde.....	110
Table 34	Results in vertical fReactor system	116
Table 35	Reaction progress with ADH and ATH carried out alternately.	122
Table 36	Results of ADH of 1-phenylethanol.....	130
Table 37	ADH of HIV protease mode substrate.....	132
Table 38	ADH of 67	133
Table 39	ADH of challenging substrates	135
Table 40	ATH of 27	138
Table 41	ATH of 49	139
Table 42	Screening of catalysts for ATH of 53	140
Table 43	Solvent effect of catalyst C.5	141
Table 44	Reactions without MeOH.....	142
Table 45	ATH of 57	143

Table 46 Results of the telescoped continuous flow synthesis of (<i>R</i>)-eslicarbazepine acetate	157
Table 47 Screening of reaction conditions.	163
Table 48 Components details of reactor system	253

Table of Schemes

Scheme 1 Process scheme of high-pressure hydrogenation combining inline analysis.....	40
Scheme 2 Asymmetric hydrogenation of 3 in batch.....	47
Scheme 3 deprotection step to synthesize Ezetimibe.....	53
Scheme 4 Two steps process scheme for synthesis of ezetimibe	56
Scheme 5 Synthetic route of eslicarbazepine acetate.....	57
Scheme 6 Multi-step synthesis of (<i>R</i>)-eslicarbazepine acetate.	60
Scheme 7 Synthesis of Biotin.....	63
Scheme 8 Cyclic slug flow reactor.....	64
Scheme 9 Two Set-ups of a continuous fReactor Hydrogenation System	72
Scheme 10 Hydrogenation of nitrobenzene.....	78
Scheme 11 Benchmark reaction for hydrogenation by fReactor	91
Scheme 12 Synthesis of standard substrate.....	92
Scheme 13 Hydroformylation of 1-octene	99
Scheme 14 Hydroformylation cycle and isomerization cycle	100
Scheme 15 process diagram of flashstop reactor	104
Scheme 16 Single unit flashstop reactor	108
Scheme 17 Initiation of hydroformylation catalytic cycle	110
Scheme 18 Ligands adopted in this study	112
Scheme 19 process diagram of vertical fReactor system	115
Scheme 20 ADH of 1-phenylethanol.....	118
Scheme 21 Catalysts adopted in the study.....	122
Scheme 22 An example of continuous flow system for single diastereomer synthesis.....	123
Scheme 23 Immobilized asymmetric hydrogenation catalyst.....	124
Scheme 24 Synthetic route of HIV protease inhibitor and mechanism	125
Scheme 25 Synthetic route of substrates.....	126
Scheme 26 Synthetic route of α -carbonyl- β -amino acids	127
Scheme 27 Mechanism of step 2 in route 4	128
Scheme 28 Route 5 for synthesis of α -carbonyl- β -amino acids.	128
Scheme 29 route 6 for synthesis of α -carbonyl- β -amino acids.....	128
Scheme 30 Synthesis of 2-nitropropiophenone	129
Scheme 31 Process combining ADH and AH.....	145

Chapter 1: Introduction

A chiral molecule is one that cannot be superposed on its mirror image by any combination of rotations and translations.^[4] The concept of chirality is of great importance in understanding the physical and theoretical reasons behind the formation and structures of numerous organic molecules, metal complexes and biomolecules.^[5] Nowadays, the origin of chirality in life's chemical building blocks and amplification of chirality are still an unsolved scientific problem.^[6]

Recent developments in reactor technology, especially continuous flow reactor technologies, are bridging the gap between chemical engineering and chemistry, which is opening opportunities to tackle chirality problems. Flow chemistry can provide several benefits over batch methods, such as improved consistency of mixing, increased control over thermal characteristics and gas liquid mass transfer owing to the high gas surface-area to liquid volume ratio.^[7] These characteristics facilitate process intensification and allow operation under extreme conditions (high temperature and high pressure in this thesis), which can improve the efficiency of process and TOF of catalysts. The precise control of residence time can help us extract the kinetic information on the second scale, even for the challenging pressurized gas liquid reactions.^[8]

1.1 Homogeneous catalytic hydrogenation

Homogeneous hydrogenation is one of the most extensively studied reactions in homogeneous catalysis. It can be carried out by using molecular hydrogen as reductant and it is also possible to adopt other molecules acting as hydrogen donors, such as alcohols or formic acid, which are called transfer hydrogenations. A wide variety of soluble transition metal complexes that are active in catalytic homogeneous hydrogenation under mild conditions have emerged with development of organometallic chemistry in the late 20th century. It was found that transition metals have the appropriate orbital to interact with molecular hydrogen, forming metal hydride and allowing the transfer of the hydride to the unsaturated compounds. Pioneer complexes are shown in Figure 1.^[9]

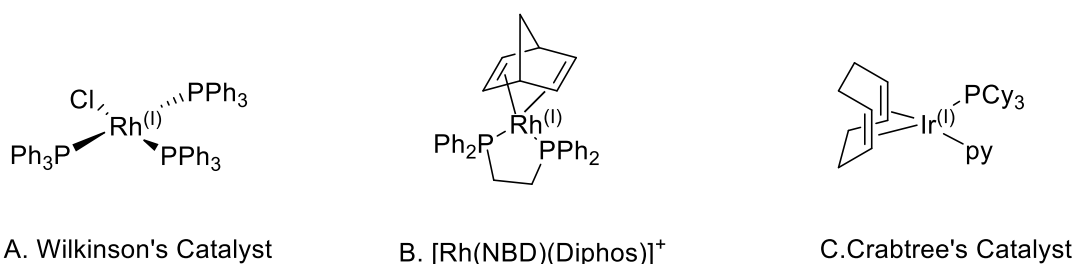


Figure 1 Homogeneous hydrogenation catalysts.^[10]

The study of rhodium catalysts sheds initial light on the mechanism of homogeneous hydrogenation.

^[10] Two types of catalysts were found, namely monohydride and dihydride catalysts, Figure 2. The hydride route of monohydride catalysts involves the initial heterolysis of molecular hydrogen followed by coordination of the substrate. A second possible route is that which begins by coordination of the substrate followed by interaction with molecular hydrogen. The cationic catalyst, $[\text{Rh}(\text{NBD})(\text{Diphos})]^+$, is an example.^[11]

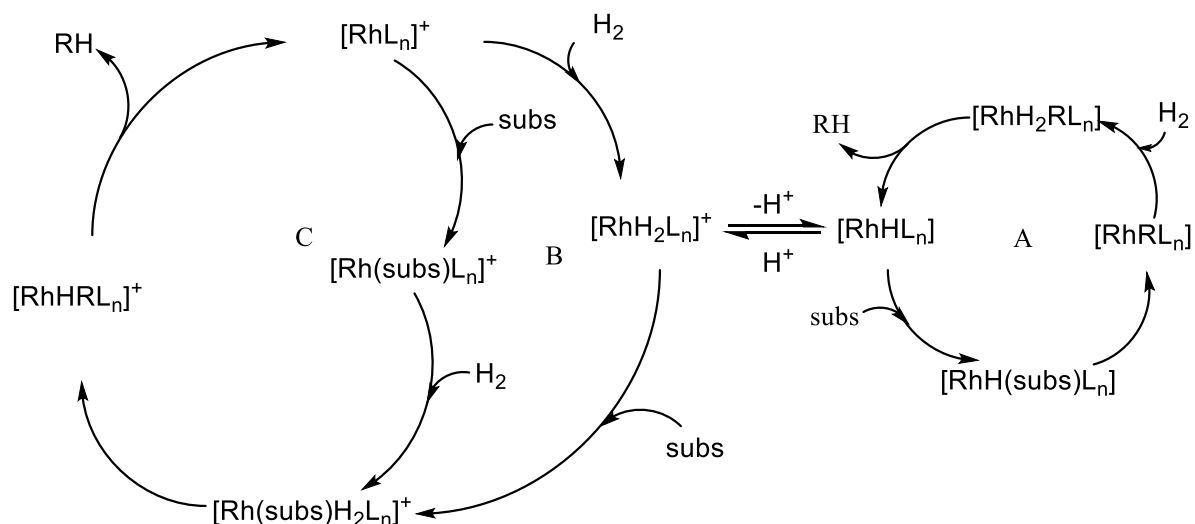


Figure 2 Monohydride (A) and dihydride (B and C) Rhodium hydrogenation catalyst

Catalytic systems with multi-equivalent phosphorus ligand and coordination solvent have been found to work well for rhodium, such as $[\text{RhCl}(\text{PPh}_3)_3]/\text{MeOH}$. In the rhodium system, the reaction adopted a PR_3 to Rh ratio of 2:1 to avoid the ligand dissociation. MeOH was easily lost resulting in a vacant site for substrate coordination. However, the Ir(III) complexes $[\text{IrH}_2(\text{MeOH})_2(\text{PPh}_3)_2]^+$ were less labile and less active in MeOH than its Rh analogues due to the strong metal ligand bond. Consequently, iridium catalysts developed in the early era underperformed.^[12]

By combining mono-equivalent phosphorus ligand catalysts with non-coordinating solvents, an effective iridium catalytic system was found. Since solvent dissociation was needed to generate a vacant site for substrate binding, the use of CH_2Cl_2 that is non-coordinating could enhance the catalytic rate and expand the substrate scope. Halocarbon solvents in general had been less favoured for Rh catalysts, because of the risk of C-Cl oxidative addition to Rh(I). This was not observed in iridium catalytic systems, because the resting state of iridium complexes is Ir(III)(versus Rh(I)) that has cationic nature. The catalyst, $[\text{Ir}(\text{COD})(\text{PCy}_3)(\text{pyridine})]\text{BF}_4$ that is usually referred to as Crabtree's catalyst, is coordinated with one phosphorus ligand and proved to be most effective. After hydrogenating COD, a vacant site is available for interacting with the molecular hydrogen and the substrate. The TOF for reduction of alkenes at 0 °C by Crabtree's Catalyst are as followed: *t*-BuCH=CH₂, 8300 h⁻¹; 1-hexene, 6400 h⁻¹; cyclohexene, 4500 h⁻¹; 1-methylcyclohexene, 3800 h⁻¹; Me₂C=CMe₂, 4000 h⁻¹. The above-mentioned rates can be compared with those for other catalysts under similar conditions: $[\text{RhCl}(\text{PPh}_3)_3]$

at 0 °C (1-hexene, 60 h⁻¹; cyclohexene, 70 h⁻¹; 1-methylcyclohexene, 20 h⁻¹) is far slower and [RuHCl(PPh₃)₃] at 25 °C in C₆H₆ (1-hexene, 9000 h⁻¹; cyclohexene, 7 h⁻¹; 1-methylcyclohexene, Me₂C=CMe₂ 0 h⁻¹) showed a high activity only for the reduction of terminal alkenes.^[13]

Ruthenium catalysts attracted attention in the 1990s, especially due to their application in asymmetric hydrogenation.^[14] RuCl₂(PPh₃)₃ with three bulky triphenylphosphine ligands prevents the coordination of other large ligands in a coordinatively unsaturated d⁶ complex. In the catalytic cycle as shown in Figure 3, this complex coordinates with the ketone by hydride addition to the double bond. In the turnover-limiting step, dihydrogen coordinates and becomes acidic. Proton transfer to the oxygen releases the hydrogenated product and regenerates the starting hydride. When a chiral ligand is coordinated, the chirality can be induced by the addition of dihydrogen to the double bond through cis stereochemistry.^[15]

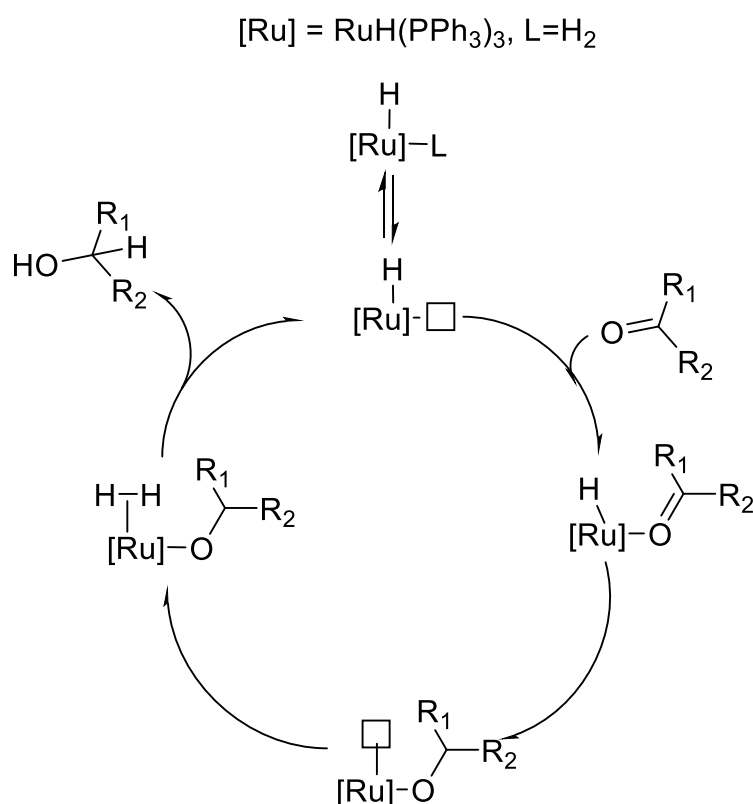


Figure 3 Conventional mechanism for the H₂-hydrogenation by Ru Catalyst

Many processes manufacturing chiral compounds employ the platinum-group metal (rhodium, ruthenium, and iridium) catalysts, due to their remarkable activity and enantioselectivity. However, the cost of noble metals is expensive and the price volatile. The aim of reducing costs in the pharmaceutical industry causes the trend in current research to shift their interest to first-row transition metals, such as iron, cobalt, manganese, nickel, and copper. The achievements in this field indicate that first-row transition metal hydrogenation catalysts can provide an alternative to noble metal catalysts, but activity, productivity and catalyst recycling still remain a major challenge.^[16]

1.2 Asymmetric hydrogenation catalysts and reactions

The asymmetric reduction of unsaturated double bonds by H₂ catalyzed by chiral transition metal catalysts is an efficient and environmentally friendly method to produce chiral compounds at large scale.^[17] Compared with resolution methods (diastereomeric crystallization, enzyme and chromatography),^[2b] it generates less waste and saves cost. Hydrogen is inexpensive and readily available. Hydrogen gas can be used in excess to drive reactions to completion, avoiding the need for further purification. It is non-toxic, but does give safety and handling problems.^[2a] Catalytic homogeneous asymmetric hydrogenation (AH) has diverse industrial uses in food industry, petrochemical industry, and pharmaceutical industry. Over 70% of commercial chemical chiral catalytic processes are asymmetric hydrogenation reactions.^[2b] Some examples of industrial applications of AH include Monsanto's L-DOPA synthesis (AH of a dehydroamino acid, 94 % ee, 20,000 turnovers with a Rh-DIPAMP complex)^[18], synthesis of a key intermediate of carbapenem (AH of ketones using a Ru-DTBM-segphos catalyst through dynamic kinetic resolution, 99% ee, 98% de over 100 tons/year),^[19] Recently, several launched drugs such as tipranavir for treating HIV infection,^[20] rozerem for treating sleep-onset insomnia,^[21] sitagliptin that is an anti-diabetes drug,^[22] and aliskiren that is used to treat high blood pressure,^[23] relied on AH in their synthesis.

By replacing triphenylphosphine of the Wilkinson's catalyst [RhCl(PPh₃)₃]^[24] with resolved chiral bisphosphines, two breakthroughs were made in AH in the late 1960s by Kagan and Knowles.^[18, 25] Kagan reported the first bisphosphine ligand, DIOP (Figure 4a), for Rh-catalyzed AH. Chelating bisphosphorus ligands could lead to superior enantioselectivity compared to monodentate phosphines. C₂ symmetry was an important structural feature for developing new efficient chiral ligands. Kagan's work led to the rapid development of chiral bisphosphorus ligands.^[26] Knowles made his significant discovery of a C₂-symmetric chelating P-chiral bisphosphine ligand-DIPAMP (Figure 4b). Due to its high catalytic efficiency in Rh-catalyzed AH of dehydroamino acids, DIPAMP was quickly employed in the industrial production of L-DOPA.^[18]

Following significant contributions by Knowles and Kagan, hundreds of chiral phosphorus ligands have been developed for AH.^[27] Noyori's research on Ru-BINAP catalysts for AH opened up opportunities for efficient hydrogenations of a variety of substrates. Initial application of Noyori's Ru-BINAP (Figure 4c) system was olefin reduction,^[28] and afterward the system was found to be useful for hydrogenation of ketones by chelating the Ru-BINAP complex with chiral diamine ligand. It was found that the NH group enables the formation of a six membered ring intermediate in the catalytic cycle, which is known as "NH effect".^[29] Thus a wide variety of prochiral ketone substrates were hydrogenated with excellent enantioselectivities.^[30] In the 1990s, significant progress was also achieved in Rh-catalyzed AH with the introduction of some efficient chiral bisphosphorus ligands such

as DuPhos (Figure 4d) and BPE (Figure 4g) developed by Burk^[31] and the substrate scope has been broadened.

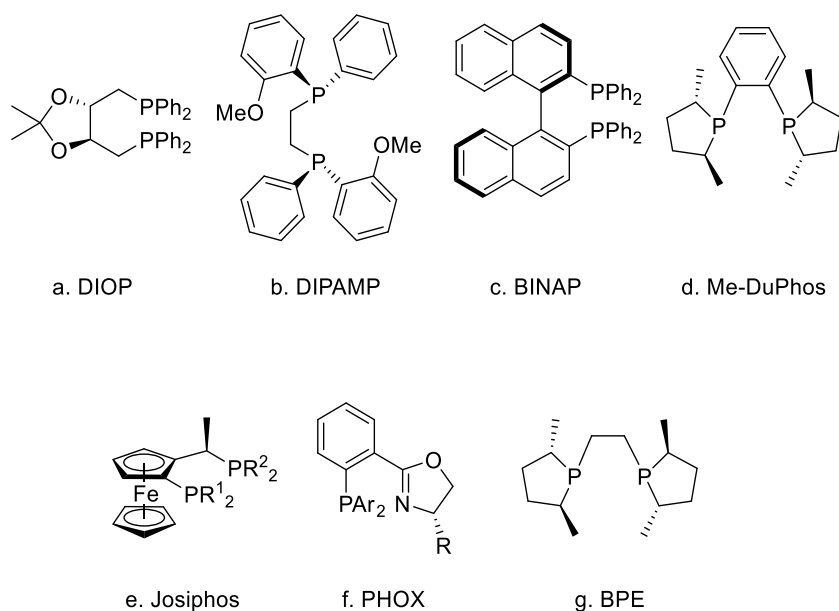


Figure 4 Pioneering ligands for asymmetric hydrogenation.

Chiral bisphosphorus ligands, such as TangPhos (Figure 5h),^[32] DuanPhos (Figure 5i),^[33] ZhangPhos (Figure 5j),^[34] Binapine^[35] and Tunephos (Figure 5k),^[36] designed and synthesized by the Zhang group, are highly electron-donating in nature and have a well-defined chiral environment. To accelerate the reaction rate, it is important to develop a strategy to reduce substrate and product inhibition towards catalysts. The strong trans effect of electron-donating phosphines is employed to reduce product inhibition and this will allow high turnover and turnover frequency to be achieved. TangPhos was developed as a highly effective P-chiral ligand toward a broad range of substrates, including functional olefins, ketones, and imines with a TON up to 100000. The history of Zhang's group ligand is as follows: Only one enantiomer of TangPhos is available through (-)-sparteine assisted reaction, DuanPhos that can be prepared as two enantiomers in a convenient route was developed. Compared with TangPhos, DuanPhos is air-stable and also more rigid due to the fused aromatic moiety, giving excellent ee's in Rh-catalyzed AH.^[34] Tunephos are biphenyl ligand connected by carbon chains with different length that results in different bite angle and an increased conformational rigidity. It was found that different substrates can be reduced with high enantioselectivity by catalysts of different bite angles. Its Ru complex gave a good performance in asymmetric reduction of a series of keto ester and reductive amination of simple ketone by inorganic amine source. For example, high turnover, up to 100000, in hydrogenation of ethyl (2-chloroaceto)acetate can be achieved using C3-tunephos, while reaction TON using BINAP was 1000.^[36d]

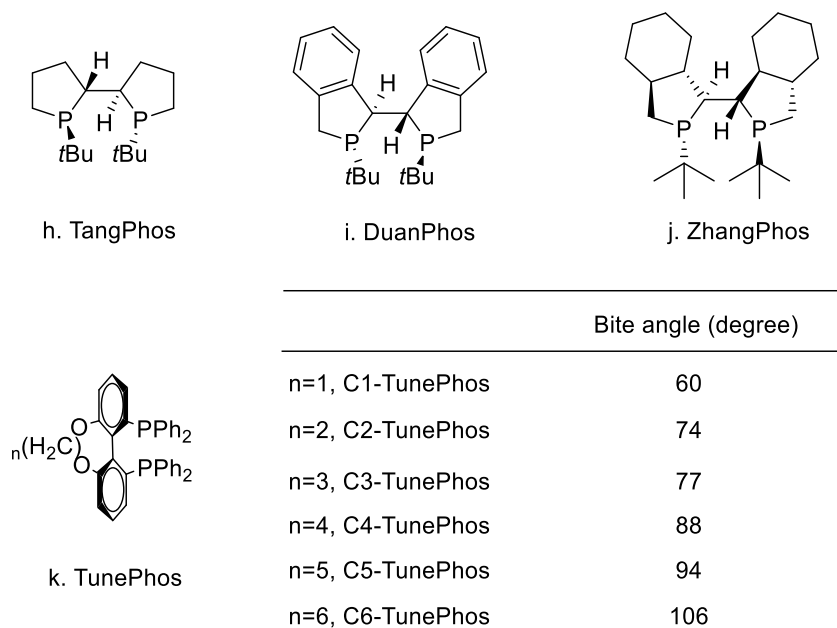


Figure 5 Diphosphine ligands developed in Zhang's lab

Compared to diphosphines, tridentate ligands are more rigid and electron donating. They can create a deeper catalytic pocket around the reaction site (transition metal). Catalysts of tridentate ligands could have better performance when catalyzing reactions. In 1989, Nishiyama synthesized a tridentate ligand, Pybox (Figure 6l), that successfully catalyzed asymmetric cyclopropanation, Diels-Alder reaction, 1,3-dipolar cycloaddition, Adol reaction, coupling reactions and so on.^[37] Zhang designed and synthesized (*R*)-Ph-ambox (Figure 6n) and (*S,R*)-indan-ambox (Figure 6o) that contained chiral ambox. It was proven that the structure motifs, NH, served an important role in increasing catalyst's activity and selectivity in asymmetric hydrogenation and transfer hydrogenation of simple ketone.^[38] In 2001, Zhou successfully synthesized tridentate ligand, SpiroPAP (Figure 6m), that achieved high activity and enantioselectivity in AH of simple ketone.^[39] Tridentate ligands also showed potential in AH by earth abundant metal catalysts, including, iron, cobalt, nickel and magnesium catalyst.^[16]

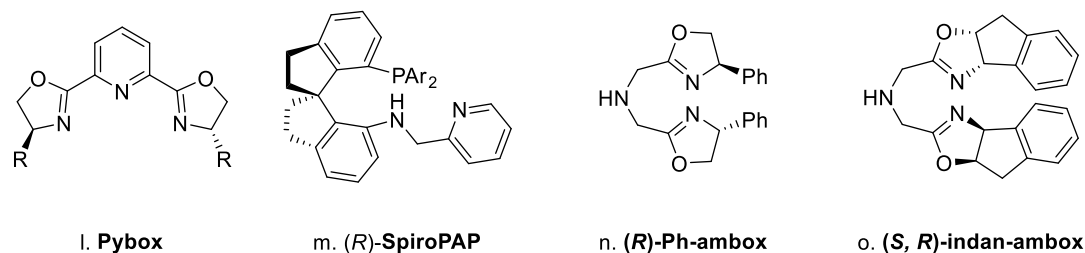


Figure 6 Pioneering tridentate ligands

In recent years, by incorporating NH effect with rigid ferrocene moiety, Zhang developed a series of ferrocene-based tridentate ligands, including f-amphox (Figure 7p),^[40] f-amphol (Figure 7q),^[41] f-ampha (Figure 7r)^[42] and f-amphamide (Figure 7s)^[43]. Simple ketone can be reduced with high turnover (up to 1000000) and high enantioselectivity catalyzed by f-series ligand iridium complexes. Ir/f-amphox can

be used to produce Ezetimibe, Ramipril, (S)-phenylephrine, Denopamine and so on. Ir/f-amphol and Ir/f-ampha also have wide applications in drug synthesis.^[44]

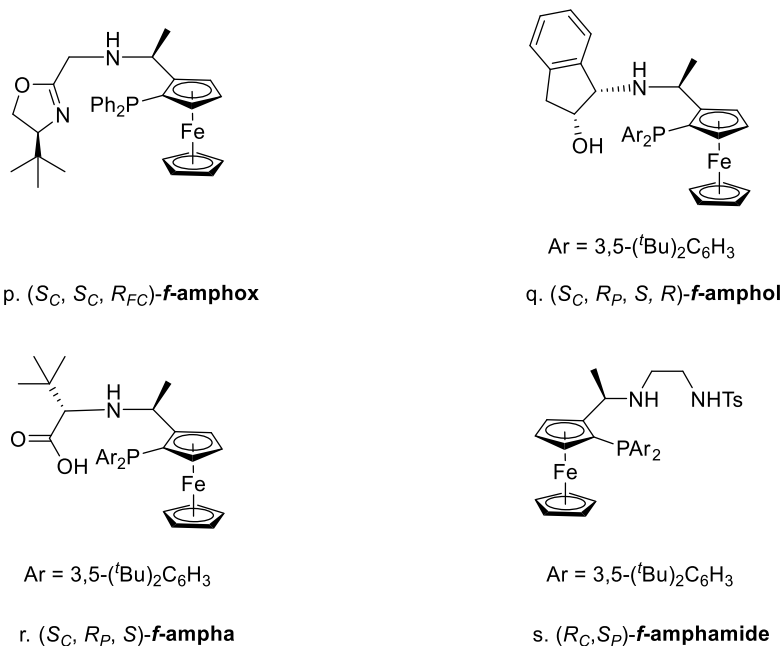


Figure 7 Ferrocene based tridentate ligand---f-series ligands.

The classical asymmetric hydrogenation used gaseous hydrogen, while asymmetric transfer hydrogenation (ATH) utilizes substances contained in the reaction mixture as hydrogen source, such as propan-2-ol or the azeotropic mixture of formic acid and triethylamine.^[45] The absence of gaseous hydrogen prevents the requirement of pressure reactors, which lowers the overall cost of the process and minimizes the explosion hazard.^[46] Homogeneous Ru catalysts to be applied in ATH of prochiral ketone and imine compounds were introduced by Noyori between 1995 and 1996 and extended to Rh and Ir catalysts by the Blacker group.^[47] The catalysts shown in Figure 8u contained ruthenium(II) as the central atom, enantioenriched chiral diamine ligand, such as *N*-(2-amino-1,2-diphenylethyl)-4-toluenesulfonylamide (TsDPEN) and η^6 aromatic ligand (e.g., benzene, *p*-cymene or mesitylene).^[48] The main advantage of these complexes lies in their high modularity. The structure of these complexes can be relatively easily modified to enhance their catalytic properties to better fit the hydrogenated substrate. Some examples of ATH catalysts are shown in Figure 8.^[49] In 2004, to minimize the rotation of the η^6 -arene and improve the catalytic properties, Wills et al. tethered the chiral diamine ligand and η^6 aromatic ligand in Noyori type rhodium and ruthenium catalysts shown in Figure 8v. Tethered **complex v** was found to be highly active in reduction reactions under transfer hydrogenation conditions. For example, acetophenone ([S]=2M, FA/TEA) reduction using 0.5 mol% of **v** at 40 °C achieved >99% conversion within 3 h (without significant erosion of ee), whereas the same reaction with an untethered catalyst required 24h.^[50]

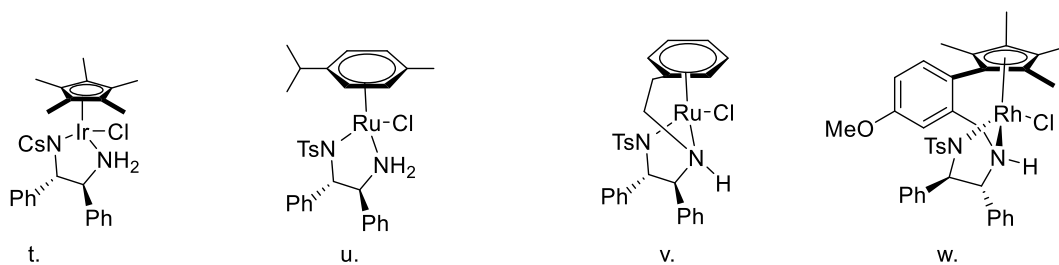


Figure 8 Some examples of asymmetric transfer hydrogenation catalysts

Current continuous processes rarely involve catalytic enantioselective transformations.^[1] AH is one of the most powerful synthetic tools to obtain chiral molecules in pharmaceutical industry.^[2] However, practical homogeneous hydrogenation with a low catalyst loading typically requires a long reaction time (more than 24 hours), which poses challenges for continuous operation, because the microreactor is adaptable to reactions with short reaction time.^[3] Immobilization of the catalyst for homogeneous hydrogenation has been demonstrated to be a practical strategy, using catalyst loadings decreased to a minimum of 0.02 mol%.^[51] But continuous flow AH has still been an underdeveloped area. To the best of knowledge, several kinds of reactors have been developed for catalytic homogeneous gas liquid reactions and there has been only one report on the application of AH as the key step in a multi-step flow synthesis of chiral molecules, in which the 2.5 mol% catalyst loading was far from ideal.^[52]

1.3 Flow chemistry and microreactor

Flow chemistry is a recent subject that looks at producing chemicals in a continuous instead of batch mode. With micro-structured devices, reactions or separations can be carried out with high efficiency and controllability in the micro or submillimeter confined space.^[53] By applying a number up strategy, the microreactor system can be scaled quickly by integrating more reactor units without loss of yield or selectivity.^[54] The majority of microreactors are tubular and rely on passive mixing. To create turbulent flow, baffles of different shapes are fused into the microchannels, for example, the heart design of Corning reactors shown in Figure 9a. Another type of reactor is the miniature CSTR that relies on active mixing. The Jensen group reported one design that relies on manifolding the CSTRs back-back.^[55] The Blacker and Kapur groups designed another lab CSTR called the fReactor that bear mixing units inside the reactor and connect to each other by PTFE tubes as shown in Figure 9b.^[55-56]

Microreactors hold several advantages against traditional batch reactors:

1) Good mass and heat transfer.^[8]

The mixing time in microchannels can be lower than 1 ms due to short diffusion length.^[57] Compared to a traditional stirred tank, the mixing in microreactor is faster, which leads to better reaction control and high selectivity. In terms of heat transfer, the high surface area per unit volume also gives good

heat transfer and control. When a gas liquid reaction takes place in a micro reactor, the mass transfer can be quicker than in traditional batch reactor because the interfacial surface area (gas liquid contact area per unit liquid volume) can be higher. A comparison is shown in Table 1. The interfacial surface area is 3500-18000 $\text{m}^2 \text{m}^{-3}$ in microchannels, while 141 $\text{m}^2 \text{m}^{-3}$ in a 5 mL round bottom flask.

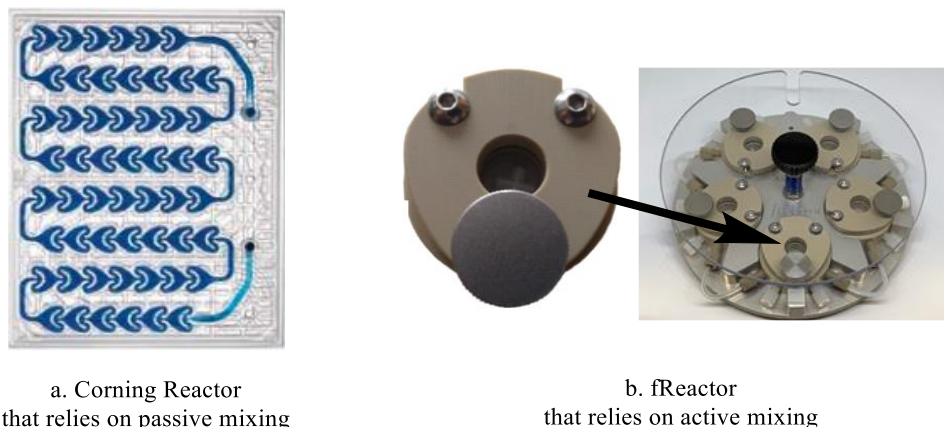


Figure 9 Microreactors adopting passive mixing (a) and active mixing (b)

Table 1 Interfacial surface areas for various reactors^[8]

Reactors	Interfacial surface area ($\text{m}^2 \text{m}^{-3}$)
5 mL round-bottom flask (rbf) ^a	141
50 mL rbf ^a	66
250 mL rbf ^a	38
Tube reactors, horizontal and coiled	50-700
Tube reactors, vertical	100-2000
Gas-liquid microchannel	3400-18000

a. calculated for half-filled round-bottom flasks when the liquid is static.

2) The safety^[58]

Small reactor size means a low inventory of reaction medium, which makes production under high temperature and pressure safer in microreactors than in traditional batch reactors.

3) Expanded chemical space^[59]

The pressurized reactor allows the operation temperature to be higher than the boiling point of the solvent. This can enhance productivity. Furthermore, the small dimensions of the reactor can also benefit photochemistry, electrochemistry, and micro-wave chemistry in scaling up.^[54] The fast mixing and precise control of residence time make it possible to obtain the kinetic product in high yield instead of thermodynamic product, which is impossible in batch and gives a new area called “flash chemistry”.

4) Precise control and easy to scale up.^[7a, 54b]

The well-defined mixing and thermal characteristics at steady state are useful in providing consistency but can also be used to predict process behaviors. The high-quality data increases the

success of scale-up and robustness of the product's quality. In addition, the conditions can be kept the same by the number up strategy, when a process is scaled up.

5) Automated and intelligent process^[60]

Flow chemistry processes consist of pumps, reactors, and valves, which makes the process easier to be automated than traditional batch processes. This allows the establishment of unmanned processes that can reduce human manipulation and avoid human error. The reproducibility of the data can be improved. The data can be further processed by algorithms to develop a self-optimizing machine for automated optimization of chemical reactions and accelerate chemistry research.^[60]

To conclude, continuous flow has been widely applied to a vast number of reactions both in industry and research communities over the past decade. Microreactors outperform batch reactors in carrying out several kinds of reactions. Firstly, biphasic reactions, especially gas-liquid reactions, are becoming more common in flow to avoid mass transfer limitations. Operation under high pressure and high temperature in microreactors to have higher productivity can also be safer than in batch.^[3] Secondly, extremely fast reactions, notably flash chemistry, are facilitated by sub-second mixing enabled by micro-structured devices.^[61] Thirdly, in photochemistry, the small dimensions of flow reactors avoid the appearance of dark area, which makes the scale-up of photo-reactions feasible in industry.^[62] While electrochemistry remains underdeveloped by comparison, it remains a promising field since the precise control of potential energy can improve selectivity of reactions. Flow technology can reduce the use of electrolytes that reduce the cost and waste in industrialization.^[63] Finally, automated and self-optimizing systems are promising for accelerating chemistry research and liberating chemists from labor intensive works. Online and inline analytics enable feedback optimization, and useful kinetic and mechanistic details can be gleaned from the data.^[60]

1.3 Reactor designs for biphasic catalytic gas liquid reactions

AH is one of the major ways to obtain chiral compounds in the pharmaceutical industry.^[2] However, scaling-up is usually a problem due to complicated safety control and poor gas-liquid mass transfer in batch reactors. Continuous microfluidic reactors have emerged as an important tool to carry out organic synthesis. Continuous flow hydrogenation can benefit from being carried out this way for two reasons. Firstly, since hydrogenation is a bi or multiphasic reaction, the reaction rate is often limited by mass transfer between the phases. Micro-reactors can facilitate the reaction with their efficient mixing and high surface area-to-volume ratio. Secondly, hydrogen gas is highly flammable and explosive when it is mixed with oxygen (and therefore air). Since flow reactors typically have less reaction mass than batch reactors, this can reduce the hazard.^[8, 52b, 52c]

The reactors used for biphasic hydrogenation reactions are classified into three types presented in

Figure 10: the stirred tank reactor (batch), the continuous stirred tank reactor (CSTR) and the plug flow reactor (PF).^[64] The total contact area between the gas and liquid (interfacial area) is the key factor to consider during the design of the reactor since the gas-liquid mass transfer is important for the rate of hydrogenation. To carry out reactions successfully in continuous reactors, residence time (flow rate to reactor volume) ideally need to be less than an hour, otherwise batch systems are better. A batch reactor is a tank where starting materials are charged in the beginning; while the reaction is carried out, nothing else is put in or taken out until the reaction is done. As the batch reactor is scaled up, the surface area-to-volume ratio decreases, and if mass transfer is limiting, the reaction rate consequently slows down. A version of this is the fed-batch reactor in which one or more reactants are continuously added, and without an outflow the volume increases. Fed-batch reactors can improve the operational safety of a batch reaction as the feed rate allows control of the reaction rate and therefore any exo- or endotherm. Plug flow or tubular reactors consist of a hollow pipe or tube through which reactants flow in and product flows out. In the plug flow reactor, gases and liquids are separated into gas bubbles and liquid slugs, also referred to as segmented flow. The liquid slugs require a high flow rate to create recirculating flow patterns (Taylor Flow) to generate radial mixing inside the liquid slug.^[65] High flow rates usually results in short residence times. However, most asymmetric hydrogenation reactions take several hours. Hence, plug flow reactors are not suitable to hydrogenations with long reaction time.

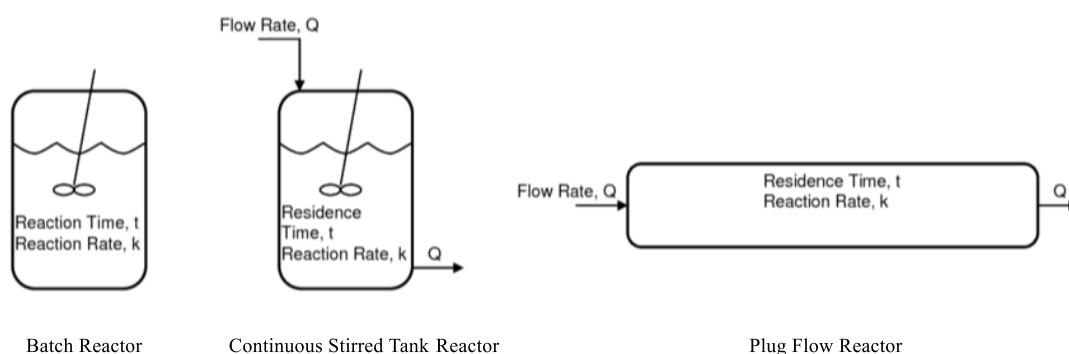


Figure 10 Examples of reactors used for biphasic hydrogenation reactions

Continuous stirred tank reactors are fed with a continuous flow of reactants and the fluids outflow equals the inflow so that a constant volume is maintained. The reactor provides a uniform composition throughout the reactor and exit stream has the same composition as in the tank. Equation 1 is the mole balance of a CSTR in steady state. v_0 is inlet flow rate. v_R is outlet flow rate. C_0 is reactant concentration of inlet. C_R is reactant concentration of outlet. r_R is reaction rate of reactant that is equal to opposite number of multiplications of k (rate constant) and C_R , which is illustrated by equation 2. V is reactor volume.

$$0 = v_0 C_0 - v_R C_R + r_R V \quad \text{Equation 1}$$

$$r_R = -k C_R \quad \text{Equation 2}$$

Unlike plug flow reactors that are mixed by passive frictional forces, CSTR has a stirrer that can provide energy input and maintains active mixing.^[56] It creates a population of gas bubbles within the liquid phase. Therefore, the interfacial area is high, and the high flow rate is not required for creating mixing patterns. The residence time could be prolonged to adapt reactions that take hours. Continuous stirred tank reactors can, therefore, be feasible for long reaction time asymmetric hydrogenation reactions.

The idealized plug-flow and batch reactors are the reactors in which all the atoms in the reactors have the same residence time, whilst for CSTR, there is a distribution of residence time of the materials. It is assumed that the feed introduced into a CSTR is well mixed with the medium. Thus, some of the atoms entering the CSTR leave it almost immediately because material is being continuously withdrawn from the reactor; other atoms remain in the reactor in a longer period because all the material is never removed from the reactor at one time. The distribution of residence times can significantly affect its performance. When using CSTR, a series of reactors are connected to narrow down the residence time distribution.^[66]

Several types of continuous reactors for AH have been developed and results are shown in Table 2. They are all classified as plug flow reactors. In 2004, Bellefon firstly reported a micro-structured mesh reactor (lower left in Figure 11) that enabled the homogeneous and heterogeneous reaction in micro-reactor.^[67] Thales Nanotechnology, Inc. launched an H-tube hydrogenation reactor (upper left in Figure 11) in 2005^[68] that can be used for both homogeneous and heterogeneous hydrogenation. The productivity, however, is limited and the instrument is complicated. The highest residence time among the research was 12.5 minutes. Hessel's group reported a helicoidal single channel falling film micro-reactor (lower right in Figure 11) for AH in 2005.^[69] The gas-liquid mass transfer coefficient is not as good as in well-behaved bench top pressure reactors. The merit of this reactor is that the consumption of chiral ligand is low because the medium volume is small. Ley's group developed a tube-in-tube reactor (upper right in Figure 11) for hydrogenation in 2012.^[52b, 52c] AH could be conducted in this reactor. The residence time was 8 seconds; however, the pressure rate was 20 bar. There was also research about using tubular fixed-bed reactor^[51a, 70] and trickle bed reactor^[71] for heterogeneous hydrogenation. They all have a common drawback that the residence time is short and mixing of gas-liquid-solid is poor. Their application is limited because most of the asymmetric hydrogenation reactions require long reaction time and low catalyst loading.

Table 2 Examples of continuous reactors for asymmetric hydrogenation

No.	Catalyst	Substrate	Batch Condition	Flow (Pressure and temperature)	Reactor	Volume	Residence time or flow rate	Conversion (%)	ee (%)
1	A series of homogeneous catalyst	alkene		20 bar	Tube-in-tube Reactor	0.28 mL	0.16-0.25mL/min	42-99	59-78
2	A series of homogeneous catalyst and Pt/Al ₂ O ₃	alkene	30 min, 2-10 bar, conv: >98 % ee: 95%	20-40°C, 2-10 bar	A micro-structured mesh contactor	0.1 mL	1 min, 0.1 mL/min	>96	31-98
3	[Rh(COD)((S)-MonoPhos) ₂] ₂ BF ₄ /PTA/Al ₂ O ₃	alkene		20°C, 1-30 bar	H-Cube reactor	3mL	0.1-0.4mL/min	>99	96 – 97
4	[Rh (COD) ₂]/PTA/Al ₂ O ₃	alkene	5 bar, RT, 72 min	1 bar, 25°C	H-cube reactor	1.6 mm ³	1 s	90-99	97
5	rhodium/chiral diphosphines	alkenes	k _{ia} = 1-2 s ⁻¹	1bar, 20-70°C	helicoidal single channel falling film micro-reactor	0.02-0.35 mm ⁻³	3–22 min (depend on solvent)	0-94	-7.6-99
6	Homogeneous or heterogeneous			RT–150°C, 20 bar	Vapourtec™ gas/liquid reactor		0.01–9.99 mL/min		
7	Pt/Al ₂ O ₃ modified with O-methyl-cinchonidine	Activated Ketone		20°C, 150 bar TOF: 900 h ⁻¹	continuous stainless-steel tubular fixed-bed reactor	30 mL	1mL/min	80-95	80-90
8	self-assembled metal–organic frameworks	alkene		3 bar TOF: 97 h ⁻¹	continuous stainless-steel tubular reactor		0.05 mL/min	99	90-98

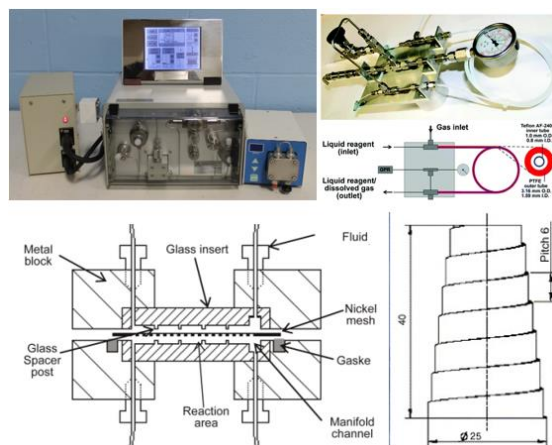


Figure 11 H-cube Reactor (upper left); tube-in-tube Reactor (upper right); micro-structured mesh reactor (lower left); helicoidal single channel falling film micro-reactor (lower right)

Pipe-in-series reactor is a type of continuous reactor that has been applied to a wide range of diphasic reactions, as shown in Figure 12 and Table 3.^[72] It can work under high temperature (up to 140 °C) and high pressure (up to 80 bar) and can give a residence time of 9 hours. Both industrial scale version (up to 400 L) and research scale (12 mL) have been developed in America and Japan. It has shown high ability in improving productivity, selectivity, and safety. The pipe-in-series, in which short wide tubes were filled mostly by liquid and long narrow tubes contained slug flow were connected in series, was derived from coiled tube. Eli Lilly found that by installing pipes with large inner diameter vertically, the gas flow rate and liquid flow rate can be decoupled. The gas flowed out of the tube quicker than the liquid, which prolong the residence time of liquid. This makes it possible to carry out the catalytic reactions with low metal catalysts loading in flow, while traditional flow reactors do not allow reactions with a residence time of hours. Pipe-in-series reactors were firstly applied in gas liquid reactions, including asymmetric hydrogenation^[73] and hydroformylation^[74]. High conversion (63-99%) and high ee (79-97%) can be achieved. In recent years, the Leuckart-Wallach reaction,^[75] aza-Henry Reaction,^[76] asymmetric transfer hydrogenation^[77] and Chan Lam Coupling^[78] have been successfully done in this reactor. The enlargement of tube's diameter can have a negative effect on the mass transfer, although static mixing can improve this. Static mixing involves elements that interrupt the linear flow and cause eddies and recirculation, like rocks in a stream.

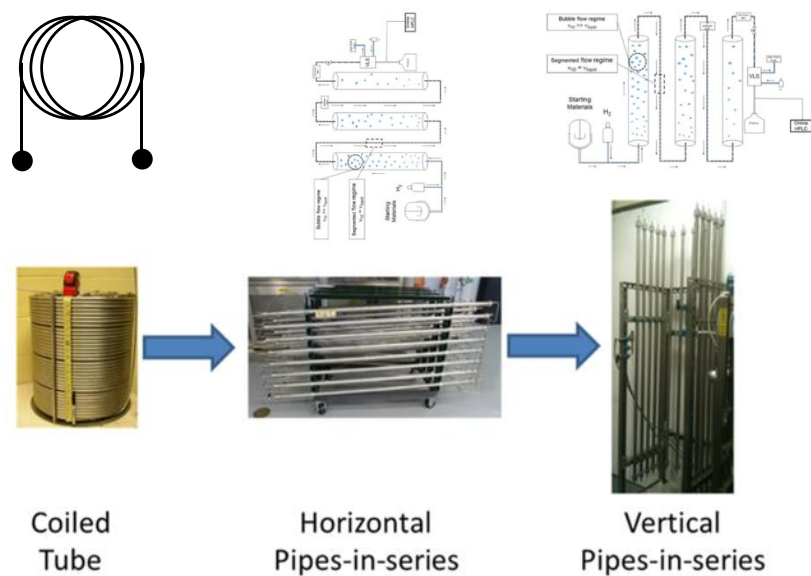


Figure 12 Three generations of pipe-in-series reactors

Table 3 Examples of diphasic reactions carried out in pipe-in-series reactors.

No.	Catalysts	Reaction	Conditions	Reactor volume	Residence time	Conversion (%)
1	Ir catalyst	Reductive amination	28-69 bar, RT	412 mL	4-20 h	90-95
2	Rh-Ph-BPE	Hydroformylation	14-56 bar, 80 °C	360 L	7.5-8.3h	63-97
3	Ir-BINAP	Reductive amination	68 bar, 110 °C	32L	2-8h	90-93
4	Rh-diphos	Asymmetric hydrogenation	70 bar, 70°C	200L	10-13 h	90-99
5	Rh-diphos	Asymmetric hydroformylation	10-60 bar, 60°C	24 mL	7-8.5 h	98
6	N.A.	Leuckart-Wallach Reaction	110 °C	200 mL	>10 mins	99
7	N.A.	Aza-Henry Reaction	87-95 °C	12 mL	33-40 mins	82-84.5
8	(<i>R,R</i>)-Ts-DENEB	Transfer Hydrogenation	9.5 bar, 85 °C	100L	6 h	96
9	Cu catalyst	Chan Lam Coupling	28 bar, 60 °C	200 L	4 h	90

In 2017, Blacker and Kapur's groups reported a miniaturized CSTR reactor (Figure 13) designed to tackle this problem, named as fReactor.^[56] The reactor proved to be adaptable to hydrogenation (solid-liquid-gas), enzymatic reactions (organic-aqueous phases), slurries (solid-liquid), all requiring effective mixing and long residence times. In a plug flow reactor, when the flow rate is decreased, the mixing time in the T-junction or other mixer is prolonged. By adopting active mixing, this decoupled it from the flowrate and ensures good mixing even at low flowrates. A fixed bed reactor is often used for reactions catalyzed by solid catalysts, in which the solid is static and mixing relies on the flow velocity. The fReactor offers full agitation for gas, liquid and solid in whatever combination.^[79] Apart from the fReactor, another version of miniature CSTR was designed and constructed by the Jensen's group. Its design avoids using connecting pipes between the CSTRs by fitting reactors back-to-back with a gasket seal between. But the problem is that it is very hard to form a good seal between the CSTRs so that it cannot be used under pressure.

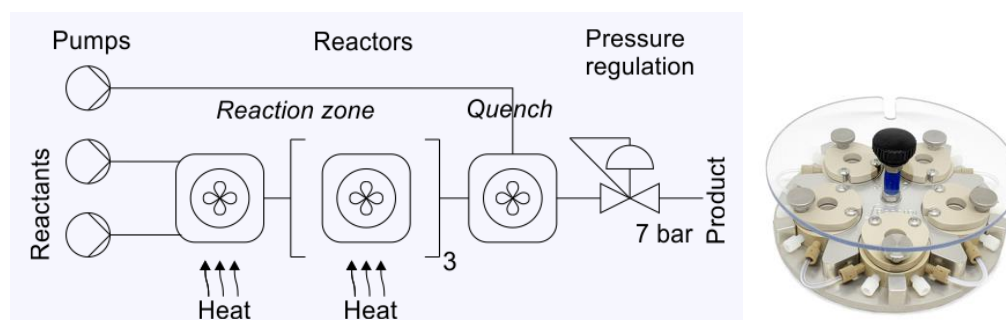


Figure 13 fReactor flow system^[56]

1.4 Controlling diastereoselectivity

Today, most new drugs and those under development consist of a single optically active isomer.^[80] Whilst asymmetric control of single chiral centres^[81] is, arguably now straightforward, much harder is stereocontrol of compounds with multiple chiral centres. According to a survey, 54% of APIs containing chiral centres have an average of two per compound.^[82] Thus, effective diastereoselective hydrogenation is greatly needed. This is exemplified by drugs shown in Figure 14.

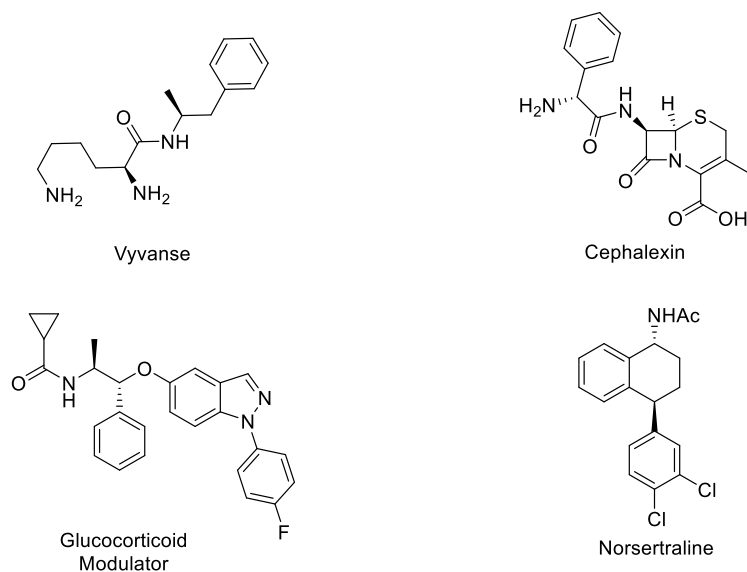


Figure 14 APIs with multiple chiral centres^[12-15]

A second part of the work described in this thesis, integrates hydrogenation and dehydrogenation methods to assist in the control of diastereoselective reactions. There are two strategies to improve diastereoselectivity for reduction of carbonyl or imine compounds as shown in Figure 15.^[83] One method applies the Felkin-Anh and Cornforth–Evans models (relevant to α -halogenated carbonyl derivatives and silyl ethers) to predict the enantioselective outcome of the reaction. The Felkin-Anh rule states that if there is not an unusually electronegative atom on the carbon adjacent to the carbonyl, the largest group prefers a conformation where it is perpendicular to the carbonyl. The medium and smallest groups differ in their proximity to the carbonyl oxygen and the (nucleophile) hydride will attack the position that is nearest to the smallest group, Figure 15. If there is an electronegative atom or group at the site α - to the carbonyl, there is a slight change. The energy of the C-X σ^* antibonding orbital is rather low, and so it overlaps with the π^* of the carbonyl to make a new, lower energy LUMO (lowest unoccupied molecular orbital). What this means is that the conformational arrangement where C-X and adjacent carbonyl group overlap with each other is more favourable than any other. This is Cornforth–Evans rule. If the configuration of the existing chiral centre is fixed, only one enantiomer is favourable, and it might not be the desired isomer. Thus, the less-favoured diastereomer under steric control (anti-Felkin-Anh) could not be obtained and consequently, the application may be limited.

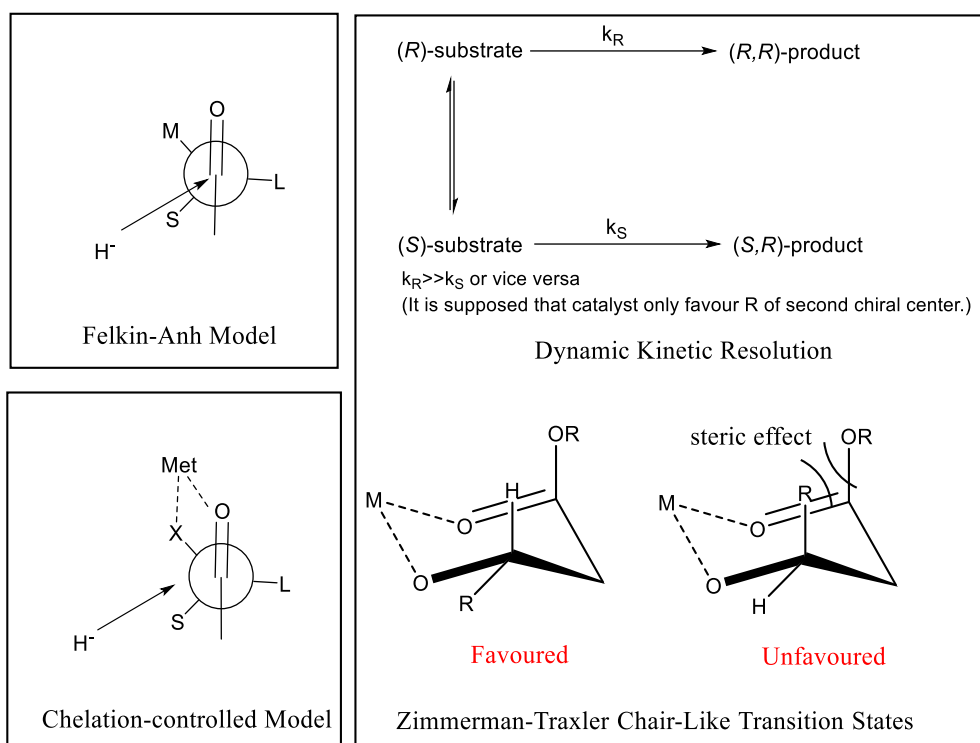


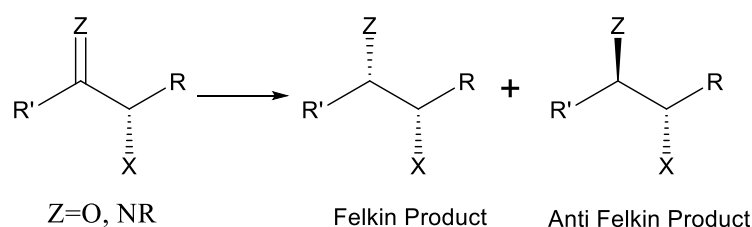
Figure 15 Strategies for obtaining compounds with two chiral centres

Chelation-controlled models are currently the major way to get anti-Felkin configurations.^[83b, 84] A Lewis acid coordinates with the carbonyl group and the α -coordinating group. Thus, it always requires a chelating group, such as a methoxy group and a carbonyl group, to form a six-centred ring structure between the substrate and the catalysts. However, substrates with sterically demanding and weakly coordinating groups, such as SiR_3 , halogen and vinyl groups, disfavour coordination to metals, and additions proceed through Felkin-Anh pathway and result in Felkin-Anh products. In order to obtain anti Felkin-Anh products, Lewis acid reagents, such as ZnCl_2 , can be added to facilitate chelation to the carbonyl addition reactions. Low temperature and weakly coordinating solvents are required to achieve good enantioselectivity.^[83b] The other method is hydrogenation through dynamic kinetic resolution.^[85] This is achieved by racemization. In a dynamic kinetic resolution process, the kinetic resolution occurs with an *in-situ* racemization and then the substrate can be hydrogenated into the favoured single diastereomer. According to Zimmerman-Traxler chair-like transition states,^[86] the metal chelate with a heteroatom in the substrate will form a chair like transition state for certain substrates, such as β -ketoester. The asymmetric hydrogenation and transfer (de)hydrogenation of a substrate possessing an achiral

stereocenter could generate one enantiopure diastereomer. There is also the strategy of catalyst-controlled diastereoselection by adding a steric hindered group on the substrate to interact with the configuration of catalyst.^[83b]

Substrate scope of two strategies is summarized in Table 4. There is no method to get the anti Felkin-Anh products of a substrate that coordinate weakly with Lewis acids. The substrate scope is usually limited by the requirement of the additional interaction. Furthermore, not all enantiopure configurations can be synthesized by a single method. In conclusion, a general methodology to broaden the scope of substrates and obtain all four diastereomers is still greatly needed.

Table 4 Groups adaptable to Felkin–Anh and chelated control pathway^[87]



X	Felkin Product	Anti-Felkin Product
OMe, OBn, Ester	Favoured	Lewis Acid required (metal catalyst)
OSiR ₃ , Halogen, vinyl group	Favoured	Zn reagent required
Weakly Coordinating Group	Favoured	disfavoured

Hydrogenation and dehydrogenation can both be adopted for asymmetric reaction and from a mechanistic perspective, they have the same catalytic cycle in opposite directions, as shown in Figure 16.^[88]

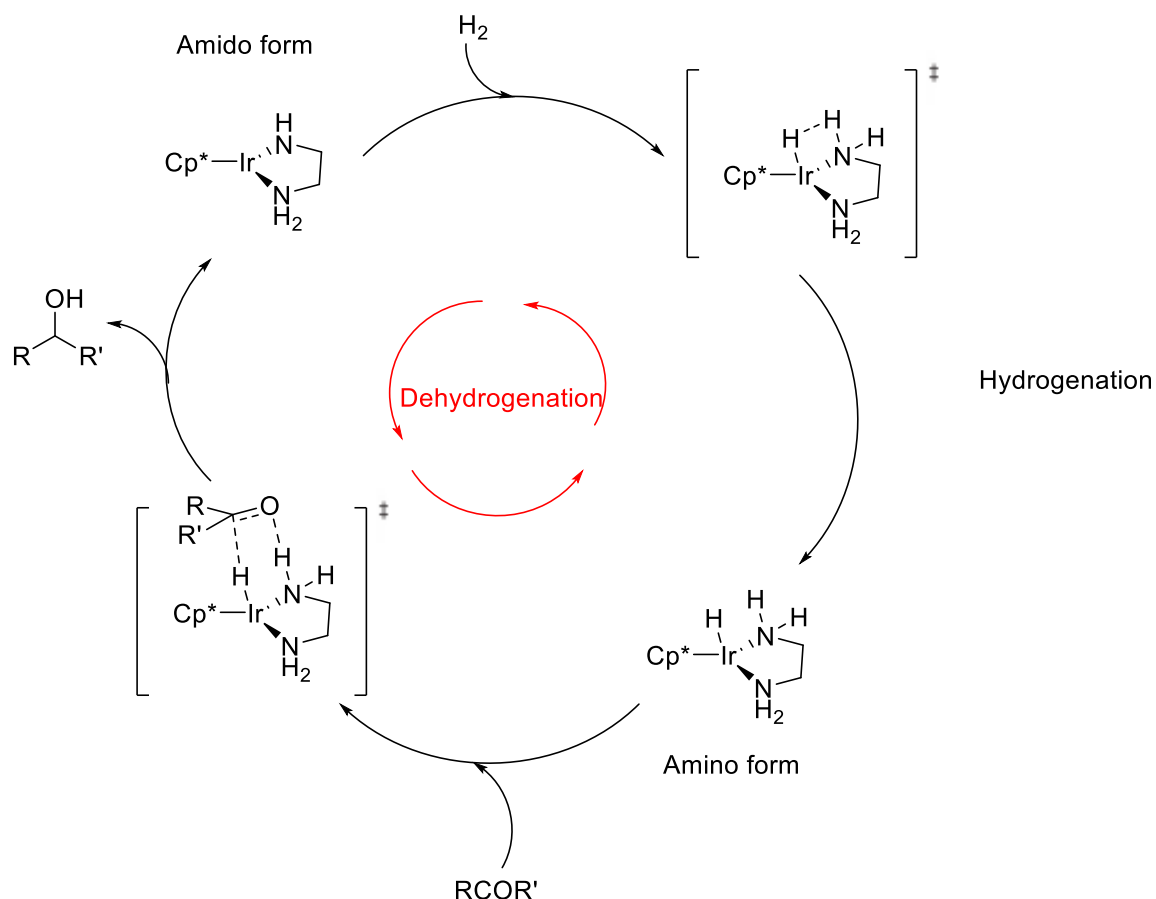
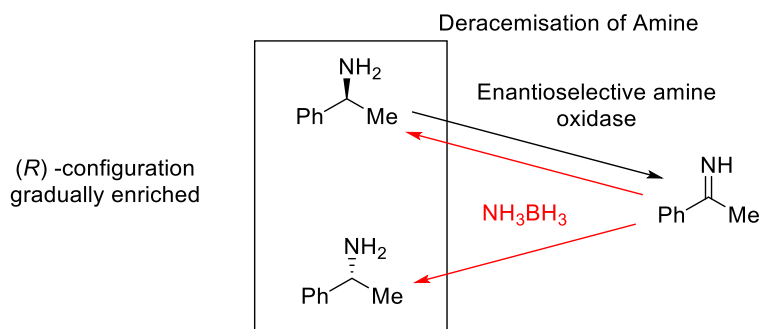


Figure 16 Mechanism of hydrogenation and dehydrogenation^[88]

A chiral product can be produced by AH to start, and if the selectivity is unsatisfactory, the product with undesired configuration can be dehydrogenated by a chiral catalyst to regenerate the starting material which can be rehydrogenated etc, to enrich the desired configuration. Substrates can go through a recirculating process until the desired enantio- and diastereoselectivity are achieved. Recirculation in this way has been achieved with enzymatic but not chemocatalysts, to deracemize the racemic amines.^[89] Turner has shown that an enantioselective amine oxidase can oxidize selectively one enantiomer of a racemic amine, the imine formed can then be reduced non-selectively by ammonia borane and enrich the residual amine enantiomer, recirculating several-times results in a single amine enantiomer, Figure 17.

Previous Work:



Our Work:

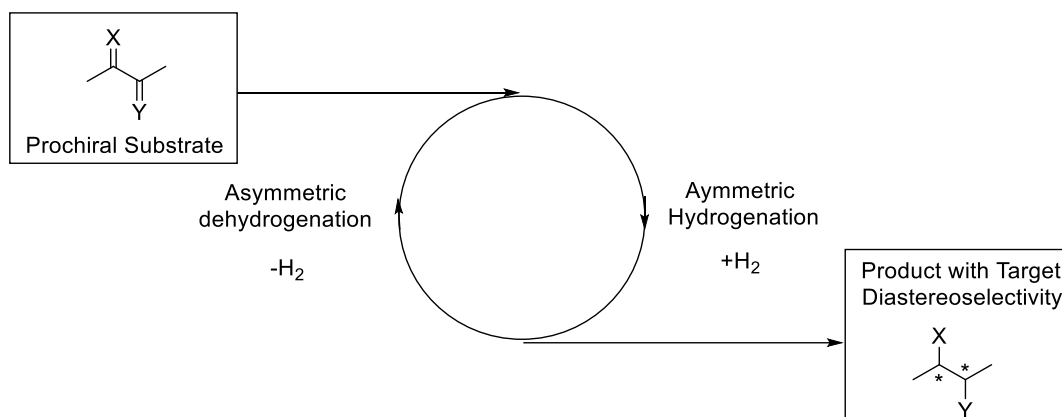
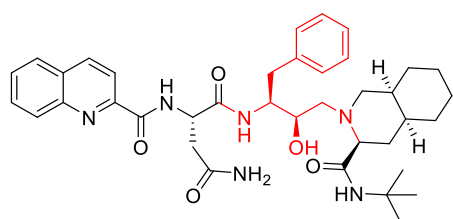


Figure 17 Continuous Reactor System to Obtain Diastereomers

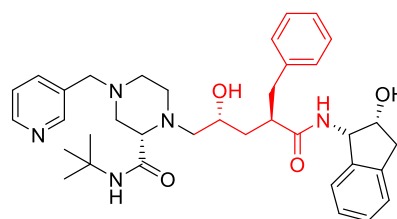
Whilst asymmetric dehydrogenation has been applied for the synthesis of compounds with one chiral centre,^[90] this project will test these in diastereoselective dehydrogenation to allow the cycle for improving controllability of diastereoselectivity shown in Figure 17. Since hydrogenation and dehydrogenation can be carried out under different conditions, a continuous reactor system is designed to separate them from each other, and two reactions can be carried out as a cycle. A continuous reactor system will be developed which combines heterogeneous hydrogenation, heterogeneous transfer (de)hydrogenation and possible additional crystallisation to gain compounds with more than one chiral centre.^[45b, 91] The project tests the concept of multi-catalysis.^[92] This is when two or more catalytic cycles are used to interact with one substrate in one vessel, which raises the efficiency and reduces cost of separation. Conducting multicatalytic reactions in one pot increases the probability of having side reactions. Using a continuous reactor system, catalytic cycles that have interference can be separated into different parts or compartmentalized. This can reduce the disturbance between catalytic cycles. Furthermore, some preferred conditions may differ between the catalytic reactions and these can be optimized and controlled separately, eg.

temperature, concentration, residence time.

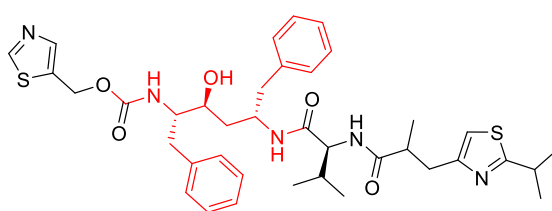
HIV is an important social problem that threatens well-being.^[93] A series of drugs have been developed to manage HIV shown in Figure 18. One class of these are protease inhibitors that target a C₂-symmetric homodimeric structure. This feature within protease active site allows it to selectively cleave the Phe-Pro (Tyr-Pro) moiety of the virus polyprotein. The drugs are designed as hydroxyethylene isosteres, diaminoalcohols, and other related molecules shown in Figure 18, all of which have chiral centres at their core. The current methods of synthesis require chiral starting materials and the synthetic route always require harsh conditions. In our case, we hope to start from cheap achiral compounds to get the enantiopure product by a new continuous reactor system. In addition, this series of substrates includes diastereomers favoured (for example, hydroxyethylene) and less-favoured (for example, diamino diol) by Felkin-Anh rule, which allows us to test the effectiveness of the methodology and better understand the origin of diastereocontrol.



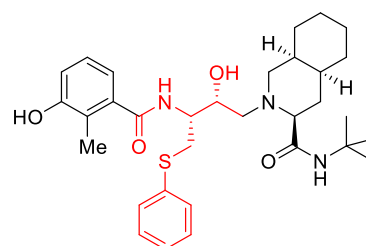
Saquinavir



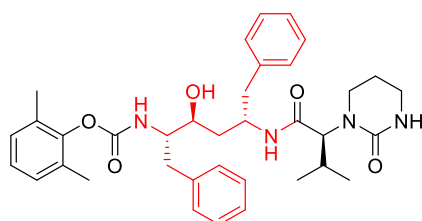
Indinavir



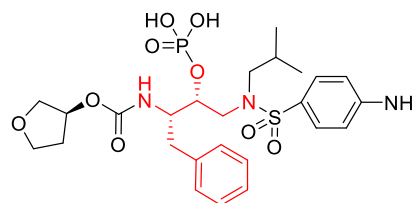
Ritonavir



Nelfinavir mesylate



Lopinavir



Fosamprenavir

Figure 18 HIV Protein Inhibitors with multiple chiral centres requiring diastereocontrol^[93a]

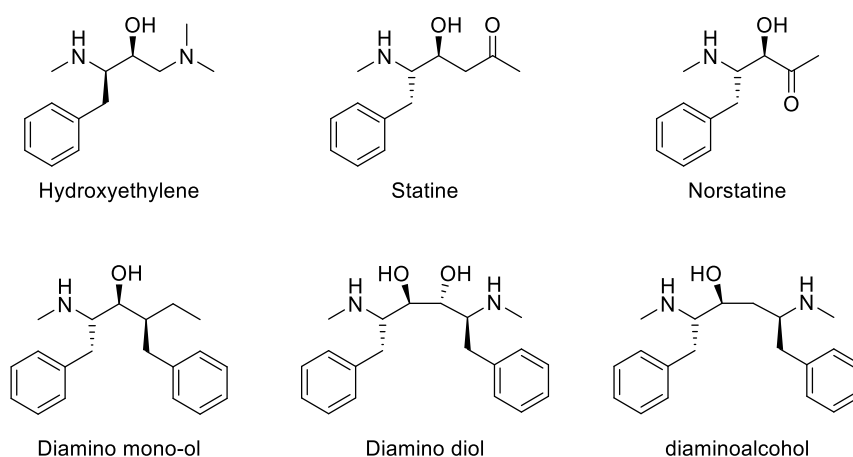


Figure 19 Core Molecule of HIV Protein Inhibitor^[93]

Another target of this work is to develop a new synthetic route to the taxol side chain through our new methodology. Plant derived natural taxol from the bark of *Taxus brevifolia* is the most promising anticancer agents discovered. Due to the limited amounts of taxol which can be derived from the plants, a semisynthetic route starting from the more abundant 10-deacetylbaccatin III is promising for obtaining large quantities. The side chain being attached to the main ring of baccatin III is N-benzoyl-(2*R*,3*S*)-phenylisoserine.^[94] The building block, β -amino α -hydroxy ester, also serves in the synthesis of other drug molecules shown in Figure 20.

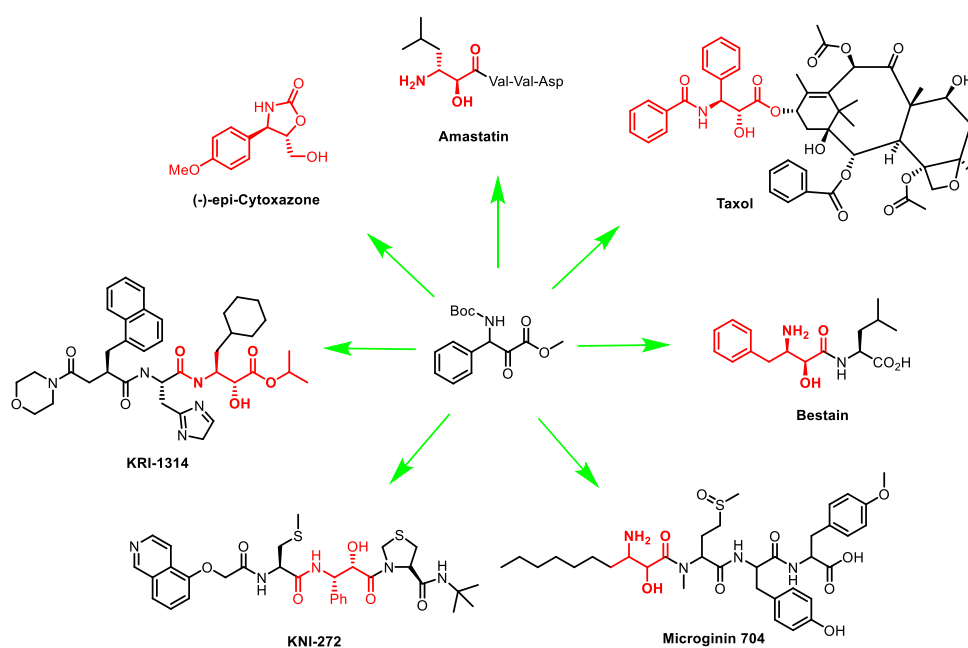


Figure 20 Drug molecules containing building block of β -amino α -hydroxy ester.

1.5 Objectives

This research aims to develop new continuous flow reactor catalytic hydrogenation methods that enable high efficiency.^[95] Current continuous processes rarely involve catalytic enantioselective transformations on a large scale.^[1] AH is one of the most powerful synthetic tools to obtain chiral molecules in pharmaceutical industry.^[24] The work here tests novel microreactor technology in catalytic gas liquid reactions, especially asymmetric hydrogenation and hydroformylation. This work will enable the flow synthesis of chiral compounds through achiral materials and acquirement of kinetic data for high-temperature and high-pressure gas liquid reactions. Furthermore, a new strategy combining asymmetric (transfer) hydrogenation and dehydrogenation using immobilized catalysts will be developed to further improve the diastereoselective synthesis of drug compounds. The methods can be applied to automated chemical synthesis which is revolutionizing the end-to-end continuous-flow production of active pharmaceutical ingredients (APIs).

Chapter 2: The high-pressure gas-liquid slug flow reactor and application in asymmetric hydrogenation.

AH of acetophenone by f-amphox-Ir was selected as the benchmark reaction. Figure 21 shows the kinetic profile in batch. There was a long activation period of 140 minutes. It was proved that by increasing pressure, the activation period can be shortened (unpublished work from Prof. Jialin Wen). After the activation period, the catalyst showed a high activity, which could turn mass transfer as the limiting factor when the reaction is scaled up. In this case, micro-reactor can reduce the scale up effect. Therefore, a high pressure microreactor system could facilitate the reaction by reducing activation period and facilitating mass transfer in this catalytic system.

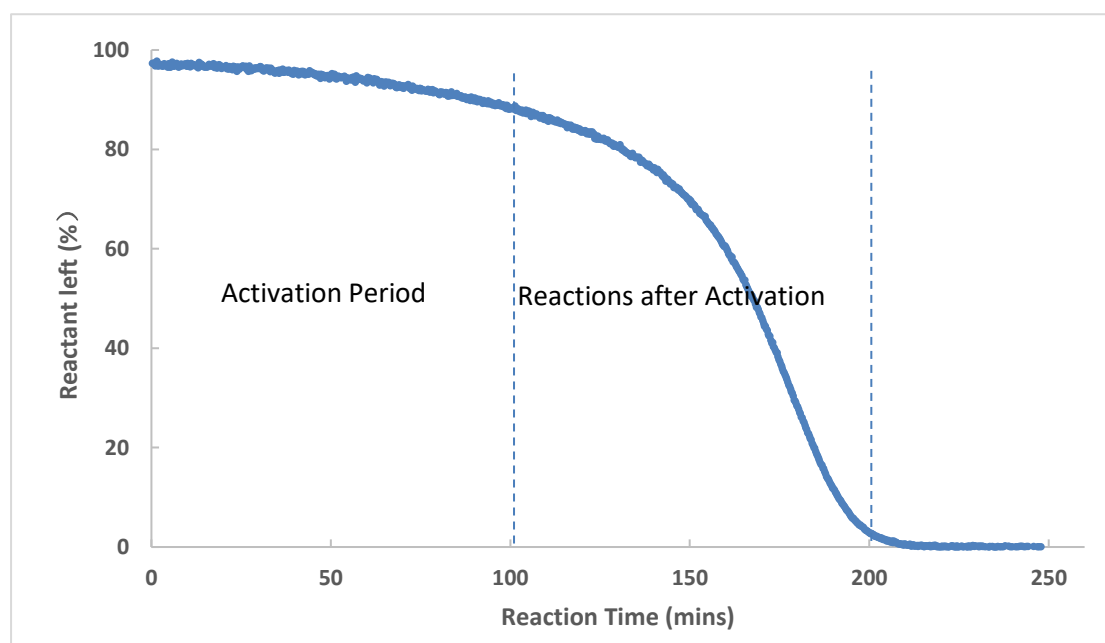
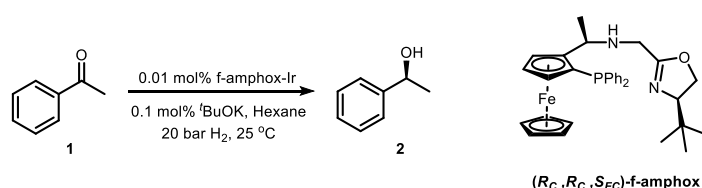


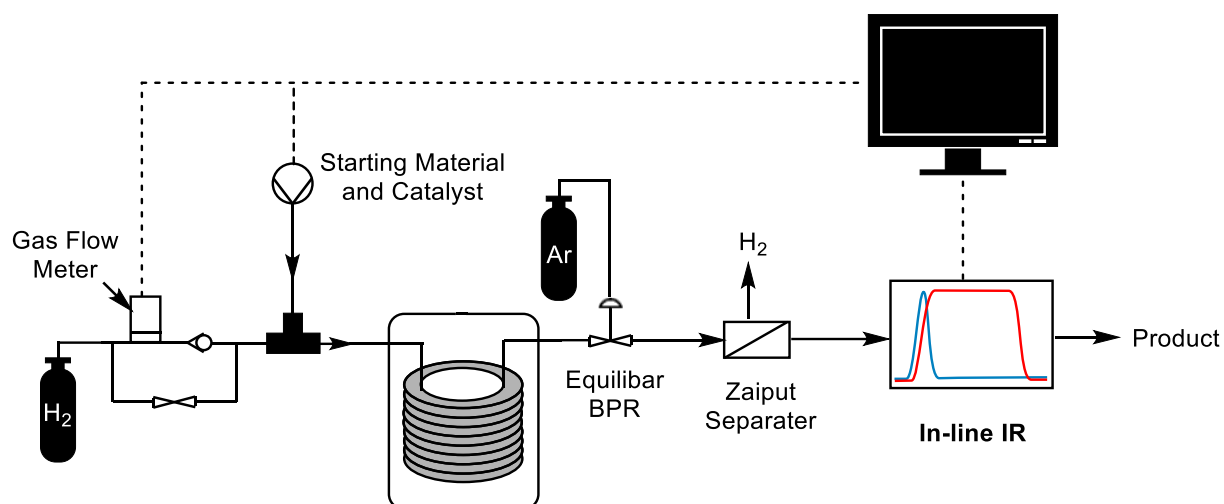
Figure 21 Kinetic profile for asymmetric hydrogenation in batch

2.1 Equipment

High pressure and temperature can increase the turnover frequency (TOF) in a catalytic gas liquid reaction and therefore shorten the reaction time, making a micro-reactor suitable for carrying out AH. According to our investigation, commercially available reactors do not meet the requirements for hydrogenation with high TON and TOF (residence time around 10 minutes and extreme pressure). The system we designed was able to work under high pressure (60 ~ 150 bar) and temperature (80 ~ 150 °C) and is suitable for screening catalysts and conditions, to deliver products quickly and safely and be applied in multi-step flow synthesis. The customized set-up is shown in Scheme 1 and Figure 22. To accommodate the anticipated pressures, all components of reactor system were made of 316 SS with valve and fittings of >500 bar pressure rating.

The HPLC pump was rated to 150 bar,^[96] and gas flow meter was a customized high-pressure unit (outlet pressure rating: 400 bar).^[97] To generate a stable gas liquid flow, a diaphragm-type back pressure regulator was used.^[98] The segmented flow pattern was generated by a T-junction with a liquid and gas inlet. The reactor outflow passed through a hydrophobic membrane-based gas-liquid separator,^[99] and the reaction solution passed across a customized in-line IR probe. A remote-control application as shown in Figure 23 (code in appendix) was developed to realize safe and automated operation, able to vary pump speed affecting the residence time and gas-liquid ratio. All gas flow rates were calculated by non-ideal gas law, which is explained in the appendix.

The tridentate ligands f-amphox (Figure 7p) and f-amphol (Figure 7q)^[40-41] were applied since the tridentate complexes with iridium are more stable under high temperature and pressure than Noyori's ruthenium/bisphosphine-diamine catalysts that are prone to loss of reactivity by dissociation of diamine ligand.



Scheme 1 Process scheme of high-pressure hydrogenation combining inline analysis.

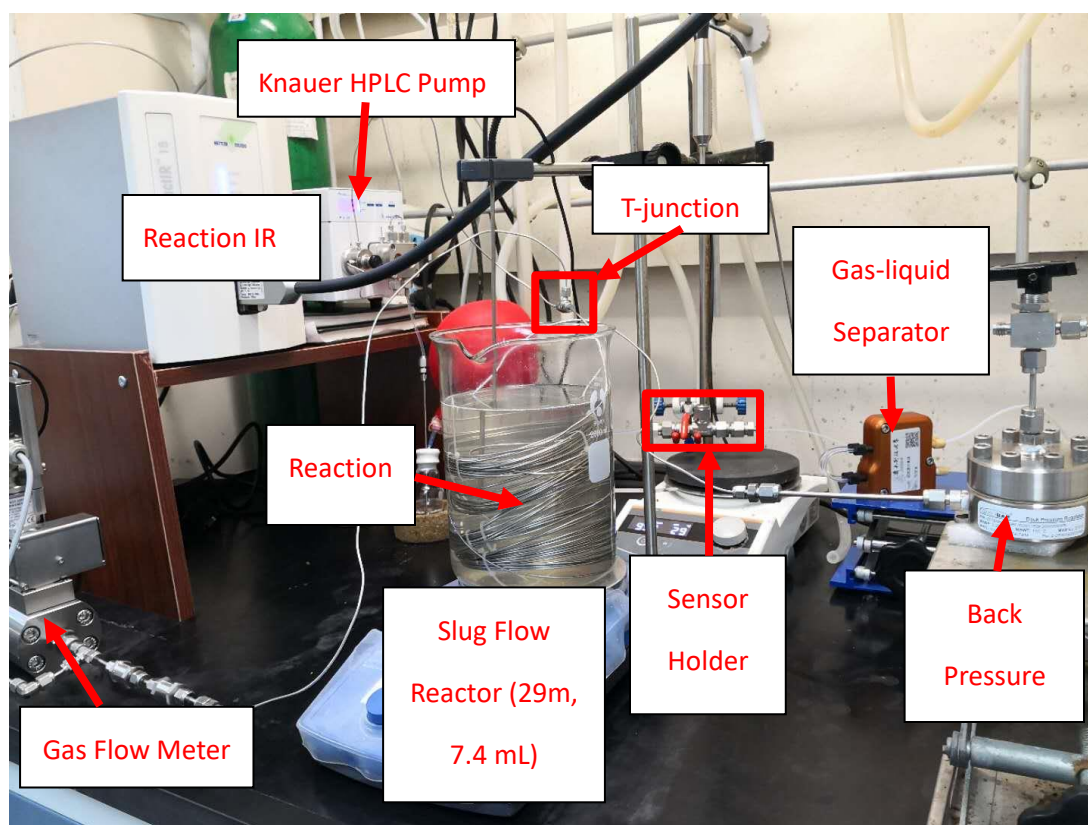


Figure 22 Set-up for high-pressure hydrogenation combining in-situ IR analysis.

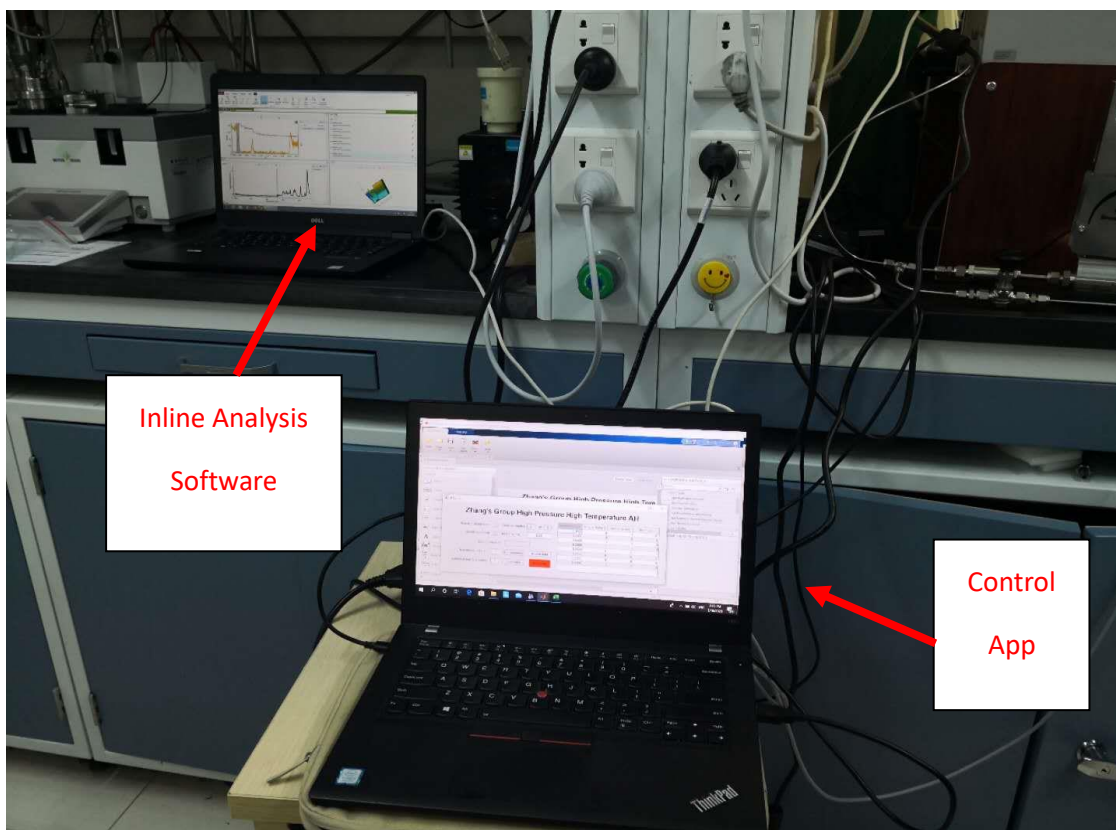


Figure 23 Remote control system and inline analysis system

2.2 Formation of stable slug flow

Batch hydrogenation reactors classically provide hydrogen by stirring and bubbling. The reaction rates are usually gas-liquid mass transfer limited. When implemented in a microchannel-reactor, in our case 1/16-inch OD 316 SS tube, the reaction medium containing the catalyst, substrate and base is mixed with hydrogen in a T-junction and pumped through the reactor. The homogeneous catalyst exists with the product at the end of the reactor. Different flow regimes can be obtained by varying the gas liquid volume ratio and linear velocity, and including bubbly, slug, churn, slug-annular and annular, Figure 24.^[100] The type of flow has a significant effect on reaction conversion.^[62, 89b] Among them, gas-liquid slug flow is beneficial as the frictional forces create Taylor flow micromixing, illustrated in Figure 21 giving more reproducible results with good mass transfer and narrower residence time distribution.^[101] Slug flow is characterized by a series of equi-volume elongated bubbles separated from each other by liquid slugs and surrounded by liquid film, which results in

surface-area-to-volume ratios of $40\sim 230\text{ cm}^{-1}$.^[102]

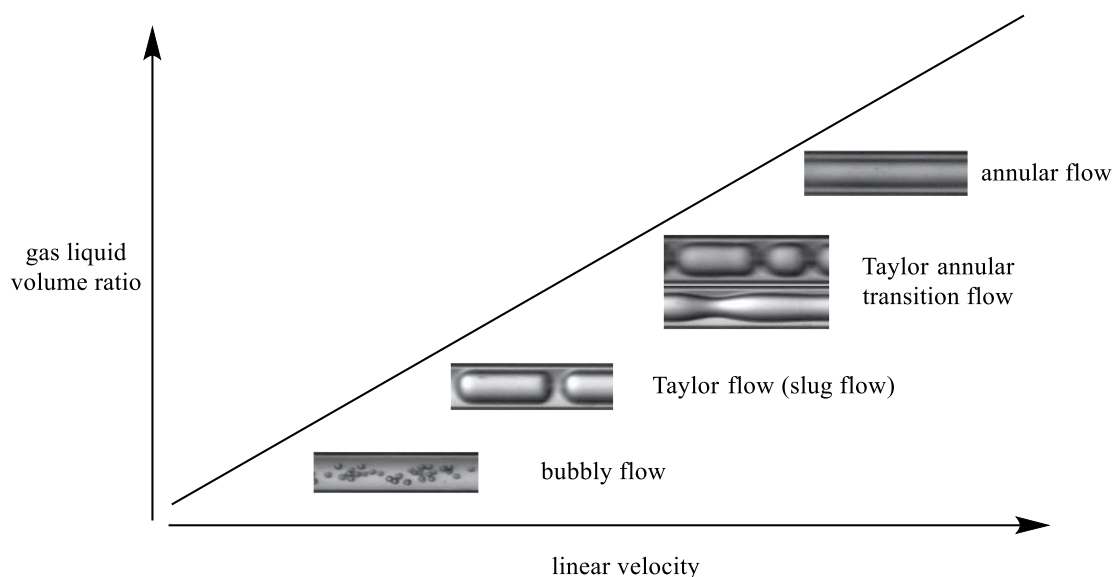


Figure 24 Factors related to mass transfer in Taylor Flow^[100b]

The dimensions and linear velocity of slug flow determine the mass transfer, which is explained in Figure 25. The channel size, mixing geometry, pumps, back pressure regulator, wall wetting properties and fluid properties (solvent type, substrate and gas) all affect the properties of the flow.^[102b] Apart from the factors mentioned above that are predetermined by a process and a target reaction, the linear velocity and gas liquid flow ratio are two factors that can be optimized in a process. The shorter the liquid slug and gas bubble formed by high linear velocity, the higher the surface-area-to-volume ratio, which facilitates gas liquid mass transfer. Higher linear velocities can accelerate the vortex speed in liquid slug as well. In addition, increasing the gas liquid volume ratio leads to a high surface area-to-volume ratio.^[62, 100c] However, increasing the gas liquid volume ratio and the linear velocity can also destabilize the slug flow and turn it into Taylor annular transition flow or annular flow.

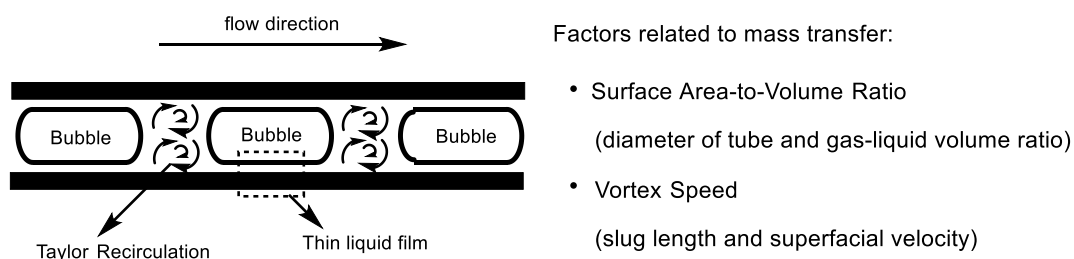


Figure 25 Factors related to mass transfer in Taylor Flow^[100c]

A gas-liquid flow regime universal map, in microchannel at atmospheric pressure, has been proposed under a series of flow superficial velocity and gas-liquid volume ratios. Kraus found that when the segmented flow was pressurized, the slug flow is destabilized and could transfer to annular flow under high linear velocity due to the pulse of pump and back pressure regulator, and then restore to slug flow after several seconds.^[103] This phenomenon was also observed in this process. However, this group did not propose a universal map of flow regime under elevated pressure. Furthermore, a syringe pump with low pulsation was used in his study instead of an HPLC pump as used in this work. Hence, the conditions to form stable slug flow were studied here by visualizing the flow through transparent PTFE tubes. Figure 26 shows a universal map of gas-liquid (H_2 and isopropanol) velocity and ratio in a microchannel at 15 bar gas pressure. The pressure was relatively low, compared with the conditions (30-100 bar) used elsewhere in this research, because PTFE tube fittings were unable to withstand pressure of more than 25 bar. It was found that at low linear velocity and gas liquid volume ratio, the liquid slug is longer than 5 cm, and leads to a slower Taylor mixing. When the velocity and gas liquid ratio are high, the pulse of back pressure equipment can turn the slug flow into intermittent, unstable, annular flow. Stable slug flow is achieved in the area shown in red. The area along the dashed line is the transient area.

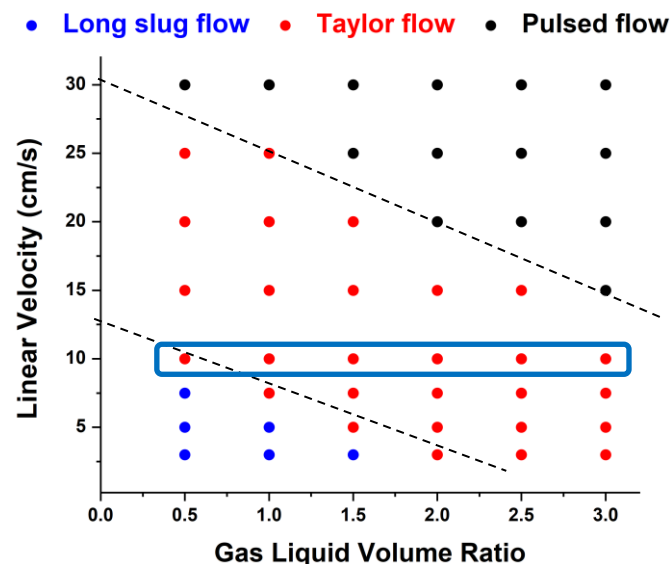


Figure 26 A universal map of gas liquid (H_2 and isopropanol) flow in a microchannel at 15 bar gas pressure

Figure 27 shows the short uniform slug flow. Figure 28 shows the long slug flow that is around 5 cm. Figure 29 shows the breakage of the flow caused by the pulse of the pump and BPR.

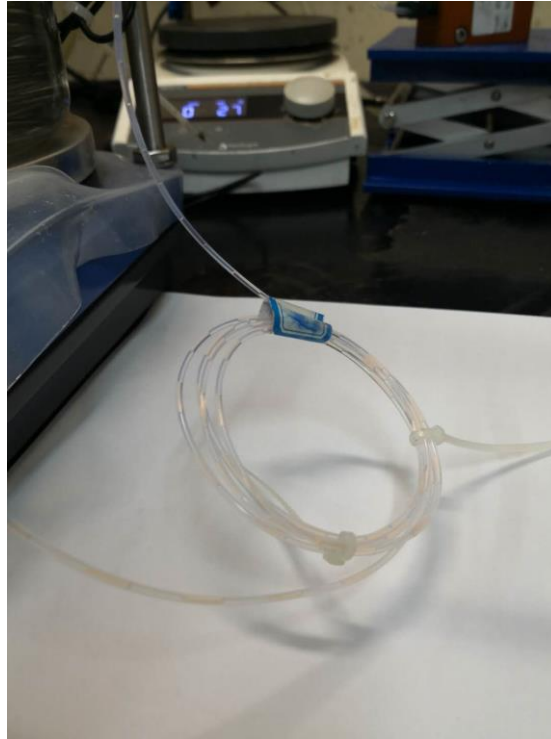


Figure 27 Uniform slug flow ($r = 1.5$; $g = 0.68$ mL/min; $l = 0.46$ mL/min)

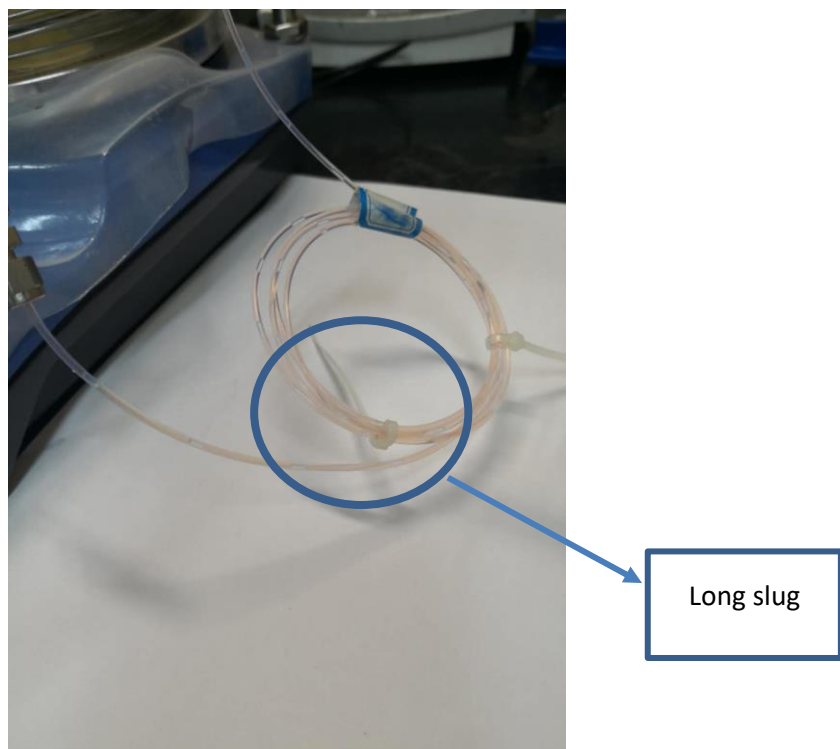


Figure 28 Slug flow with long liquid slug length ($r = 0.5$; $g = 0.38$ mL/min; $l = 0.75$ mL/min)

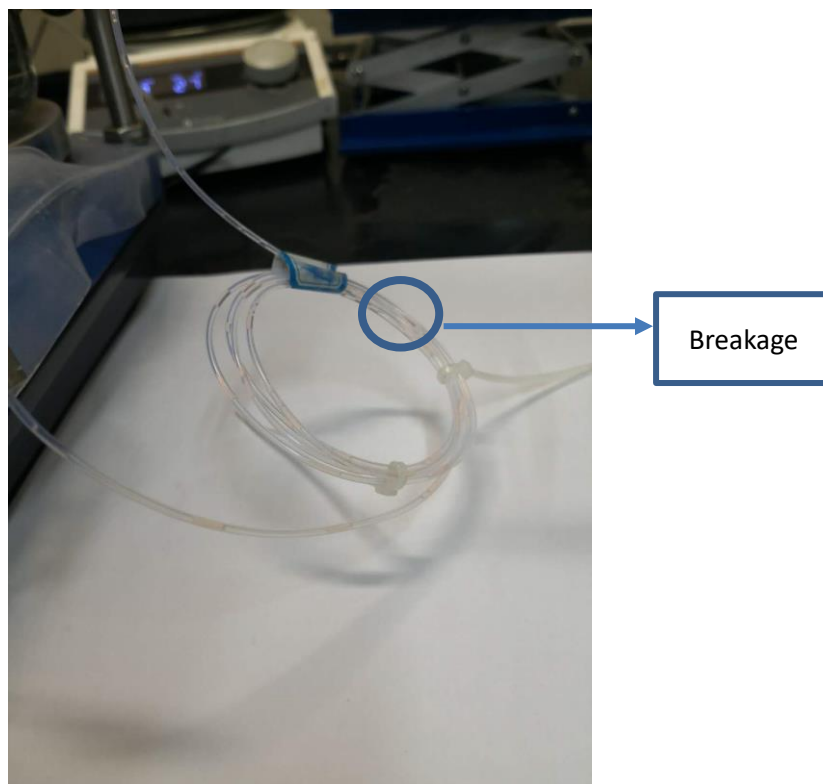
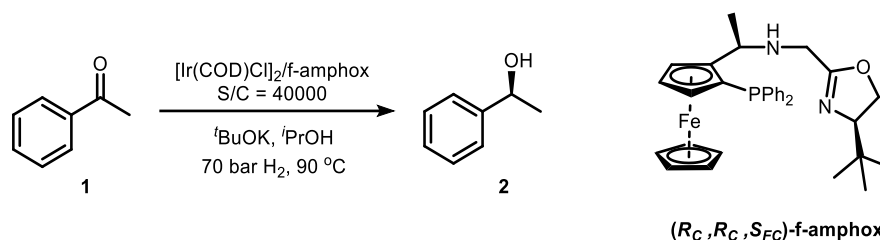


Figure 29 Pulsed slug flow with breakage caused by pulse ($r = 3$; $g = 2.5$ mL/min; $l = 0.85$ mL/min)

A stable slug flow with relatively long residence time, linear velocity of 7.3 cm/s and gas liquid volume ratio of 1.5 were selected as the starting point of optimization. The benchmark reaction used was AH of acetophenone catalyzed by f-amphox iridium complex. This gave full conversion to the alcohol in 99% ee with 0.0025 mol% catalyst loading and residence time of 8.75 min, giving a remarkably high TOF of $274,000$ h⁻¹ under 70 bar and 90 °C, which was 27 times higher than in batch as shown in Table 5.

Table 5 Results of AH of acetophenone.

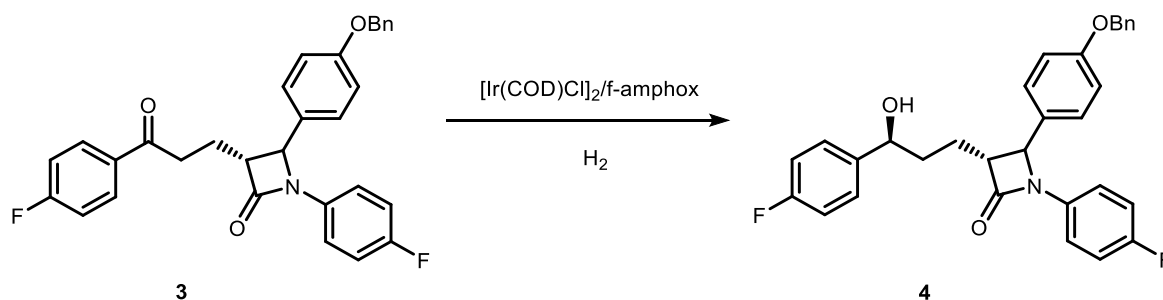
	7.4 mL Micro-reactor	50 mL Batch (20 bar, RT)
Conversion	>99%	>99%
ee	99%	99%
Residence Time	8.8 min	3.5 h
Productivity	6.7 g/h; 55.2 mmol/h	0.68 g/h ;5.7 mmol/h
TON	40000	40000
TOF	274000 h ⁻¹	11400 h ⁻¹
Space time yield (kg·L ⁻¹ ·h ⁻¹)	910	13.9

The volume of the reactor shown in scheme 1 was 7.4 mL and the space-time yield was calculated to be 910 kg·L⁻¹·h⁻¹ that was almost 70 times as high as that in batch. The productivity was 6.7 g/h that was 10 times as high as in batch. This result demonstrates the efficiency of AH in a high-pressure slug flow reactor. Afterwards, two drug intermediates were prepared by this methodology.

2.3 Optimization of reaction conditions for the synthesis of Ezetimibe

Our study on the synthesis of APIs in continuous flow commenced by producing ezetimibe, a blockbuster drug used to lower cholesterol level in blood.^[104] A dilemma, encountered at the start, was that reactant **3** was soluble in toluene but less so in *i*-PrOH, while the product **4** was soluble in *i*-PrOH but less so in toluene. To avoid blocking and increase reaction efficiency, the microreactor, 0.5 M of **3** in toluene/*i*-PrOH (1:1) was adopted. The reaction conditions were firstly screened in batch and it was concluded as shown in Table 6 that CsOH and Cs₂CO₃ (entries 2 and 3) gave better enantioselectivity and conversion than *t*-BuOK (entry 1). CsOH is more soluble than Cs₂CO₃ in the toluene/*i*-PrOH mixed solvent. Therefore, CsOH will be used as

base in flow reactions.



Scheme 2 Asymmetric hydrogenation of **3** in batch

Table 6 Asymmetric hydrogenation of **3** in batch

Entry ^a	Base	Reaction Time (h)	Conversion (%) ^b	de (%) ^b
1	2 mol% ^t BuOK	4	65	92
2	2 mol% CsOH	4	85	95
3	1 mol% Cs ₂ CO ₃	4	85	95

[a] Toluene: ⁱPrOH = 1:1; Room Temperature; 60 bar; Substrate concentration: 0.5 M; Catalyst Concentration: 0.0001 M; S/C=5000. [b] conversion and de were determined by UPLC via semi quantitative analysis.

2.3.1 Gas liquid ratio

It was shown that Taylor mixing increases with the superficial velocity of the fluids, with short, fast-moving slugs preferred. The effect of the gas-liquid volume ratio was studied over 0.5 to 3.0 in a 7.4 mL reactor with 6.5 mins residence time under 80 bar and 90 °C, 2 mol% CsOH, 0.02 mol% f-amphox-Ir, which is explained in Figure 30. The concentration of substrate was 0.5 M.

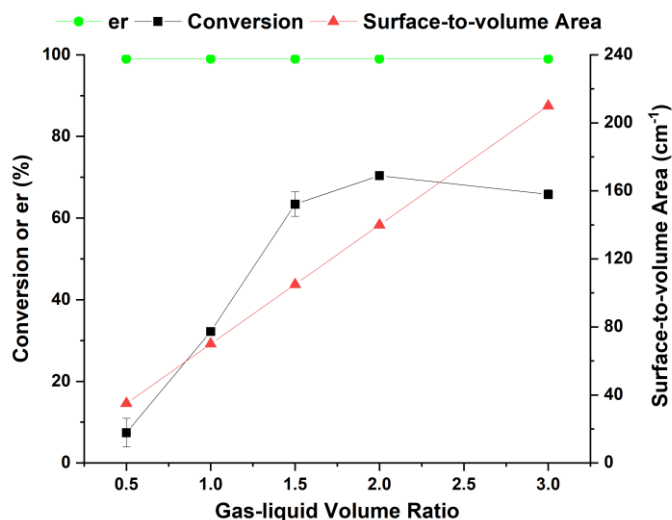


Figure 30 Effect of gas liquid ratio in continuous flow hydrogenation

The flow regimes were altered from long slug flow to short slug flow, which were marked by blue box under 15 bars in Figure 26. Similar changes in flow along with gas-liquid ratio might also be observed under 80 bars. As shown in Figure 30, the surface area to volume increased from 40 to 210 cm⁻¹ giving an increase in mass transfer explained by the following equation:

$$a = 4r/d \quad \text{Equation 3}$$

where a is the surface area to volume ratio (cm⁻¹), d the inner tube diameter (0.057 cm in this case) and r the gas-liquid volume ratio (for the derivation of Equation 3, see appendix). The conversion was increased from 8% to 64% when the gas-liquid ratio was increased from 0.5 to 1.5 and is explained by improved mass transfer. When the ratio was increased further to 2 or 3, the conversion remained similar (~ 67%), showing the gas-liquid ratio, hence mass transfer, was no longer rate limiting. A gas-liquid ratio of 1.5 was adopted for all reactions.

2.3.2 Pressure and temperature

The effect of pressure was studied under 90 °C, 2 mol% CsOH, 0.02 mol% f-amphox-Ir. As shown in Figure 31, as the pressure was elevated, the conversion increased and the d_e was all 95% in all entries.

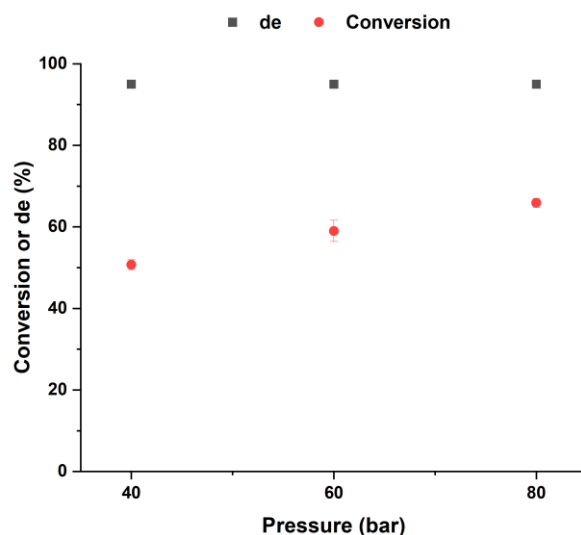


Figure 31 Effect of pressure in continuous flow hydrogenation

The effect of temperature was studied under 80 bar, 2 mol% CsOH, 0.02 mol% f-amphox-Ir. As shown in Figure 32, the de was maintained at 95% between temperatures of 40 °C and 100 °C. The conversion increased from 54% to 84%, when the slug flow reactor was heated from 40 °C to 60 °C. As the temperature was raised further to 80 °C and 100 °C, the conversion dropped to 59% and 46%. Therefore, 60 °C is the optimal reaction temperature.

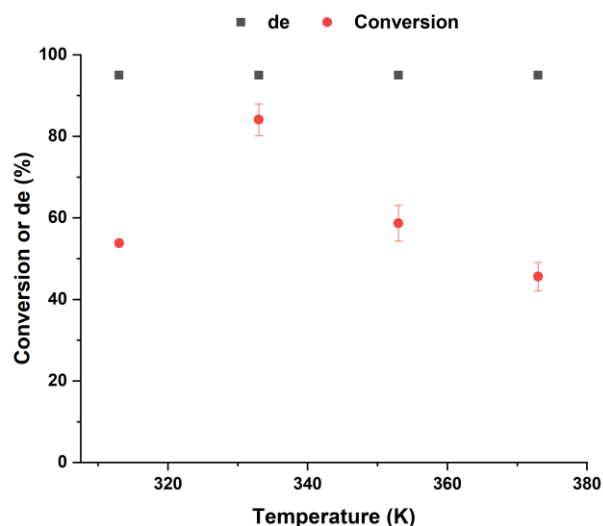


Figure 32 Effect of temperature in continuous flow hydrogenation

2.3.3 Catalyst loading

The effect of catalyst loading in continuous flow hydrogenation was studied and the results

are shown in Table 7. A catalyst loading of 0.01 mol% was tried in the beginning, however there was no conversion, which can be explained by an activation period, entry 4. The catalyst was inactive at this catalyst concentration in 6.5 minutes. Increasing the concentration of the Ir complex to 0.02 mol%, the conversion was increased to 94% in a 95% de, entry 5. By further increasing the concentration of the catalyst, full conversion was achieved with a S/C = 2500, entry 6.

Table 7 Effect of catalyst loading in continuous flow hydrogenation.

Entry ^a	S/C	conv. (%)	de (%)
4	10000	0	N.A.
5	5000	94	95
6	2500	>99	95

[a] substrate concentration: 0.5 M; Toluene/*i*PrOH = 1:1; CsOH: 2 mol%; liquid flow rate and gas flow rate are 0.46 mL/min and 0.68 mL/min under 100 bar and 60 °C; conversion and de (diastereomeric excess) values were determined by HPLC via semi-quantitative analysis; reactor volume: 7.4 mL; residence time: 6.5 mins.

2.3.4 Residence time

Normally, in batch, elongating the reaction time causes a higher conversion, however, it was interesting to find that when the residence time was prolonged from 5.2 to 10.4 minutes (Table 8, entries 7 and 8) by decreasing gas and liquid flow rate, the conversion dropped to 2%. This was probably caused by reduced Taylor flow mixing that caused the reduction of hydrogen concentration and slowed down the catalyst activation.

Table 8 Effect of residence time in continuous flow hydrogenation

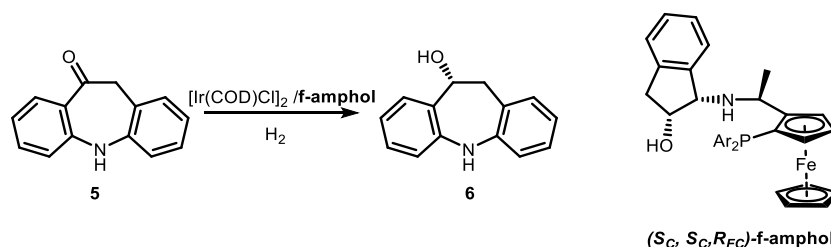
Entry ^a	S/C	linear velocity (cm/s)	residence time	conv. (%)	de (%)
			(min)		
7	5000	7.3	5.2	51	95
8	5000	3.6	10.4	2	N.A.

[a] substrate concentration: 0.5 M; Toluene/*i*PrOH = 1:1; CsOH: 2 mol%; liquid flow rate and gas flow rate for 8, it was 0.23 mL/min and 0.33 mL/min, while for Entry 7 are 0.46 mL/min and 0.68 mL/min under 80 bar and 90 °C; conversion and de (diastereomeric excess) values were determined by HPLC via semi-quantitative analysis. Reactor volume: 5.9 mL.

2.4 Optimization of reaction conditions for the synthesis of eslicarbazine acetate

AH of dibenzazepinone **5** is the key step in the synthesis of eslicarbazine acetate **9**, an anticonvulsant for the treatment of partial onset seizures.^[105] In a batch reaction with 0.1 mol% Ir/*f*-amphol catalyst and 5 mol% ^tBuONa in mixed solvent DCM/*i*PrOH (1:1, v/v) at ambient temperature under 60 bar hydrogen, >99% conversion and 98% ee were achieved in 24 h. AH in continuous flow provides short reaction times that facilitate fast screening of conditions. To assist this, inline AFT-FTIR was incorporated at the outflow to give real-time data on the concentration of components in the reaction mixture using the Lambert-Beer law and calibration. The carbonyl group of **5**, absorbing at 1661 cm⁻¹, was selected as a strong and unique signal to measure conversion. Detailed analytical protocols and reaction procedure can be found in the Experimental Chapter. The conversion was the average conversion at steady state. Table 9 shows the results of testing different reaction conditions and Figure 33, Figure 34 and Figure 35 shows the IR traces recorded.

Table 9 Asymmetric hydrogenation of **6** in continuous flow.^a



Entry	S/C	T (°C)	conv. (%) ^b	ee (%) ^c
9	1000	60	98	98
10	2500	60	98	98
11	2500	40	61	98
12	5000	60	22	98
13	5000	80	77	98
14	5000	100	43	97

[a] substrate concentration: 0.5 M; DCM/*i*PrOH = 1:1; ^tBuONa: 5 mol%; reactor volume: 7.4 mL; pressure: 90 bar. [b] Conversion was determined by inline IR. [c] ee was determined by HPLC.

After quintuple residence time, the reactor achieved steady state, where conversion was calculated. 98% conversion and 98% ee were achieved at 60 °C and 90 bar hydrogen, at gas liquid ratio 1.5 and residence time of 6.5 mins, with catalyst loadings of 0.1 mol% and 0.04 mol% (entries 9 and 10). However, the conversion decreased markedly to 22% with a lower catalyst loading of 0.02 mol% at the same temperature (entry 12) but recovered to 77% when the temperature was increased to 80 °C (entry 13), equating to a TOF of 37000 h⁻¹. At 100 °C the conversion decreased to 43% and this may reflect the decreasing of catalyst stability (entry 14). With low catalyst loading of 0.02 mol%, the conversion becomes fluctuating as shown in Figure 35. It can be concluded that under high catalyst loading (S/C = 1000 and 2500), the reactor system can offer a stable steady state, while under low catalyst loading (S/C = 5000), the reactor system was prone to be influenced by minor changing of flow regime, which leads to the fluctuation of the conversion.

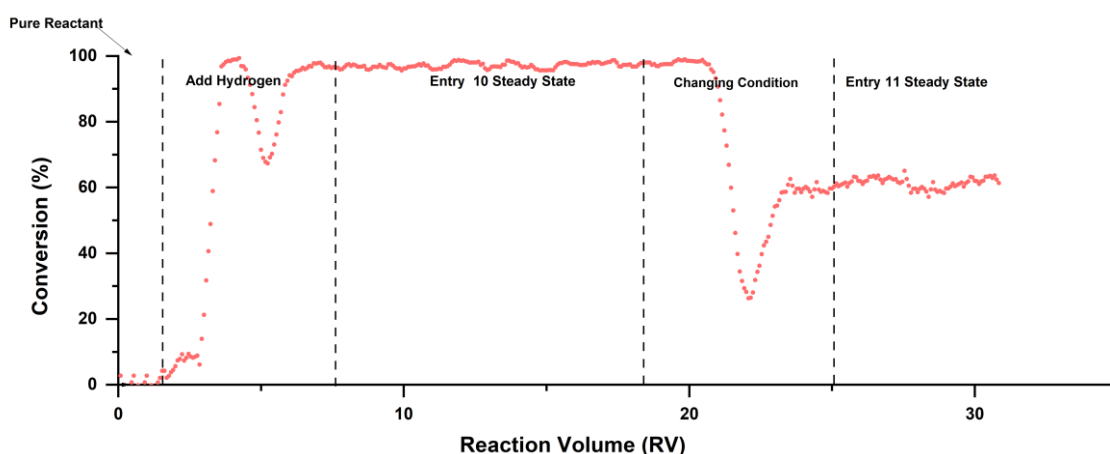


Figure 33 Inline analysis by in-situ TFIR for the condition optimization. (Entry 10 and 11)

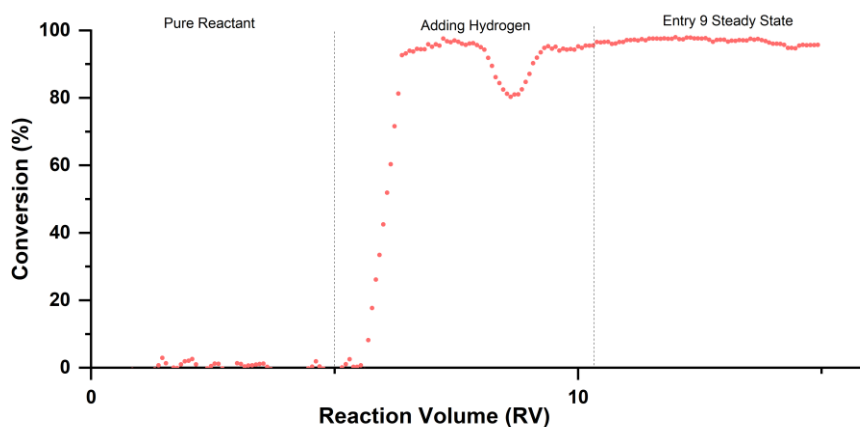


Figure 34 Hydrogenation of Asymmetric hydrogenation of 5 (Entry 9)

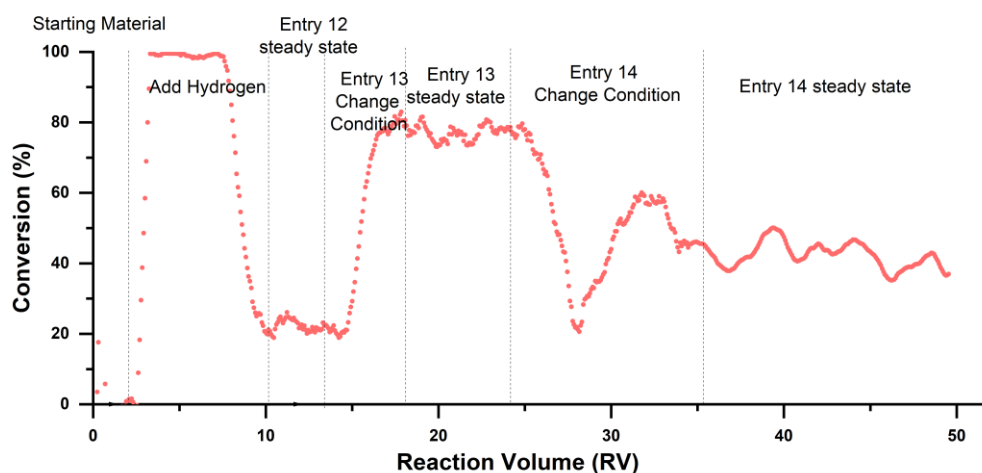
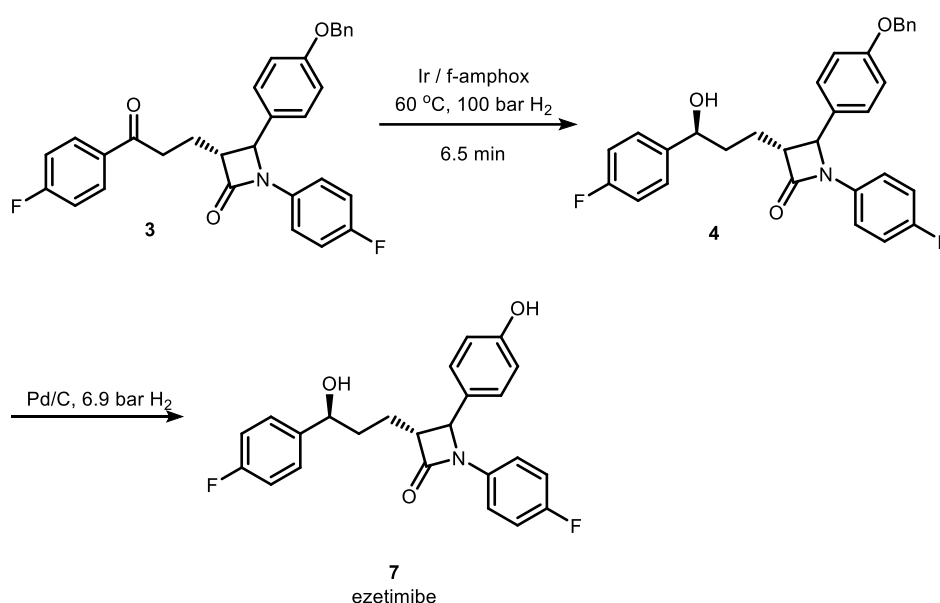


Figure 35 Hydrogenation of Asymmetric hydrogenation of **5** (Entry 12, 13, 14)

2.5 Multistep continuous flow synthesis of Ezetimibe

2.5.1 Optimization of the deprotection step using a batch and flow fReactor

In the synthetic route shown in Scheme 3, debenzoylation of intermediate **4** is required to yield ezetimibe **7** and relies on hydrogenation with palladium on activated charcoal. This heterogeneous triphasic reaction relies on good mixing for high efficiency. The fReactor, that incorporates active mixing, even at low flow rates allowing for long residence times, was adopted for carrying out the downstream reaction.^[56]



Scheme 3 Deprotection step to synthesize Ezetimibe.

The batch process is shown in Figure 36. Table 10 shows the results of deprotection of **4** in both the batch and flow fReactor system.

Table 10 Optimization of debenzylation in fReactor system

Entry ^a	Catalyst Type	Catalyst Loading (mol %)	Temperature (K)	Reaction Time (mins)	Conversion (%) ^c
15	5% Pd/C	4	298	30	20
16	10% Pd/C	4	298	30	85
17	10% Pd/C	4	353	15	99
18	10% Pd/C	20	353	2.5	99
19 ^b (In flow)	10% Pd/C	750 mg in 9 fReactor	353	2.5	90

[a] substrate **4** concentration: 0.5 M; Toluene/PrOH = 1:1; v:v. [b] liquid flow rate was 0.46 ml/min and gas flow rate were 45 sccm. 6.9 bar BPR was used. [c] The conversion was obtained by ¹H NMR.

Since the gas liquid flow comes out of the asymmetric hydrogenation module, it is delivered directly to the debenzylation module. The concentration, solvent and flow rates were all the same as the resulting reaction medium from module 1. The reaction time was shortened by increasing catalyst loading and temperature, and a 2.5-minute residence time was used with nine fReactors in series. It was found as shown in Table 10 that the reaction achieved 99% conversion using 20 mol% Pd/C within 2.5 mins under 80 °C, entry 18 in Table 10. The reaction conditions of entry 18 was transferred into flow process with 9 fReactors in line, which gave a 90% conversion in entry 19.

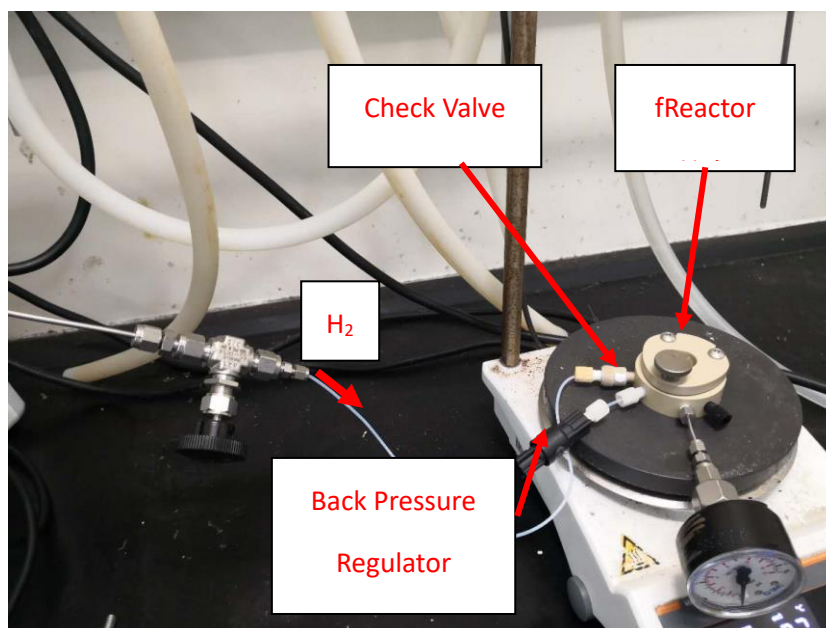


Figure 36 Batch mode fReactor

2.5.2 Optimization of the multi-step flow reaction

The overall multi-step process is shown in Figure 37 and Scheme 4. The AH step was carried out under 100 bar and 60 °C. It afforded the alcohol in 99% conversion and 95% de with a residence time of 6.5 minutes, 2 mol% CsOH and a TON of 2500. Experimental details can be found in the Experimental Chapter. The reaction medium of module 1 was delivered directly to module 2 without gas liquid separation. The excess H₂ was used for deprotection step and nine fReactors were filled with 750 mg 10% Pd/C in total and heated to 80 °C with two step residence time of 9 minutes. The yield of Ezetimibe over both steps was 84% with 95% de and the production rate was 4.8 g/h.

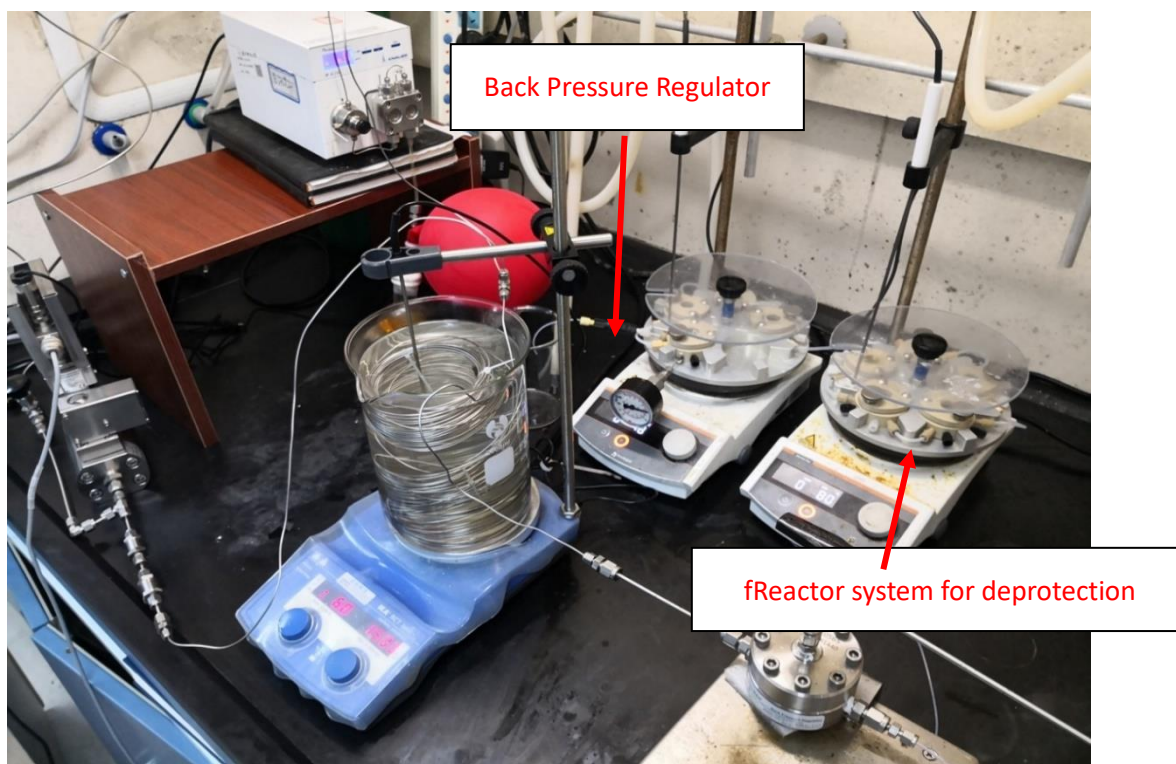
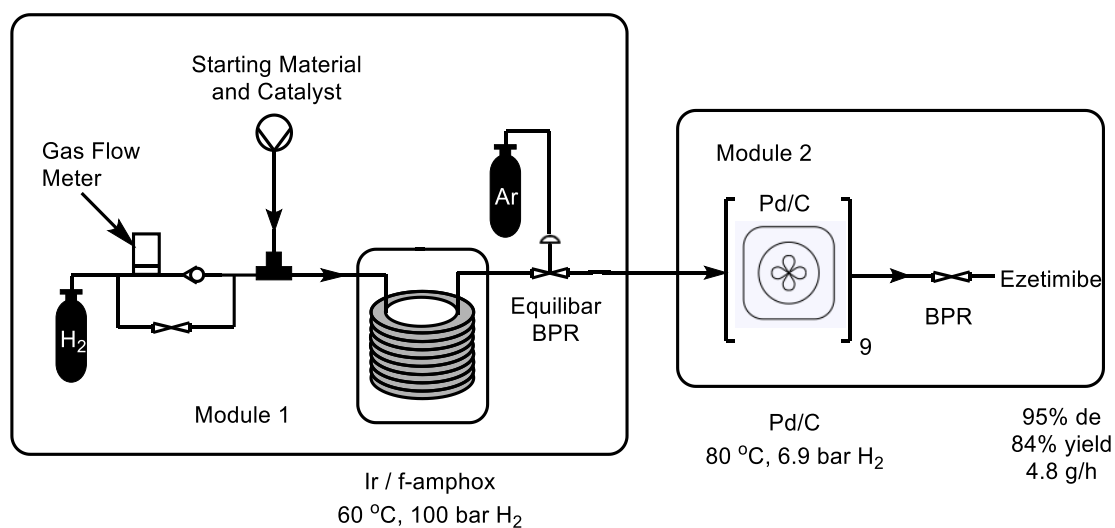


Figure 37 Two steps process for synthesis of ezetimibe

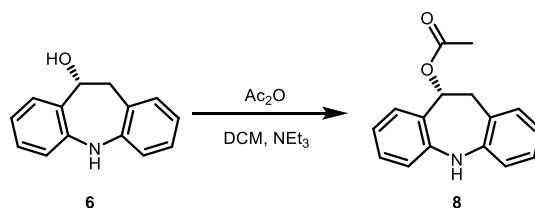


Scheme 4 Two steps process scheme for synthesis of ezetimibe^[106]

2.6 Multistep continuous flow synthesis of Eslicarbazepine Acetate

2.6.1 Optimization in batch of step 2 and 3

Route selection for multi-step flow synthesis is different from that of batch synthesis. Two criteria need to be considered: all the reactants, products and additives should be soluble

Table 11 Optimization of acylation step

Entry ^a	Catalyst	Temperature	Reaction time	Ac ₂ O	NEt ₃	Conversion ^b
		(°C)	(h)			
20	N.A.	R.T.	12	3 eq.	2 eq.	>99
21	N.A.	60	5	3 eq.	2 eq.	>99
22	N.A.	90	0.5	12 eq.	2 eq.	>99
23	DMAP	R.T.	0.5	12 eq.	2 eq.	>99
24	DMAP	60	0.3	3 eq.	2 eq.	>99
25	DMAP	60	0.3	1.5 eq.	1.5 eq.	>99
26 ^c	DMAP	60	0.3	10 eq.	1.5 eq.	>99

[a] substrate concentration: 0.5 M; 5 mol% DMAP [b] reaction was monitored by TLC; Conversion was measured by ¹H NMR. [c] Isopropanol:DCM (1:1, v:v).

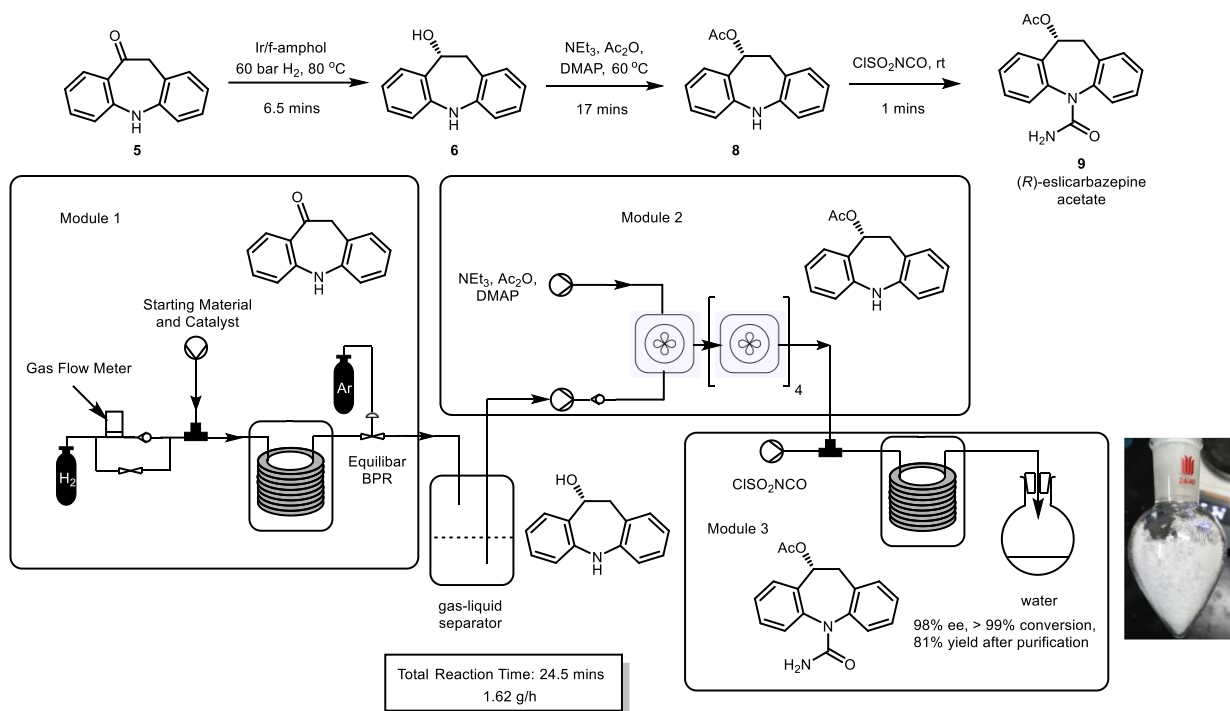
Raising the temperature and increasing the equivalent of Ac₂O accelerated the reaction in entries 20-22, but 30 minutes reaction time was still too long for the fReactor process. It was found that using 5 mol% DMAP, the reaction time can be shortened to 18 minutes, Table 11 (entry 24) from 5 hours (entry 21). The molar equivalence of triethylamine and acetic anhydride were decreased to 1.5 without prolonging the reaction time in entry 25. However, it was found that the isopropanol left in step 1 can react with acetic anhydride and chlorosulfonyl isocyanate. In the flow reaction, 10 eq. acetic anhydride in the presence of isopropanol was added to push the reaction to completion. The conditions of entry 26 were transferred to a flow reactor system consisting of five fReactors in series. The ureation step achieved 100% conversion in 5 minutes with 1.1 eq. chlorosulfonyl isocyanate in batch and the resulting medium was mixed with water for 1 hour to get the product. 2 eq. chlorosulfonyl

isocyanate were added to the flow reactions to avoid the influence of the isopropanol and acetic anhydride. The residence time of the ureation step in tubular reactor was 1 minute.

2.6.2 Optimization of the multi-step synthesis of (*R*)-eslicarbazepine acetate in continuous flow.

The process for asymmetric synthesis of eslicarbazepine acetate is shown in Scheme 6 and Figure 38. In module 1, ketone 6 was hydrogenated to alcohol 7 under 90 bar hydrogen and 80 °C with a TON of 1000, 5 mol% ^tBuONa, which afforded the product with 98% conversion and 98% ee. The reactor was a 7.4 mL tube giving a residence time of 6.5 min. After steady state was achieved, the outlet stream was collected in a gas liquid separator (Schlenk flask) and the hydrogen was discharged through a tube filled with argon. The resulting alcohol 6 was pumped into a fReactor (module 2 in Figure 39) at 0.23 mL/min, set for a reaction temperature of 60°C, and mixed with a stream containing NEt₃, Ac₂O and DMAP (0.26 mL/min) before flowing through another four fReactors to give a residence time of 17 minutes for full conversion. The acetylated product was pumped through a 1 m cooling coil (module 3 in Figure 40

) and mixed with a stream (0.069 mL/min) of neat chlorosulfonyl isocyanate. In batch, intermediate 8 was fully consumed in 1 minute so the flow process was designed with the same residence time. The resulting mixture was collected in a round-bottom-flask with water quench during which chlorosulfonyl group was hydrolyzed. After flash chromatographic purification, 9 was obtained in 81% yield and 98% ee. The total reaction time was 24.5 mins and 2.7 g pure API could be produced in 100 minutes. Figure 41 presents the comparison of crude product and pure product ¹H NMR. Only trace amount of impurity was observed.



Scheme 6 Multi-step synthesis of (*R*)-eslicarbazine acetate.^[106]

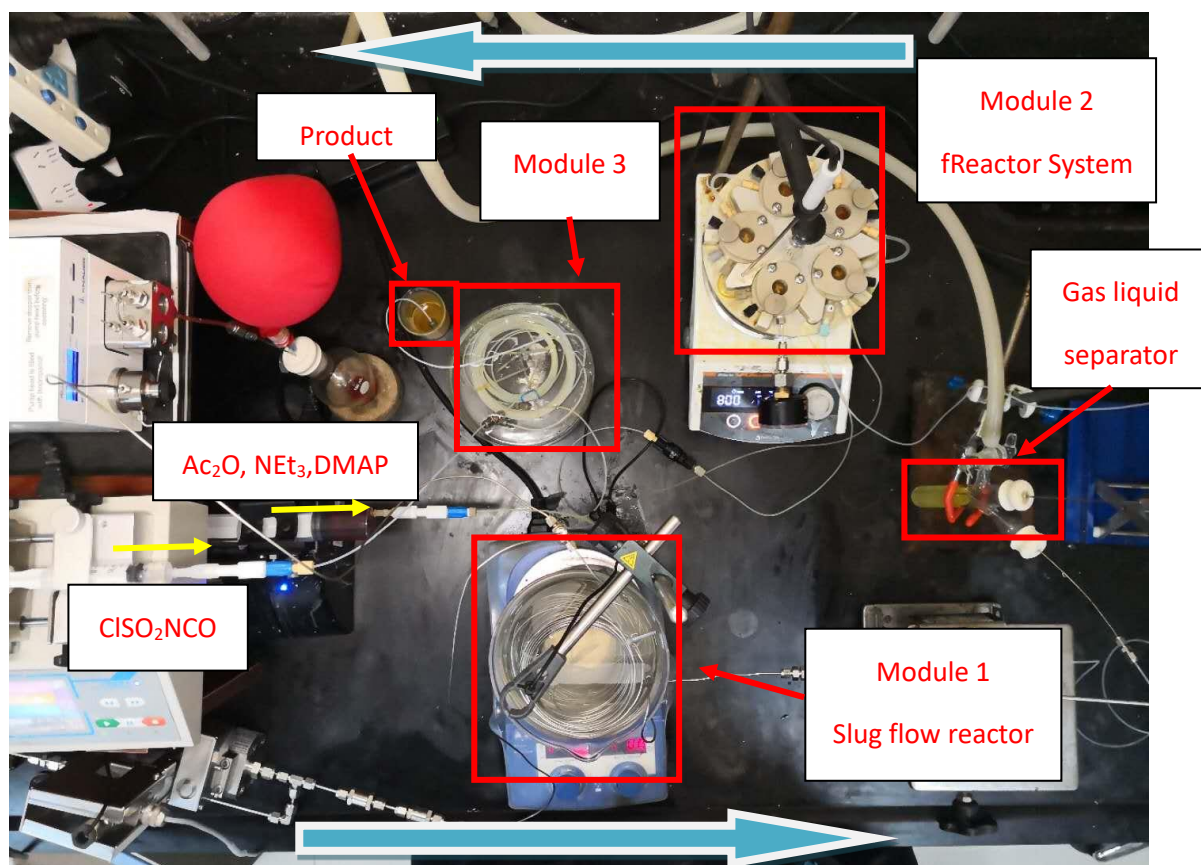


Figure 38 Multi-step synthesis of (*R*)-eslicarbazine acetate.

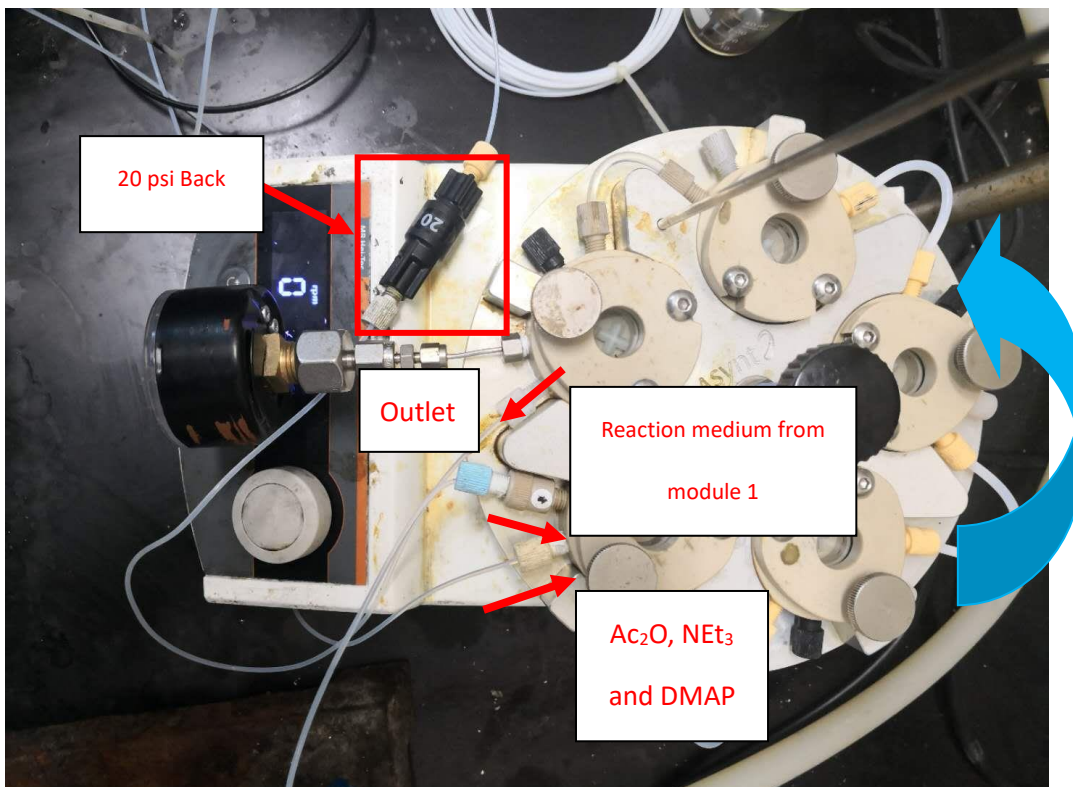


Figure 39 Module 2 for synthesis of eslicarbazepine acetate

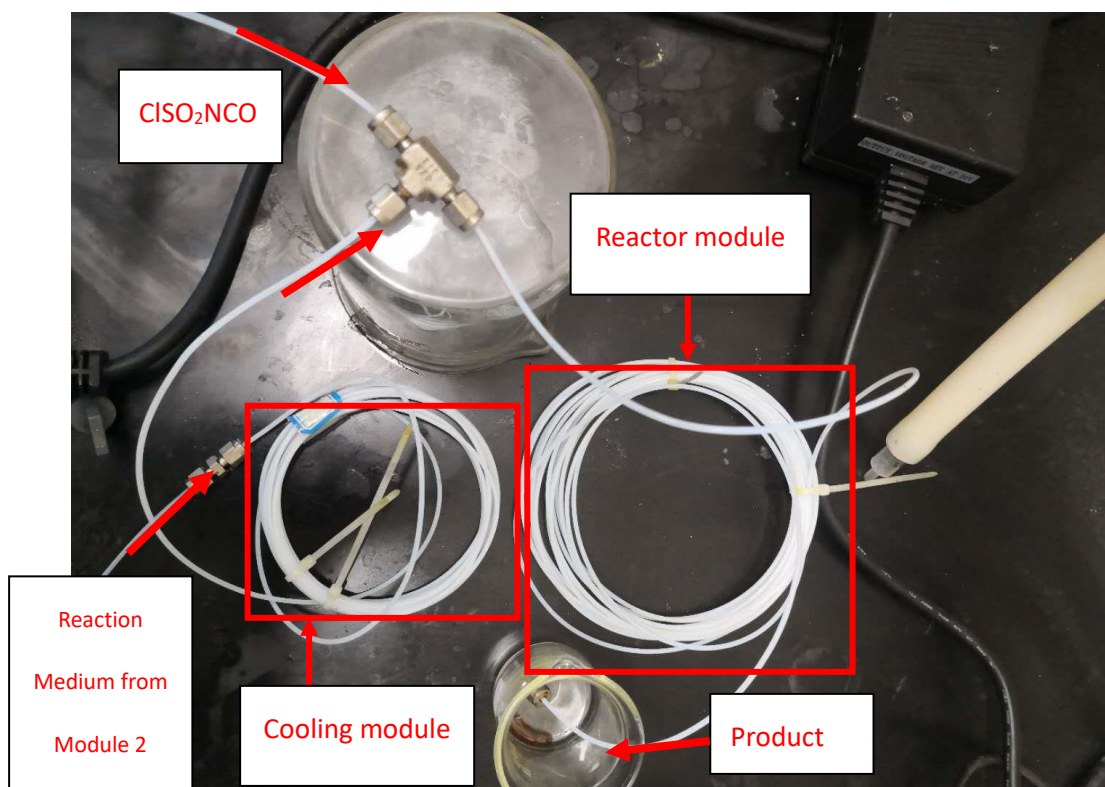


Figure 40 Module 3 for synthesis of eslicarbazepine acetate

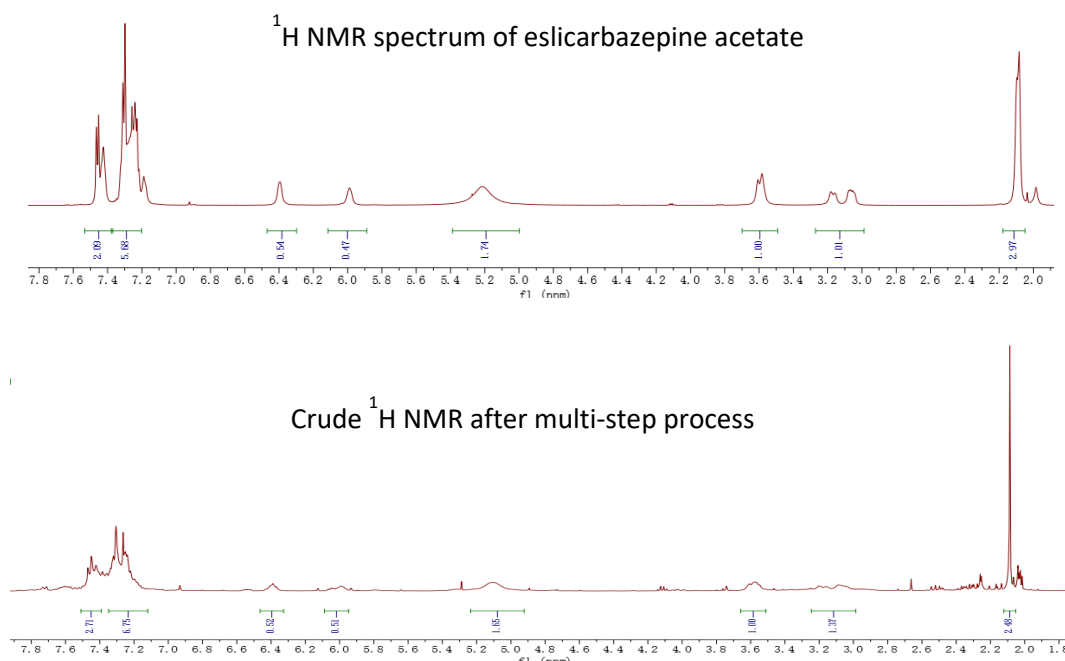
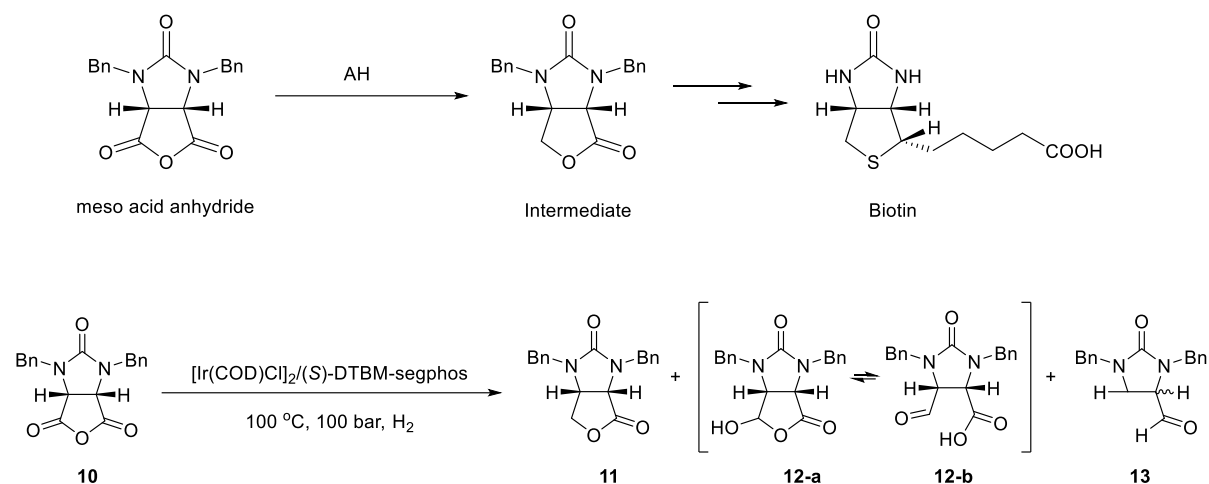


Figure 41 Comparison of the crude product and the pure product by ^1H NMR.

2.7 Asymmetric synthesis of biotin in a cyclic slug flow reactor

The asymmetric desymmetrization (ADS) of prochiral molecules in symmetrical bifunctional compounds has proven to be a straightforward and powerful strategy in asymmetric syntheses.^[108] In particular, ADS of meso compounds is a remarkably valuable transformation in organic synthesis because it breaks the symmetry of the molecule without incorporating new stereogenic centers.^[109] Among many important chiral lactones, water-soluble B-vitamin biotin plays a crucial role in biochemical processes and overall physiological metabolism in human beings. Furthermore, it not only acts as a coenzyme in carboxylation reaction but also an essential growth factor in living cells.

Biotin is synthesized by the synthetic route in Scheme 7.^[110]



Scheme 7 Synthesis of Biotin

Compound **11** is the desired product of AH and **12** is the reduction intermediate, whilst **13** is the product of decarboxylation. As shown in Table 12, when reaction was conducted in batch on a 1 mmol scale, the two byproducts were formed in trace amount, however at 40 mmol scale in entry 28, the quantity of by-product rose to 20.8% for **12** and 6.4% for **13**. The reason was that the temperature distribution in the batch reactor was uneven, and decarboxylation happened in the higher thermal zone, while product was incompletely reduced in the low temperature part, which made the product distribution worse. The temperature distribution in microreactor is more uniform, because of its small dimensions and higher surface area to volume, which was considered as a solution to improve product distribution.

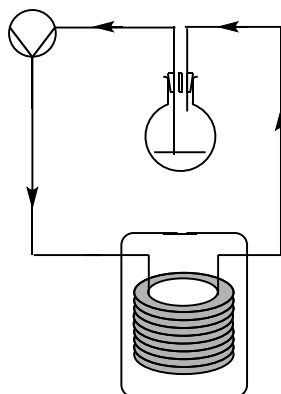
Table 12 Results in Batch

Entry ^a	Scale (mmol)	TON	Time (h)	Conversion (%)	Conv. (11)	12-a, b	13	ee (%) ^b
27	1	20000	24	93	91.7	trace	Trace	96.1
28	40	20000	36	83	55.8	20.8	6.4	96.0

[a] 100 bar, 100 °C, THF [b] conversion and ee were determined by HPLC.

The cyclic slug flow reactor shown in Scheme 8 was used to prolong the reaction time.^[95f] The reaction medium was flowed through the reactor as a semi-batch recirculation cycle. The product was collected in a flask and re-pumped into the reactor system afterwards. Table 13

shows the results in cyclic flow reactor. A good product distribution was achieved in the microreactor. In the entry 30, the yield was 94.3%, and the ee was 97.6%, a little higher than batch. The impurities **12** and **13** were formed in only 1.7% and trace. However, the solubility of the substrate was bad and when the reaction was run in recirculation, the solvent could evaporate, which caused the precipitation of the reactant that blocked the pump.



Scheme 8 Cyclic slug flow reactor

Table 13 Results in Cyclic Flow Reactor

Entry ^a	Reactor	TON	Time (h)	Conversion (%)	Conv. (11)	12-a,b	13	ee (%) ^b
29	Flow	5000	4	100	88.8	2.8	8.4	97.3
30		5000	1	96	94.3	1.7	trace	97.6

[a] 0.1M solution, 7.91 sccm, 0.23 mL/min reaction medium, residence time for a single cycle was 3.7 mins. 100 bar, 100 °C, THF. [b] conversion and ee were determined by HPLC.

To scale up the production in continuous mode, the data obtained from the cyclic flow reactor could be used to predict the actual reactor volume needed. This strategy is shown in Figure 42. It was calculated from the equation and data below, entry 30, that 13 minutes residence time was needed, and 4 mL reaction medium was recycled with holdup volume of 0.85 mL. The total cycle time was 60 minutes. The residence time in continuous mode calculated in Equation 4 is the time each mL liquid stays in the tube.

residence time of continuous production

$$= \text{total reaction time} \frac{\text{holding volume of a single module}}{\text{total volume of reaction medium}}$$

$$= 60 \text{ min} * \frac{0.85 \text{ mL}}{4 \text{ mL}} = 13 \text{ mins}$$

Equation 4

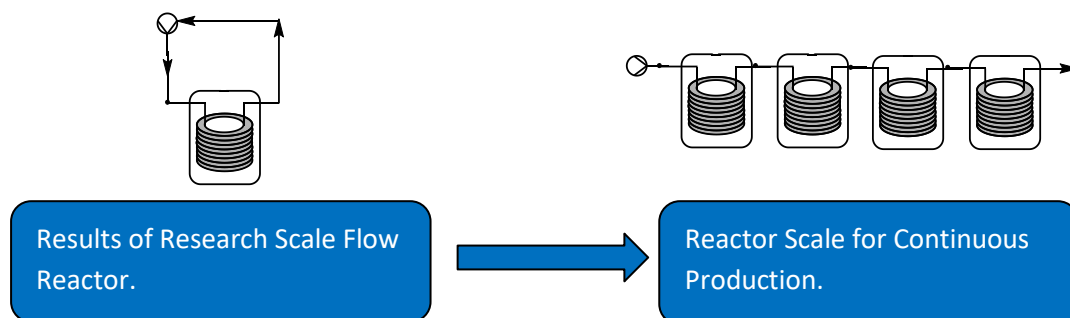


Figure 42 Scale up from cyclic flow reactor to continuous production.

For further scale-up, an active mixing DRAT-DM reactor from AM Technology to allow a long residence time (15 mins-2h) was employed to avoid blocking due to the bad solubility of biotin. This reactor offers active mixing by a mixing bar that rotates inside a larger tube. The baffles curved on the bar creates micro-mixing. The reaction medium and gas mixed from one side of the reactor and comes out of the reactor from the other side. The pressure rate was 50 bars. It was found in Table 14 that under 50 bars, the transformation stopped at the intermediate, even with prolonged reaction time, accelerated mixing frequency and elevated temperature. Therefore, a higher-pressure rate reactor needs to be used to carry out this reaction.

Table 14 Results in DRAT-DM reactor

Entry	Mixing Frequency (rpm)	Temp. (°C)	Residence Time (min)	Conv. (%) ^b	11	12-a,b	13
31 ^a	100	100	13.3	25	0	25	0
32 ^a	300	100	13.3	44	0	44	0
33 ^b	300	100	26.6	38	0	38	0
34 ^a	300	120	13.3	42	4	38	0

[a] Liquid flow rate: 0.24 mL/min, 18 sccm.; b. liquid flow rate: 0.12 mL/min, 10 sccm. [b] conversion was determined by HPLC.

2.8 Conclusions

To conclude, two multi-step asymmetric flow synthesis of ezetimibe and eslicarbazepine acetate are reported. This was enabled by AH in a continuous slug flow reactor able to operate at pressures up to ~ 150 bar and temperature ~ 100 °C and real-time quantitative analysis was performed by in-situ IR spectroscopy followed by a longer residence time reaction within the fReactor CSTR cascade. A remarkably high TOF of $274,000 \text{ h}^{-1}$ was observed in the hydrogenation of acetophenone. Two optically active APIs, ezetimibe and eslicarbazepine acetate, were successfully synthesized by the multi-step flow system with high efficiency (4.8 g/h, $32,195 \text{ h}^{-1}$ for ezetimibe and 1.62 g/h, 16100 h^{-1} for eslicarbazepine acetate) and enantioselectivity. It was found that changing of flow regime can have a significant effect on the reaction conversion in the slug flow reactor with optimal gas-liquid flow rate and ratio determined. Synthesis of Biotin was tested by a cyclic reactor and optimized in a DRAT-DM reactor. However, since the pressure rate of DRAT-DM reactor was only 50 bars, the reaction stayed in intermediate. Continuous flow AH is usually quantitative, with no by-product and few impurities, so requires no purification before carrying through to the next reaction. Continuous flow AH with low catalyst loading will become an important tool in end-to-end enantioselective flow synthesis of chiral compounds.

Chapter 3: A horizontal micro-fluidics CSTR and its application in heterogeneous and homogeneous hydrogenation

The slug flow regime used in a microreactor has three disadvantages in gas-liquid reactions. Firstly, low catalyst loading resulting in long reaction times (usually more than 24 hours) and therefore requiring low flow rates or long lengths of tubing. However, reducing the flow rate slows down the Taylor flow micro-mixing, which worsens the mass transfer. Secondly, a high gas liquid ratio allows more concentrated reaction medium and higher reaction rate, but in microchannels, this can turn Taylor flow into an unstable annular flow. Thirdly, the thin tubes in a microreactor get blocked easily when solids are present or formed during a reaction which limits the range of reactions.

The miniature CSTR (fReactor), adopting active mixing, decouples the flow rate with mixing. This allows the flow reaction to operate under low flow rate to prolong reaction time without slowing down the mixing. Thus, the residence time can be several hours. In addition, reactions involving solid catalyst or even precipitations can be done in flow with the help of active mixing. In this work, homogeneous and heterogeneous hydrogenation in the fReactor system will be studied.

3.1 Design of Experiment

The 'Design of Experiment' (DoE) technique will be adopted for defining the optimal conditions. This is a statistical approach to reaction optimization that allows the variation of multiple factors simultaneously to reduce the number of experiments required and to understand interactions between variables. ^[111] A traditional 'one variable at a time' (OVAT) approach can fail to optimize even two factors of a reaction if interactions between the factors are present.

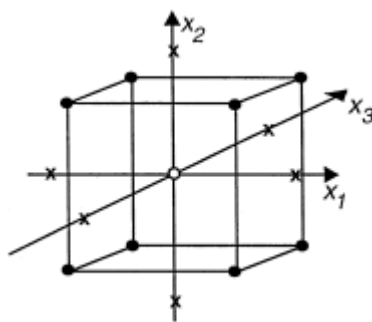


Figure 43 A central composite design for three variables^[112]

DoE works by initially exploring the reaction parameter space by determining the range of variables, known as the design space. Then, a common space-filling approach is used to construct the design, a central composite design in this project. A mathematical model is built from results of experiments by correlating the responses with the experimental conditions. A model for a 2-variable design space is shown below in equation 5:

$$Y = b_0 + b_1X_1 + b_2X_2 + b_{12}X_1X_2 + b_{11}X_1^2 + b_{22}X_2^2$$

Equation 5

Where X_1 = Variable 1; X_2 = Variable 2; Y = Response; b_n = Coefficient terms

From the mathematical model obtained, the importance of the variables can be identified, and unimportant variables can be removed in future experiments. Experiments with conditions that have not been conducted can be predicted. Finally, it can also be represented graphically - this allows the behavior of the variables to be more easily understood and interpreted, as well as allowing predicted response maxima and minima in the design space to be easily identified. This method allows us to identify critical conditions and predict optimum reaction conditions efficiently.^[113]

There are four parameters for evaluating a basic statistical model. For four parameters, 1 is perfect = 100%. R^2 shows the model fit; less than 0.5 is a model with rather low significance. Q^2 shows an estimate of the future prediction precision. Q^2 should be greater than 0.1 for a significant model and greater than 0.5 for a good model. Model validity is a test of diverse model problems. A value less than 0.25 indicates statistically significant model problems, such as the presence of outliers, an incorrect model, or a transformation problem. Reproducibility is the variation of the replicates compared to overall variability. A value greater than 0.5 is warranted.^[113]

3.2 Equipment



Figure 44 Parr Hydrogenator (upper left); Flask with hydrogen balloon (upper right); Gas pumping step of batch mode fReactor (lower left); Batch mode fReactor (lower right).

The batch mode fReactor was also tested. Conducting hydrogenation in the fReactor is simple, safe and with better mixing. Compared to the Parr Reactor shown in Figure 44 (upper left), the equipment is simpler and easier to handle for its small size. Hydrogen is pumped into the reactor by a syringe with a calculated volume for the given pressure, which is shown in Figure 44 (lower left). Several fReactors can be run in parallel on a single stirred hot plate, which is shown in Figure 44 (lower right). Most labs tend to use hydrogen balloon to carry out hydrogenation, which is shown in Figure 44 (upper right). This is not very safe and only allows the reaction to occur under atmospheric pressure. Continuously feeding hydrogen by coupling to a hydrogen cylinder is also possible. In this way as illustrated in Figure 45, gas is continuously added to keep a constant pressure in the reactor. The specifications of the reactor are shown in Table 15.

Table 15 Technical specifications of Parr, “balloon” reactor and fReactor

Property	Parr Reactor	“Ballon” Reactor	fReactor
Reactor Volume (mL)	40-600	100	1
Maximum Working Pressure (bar)	70	1	10
Temperature Range (°C)	-10-300	RT	-20-100
Material	Hastelloy	Glass	PEEK

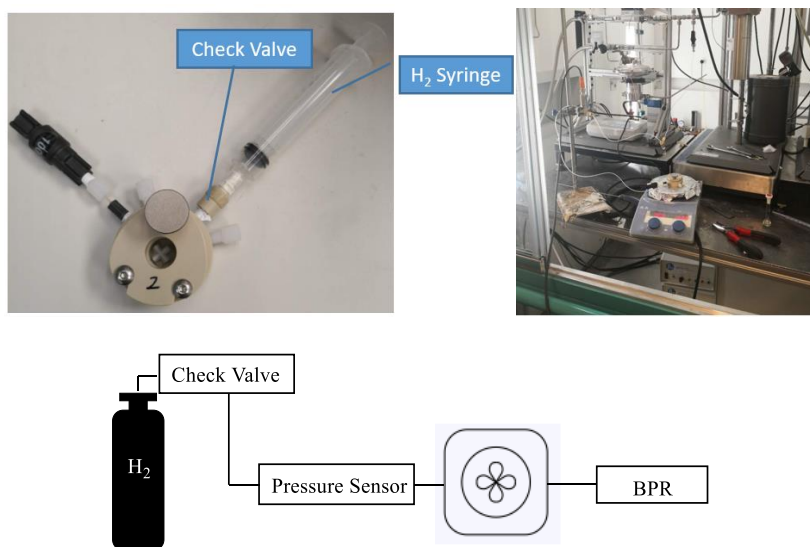


Figure 45 Batch mode fReactor with hydrogen syringe (upper left); Batch mode fReactor with continuous feeding of hydrogen (upper right and lower)

When a particulate catalyst is used, the frit in ferrule can be adopted to compartmentalize the catalyst within the fReactor, shown in Figure 46, but, as opposed to a fixed-bed catalyst, is well mixed and slurried. The common method to use a solid catalyst is to pack it into a cartridge or tube. An example is provided by the H-cube reactor, in which gas and liquid are simultaneously pumped into the cartridge containing heterogenous hydrogenation catalyst. The catalyst becomes a static mixer, and the mixing efficiency depends upon the flow rate. Low flow rates provide poor mixing with hydrogen segregating from the liquid. In the fReactor, all three phases are actively mixed (i.e., energy input) by a stir bar and the gas, liquid and solid can be uniformly distributed inside the reactor. This can maximize the efficiency of catalyst. fReactor could also be used as gas liquid separator, as shown in Figure 47.



Figure 46 Frit in a ferrule

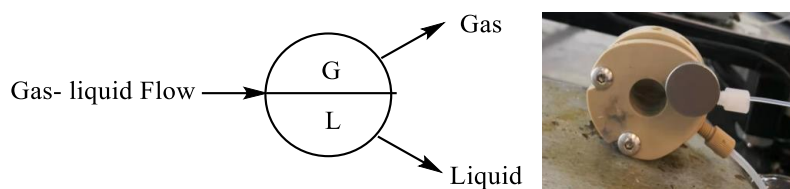
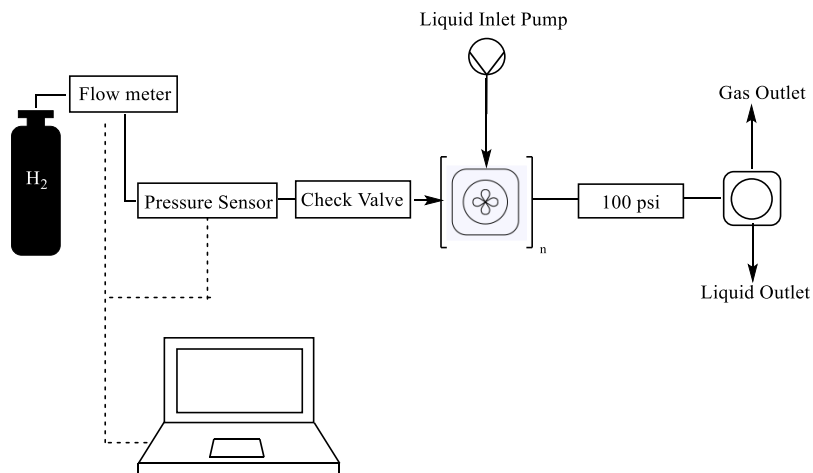


Figure 47 Gas-liquid Separator (vertical fReactor)

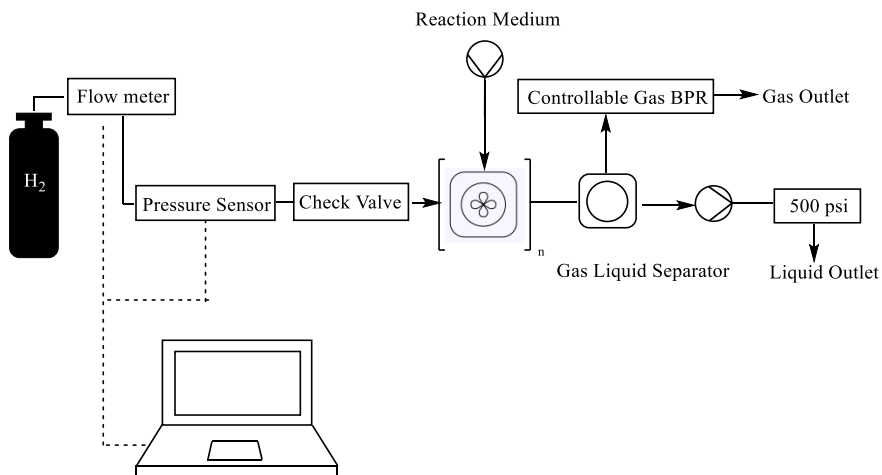
Then hydrogenation can be operated in batch and then reconfigured into a continuous system. Factors including flow rate, residence time, pressure, gas-liquid ratio, concentration of catalyst and substrate and frequency of stirring will be studied in this work. Two setups of the fReactor flow system are shown in scheme 9. Setup A is used for this work. The gas and liquid inlets were connected to the first fReactor. A check valve was installed to avoid liquid back flow. The last fReactor in the cascade was placed vertically without a stir bar to act as a gas liquid separator. The gas-liquid flow flows through the inlet in the middle, whilst liquid exits from the lower outlet and gas leaves from upper outlet, which is illustrated in Figure 47. The reaction pressure was monitored by an in-line pressure transducer. Since the check valve is placed between reactor and pressure sensor, the measured pressure is 1 bar higher than the system pressure. This setup has two disadvantages: the pressure in the system depends on the back pressure regulator, it can be tuned only by changing back pressure regulator; pressure cannot be kept stable by cartridge back pressure regulator. In Setup B, a gas liquid separator that can be a fReactor without stir bar or a T-junction is added after reaction mode reactors. A controllable back pressure regulator is connected to the gas outlet for controlling pressure. A pump with a back pressure regulator after the outlet is to add pressure and pump liquid out. Using this process, the pressure in the system can be controlled by the gas back pressure regulator and adjusted to any value that is lower than pressure of back pressure regulator of liquid outlet pump. The separation of gas and liquid can prevent fluctuation of pressure that is caused by cartridge back pressure regulator. Setup A was used for its concise design that

doesn't require an additional pump.

Setup A



Setup B



Scheme 9 Two set-ups of continuous fReactor hydrogenation systems

Figure 48 shows two diagrams of components used to construct the continuous hydrogenation system (Set-up A). The computer and electronic board were used to monitor the pressure and gas flow rate.



Figure 48 Components of a continuous fReactor hydrogenation system

Initially Setup A was used to try and obtain a stable gas-liquid flow. The residence time range chosen was 10-180 minutes giving a liquid flow rate of 0.05 mL/min to 0.5 mL/min and gas flow rates from 2 sccm to 100 sccm. Setup B was not built. When the gas flow rate was more than 20 sccm under 6.9 bar, a pressure increase of 3-5 bar was observed over 10 minutes, so gas flow rate was reduced to <5 sccm. When the liquid flow rate was varied, it was found that there was a pressure increase for all flow rates used: 0.1 mL/min and 0.2 mL/min gave an increase of 1 bar in 20 minutes, shown in Figure 49. When liquid flow rate was more than 0.3

mL/min, pressure increased more quickly and there were intermittent pressure releases as the BPR opened and closed due to the spring-based release mechanism. Consequently, a wave-like pattern was observed, Figure 49.

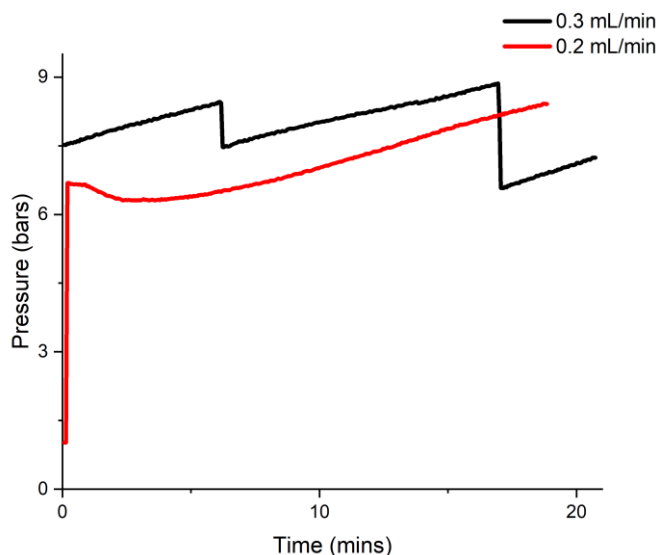


Figure 49 Pressure Pattern under different liquid flow rates

3.3 Gas liquid mass transfer in fReactor

The rate of triphasic hydrogenation, such as hydrogenation by Pd/C, is influenced by a combination of factors: (a) the mass transport of hydrogen gas through the gas/liquid interface; (b) the transport of hydrogen and substrate from liquid bulk to liquid/solid interface; (c) adsorption and desorption of reactants on the catalyst surface; (d) the intrinsic rate of the chemical reactions. The fReactor offers intense mixing which will affect the transfer rate of hydrogen and substrate to active site of heterogeneous catalysts.^[114]

The transport of hydrogen from gas to liquid phase can have a negative effect on conversion. It is an important factor when stirring is inefficient or when catalyst activity or loading are high. In such cases the observed rate will only depend on the concentration of hydrogen and can be described by Equation 6:

$$V = k_L a (C_{H_{2g}} - C_{H_{2l}}) \quad \text{Equation 6}$$

where V is the mass transfer rate, and C_{H_2g} and C_{H_2l} are the concentration of hydrogen in the gas and liquid phase, respectively. The constant k_{La} (volumetric mass transfer coefficient) is an important parameter that is often calculated to estimate the efficiency of hydrogenation equipment. It varies hugely with reaction scale, ranging typically from 2.1 s^{-1} for a 1 litre vessel to 0.05 s^{-1} for a 24,000 litres reactor.^[8] As a consequence, the bigger the scale the harder it becomes to set up a process outside the boundaries of the mass transport limitation.

In the fReactor, the mixing, power input per unit volume, is intense. Micro-mixing rates have been measured, which is at 10-100 ms (unpublished work of Prof. John Blacker and Prof. Nikil Kapur). Intense mixing creates a large gas-liquid contact surface that facilitate the gas liquid transfer rate. In addition, the mixing assists the diffusion of substrate and hydrogen to the catalyst, which avoids the formation of concentration gradients inside the liquid bulk.

Hydrogen mass transfer rates have been measured in larger reactors, however, the small-scale of the fReactors makes them useful for kinetic measurement.^[115] Using this rapid reaction and fast response pressure transducer, the overall mass transfer coefficient (k_{La}) could be measured directly by continuously monitoring the pressure drop, Figure 50. This shows the effects of r , and magnetic stir-bar speed, on the k_{La} in a fReactor (details in Appendix). The ratio of gas-liquid volume in a reactor is r . With 1 mL of liquid ($r=0.7$), and a stirrer speed of 200 rpm, the k_{La} is 0.25 s^{-1} . Increasing the mixing to 1500 rpm, the k_{La} increases to 1 s^{-1} . Significantly, as the fReactors sit off-centre from the magnetic stirrer, at high speeds the stir-bars start to bounce around the chamber, which increases the gas-liquid interface and k_{La} . Changing the gas-liquid ratio from 0.7 to 2.4, gives almost 3 times the rate, because of an increase in gas-liquid surface area. Under the same stirring rate, the fReactor shows a five-fold higher mass transfer rate, 2.7 s^{-1} , than the much larger overhead-stirred 600 mL Parr reactor for which individual component mass transfer rates have been previously measured, 0.54 s^{-1} .^[115c] The power per unit volume in the fReactor is estimated at 200 mW/mL, and compares with a well-mixed hollow-shaft hydrogenator.^[114]

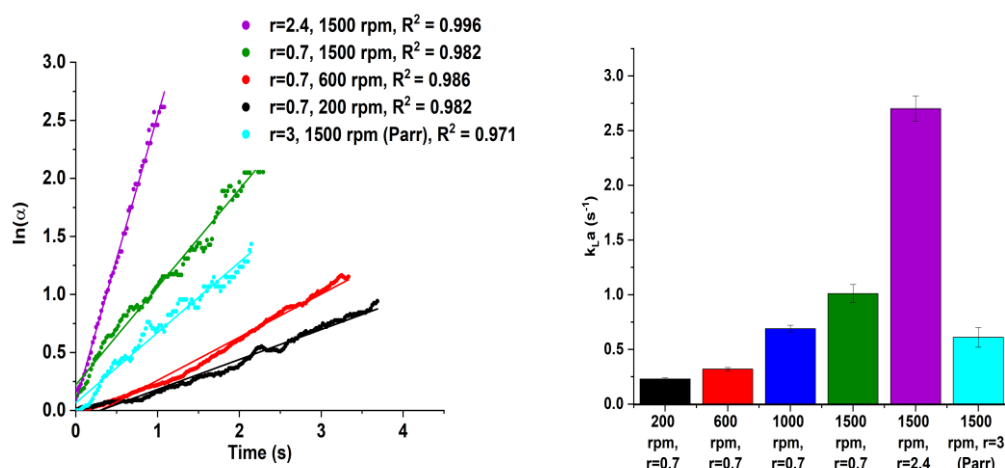


Figure 50 Left, Characterization of gas–liquid mass transfer $\ln(\alpha)$ via hydrogen uptake in batch. Right, A bar chart showing the mass transfer coefficient ($k_{L,a}$, for calculation see appendix) under different conditions; r = volume of gas/volume of liquid.

3.4 Heterogeneous hydrogenation in fReactor system

Figure 51 shows the typical kinetics for heterogeneous hydrogenation of nitrobenzene under batch mode. When the mixing is efficient, the limiting factor will be the intrinsic reaction rate, the rate of absorption and desorption. In this case, the reaction is zero order and lies in phase 1, which means it is independent of substrate and hydrogen. In this phase, catalyst efficiency can be maximized. As the concentration of substrate decreases, the reaction will become first order in substrate as described in phase 2. When hydrogenation is transferred into flow, the reaction will be kept in the phase 1. The reaction is zero order and concentration of hydrogen and substrate are not limiting factors of reaction rate.

Our study looked at optimizing fReactor system in batch mode by factors, including pressure, reaction time, the ratio between substrate and catalyst and mixing frequency. The end point of phase 1 (red point in Figure 51) is the target condition. Based on the conditions obtained in the batch experiments, the continuous flow mode fReactor system can be developed.

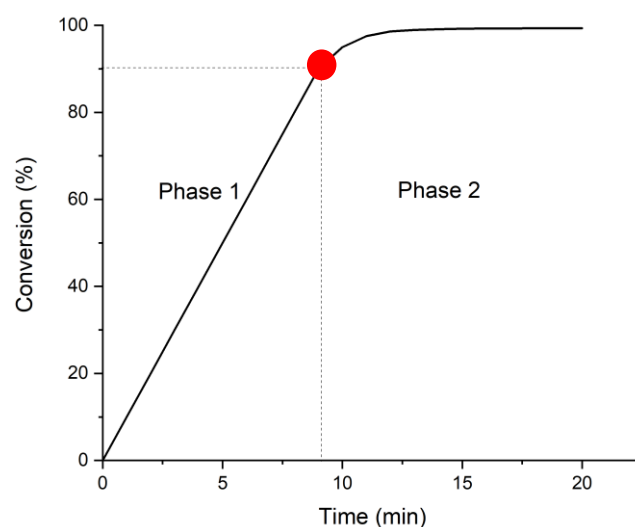


Figure 51 Kinetics of hydrogenation in batch reactor

To extend the use of the fReactor to multi-phasic reactions, heterogeneous hydrogenation and an air-sensitive homogenous hydrogenation were selected as test reactions. The hydrogen uptake rate, reaction rate and effect of stirring rate were studied and the results compared well with larger Parr reactors.

Since the fReactor can be used in both batch and flow mode, a new strategy was developed allowing identification of conditions in batch, then reconfiguring the same reactor (with same mass transfer characteristics - $k_L a$) for use in continuous flow, Figure 52. It also saves starting materials and catalyst.^[116] A wide range of conditions were screened so that the reaction in flow could be defined.

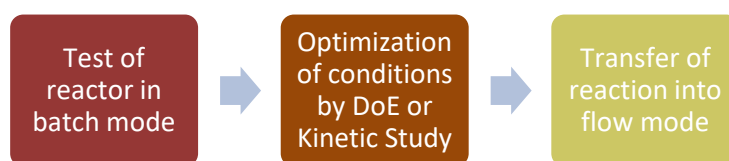


Figure 52 Strategies of conducting flow reaction in fReactor

3.4.1 Optimization in a batch fReactor system by DoE

The hydrogenation of nitrobenzene (Scheme 10), which is commonly used in pharmaceutical industry, was selected to test the gas-liquid-solid triphasic reaction in the

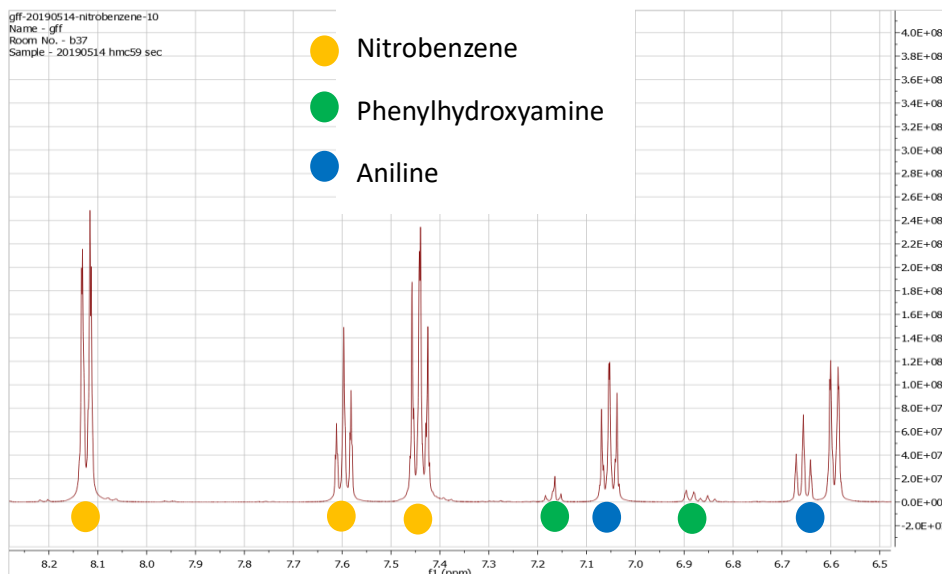


Figure 54 ^1H NMR of spectrum reaction medium after hydrogenation (CDCl_3 , 400 MHz)

Figure 55 shows the pressure changing in the batch-mode fReactor. The blue line shows the pressure without a reaction. For 3.5 minutes reaction, there was only a 0.04 bar pressure drop, showing the fReactor can hold pressure for a batch reaction. The red line shows the pressure of the fReactor during a hydrogenation. 30 mL H_2 was syringed into the fReactor to raise the pressure to 8.5 bar and 0.5 mL reaction medium was added. The stirrer speed was 1500 rpm and the concentration of nitrobenzene was 0.2 M. The reaction finished in 40 seconds with no more pressure drop and GC analysis showed >99% conversion to the aniline product. The pressure sensor gives a direct measurement of the rate and extent of the reaction as hydrogen is consumed the pressure drops. The experiment showed that the fReactor could be used in batch mode to carry out pressure hydrogenations.

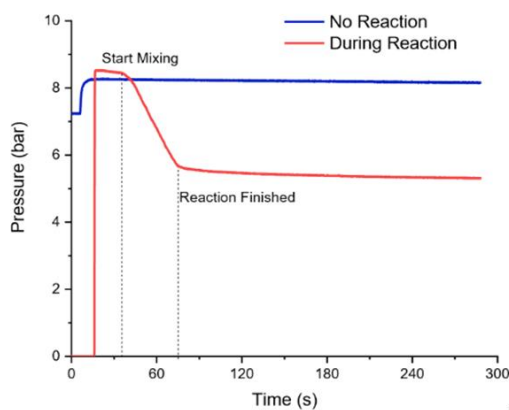


Figure 55 Pressure changing of a batch mode fReactor

Figure 56 compares a hydrogenation carried out in the fReactor and Parr reactor. In the fReactor, 1 mL reaction medium was added and pressurized to either 1, 4.5 or 7.5 bar with S/C = 400 and mixed at 1500 rpm and the nitrobenzene reacted over 10 minutes. In the Parr reactor, 40 mL reaction medium was used and reacted under the same pressure with S/C = 400 for 10 mins, and the stirrer speed of 1500 rpm. Hydrogen uptake and yield were measured to compare two reactors. With higher pressures the hydrogen uptake and yield increased. Under atmospheric pressure, the aniline yield in the fReactor was 18% and was similar to the Parr Reactor. At higher hydrogen pressures, the fReactor used the gaseous hydrogen more quickly than the Parr Reactor and the yield was higher. This is partly due to the higher liquid surface area to volume but also that the fReactor has more intense mixing (power per unit volume) which improves mass transfer and reduces the soluble hydrogen concentration gradient from the gas to the liquid to the solid catalyst. When the pressure was raised to 7.5 bar, the yield reached 99% for fReactor, but only 86% for Parr reactor. In conclusion, the fReactor enables a greater hydrogen uptake rate than the Parr reactor for pressurized hydrogenations.

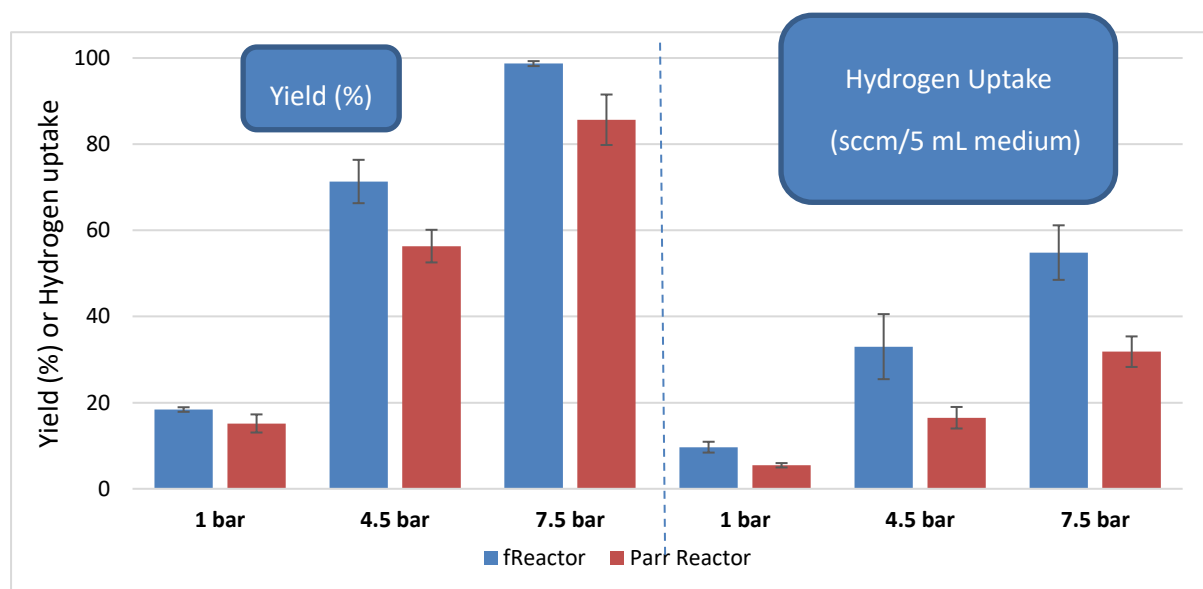


Figure 56 Hydrogen uptake and yield of hydrogenation in fReactor and Parr Reactor

The effect of stirrer speed, from 0-1500 rpm, was studied and results are shown in Figure 57. Both experiments were done at room temperature and the S/C was 400. At 1.5 bar pressure and 20 minutes reaction time, the yield increases as the stirring frequency increases

from 0 rpm to 1000 rpm showing the reaction rate is mass transfer limited. The stirring rate can speed up the uptake of hydrogen by increasing gas-liquid interfacial area and generating uniform distribution of solid catalyst and concentration of reactants (hydrogen and starting materials). When the mixing frequency was >1000 rpm, the yield did not increase any further. This shows the reaction has switched from being limited by hydrogen mass transfer to the chemical reaction rate. The adsorption of reactants and desorption rate of products have become the limiting factors. When pressure was 2.5 bar and reaction time was 10 minutes, the yield increased as the stirring frequency increased to 1500 rpm. Under higher pressure, concentration of hydrogen in the reaction medium was higher, which speeded up absorption of reactants and desorption of products by pushing the equilibrium to the hydrogenation direction. Therefore, gas liquid mass transfer rate is still limiting the reaction rate.

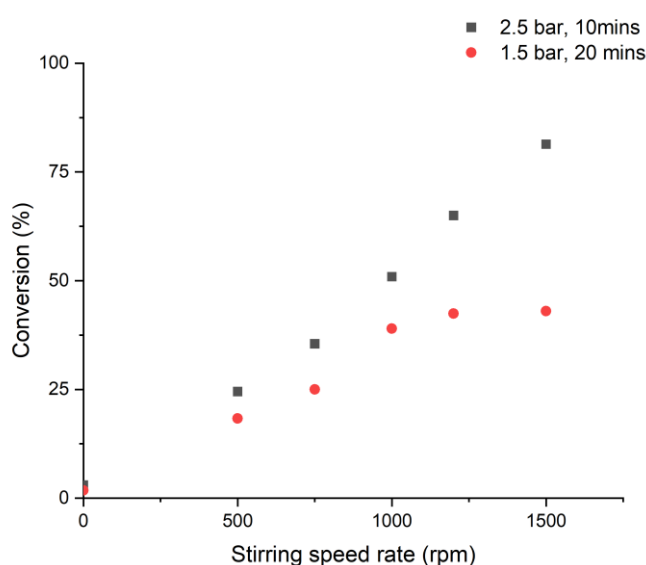


Figure 57 Effect of stirring rate.

To transfer the hydrogenation of nitrobenzene into flow-mode, the reaction conditions were firstly screened. The DoE data was processed by Modde and a model was generated to help predict performance across different conditions. The ranges screened were pressure from 1 to 4.5 bar; the reaction time from 10 to 30 minutes; S/C from 200 to 2000. The results are shown in Table 16.

Table 16 Screening of reaction conditions for hydrogenation of nitrobenzene

Entry	Pressure (bar)	Reaction time (min)	S/C ^a	Conversion ^b (%)	Phenylhydroxy amine ^c (%)	Yield ^b (%)
35	1	10	200	22	<1	22
36	4.5	10	200	>99	<1	>99
37	1	30	200	27	2	25
38	4.5	30	200	>99	<1	>99
39	1	10	2000	1	<1	1
40	4.5	10	2000	16	2	14
41	1	30	2000	4	<1	3
42	4.5	30	2000	28	1	27
43	2.75	20	1100	36	1	35
44	2.75	20	1100	34	<1	34
45	2.75	20	1100	32	1	31

[a] 5.3 mg (0.0025mmol Pd) catalyst 1 mL reaction medium with different substrate catalyst ratio (200 – 2000) under 6.3 bar and 1500 rpm were added into a reactor for each run. [b] Conversion is the mole percentage of nitrobenzene that reacts. Yield is the mole percentage of aniline that generates. They are all determined by ¹H NMR. [c] Phenylhydroxyamine was the only intermediate that was more than 1% in most of entries.

Figure 58 summarizes the four parameters of the DoE model. R² is 0.98, Q² is 0.96, model viability is 0.65 and reproducibility is 0.97. The model can be used to evaluate the importance of factors. Figure 59 represents graphically how the yield changes with pressure and catalyst loading. The reaction can reach high yield by increasing pressure and catalyst loading.

It can be concluded from the coefficients of variables in Figure 60 that the pressure, catalyst loading and pressure*S/C were all significant terms in the model, but the reaction time was insignificant. This means that when the catalyst loading was high, the reaction was in phase 2 (Figure 51) where reaction rate was decreasing. When catalyst loading was low, the reaction

rate was so low that the yield did not increase much during this time. To obtain the optimal conditions, located in Phase 1 (Figure 51), the reaction should be screened in a narrower area. In this case the reaction time could be reduced to 2-10 minutes and the catalyst loading from 0.25 mol%-0.125 mol%, to reach the target full conversion. Because a 6.9 bar BPR was used for both batch and flow reactions, a 6.3 bar reaction pressure was chosen for the optimization.

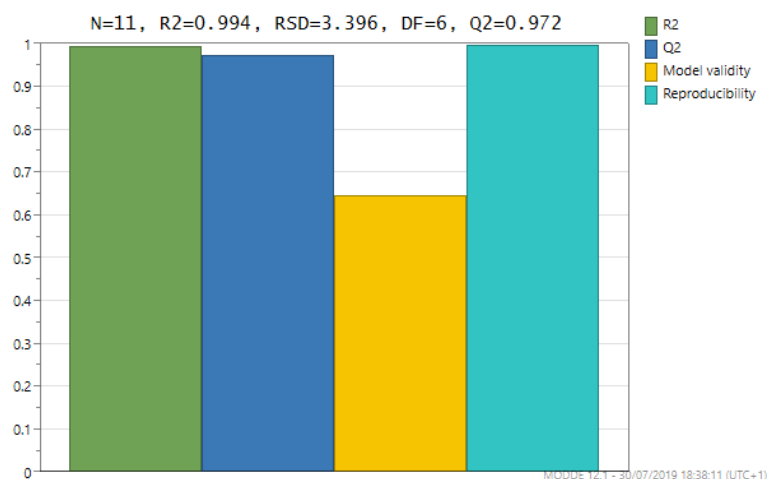


Figure 58 Summary of fit for screening step

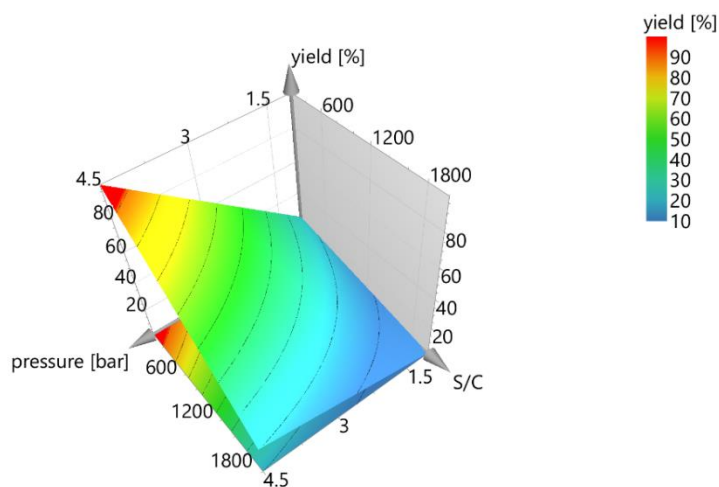


Figure 59 Response surface plot of screening step

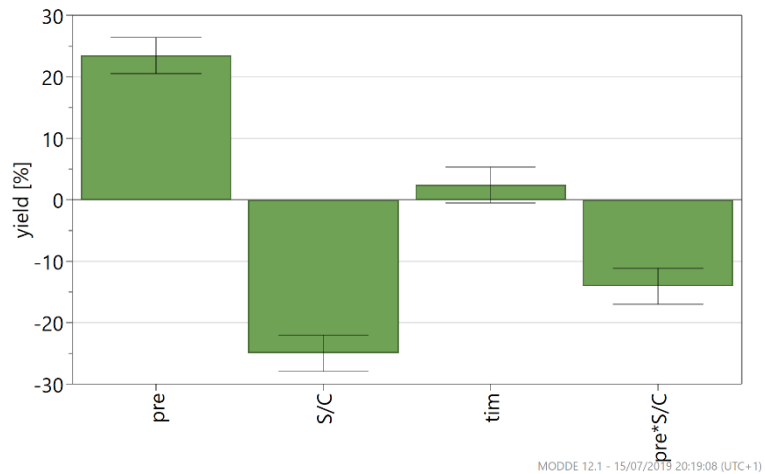


Figure 60 Coefficient plot of screening step

The reaction was optimized in a narrow range to have a more precise model to get the optimal point for flow mode. Pressure was fixed as 6.3 bar, because 6.9 bar BPR was used. Reaction time was screened from 2 to 10 minutes and catalyst loading from 400 to 800. The results were shown in Table 17.

Table 17 Optimization of reaction conditions

Entry	Reaction time (min)	S/C ^a	Conversion ^b (%)	Phenylhydroxyamine ^c (%)	Yield ^b (%)
46	2	400	43	2	41
47	10	400	>99	1.0	99
48	2	800	21	3	18
49	10	800	72	2	70
50	2	600	23	4	19
51	10	600	98	1	97
52	6	400	76	1	75
53	6	800	40	4	36
54	6	600	52	3	49
55	2	400	43	2	41
56	10	400	>99	1	99

[a] 5.3 mg (0.0025mmol Pd) catalyst 1 mL reaction medium with different substrate catalyst ratio (400-800) under 6.3 bar were added into a reactor for each run. [b] Conversion is the mole percentage of nitrobenzene that reacts. Yield is the mole percentage of aniline that generates. They are all determined by ¹H NMR. [c] Phenylhydroxyamine was the only intermediate that was more than 1% in most of entries.

Coefficient plot, summary of fit and response surface plots are presented in Figure 61, Figure 62 and Figure 63. These show that the reaction time and catalyst loading are both significant factors in Phase 1. They are independent with each other. The reaction lied in phase 1 under the time period and the catalyst loading optimized. R² is 0.95. Q² is 0.92. Model viability is 0.64. Reproducibility is 0.95. Thus, model is reliable for prediction. It is predicted that when catalyst loading is 0.25 mol% and reaction time is 9.2 min, the conversion can achieve 95% under 6.3 bar. This condition is chosen for transferring reaction into flow mode.

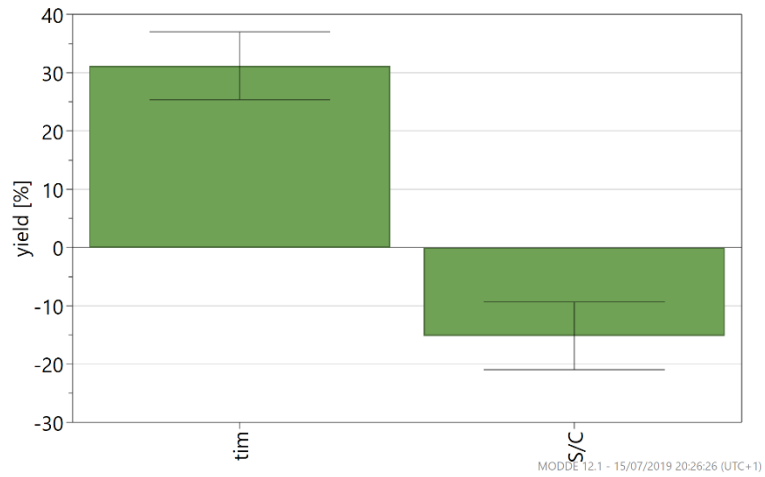


Figure 61 Coefficient plot of optimization step

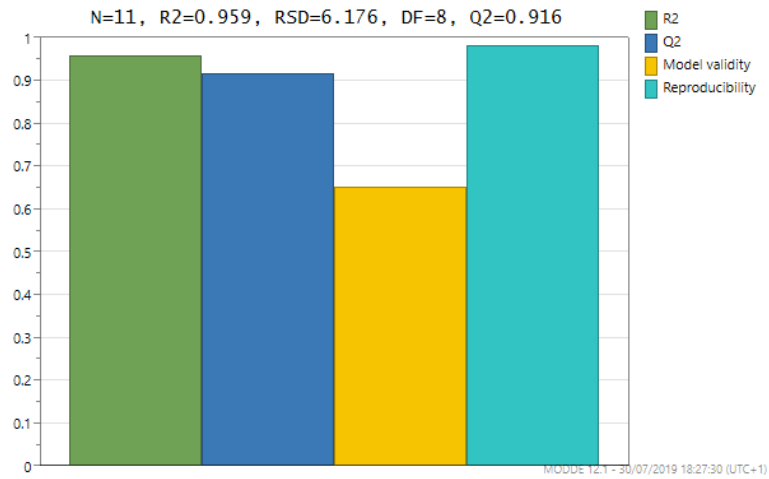


Figure 62 Summary of fit for optimization step

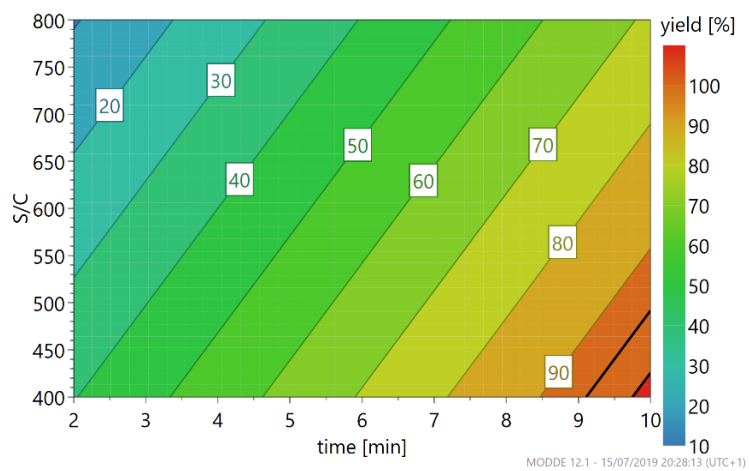


Figure 63 Response surface plot of optimization step

3.4.2 Continuous flow triphasic hydrogenation in the fReactor

Using the optimal conditions identified in batch above, the S/C was kept at 400/1 within each fReactor. It was found that at steady state each reactor contained 0.4-0.5 mL reaction medium as the liquid is blown through the cascade, which is half the volume seen in the batch-mode. Accordingly, the catalyst loading was halved, 2.8 mg Pd/C catalyst, to keep the same liquid-solid ratio. The initial hydrogenation using 4 fReactors showed an increase in pressure, perhaps due to occlusion of the in-line filter by the solid catalyst. The quantity of catalyst in each reactor decreased from 2.8 mg to 1.4 mg to avoid this and prolong the steady state reaction. So, in flow-mode, 1.4 mg catalyst was used in each reactor with 0.5 M nitrobenzene methanol solution flowing at 0.1-0.2 ml/min to give a S/C ratio of 400/1. The results are shown in Table 18. In entries 57 and 58, two fReactors were used with residence time of 4.3 minutes. In entries 59 and 60, a 1/8 inch frit in a ferrule was used instead of 1/16 inch to reduce the risk of blocking and four fReactors were used with residence time of 8.7 minutes and 9.7 minutes, which was analogous to batch reaction time.

Table 18 Reaction conditions of heterogeneous hydrogenation in flow^a

Entry	S/C in each reactor	Total catalyst loading (mg)	Concentration (M)	Reactor quantity ^b	Liquid flow rate (mL/min)	Reactor Volume (mL)	Residence time (min) ^c
57	400	2.8	0.5	2	0.2	3.4	4.3
58	80	2.8	0.1				
59	400	5.6	0.5	4	0.2	6.8	8.7
60	200	5.6	0.25		0.1		9.7

[a] 1.4 mg catalyst (0.00066 mmol) was added in each reactor connected with a 100 psi BPR in the last reactor. Gas flow rate was 5 sccm. [b] The filter could lead to blocking, therefore 2 reactors were used in parallel, instead of 4 and residence time was shortened to 4.3 min. [c] Residence time is calculated by dividing reactor volume by sum of gas and liquid flow rate under 100 psi.

Figure 64 shows the reaction profile and pressure changing during the reaction from entry

57. The reaction reached steady state at around 20 minutes (3RV) and remained until 7-8RV before the yield decreased. This was partly due to catalyst poisoning, which is well known in this system. Furthermore, the solid catalyst accumulated on the in-line filters and holes of the reactor. Entries 59 and 60 in Table 18 are experiments in which the number of reactors was increased, the residence times were longer, and the catalyst loadings were higher. The steady state conversions of entries 59 and 60 reached 88% and 95% and are higher than those of entries 57 and 58 with yields of 75% and 87%. Furthermore, the results in entries 57 and 59 show the more fReactors used in the system, the longer the reaction stayed at steady state, which increased production. There was steady rise in system pressure of all entries that could surpass the safe operating pressure. The fReactors have been pressure tested to 50 bar before failure occurred (tube fittings) but the safe recommended limit is 10 bar. Adopting this flow system, the catalyst loading was increased to S/C =2543/1 and the production rate was 0.83-4.02 mmol/h.

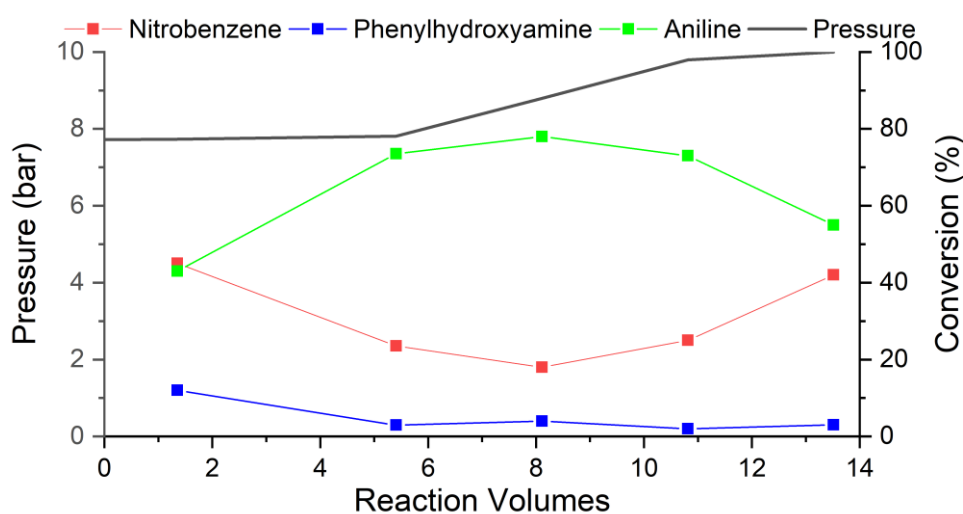


Figure 64 Continuous hydrogenation of nitrobenzene Entry 57

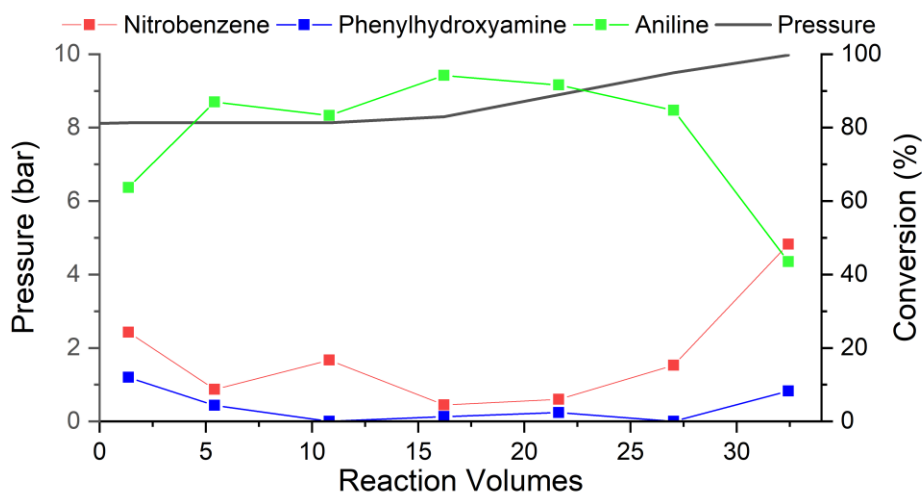


Figure 65 Continuous hydrogenation of nitrobenzene Entry 58

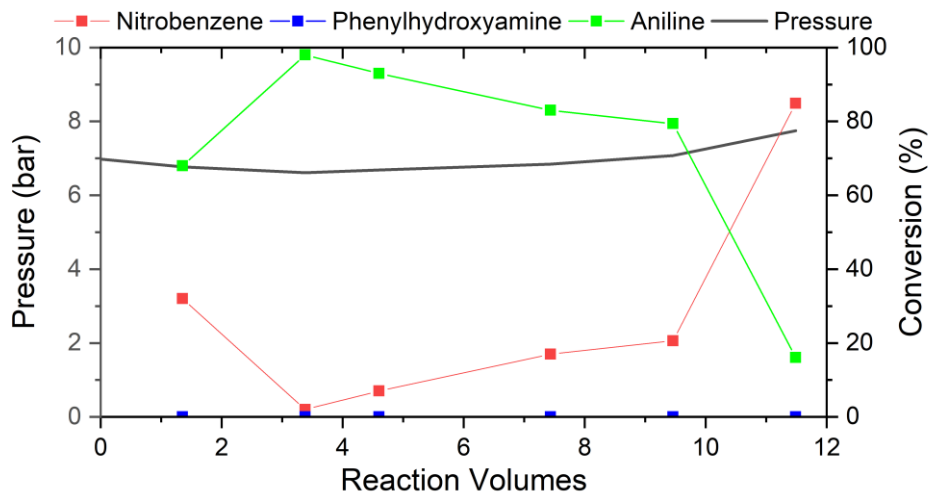


Figure 66 Continuous hydrogenation of nitrobenzene Entry 59

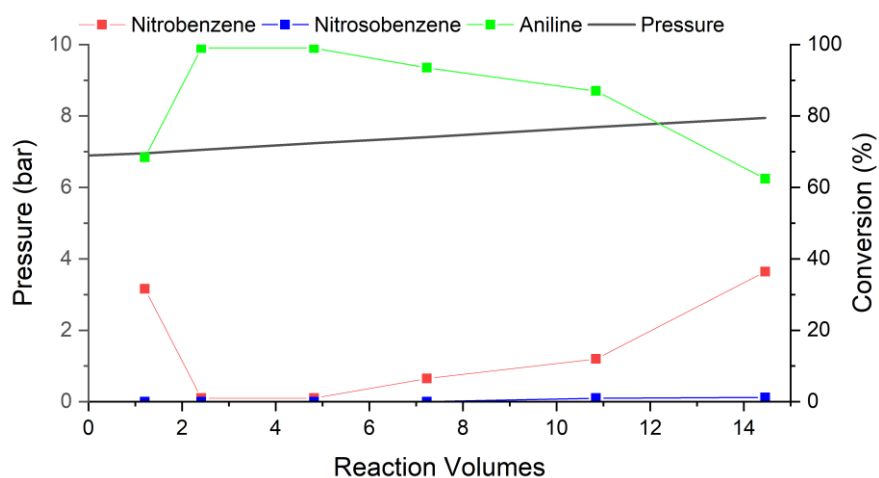


Figure 67 Continuous hydrogenation of nitrobenzene Entry 60

The results of these reactions run in continuous flow are summarized in Table 19. The values predicted by the DoE model, obtained in the batch, are close to those of the flow reactions. The reason the yields in flow-mode were higher than those in batch were that the fReactor pressure was higher than 6.9 bar, while in batch the pressure was stable at 6.3 bar. This proved that in batch-mode the fReactor has the same dimensions and mixing performance as in flow and it is feasible to predict the optimal flow conditions from those in batch. Using batch reactions to begin saves catalyst and starting material for the screening of reaction conditions.

Table 19 Results of heterogeneous hydrogenation in flow

Entry	S/C ^a in each reactor	Running time (min)	Conversion in steady state ^b (%)	Conversion predicted by model (%)	Total S/C ^c	Productivity (mmol/h)
57	400	60	75	58	2424	3.2
58	80	160	87	82	1679	0.83
59	400	100	88	99	2543	4.02
60	200	120	95	99	970	1.28

[a] The molar ratio between substrate in the reactor and catalyst loading. [b] Yield in steady state was calculated by the average yield in steady state. Aniline obtained for the whole run. For entry 57, 298 mg aniline was obtained. For entry 58, 206 mg aniline was obtained. For entry 59, 626 mg aniline was obtained. For entry 60, 239 mg aniline was obtained. [c] The molar ratio between aniline obtained for the whole run and molar catalyst.

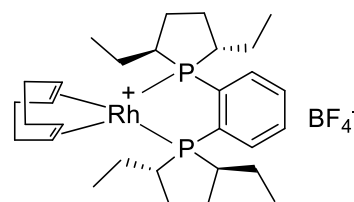
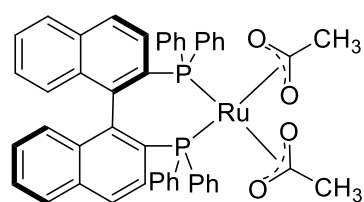
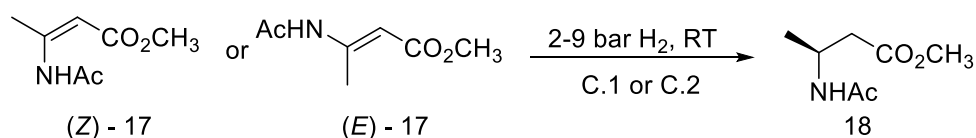
Table 20 compares the results of the fReactor with those of the H-cube from literature data. These show that the fReactor used less catalyst but achieved a similar production rate. The H-cube reactor requires 140 mg catalyst to fill in the cartridge to have a production rate of 1.8-6.2 mmol/h, while fReactor used 2.8-5.6 mg catalyst for 0.83-4.02 mmol/h. The reason for the improved performance is that in a single fReactor, the gas, liquid and solid catalyst are actively mixed, which improves mass transfer and reduces the hydrogen concentration gradient to increase the reaction rate.

To conclude, the fReactor flow system can be used for heterogeneous hydrogenation. It requires less catalyst to achieve similar production rate as H-cube reactor.

Table 20 Comparison between fReactor and H-Cube reactor

Reactor	Substrate	Pressure (bar)	Temperature (°C)	Conversion (%)	Catalyst Loading (mg)	Productivity (mmol/h)
fReactor (Entry 57)	nitrobenzene	6.9	295	75	2.8	3.8
fReactor (Entry 59)	nitrobenzene	6.9	295	88	5.6	4.02
H-cube ^[68b]	5-nitroindole	1	298	95-97	140 (10% Pd/C)	3
H-cube ^[117]	2-nitro benzamides	10	303	>99	150 (10% Pd/C)	1.8
H-cube ^[118]	4-nitro-1,8-naphthalic anhydride	10	313	98	140 (10%Pd/C)	6.2

3.5 Homogeneous asymmetric hydrogenation in fReactor system

**Scheme 11** Benchmark reaction for hydrogenation by fReactor^[119]

In 1991, Noyori reported a method to synthesize chiral β -amino esters by AH with high yield and enantiomeric excess, shown in Scheme 11.^[119a] The reaction conditions are mild, room

bars achieved >99% conversion and 63% ee at 30 minutes, entry 66, whilst under 3 bar there was no reaction, entry 67. Conducting the reaction in the Parr reactor gave 85% conversion in 30 minutes, entry 68. In this case the reaction rate and enantiocontrol were higher than that in the literature.^[119b]

Hydrogenation of (*E*)-**17** was conducted at 3.5 bar pressure, however, only 24% starting material was consumed in 1 hour, entry 70. Increasing the pressure to 6.25 bar then 9 bar, gave increased conversion. 100% conversion was achieved in 30 minutes at 9 bar hydrogen, entry 72. The enantioselectivity was 96% ee under 9 bars, higher than that in literature at 2.8 bar. Further increasing in pressure had little influence on the enantioselectivity.

Table 22 Hydrogenation by C.2

Entry	substrate	Pressure (bar)	Time (h)	Conversion ^a (%)	ee ^a (%)
66	(<i>Z</i>)- 17	9	0.5	>99	63
67	(<i>Z</i>)- 17	3	0.5	0	N.A.
68	(<i>Z</i>)- 17 (Parr Reactor) ^[119b]	9	0.5	85	60
69	(<i>Z</i>)- 17 (literature)	30	0.2	>99	47
70	(<i>E</i>)- 17	3.5	1	24	96
71	(<i>E</i>)- 17	6.3	0.5	80	96
72	(<i>E</i>)- 17	9	0.5	>99	96
73	(<i>E</i>)- 17 (literature) ^[119b]	2.8	24	>99	94

[a] Conversion and ee is determined by Gas Chromatography.

A kinetic study was done on the homogeneous hydrogenation of (*E*)-**17** in batch mode fReactor, Figure 68. Here, 0.5 mL reaction medium was used with a substrate concentration of 0.2 M and the pressure was kept at 6.3 bar and S/C was 100. It was found that under 2 bar and 3.5 bar hydrogen pressure the catalyst had an induction time of 2 hours or 30 minutes, respectively. This is explained by the hydrogenation of the cyclooctadiene ligand freeing the metal coordination site for binding and hydrogenating the substrate. When the pressure was

increased, the induction time was shortened due to a higher hydrogen concentration in solution. The reaction afforded an 84% yield under 6.3 bar with a S/C of 100 and the reaction time was 30 minutes. These conditions were selected for transferring into flow. The catalyst loading, temperature and pressure were kept the same and the residence time was 30 minutes.

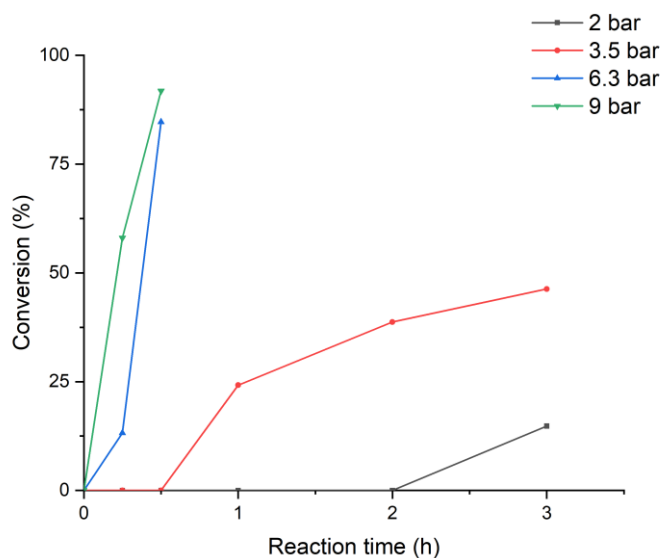


Figure 68 Kinetic Study of Asymmetric Hydrogenation by C.2

Table 23 shows the conditions for the flow reactions and Table 24 the reaction results. In entry 74 the residence time was 10.3 mins, and there was almost no reaction at steady state. In entries 74 and 75, the catalyst loading was increased to S/C=50 and the catalyst was preactivated by hydrogen from a balloon for 3 hours before adding the substrate. The (*E*)-substrate was hydrogenated with 10% yield, whilst the ee was lower than in batch. An explanation is that during preactivation there was catalyst degradation due to the ingress of air. In entry 76, there was still no conversion in steady state whilst in entry 77, the residence time was prolonged to 29.4 mins by increasing number of reactors from 4 to 10 without preactivation. The liquid flow rate was also reduced to 0.1 mL/min to increase gas liquid ratio. The steady state yield was 16 %. In entry 78, the catalyst and substrate were concentrated 4 times and the residence time was 32 minutes. The liquid flow rate was decreased to 0.05 mL/min to extend residence time and increase gas-liquid ratio. The steady state yield increased to 88% without preactivation. In the former runs, the concentration of the substrate and catalyst was the rate limiting factor, which made reaction lie in phase 2 (Figure 51), whilst after

concentrating the reaction medium in entry 78, reaction rate increased. The production rate was 0.53 mmol/h. Continuous hydrogenation of (*E*)-**17** in entry 79 afforded product with a conversion of 93% and 98% ee.

Table 23 Reaction conditions of asymmetric hydrogenation in flow

Entry	Substrate	S/C ^a	Concentration of Substrate (M)	Reactor quantity	Liquid flow rate (mL/min)	Reactor Volume (mL)	Residence time (min) ^b
74	(<i>Z</i>)- 17	100	0.1				
75	(<i>E</i>)- 17	50	0.05	4	0.2	6.8	10.3
76	(<i>Z</i>)- 17	50	0.05				
77	(<i>Z</i>)- 17	50	0.05	10	0.1	17	29.4
78	(<i>Z</i>)- 17	50	0.2	10	0.05	17	32
79	(<i>E</i>)- 17	50	0.2	10	0.05	17	32

[a] The ratio between substrate in the reactor and catalyst loading. Pressure were all 100 psi and gas flow rate are 4 sccm. [b] Residence time is calculated by dividing reactor volume by sum of gas and liquid flow rate under 6.9 bars.

Table 24 Reaction results of asymmetric hydrogenation in flow

Entry	Running time (min)	Conversion ^a (%)	ee. ^a (%)	Pre-activation ^b	Production Rate (mmol/h)
74	120	<1	N.A.	No	0
75	120	10	71	Yes	0.06
76	120	<1	N.A.	Yes	0
77	200	16	N.A.	No	0.048
78	260	88	N.A.	No	0.53
79	180	93	98	No	0.56

[a] Yield and ee were determined by Gas Chromatography. [b] The catalyst was preactivated by hydrogen for 3 hours before adding substrate.

Figure 69 shows a reaction profile for the results in entry 79. Because the liquid flow rate was 0.05 m/min, the pressure stabilized in the range of 7.5 – 8 bar. The reactor was pressurized in the beginning, then gas and liquid were added in certain flow rate. After 110 mins, the liquid came out from BPR and the first sample was collected. A sample was collected every half hour. From the second sample onwards, the conversion stabilized around 93% with a 98% ee.

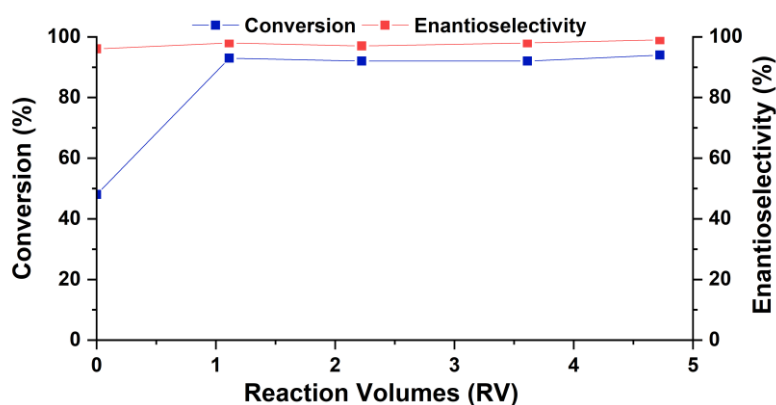


Figure 69 Reaction results of Entry 79

Table 25 compares the results of AH in different reactors. It was shown that using the fReactor in flow-mode it was able to handle air-sensitive AH. The residence time could be extended to 32 minutes using 10 fReactors in cascade and the productivity was 0.53 mmol/h, higher than that of micro-mesh reactor and H-cube reactor. A tube-in-tube reactor system for AH was used by Ley *et al* and afforded a productivity of 3 mmol/h. The set-up involved two tube-in-tube reactors in parallel, two 10 mL tubular reactor and a mixer chip, which made the set-up much more complicated than fReactor system and the pressure of 20 bar was higher than ours.

Table 25 Comparison of asymmetric hydrogenation in different reactors

Reactor	Substrate	Catalyst	Residence time (min)	Pressure (bar)	Yield (%)	S/C	Productivity (mmol/h)
fReactor (Entry 78)	(Z)- 17	<i>In-situ</i> Ethyl-DuPhos-Rh	32	6.9	88	50	0.53
Micro-mesh Reactor ^[67]	(Z)-methyl acetamido cinamate	<i>In-situ</i> Methyl-DuPhos-Rh	10	2	31	100	0.02
H-cube Reactor ^[68c]	(Z)-methyl acetamido cinamate	[Rh(COD) ₄]/PTA/ Al ₂ O ₃	1s	1	>99	1/360	0.3
Tube-in-tube ^[52c]	Trisubstituted olefins	Iridium catalyst	40	20	>99	40	3

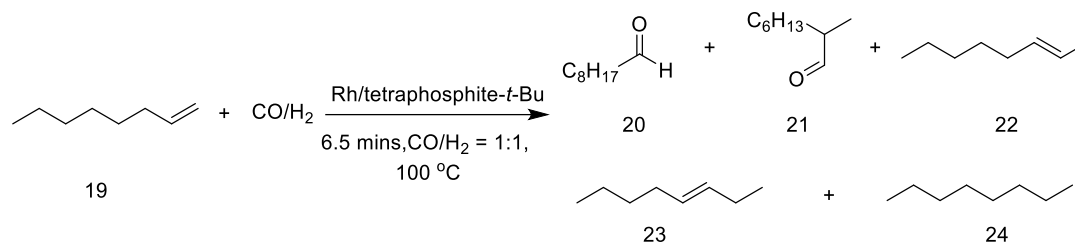
3.6 Conclusions

In conclusion, the fReactor shows great potential for assessing small scale heterogeneous and air-sensitive homogeneous hydrogenations in both batch and continuous flow. The batch experimental design data provided the basis for choosing a residence time for continuous flow operation; the benefit of using the same reactors and mixing regime is that the mass transfer coefficients are identical. The limitations of most pressure hydrogenators are their size and complexity required to ensure good mixing and safety. Many chemists avoid this by using hydrogen-filled balloons that are restricted to pressures only marginally above atmospheric. The fReactor provides a simple, small-scale, low-cost solution to batch and rapid translation to continuous flow and lab scale-up. The ability to charge hydrogen manually by syringe via a non-return valve up to ~10 bar pressure makes hydrogenations practical, and parallel reactors enable different conditions to be tested. Active mixing gives high gas-liquid mass transfer rates that can be monitored directly using an on-line pressure sensor. In a benchmark Pd/C catalysed hydrogenation of nitrobenzene, fast reactions and high conversions were achieved using high

stirrer speeds and gas to liquid ratios. The fReactor exceeded the mass transfer rates of a 600 mL mechanically stirred Parr hydrogenator. A further benchmark reaction of a homogenous asymmetric hydrogenation showed the use of an air-sensitive catalyst in both batch and flow. Using the fReactor, the hydrogenation of the (*E*)-**17** gave similar conversions and optical activities to those reported in literature. Furthermore, the known dependency of the ee on hydrogen pressure was reconfirmed, whilst the (*E*)-**17** was shown insensitive to this. Adopting a standard and easy-to-use hydrogenation platform constructed with good engineering design supports robust batch and flow experimentation and reporting of results.

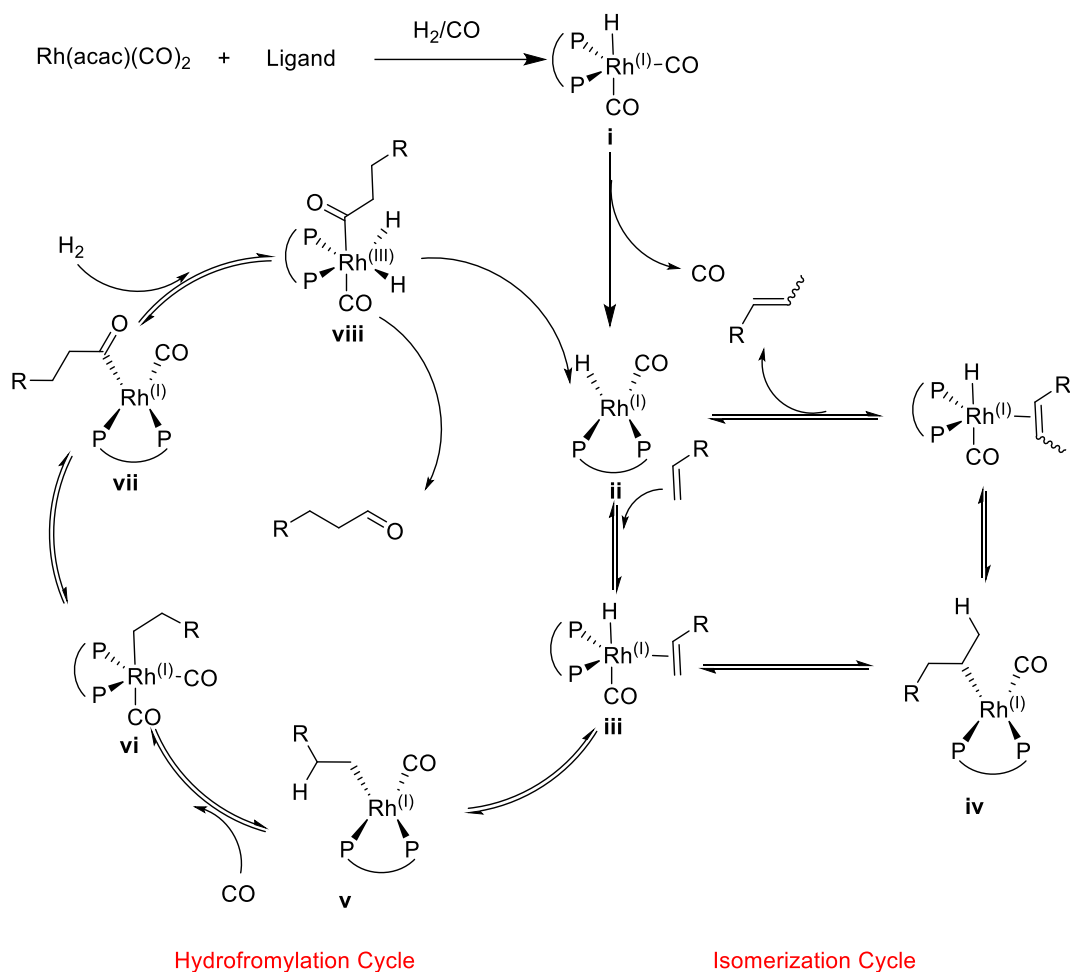
Chapter 4: Continuous hydroformylation in microreactor

Hydroformylation of olefins, discovered in 1938 by Roelen, has become one of the largest industrially applied processes which relies on homogenous catalysis. Its enormous economic importance is reflected in the number (ca. 7 million tons) of oxo products produced per year.^[121] Our research began by hydroformylation of 1-octene as shown in Scheme 13.



Scheme 13 Hydroformylation of 1-octene

Thus, starting from different Rh(acac)(CO)₂ catalyst, under syngas pressure, and in the presence of donor ligands L such as phosphines, phosphites or carbon monoxide, the trigonal bipyramidal complex **i** is formed (18 valence electron species) as a key intermediate in Scheme 14. Dissociation of one carbon monoxide from this complex generates the coordinatively unsaturated and hence, catalytically active 16 valence electron species **ii** (I). The main catalytic cycle starts with the coordination of alkene, preferably in the equatorial position, thus furnishing trigonal bipyramidal hydrido olefin complex **iii** (II). Alkene insertion into the Rh-H bond (III, hydrometallation) takes place to form the isomeric, tetragonal alkyl rhodium complexes, **iv** and **v**. Subsequent coordination of carbon monoxide yields trigonal bipyramidal complexes **vi**. Migratory insertion of the alkyl group to one of the coordinated carbon monoxide generates tetragonal acyl complexes **vii**. Oxidative addition of molecular hydrogen forms tetragonal bipyramidal rhodium (III) complexes **viii**. Subsequent reductive elimination liberates the isomeric aldehydes and regenerates the catalytically active species **ii**.^[121]



Scheme 14 Hydroformylation Cycle and Isomerization Cycle^[121]

Isomerization occurs when the alkene coordinates with the catalyst through hydride insertion and beta-elimination. The linear aldehyde can be produced through isomerization, even if a 2-olefin is used as the starting material. In industry, liquified petroleum gas that contains terminal olefin and 2-olefin can be functionalized to generate a linear aldehyde through hydroformylation.^[122]

In Scheme 14, the hydroformylation and isomerization have different catalytic cycles. In theory, to promote the isomerization, the steps in isomerization cycle need to be accelerated. To suppress the isomerization, the steps in hydroformylation cycle need to be speeded up, for example, the rate of carbonyl insertion and oxidative addition of hydrogen.

4.1 Continuous hydroformylation in slug flow reactor

The effects of pressure, temperature, catalyst loading, and residence time were studied in

a slug flow reactor and are discussed below. The process is shown in Figure 22. The reactor volume was 7.4 mL.

4.1.1 Pressure

When the pressure was increased from 10 to 15 bar, the conversion decreased from 61% to 53%, Table 26, entries 80 and 81. The results can be explained by the increasing pressure of CO that can retard or poison the catalyst. When the temperature was increased from 100 to 120°C at 15 bar, the conversion increased slightly from 53% to 54%, but with a decreasing linear to branched (l/b) ratio of 24 to 16, entry 82.

Table 26 The effect of pressure on continuous hydroformylation

Entry ^a	Temperature (°C)	Pressure (CO/H ₂)	Conversion 20 (%)	l/b ratio	19 (%)	22 (%)	23 (%)	24 (%)	TOF (h ⁻¹)
80	100	5/5	61	23	2.9	24	7.9	3.7	22700
81	100	7.5/7.5	53	24	9	30	5	4	19400
82	120	7.5/7.5	54	16	2	21	14	8	20000

[a] Liquid flow rate: 0.23mL/min, gas flow rate: 0.9 mL/min, residence time: 6.5 minutes.

4.1.2 Temperature

The influence of temperature was studied, Table 27, under 10 bar CO/H₂ (1:1). When the temperature was raised from 60 to 80 °C, the conversion was increased from 10% to 61% without deterioration in the selectivity. However, when the reaction was heated to 120 °C, the conversion decreased to 19% and the l/b ratio decreased to 10.

Table 27 The effect of temperature on continuous hydroformylation

Entry ^a	Temperature (°C)	Conversion 20 (%)	l/b ratio	19 (%)	22 (%)	23 (%)	24 (%)	TOF (h ⁻¹)
83	60	10	23	40	37	8.5	4.2	373

84	80	39	25	16	38	4.8	2.8	14300
85	100	61	23	2.9	24	7.9	3.7	22700
86	120	19	10	3.5	54	14	8	7170

[a] Liquid flow rate:0.23mL/min, gas flow rate: 0.9 mL/min, residence time: 6.5 minutes. Pressure: 10 bar.

4.1.3 Catalyst loading

The influence of catalyst loading was investigated, Table 28. It was found that there was a slight increase of conversion when mol% catalyst is increased from 0.025 to 0.1 mol%. The raw material was less than 3%. The left 30% of the raw materials were isomerized, which raised our interest to study the isomerization process to increase the conversion.

Table 28 The effect of catalyst loading on continuous hydroformylation.

Entry ^a	Catalyst Loading (mol %)	Conversion 20 (%)	l/b ratio	19 (%)	22 (%)	23 (%)	24 (%)	TOF (h ⁻¹)
87	0.025	59	23	2.9	24	7.9	3.7	22700
88	0.05	59	24	2.7	24	7	4.5	10953
89	0.1	61	23	2.7	19	8.3	5.1	5671

[a] Liquid flow rate:0.23mL/min, gas flow rate: 0.9 mL/min, residence time: 6.5 minutes. Temperature: 100 °C. Pressure: 10 bar

4.1.4 Residence time

The reaction residence time was varied by changing the linear velocity of the flow without altering the gas-liquid ratio, Table 29. It was found that the conversion was 52% at a residence time of 4.4 minutes in entry 90. By increasing the residence time to 6.5 and 13 minutes in entries 91 and 92, there was no significant change in the yield. It was noticed that the isomerization products accounted for the main by-products. In theory, the 2-octene and 3-octene can isomerize back to 1-octene and then convert into linear aldehyde but this process is slower than hydroformylation of 1-octene directly. Increasing the catalyst loading from 0.025

mol% to 0.1 mol% in entry 93 and 94 only raise the conversion by 2% and 8%.

Table 29 The effect of residence time on continuous hydroformylation

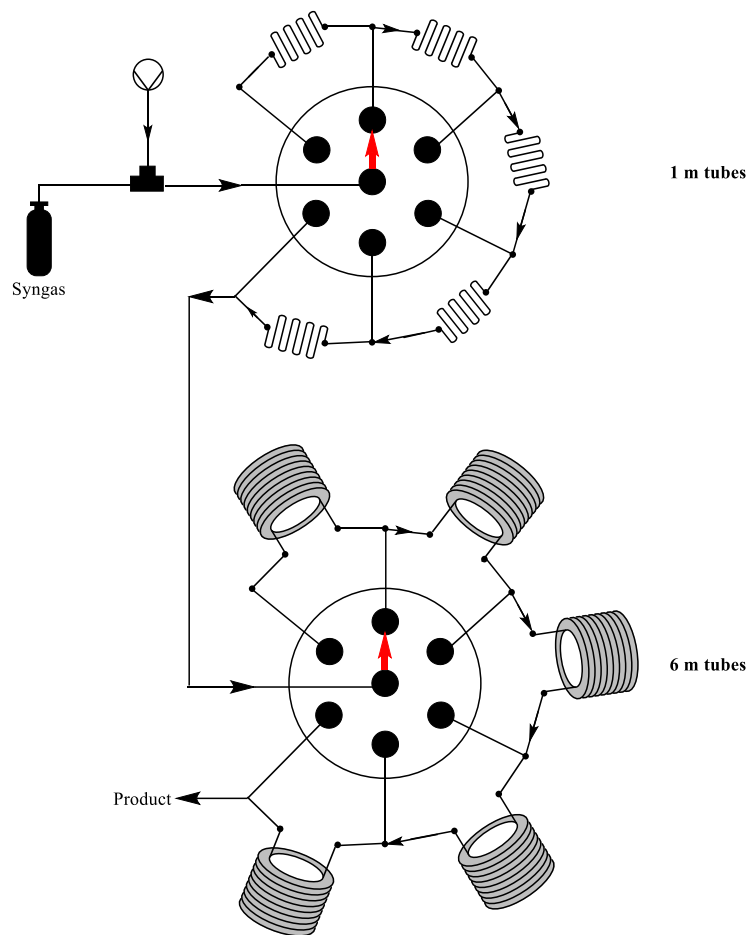
Entry ^a	TON	Residence Time (mins)	Conversion 20 (%)	l/b ratio	19 (%)	22 (%)	23 (%)	24 (%)	TOF(h ⁻¹)
90 ^b	4000	4.4	52	26	7	30	4.4	4.2	29800
91 ^c	4000	6.5	59	23	2.9	24	7.9	3.7	22700
92 ^d	4000	13	57	28	5	29	5	4	10600
93 ^c	1000	6.5	61	23	2.7	19	8.3	5.1	5671
94 ^d	1000	13	65	21	2.3	13	11	5.1	3008

[a] temperature: 100 °C, pressure: 10 bar. [b] Liquid flow rate:0.34 mL/min, gas flow rate: 1.35 mL/min. [c] Liquid flow rate:0.23mL/min, gas flow rate: 0.9 mL/min. [d] Liquid flow rate:0.12 mL/min, gas flow rate: 0.45 mL/min .

4.2 Multi-way valve reactors for kinetic study of the pressurized gas liquid reactions

Kinetic data, especially for high pressure high temperature gas-liquid reactions, can be difficult to acquire due to the high demand of reactor performance (mass transfer and heat transfer consistency, sampling speed) and suitable analytical tools. To the best of our knowledge, there are no kinetics studies in the time scale of seconds for pressurized gas liquid reaction. Acquisition of this data is difficult in batch reactors because the heating/cooling and mixing can take several minutes for each data point. Even with real time IR or UV, it usually takes an average of 15 seconds to remove noisy absorption data, which can miss information when the transformations are fast as this are in hydroformylation. On the other hand, the flow reactor stays at steady state after 3-5 times residence time, no matter how short this is, which offers a reliable method for kinetic determination. Furthermore, the microreactor heating and mixing times are much shorter than that of batch reactors. Hydroformylation of 1-octene undergoes an isomerization that will be studied using this new method.

We call the reactor a Flashstop reactor, shown in Scheme 15 and Figure 70.



Scheme 15 process diagram of Flashstop reactor

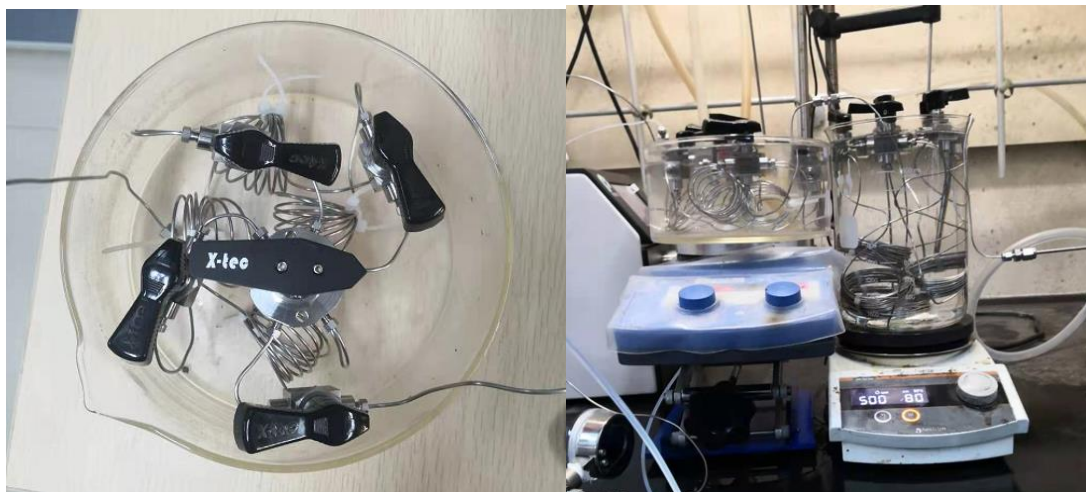


Figure 70 Flashstop reactor

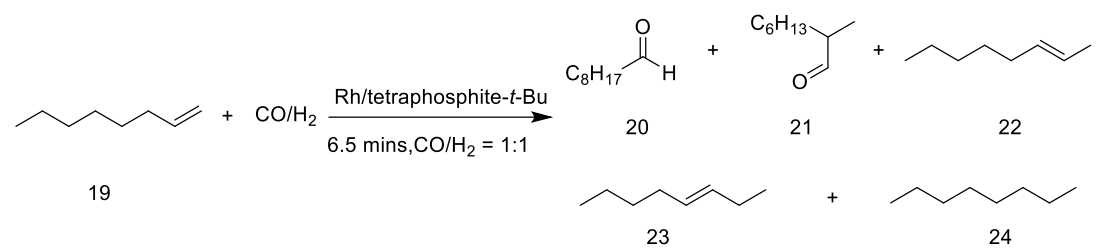
Five tubes of 1 or 6 m length and 0.057 cm inner diameter are connected between two ports of a 5-way valve, respectively. When the valve is set at a different port position, the fluid goes through reactors with different length that gives different residence time. This can offer 5 kinetics points. By connecting two 5-way valves, 24 kinetic points can be obtained. The

transient flow generated by varying the flow rate can be used to generate kinetic data without changing the length of the reactor. However, it is not adaptable to multi-phasic reactions because the changing of flow rate can change the mixing of liquid slug, even turn the Taylor flow into annular flow.

4.3 Kinetic studies in batch and flow reactors

The kinetic study was firstly done in batch by inline sampling without releasing pressure, Table 30. Figure 71 and Figure 72 show the kinetic data from entries 95 and 96, respectively.

Table 30 Conditions of kinetic in batch



Entry ^a	Temperature (°C)	Pressure (CO/H ₂)	TON	Reaction time (mins)	Conversion 20 (%)
95	100	5/5	4000	720	82
96	80	5/5	8000	60	47

[a] Concentration of 1-octene: 0.5 M. The reactor is 100 mL Mettler Toledo EasyMax 102 Advanced.

Kinetic study was firstly done in batch by inline sampling with a catalyst loading of 0.025 mol% under 100 °C and 10 bars in entry 95. In 15 minutes, 90% of 1-octene was consumed and 40% of the raw material was isomerized to 2-octene. The production of l-aldehyde slowed down after 45 minutes, because there was only 3.4% of 1-octene left. To study the rate of isomerization more precisely, the catalyst loading, and temperature was lowered in entry 96 to slow down the reaction. The kinetic data is shown in Figure 71 and Figure 72. The production of l-aldehyde slowed down after 60 minutes with 50% isomerized product, including 2-octene and 3-octene, and 5% 1-octene left. In Figure 72, 37% of 1-octene was isomerized to 2-octene and 3-octene in 5 minutes. There was 62% of reactant consumed.

The kinetic data at 5 minutes reaction was inaccurate; even though the reaction was set to

heat to 100 °C, internal temperature monitoring showed it was too short to achieve this. When the reactor was pressurized in batch, a sudden temperature increase was also observed. Therefore, a microfluidic device was designed and constructed to investigate the kinetic data.

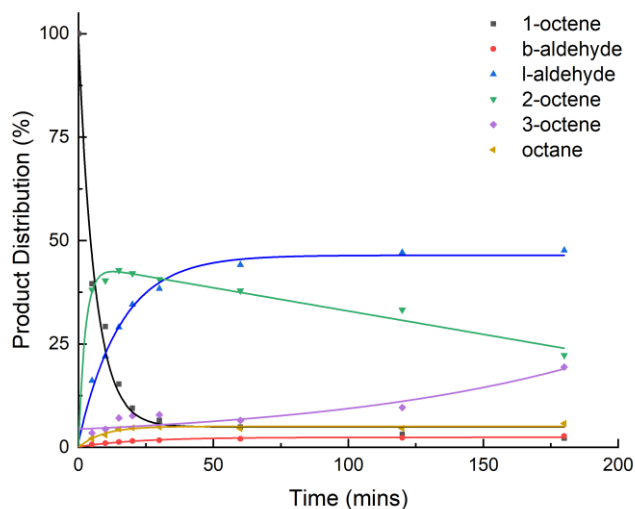


Figure 71 Kinetic in 200 minutes

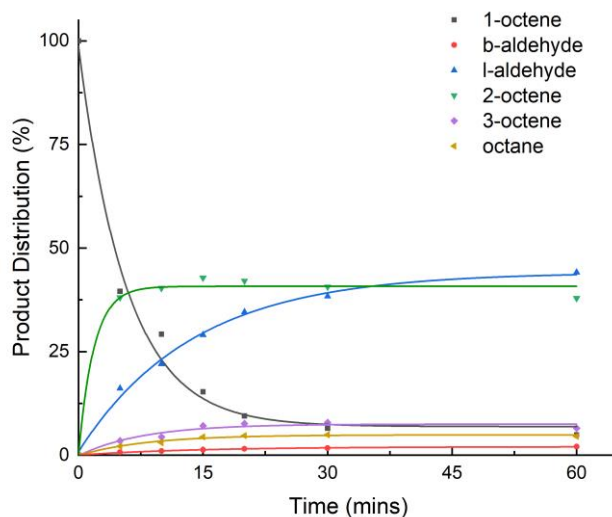


Figure 72 Kinetic in 60 minutes

This kinetic data was acquired in the micro-reactor system shown in Figure 73. Zero-order kinetics was observed in the first cycle from 6.6 s to 32 s. However, the data of the second cycle fluctuated. This could be because the reaction medium was cooled down between two sets of reactors, which caused the catalytic cycle to be interrupted. Thus, the two sets of

reactors were dissembled to avoid the cooling part.

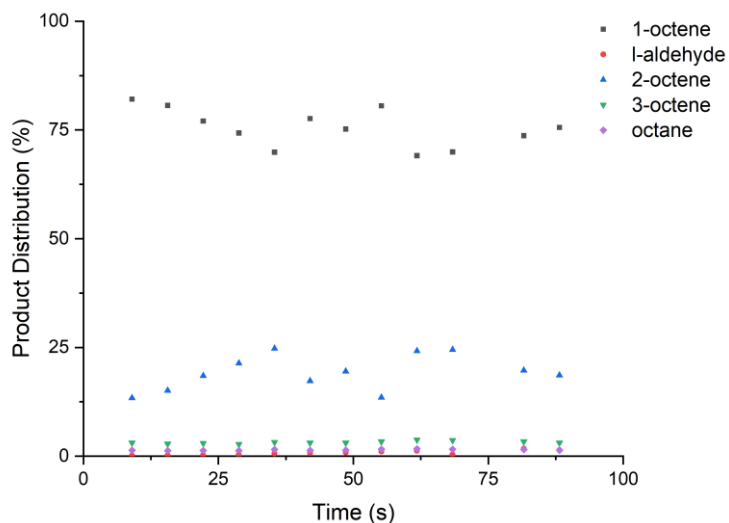


Figure 73 Kinetic in combination of two sets of microreactor

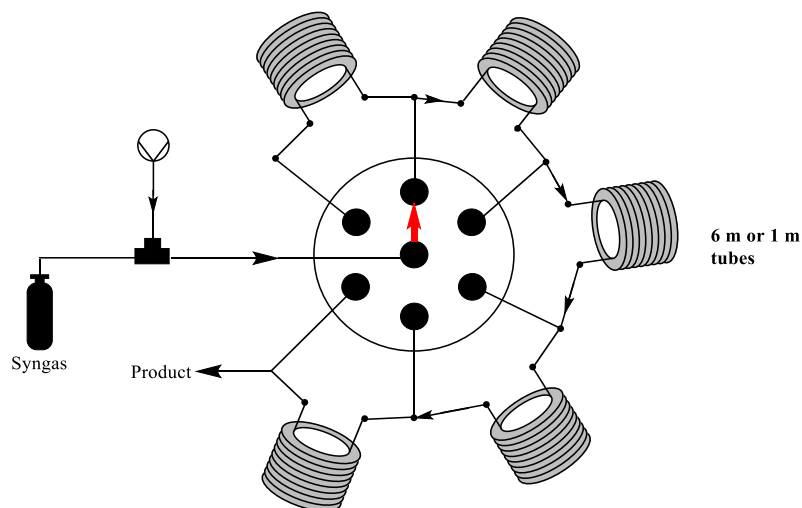
Table 31 shows the kinetic data of a reaction run at 10 bar and 80 °C (temperature limit of the valve was 80 °C.) in the 6 m tube unit flashstop reactor (Scheme 16). The gas flow rate was 6.6 sccm and the liquid flow rate was 0.23 mL/min. TON was 4000.

Table 31 The reaction rate under 10 bars in 6 m tubes unit flashstop reactor

	r (mol · L ⁻¹ · s ⁻¹)	R ²
1-octene	0.00054	0.99
2-octene	0.00027	0.98
l-aldehyde	0.00017	0.99

Continuous hydroformylation under 10 bars, with kinetic data plotted in Figure 74, shows that within 313 seconds, 70% of 1-octene is consumed and the yield of 2-octene was 40%, whilst that of l-aldehyde was 11%. 3% hydrogenation product, octane, was generated in 9 s and this increased to 4.1% in 313 s. 1-octene, 2-octene and linear-aldehyde all showed zero order kinetics under this condition.

It was noticed that in the first 9 s, 35 % of 1-octene was consumed. By 6 m tube unit, this part of kinetics cannot be resolved. Thus, a 1 m tubes unit flashstop reactor was constructed to study kinetics with smaller time slug.



Scheme 16 Single unit flashstop reactor

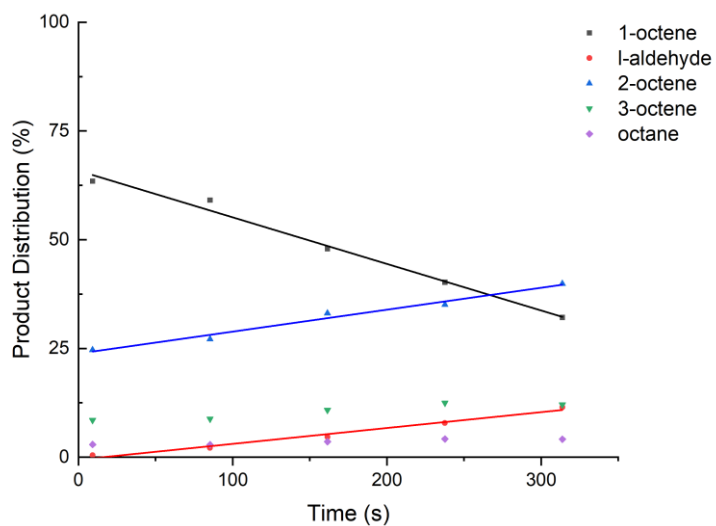


Figure 74 Kinetic under 10 bars in the 6 m tube unit flashstop reactor

Figure 75 and Table 32 show the kinetic data at 10 bars in the 1 m tube unit flashstop reactor.

Table 32 Reaction rate in a 1 m tube unit flash stop reactor.

	r ($\text{mol} \cdot \text{L}^{-1} \cdot \text{s}^{-1}$)	R^2
1-octene	0.0024	0.99
2-octene	0.0022	0.98
l-aldehyde	0.000099	0.8

In 28 s, 30% of 1-octene are consumed. The yield of 2-octene was 25%, while that of linear-

aldehyde, octane and 3-aldehyde were all less than 2%. 1-octene and 2-octene all showed zero-order kinetics under this condition. The kinetic constants determined are shown in Table 32. These are all 4 times larger, than those using the 6 m flashstop reactor. The production of l-aldehyde was slower in the beginning.

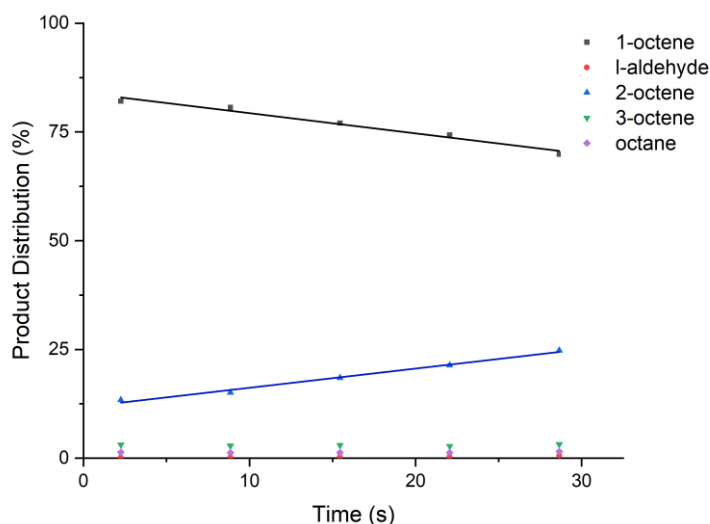
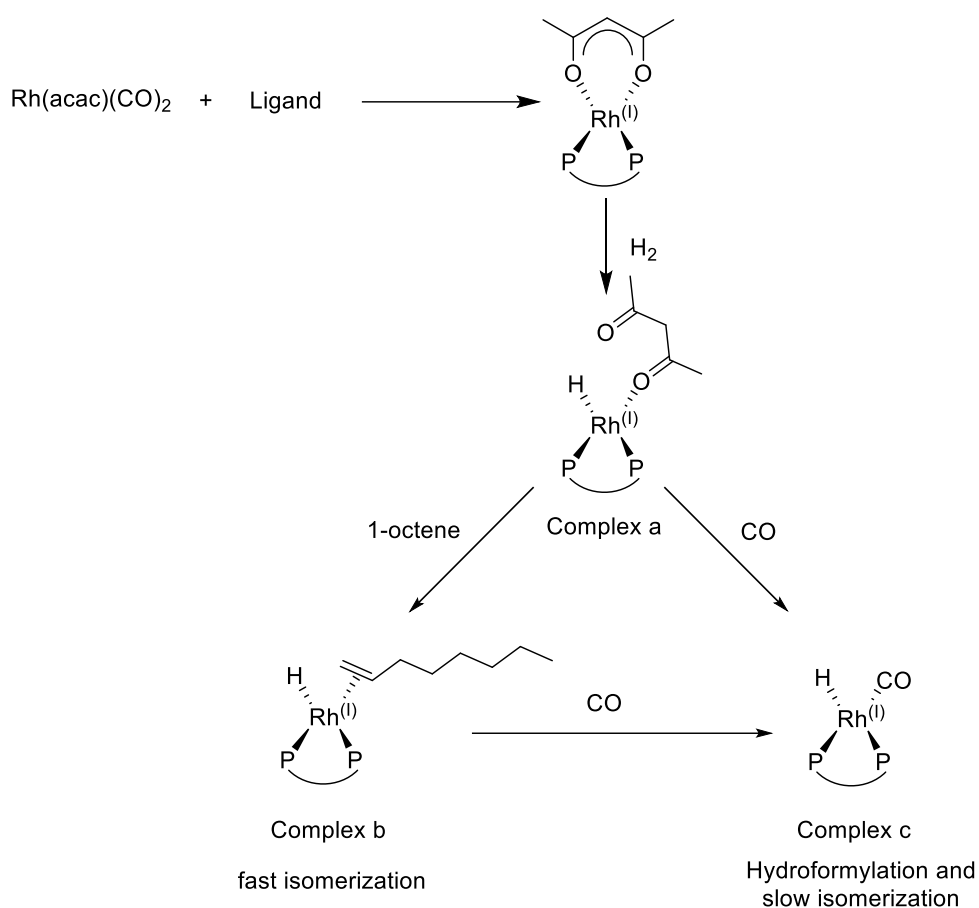


Figure 75 Kinetic under 15 bar in the 1 m tube unit flashstop reactor

The data in Figure 75 shows the isomerization kinetic constants in the initial 30 seconds were $0.0024 \text{ mol} \cdot \text{L}^{-1} \cdot \text{s}^{-1}$, which was 4.4 times that in the 85s – 330s residence time, $0.00054 \text{ mol} \cdot \text{L}^{-1} \cdot \text{s}^{-1}$. This can be explained by the formation of the monohydride complex (b) that coordinates with 1-octene in Scheme 17. $\text{Rh}(\text{acac})(\text{tetrphosphite})$ was generated by in-situ coordination. Once the reactor was pressurized, the hydride was first to formed, assisted by acac, to generate a monohydride complex that coordinates with the ketone. Both 1-octene and carbon monoxide could replace ketone as the ligand. Since the concentration of 1-octene (0.5 M) is higher than that of carbon monoxide (0.04 M under 5 bar CO and 373 K).^[123] In the initial 30 seconds, the monohydride complex (b) coordinates with 1-octene which accounts for the fast isomerization. As the 1-octene was consumed, the concentration of 1-octene decreased and was replaced by carbon monoxide. The rate of isomerization decreases and the rate of hydroformylation increases. This explains the initial fast isomerization and slowing down afterwards. With the presence of complex a, aldehyde cannot be generated, which explains the initial low production rate of aldehyde.



Scheme 17 Initiation of hydroformylation catalytic cycle

To study this further, the effect of syngas pressure was studied. Table 33 shows the rate constants under different pressures at 80 °C and Figure 76 the graphical residence time conversion data for formation of the l-aldehyde under different CO/H₂ pressures (detailed kinetics can be found in appendix.).

Table 33 kinetic constants of l-aldehyde

	$r (\text{mol} \cdot \text{L}^{-1} \cdot \text{s}^{-1})$	R^2
5 bar	0.00038	0.98
10 bar	0.00017	0.99
15 bar	0.00016	0.99
20 bar	0.00012	0.99

The reaction gave the highest yield at 5 bars. As the pressure increased, the production rate of l-aldehyde slowed down.

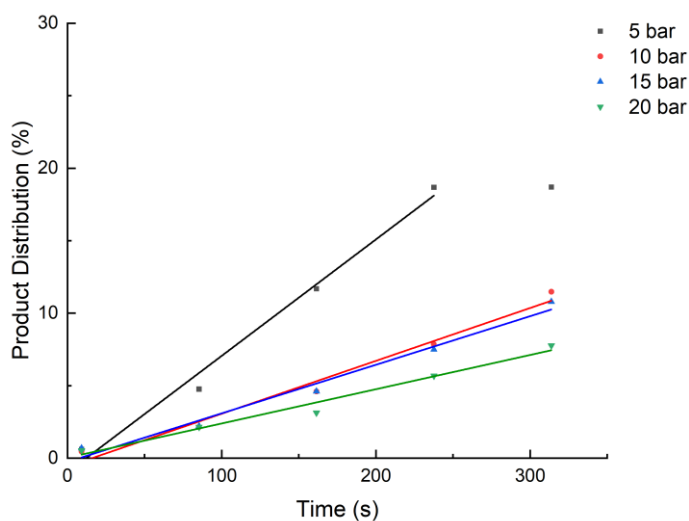


Figure 76 Effect of pressure on l-aldehyde generation

Figure 77 shows generation of the isomerized product (2-octene and 3-octene). As the pressure was increased, the isomerization rate decreased. This can be explained by the increasing pressure of carbon monoxide that facilitated the generation of dicarbonyl complex and inhibited the isomerization. Figure 78 shows the consumption rate of 1-octene. As the pressure increased, the rate decreased.

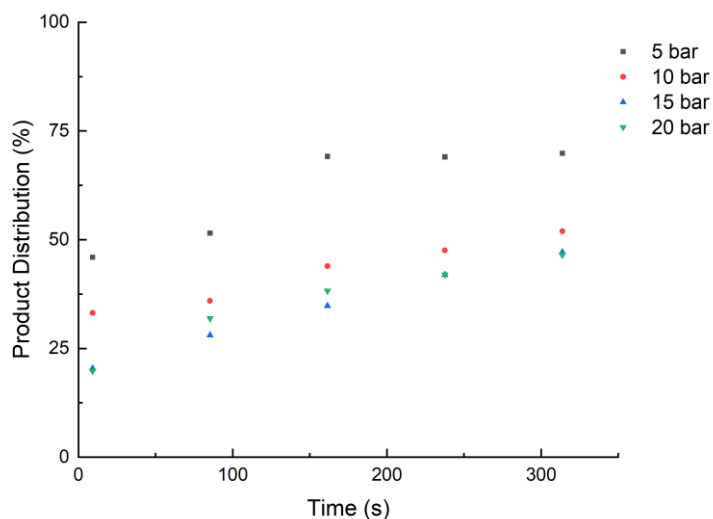


Figure 77 Effect of pressure on isomerization

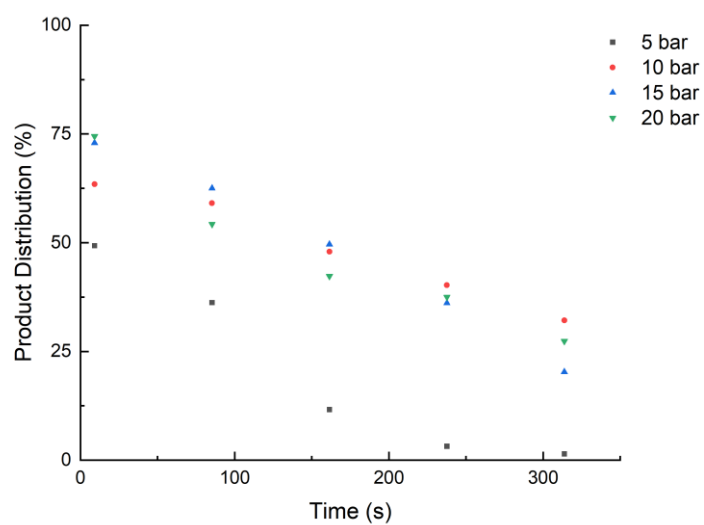
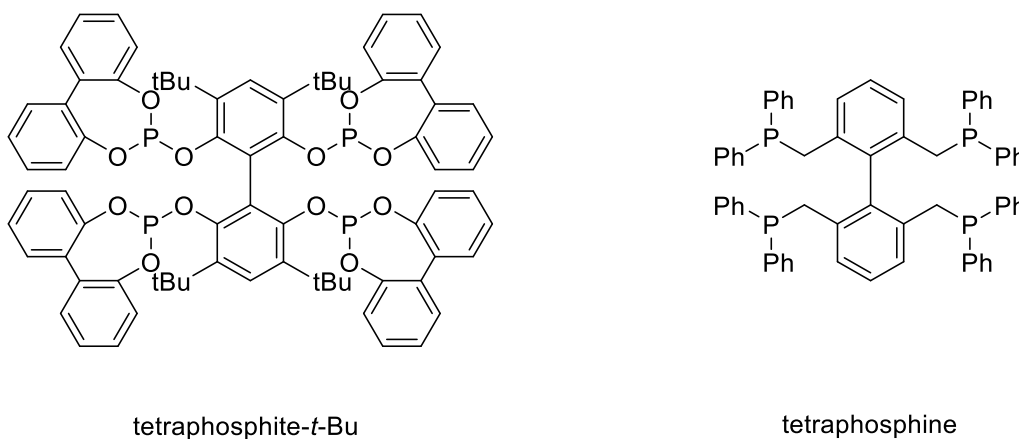


Figure 78 Effect of pressure on 1-octene consumption

To improve the catalyst, two types of ligands were compared, tetraphosphite and tetraphosphine, Scheme 18.



Scheme 18 Ligands adopted in this study

Figure 79 shows the kinetic data for the phosphite ligand under 10 bar and at 100 °C.

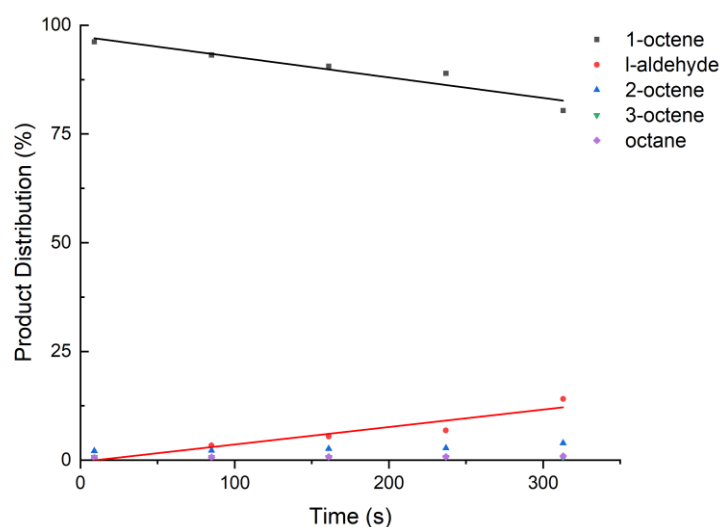


Figure 79 Kinetic study of tetrabis ligand

Since the yield of l-aldehyde was only 3% at 313 seconds residence time and 80 °C, the temperature was raised to 100 °C. It was found that the isomerization, using phosphine ligand, is much slower than that when using phosphite ligand, shown in Figure 80.

a/i is the production rate ratio between linear-aldehyde and isomerized products, 2-octene and 3-octene. At 320s, the ratio achieved 3.15 with the tetrakisphosphine ligand, whilst for the tetrakisphosphite ligand, the ratio was 0.4. This is a result of the coordination of carbon monoxide, as the hydroformylation cycle is faster when using the electron-rich phosphine ligand. However, the activity of the tetrakisphosphine-Rh was worse than that of tetrakisphosphite-^tBu. This can be explained by the coordination of carbon monoxide in the tetra-coordinated active species that deactivates the catalyst.

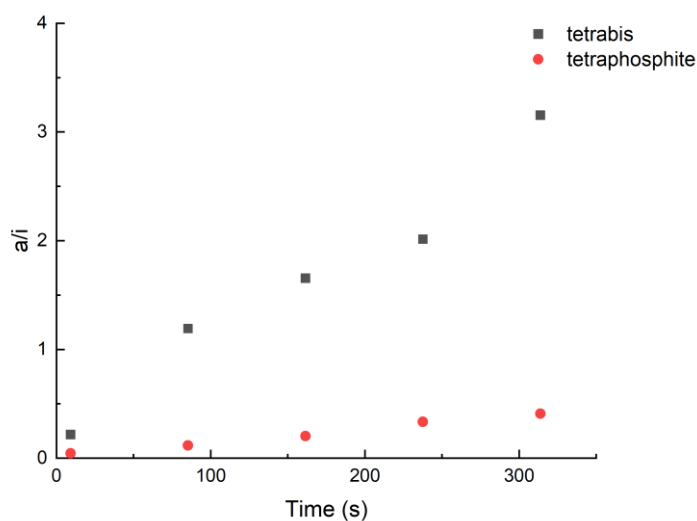


Figure 80 Comparison between tetraphosphine and tetraphosphite ligand

The kinetics for hydroformylation of 2-octene at 10 bar and 80 °C is shown in Figure 81. The reaction rate was much slower than that of 1-octene. Because the hydroformylation could happen after the isomerization, the isomerization process from 2-octene to 1-octene was slower than that from 1-octene to 2-octene.

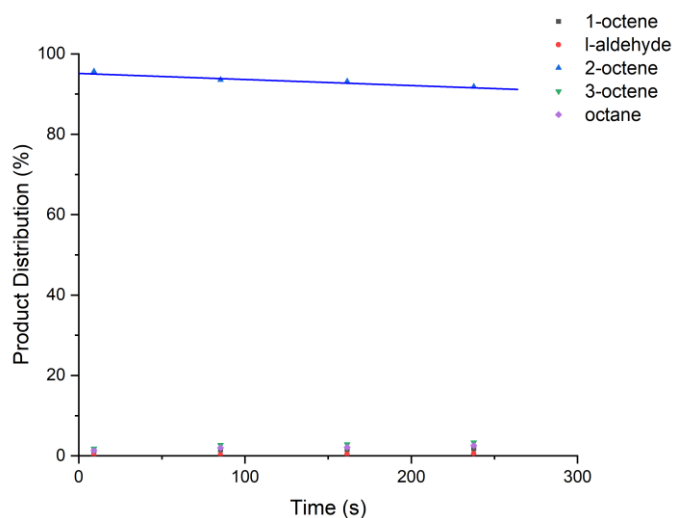
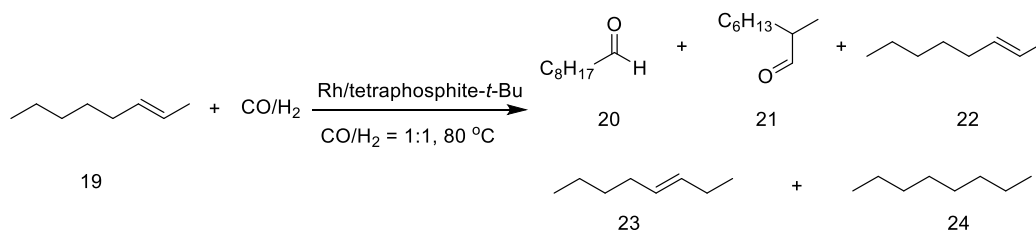
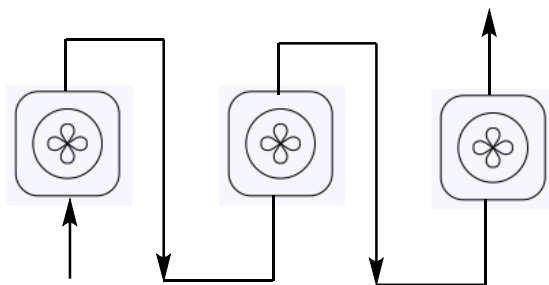


Figure 81 Kinetic study of hydroformylation of 2-octene

4.4 Continuous hydroformylation in a vertical fReactor system

The idea behind this reactor design, is to decouple the liquid and gas flow rate, scheme 19. This overcomes problems with the slug flow reactor that transports liquid slugs and gas bubbles with the same linear velocity and the slug flow become unstable when the increasing of gas liquid ratio is required for more concentrated reaction medium. When the fReactor is set up vertically, the gas flows through the reactor more quickly than liquid does. Therefore, compared to the slug flow reactor, a longer residence time can be obtained with less reactor volume. The main parts of the system are the vertical fReactors that are connected by narrow tubes. For each fReactor, the liquid inlet is the lower port of the reactor, while the outlet is the upper port of the reactor. The setup is shown in Figure 82 and Scheme 19.



Scheme 19 process diagram of vertical fReactor system

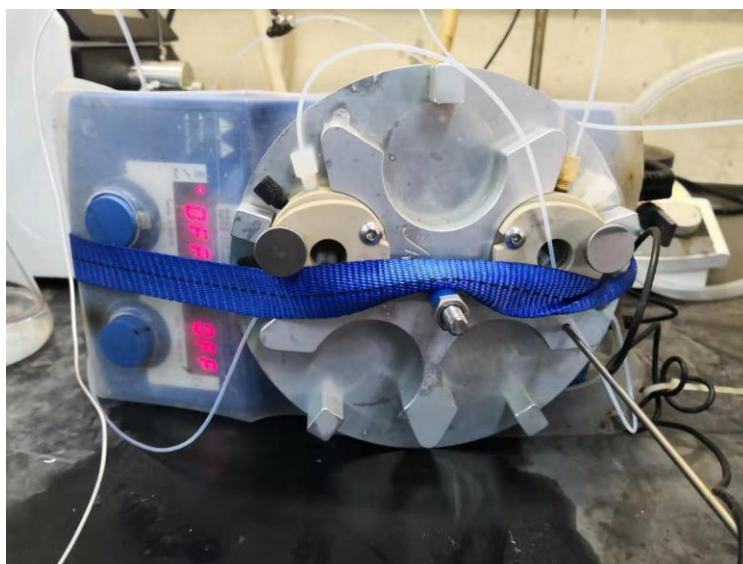
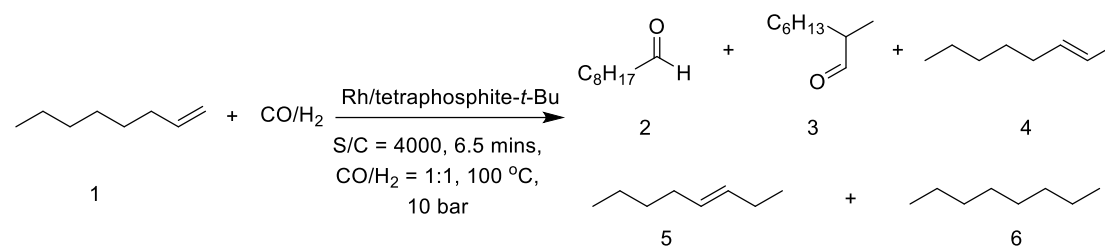


Figure 82 vertical fReactor system

Table 34 presents the results obtained using the vertical fReactor system.

Table 34 Results in vertical fReactor system

Concentration: 2.5 M

Entry ^a	gas flow rate (mL/min)	Conversion 20 (%) ^b	l/b	19	22	23	24
				(%)	(%)	(%)	(%)
97	4.5	44	13	2.3	23	20	6.9
98	9	42	15	2.4	26	21	6.4

[a] liquid flow rate:0.23mL/min; [b] conversion was determined by GC.

In this set-up, the concentration of 1-octene could be increased to 2.5M. This is impossible in the slug flow because it would require a 2.5 M hydrogen concentration, besides which the gas: liquid volume ratio is 15:1, which in a tube would give annular instead of slug flow. In the vertical fReactor configuration, the conversion was 44% and the production rate was 0.253 mmol/min, entry 97, which is 4 times that in the slug flow reactor, 0.069 mmol/min. The space time yield was 9.8 g•min⁻¹•L⁻² which was almost 10-times that of the slug flow reactor, 1.2 g•min⁻¹•L⁻². However, the ratio of linear to branched aldehyde was worse. Whilst the conditions need to be further optimized, it was shown that operating in this way is a viable method for improving the productivity of this gas-liquid reaction. Although there was active mixing in the fReactor, operating vertically gave poor stirring and both phases were stratified, which worsened the gas liquid mass transfer. Further modifications to the reactor design need to be considered to improve the efficiency of the system.

4.5 Conclusion

It was found that the initial isomerization rate of hydroformylation was very fast. In 5

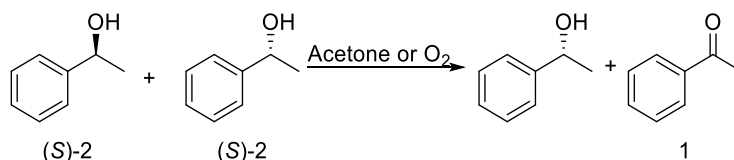
minutes, there was 60% 1-octene isomerized, which made it impossible to study this process by batch reactor. To study this quick process, a micro-reactor for acquiring kinetic data with a time scale of second for the pressurized gas liquid reactions was developed. The isomerization of alkene in hydroformylation was studied. It was found that the reaction rate of the first 30 seconds was four times as high as the first 300 seconds. This was explained by a monohydride complex without carbon monoxide presented in the first 30 seconds. The discovery of this phenomenon helps the development of catalysts enabling fast isomerization. To overcome the problem of unstable Taylor flow under high gas-liquid ratio in slug flow reactor, vertical fReactor system that decouples gas and liquid flow rate was developed to prolong the reaction time and increase the space time yield.

Chapter 5: Controlling diastereoselectivity: Integrating asymmetric (transfer) hydrogenation and transfer dehydrogenation.

A continuous reactor system was designed and evaluated with the aim of improving the diastereoselectivity in asymmetric reactions by combining hydrogenation, transfer hydrogenation and transfer dehydrogenation. A single enantiomer can be selectively oxidized by asymmetric dehydrogenation (ADH) with the production of unsaturated bond. The product can be reduced by asymmetric (transfer) hydrogenation (AH, ATH) to enrich the desired enantiomer. This strategy might outperform a single reaction, using AH or ADH alone, in terms of enantio- and diastereoselectivity, which can be used to tackle some challenging substrates.

5.1 Reaction modelling using Matlab for controlling diastereoselectivity

The asymmetric dehydrogenation of phenylethanol in Scheme 20 was firstly modelled in Matlab to validate the idea (code in Appendix).



Scheme 20 ADH of 1-phenylethanol

It was assumed that the reaction is first order to substrate, racemic alcohol in our case, and there was no catalyst deactivation. Reaction rates of the alcohols with R and S configuration can be expressed by the equations as followed where r is reaction rate, k the rate constant and c the concentration of S and R enantiomers:

$$r_S = k_S * c_S \quad \text{Equation 7}$$

$$r_R = k_R * c_R \quad \text{Equation 8}$$

Figure 83 shows the reaction progress of an asymmetric dehydrogenation reaction. It is assumed that k_R is 0.01 and k_S is 0.06. As the reaction goes on, the ee increases and the alcohol is consumed. If there is a difference between k_S and k_R , 99% ee can be achieved with certain period of reaction time. Figure 84 shows the effect of the ratio S and R rate constants on the

reaction. The blue points are the time required to reach 95% ee and the orange points the moles of alcohol remaining with 95% ee. When the ratio of k was 2, which means k_S was twice as big as k_R , the reaction time was 728 minutes and the resulting concentration of alcohol was 0.0013 M. If k_R is kept constant, as the ratio of k is increased, the reaction time falls and the resulting concentration of alcohol increases. When the ratio raises to 20, the reaction takes 36 minutes to achieve 95% ee with an alcohol concentration of 0.0428 M left after the asymmetric dehydrogenation.

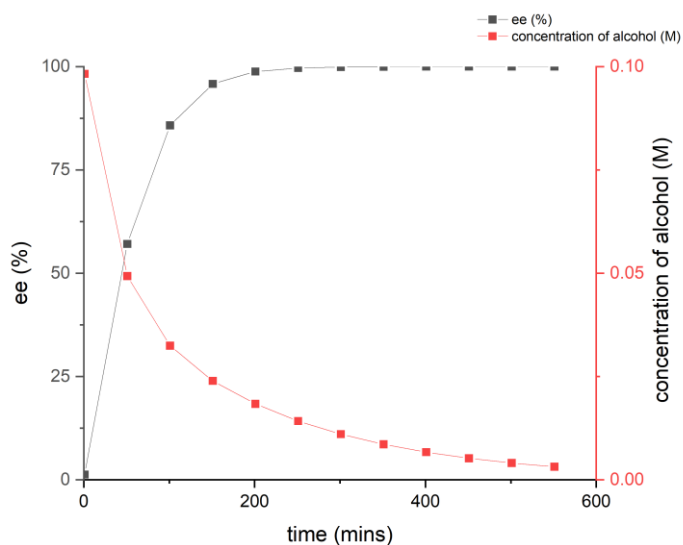


Figure 83 kinetic profile of ADH reaction

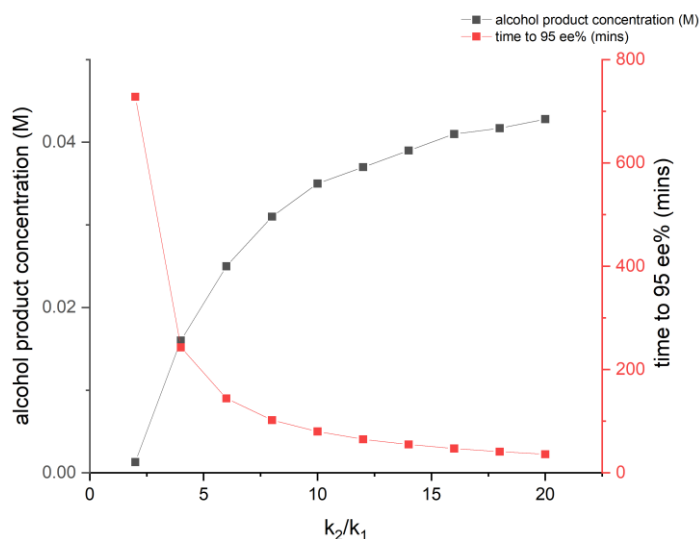


Figure 84 Effect of k_S/k_R ratio on reaction time to achieve 95% ee and alcohol product concentration.

Figure 85 shows the reaction progress when a reducing agent without enantiomeric induction is added, such as NaBH₄. It is assumed that k_R is 0.01 and k_S is 0.02. It is assumed that the reaction rate of the reducing agent is much faster than that of dehydrogenation and two reactions do not interact with each other. The ee reaches an equilibrium of 33%.

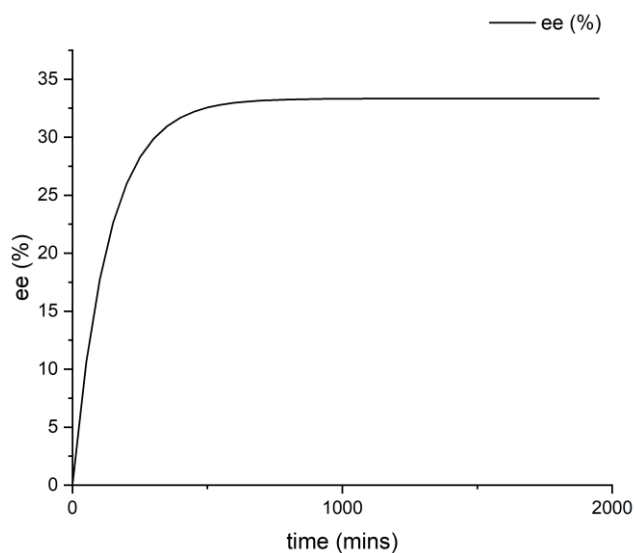


Figure 85 Reaction progress of ADH with a racemic reducing agent in the system

Figure 86 illustrates the effect of k ratio. It can be found that as the k ratio increases from 2 to 20, the equilibrium ee raises from 33.3% to 90%.

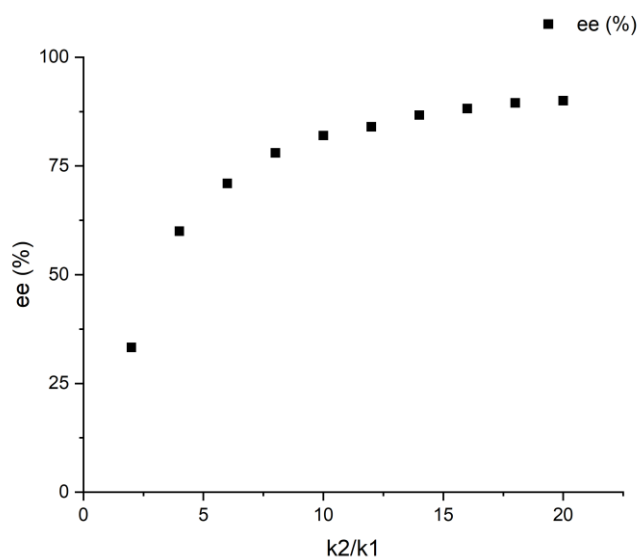


Figure 86 Effect of k_S/k_R ratio on equilibrium ee with a racemic reducing agent

Figure 87 shows the equilibrium ee when an asymmetric hydrogenation catalyst that gives

a 60% ee is mixed with an asymmetric dehydrogenation catalyst. It is supposed that the reaction rate of reducing agent is much faster than that of dehydrogenation and two reactions do not interact with each other. The equilibrium ee is increased, compared to the reaction using a reducing agent without any enantiomeric induction. It can be concluded that with the help of asymmetric dehydrogenation (k ratio equals to 10), the ee value can be raised to 95% ee, although the asymmetric hydrogenation catalyst only gives a 60% ee.

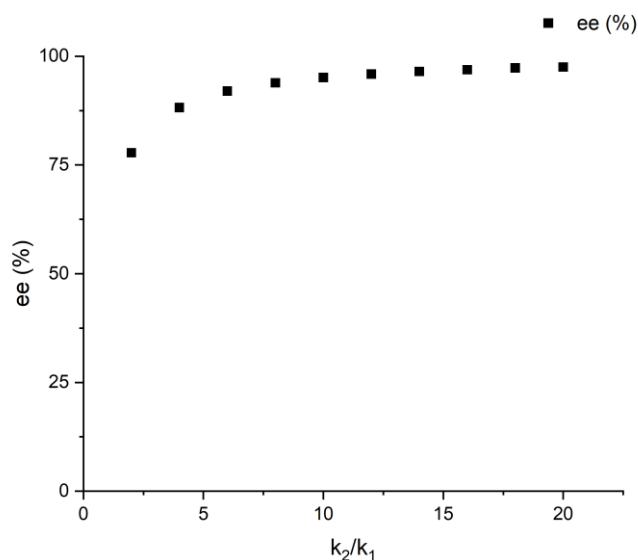


Figure 87 Reaction progress of ADH with a chiral ATH catalyst

Asymmetric hydrogenation and dehydrogenation are carried out separately in this case. It is assumed that k_R is 0.01 and k_S is 0.06. The ATH reaction is assumed to give a 60% ee and full conversion. The dehydrogenation is assumed to stop when 95% ee is achieved. Table 35 shows the results where the cycle starts with asymmetric dehydrogenation of the racemic alcohol. It can be concluded that, through 6 steps reaction, the enantiomeric excess can be raised from 60% ee when only using AH to 90% ee by combining asymmetric dehydrogenation and hydrogenation.

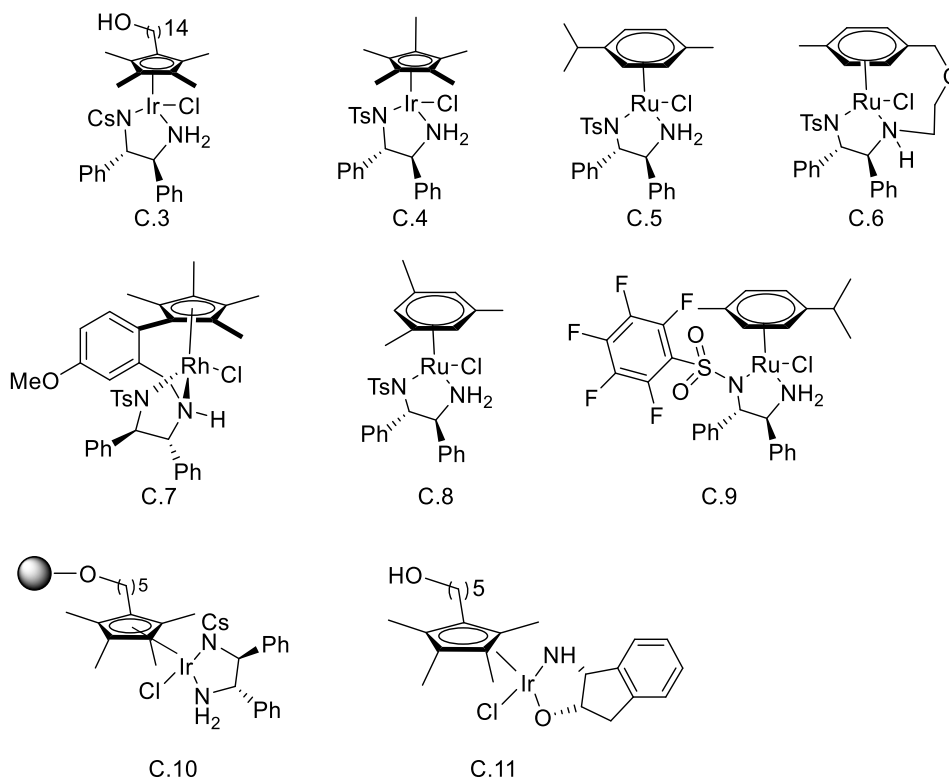
Table 35 Reaction progress with ADH and ATH carried out alternately.

#	ee (%)	Alcohol concentration (M)
	0	0.1
Step 1 (ADH)	95	0.025
Step 2 (ATH)	69	0.1
Step 3 (ADH)	95	0.058
Step 4 (ATH)	83	0.1
Step 5 (ADH)	95	0.073
Step 6 (ATH)	90	0.1

Since the reaction needs to run in cycle, a flow system containing immobilized catalyst could be a choice to automate the process, which will be explained in the next part.

5.2 Catalytic Systems

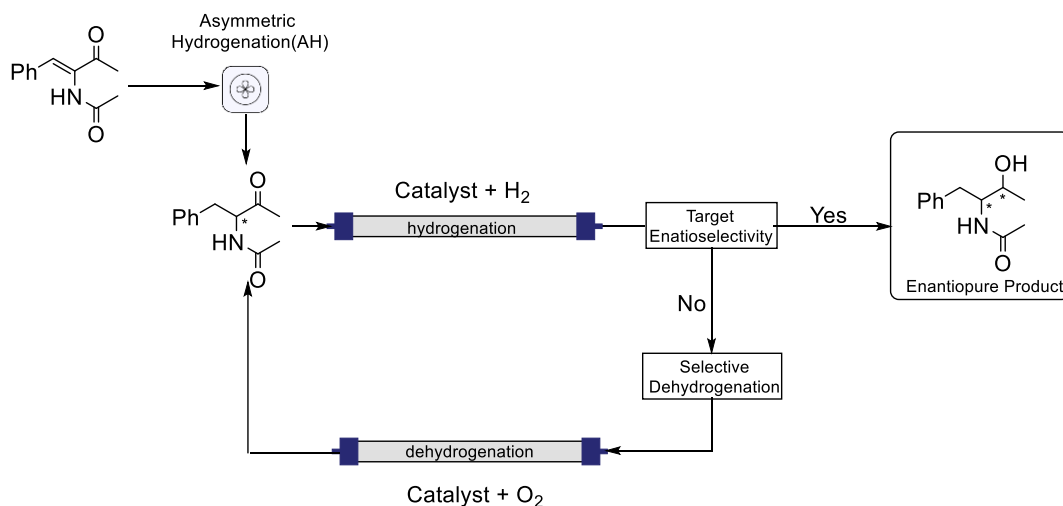
Scheme 21 shows all the catalysts used in the study. C.5, C.6, C.8, C.9 are commercially available. C.3, C.4, C.7, C.10 and C.11 were synthesized in Lab.



Scheme 21 Catalysts adopted in the study.

A continuous reactor system with multiple catalysts will be developed to hydrogenate complicated substrates, for example, anti Felkin-Anh substrates. The system will combine homogenous hydrogenation, heterogeneous hydrogenation, and dehydrogenation. The substrate for an HIV protease inhibitor was taken as an example, Scheme 22. The first step involves hydrogenating one of two unsaturated bonds to get one chiral centre. Then another catalyst is adopted for the second hydrogenation. There will be dynamic kinetic resolution during the second hydrogenation. The base and metal catalyst could racemize the existing chiral centre and the configuration favoured by the catalyst is selectively generated.

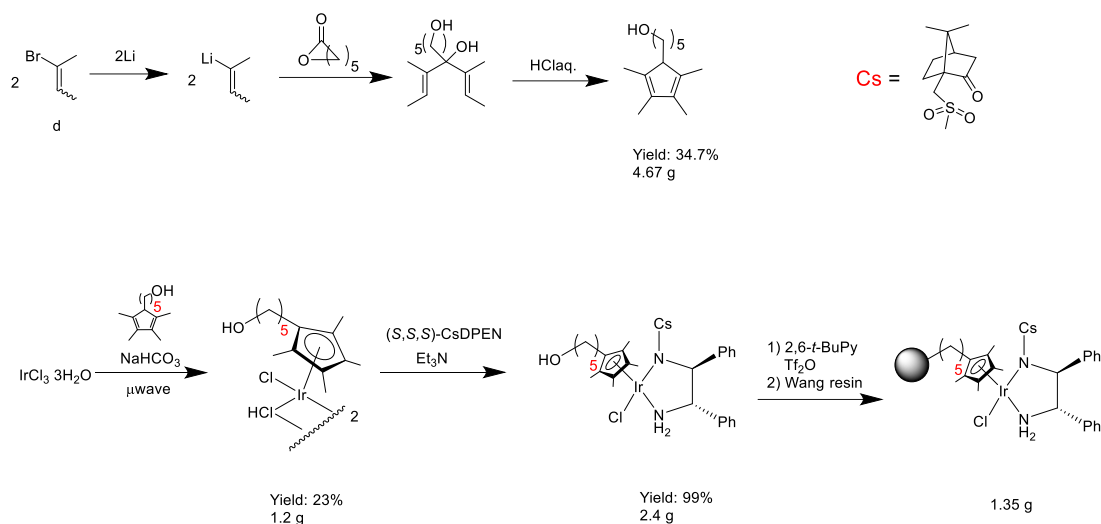
As well as hydrogenation, asymmetric dehydrogenation could be used to assist the diastereocontrol. The product could be selectively dehydrogenated by an asymmetric transfer dehydrogenation catalyst. Thus, the undesired configuration could be oxidized. The product will be hydrogenated again to enrich the desired configuration. There is decision point after transfer hydrogenation. If target enantioselectivity is achieved, sample will be collected. If not, this process could be carried on until the enantiopure compound with satisfactory purity is obtained. Scheme 22 shows the whole process for diastereocontrol.



Scheme 22 An Example of Continuous Flow System for Single Diastereomer Synthesis

$\text{Ru}(\text{OAc})_2(\text{BINAP})$ (C.1) and Rh-duphos (C.2) are chosen for the homogeneous hydrogenation of alkenes. The BINAP ligand was firstly reported for hydrogenation reaction in 1980. The Ru-BINAP ^[28, 120] and Rh-duphos ^[31a] complex were all proved to be efficient catalysts. This study will begin by using these catalysts.

The Ir[Cp*₅OH][(S,S)-TsDPEN]Cl@Wang (C.3) developed by Blacker's group was chosen as the catalyst for the heterogeneous transfer hydrogenation of alcohols.^[51f] The catalysts and synthetic route are shown in Scheme 23.



Scheme 23 Immobilized Asymmetric Hydrogenation Catalyst

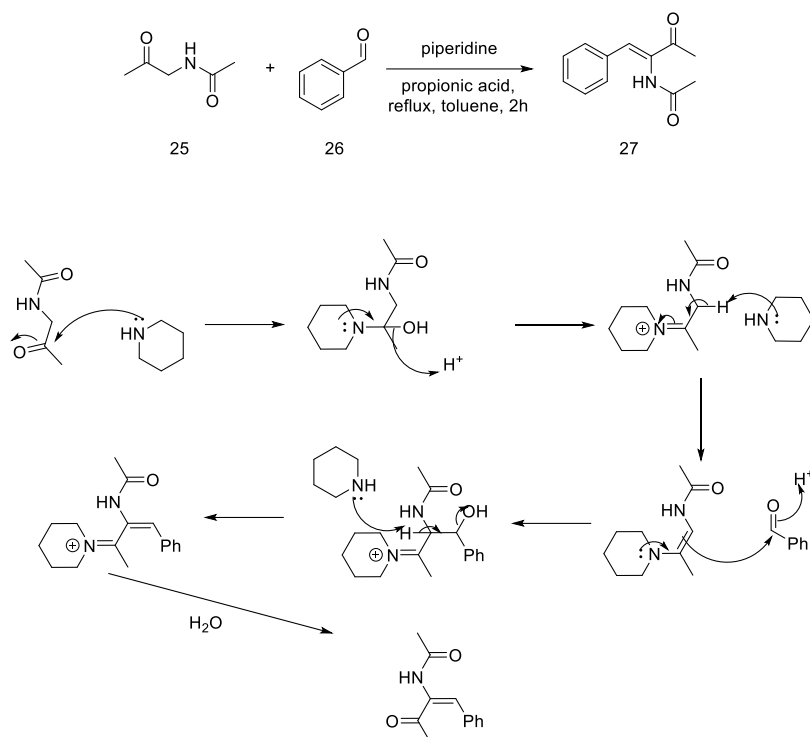
Dehydrogenation catalyst (C.11) is a new catalyst designed for asymmetric dehydrogenation. The homogeneous catalyst of ruthenium with Cp* and (1*R*,2*S*)-(+)-cis-1-Amino-2-indanol as the ligand has been proved to be effective in asymmetric dehydrogenation.^[90b] The Rhodium catalyst (C.7) has been proved to be effective in asymmetric transfer hydrogenation.^[46] It is shown in Scheme 21 and will be adopted for asymmetric transfer dehydrogenation. C.5 and C.6 are also used for dehydrogenation.

5.3 Synthesis of substrates

5.3.1 HIV protease inhibitor

The synthesis of the model substrate is enamine catalysis shown in Scheme 24.^[124] The aldol reaction is preferred in position 2, because of its stronger nucleophilicity. A Dean-Stark Apparatus was used to remove water to facilitate the reaction. The mechanism is elaborated in Scheme 24. Piperidine acts as a nucleophilic catalyst. The first step is the addition of the amine catalyst to the ketone to form an enamine. Then the loss of the proton results in the formation of a nucleophile. This *in-situ* generated nucleophile then adds to the aldehyde.

Subsequent elimination of the catalyst leads to the observed products.

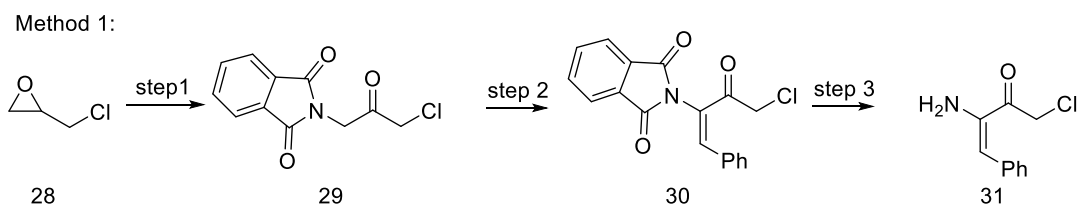


Scheme 24 Synthetic route of HIV protease inhibitor and mechanism

Two substrates that can be functionalized in the side chain were designed and synthesized. The proposed synthetic routes are shown in Scheme 25.

Method 1 is based on the synthesis of the model substrate.^[125] The imide group could be easily transferred to an amine group by step 3. Thus, it will be possible to connect other building blocks to the amine group. In addition, the chloride group can be substituted by other functional groups. The product of step 2, substrate 30, could be a basic building block for the HIV protease inhibitor. When tested, the condensation did not happen in step 2 and the reactant remained. Furthermore, epichlorohydrin and Jones solution are toxic, so this route was not further optimized.

For method 2,^[126] a Heck reaction was employed. Then the ester was functionalized by different reactions. For step 2, there is a possibility that the alkene in the product may act as an electrophile and it could perform a 1,4-addition reaction with ClCH_2I . Because LDA is adopted, the reaction condition could be harsh and difficult to handle.

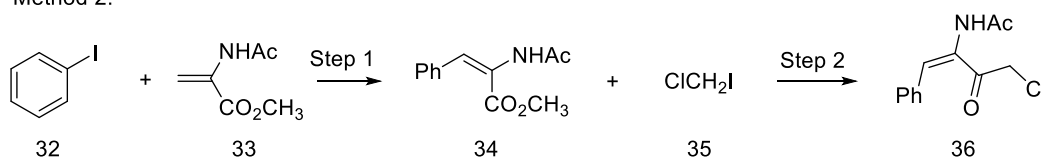


Step 1: 1 eq epichlorohydrin, 1.1 phthalimide, 0.05 eq pyridine, isopropynol, reflux, 3 h; then Dess-Martin Oxidation

Step 2: 0.015 eq piperidine, 0.03 eq propionic acid, 1.2 eq benzaldehyde, 4 h

Step 3: N_2H_4 , ethanol, reflux

Method 2:



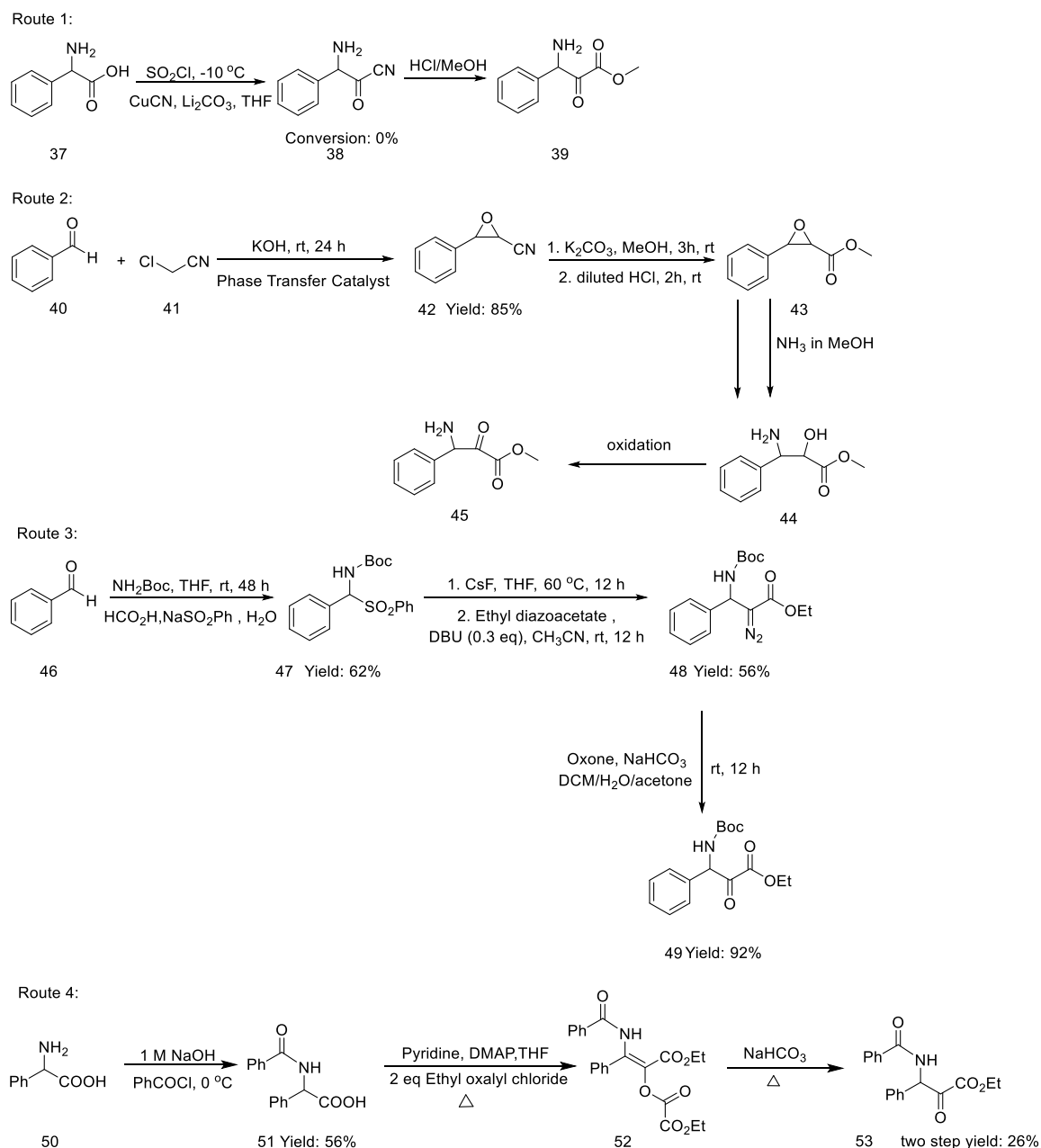
Step 1: (Heck Reaction): 4 eq olefin, 1.4 eq K_2CO_3 , 10 % Pd/C, 1 eq KCl, DMF, 100 °C, 15-24 h.

Step 2: ClCH_2I (4 eq), LDA (5 eq), THF, -78 °C

Scheme 25 Synthetic Route of Substrates

5.3.2 Paclitaxel side chain

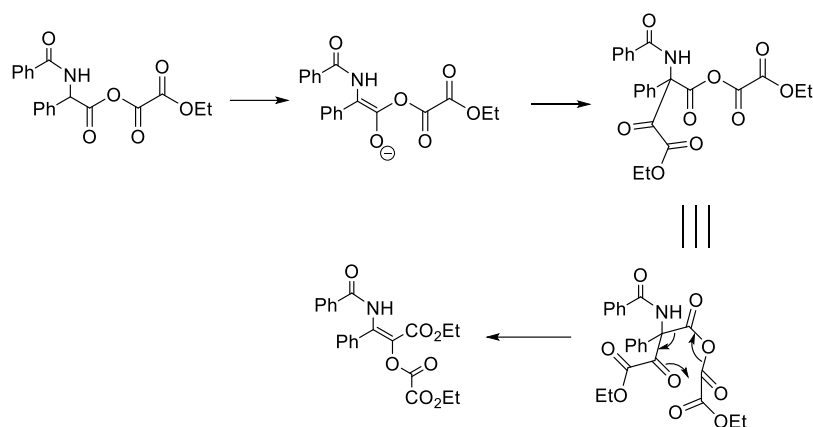
α -Hydroxy- β -amino acids and their derivatives are the indispensable moieties of many biological molecules and natural products.^[127] The side chain of paclitaxel is one of the most famous examples, which plays an important role in semi-synthesis of paclitaxel. Through retrosynthesis analysis, it can be obtained by asymmetric reduction of α -carbonyl- β -amino acids. Four synthetic routes of α -carbonyl- β -amino acids are proposed in Scheme 26.



Scheme 26 Synthetic route of α -carbonyl- β -amino acids

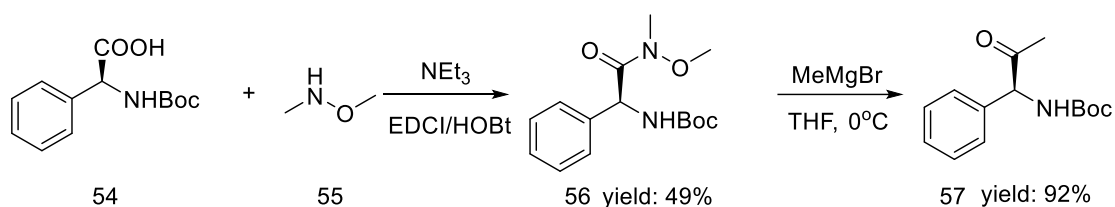
The first route was not used, because it involves sodium cyanide that is highly toxic.^[128] Copper cyanide was tried to replace sodium cyanide, but there was no conversion. The second route is an alternative way to introduce cyanide. However, the third step undergone an ester exchange by NH_3 and there was no desired product obtained. In the route 3,^[127] one of the intermediates has a diazonium salt with risk of explosion. This route was tried and proved to be viable. But the last step was not reproducible. Route 4^[129] had only three steps and started from readily available phenylglycine amino acid. The second step was a rearrangement

reaction, and its mechanism is shown in Scheme 27.



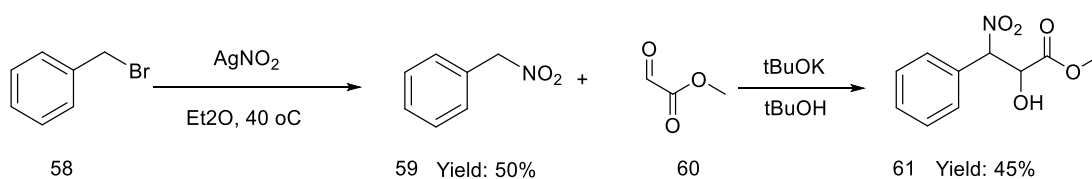
Scheme 27 Mechanism of step 2 in route 4

Scheme 28 shows the route for α -carbonyl- β -amino acids through a Weinreb ketone synthesis.^[130] In this method, the chiral center of the enantiopure amino acid can be preserved.



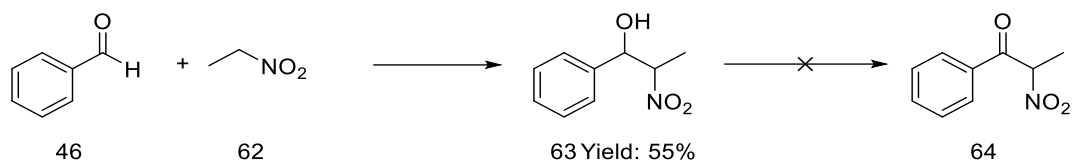
Scheme 28 Route 5 for synthesis of α -carbonyl- β -amino acids.

Scheme 29^[131] shows the synthetic route for α -carbonyl- β -amino acids by firstly synthesizing an α -nitro- β -hydroxy ester. The electron-withdrawing nitro group can assist diastereocontrol via dynamic kinetic resolution by accelerating racemization.



Scheme 29 Route 6 for synthesis of α -carbonyl- β -amino acids

2-nitropropiophenone was synthesized via nucleophilic attack of benzaldehyde by nitroethane in Scheme 30.^[132] The yield was 55%, however, oxidation of the alcohol to ketone by either Ley oxidation, TEMPO oxidation or Dess-martin oxidation resulted in a decomposition of the substrate.

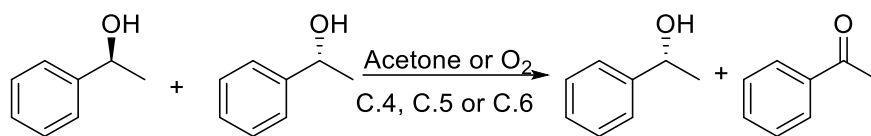


Scheme 30 Synthesis of 2-nitropropiophenone

5.4 Results of asymmetric transfer dehydrogenation

5.4.1 acetophenone

Acetone and oxygen in the air were used as oxidants for asymmetric dehydrogenation. The results are shown in Table 36. *In situ* generation C. 11 failed to work for this reaction in entry 99. C.3 is proved to give racemic product in entry 100-105, whilst RuCl(*p*-cymene)[(R,R)-Ts-DPEN] was found to be effective for asymmetric dehydrogenation. When acetone was used as the oxidant and KOH as base, phenylethanol with 79% ee was generated in entry 106 and the yield was 45% after 22h. Oxygen was also tested in entry 107, but the rate was very low, and only 12 % conversion was achieved after 24h. The reaction conditions of entry 108 were the same as that of entry 106, except it was heated to 100 °C to accelerate the reaction and make it adaptable to be carried out in microreactor. It was found that heating deteriorates the enantioselectivity of catalyst. A product of 8% ee was obtained with a conversion of 85%. The tethered Rh catalyst (C.7) had better activity than Ru catalyst in either system adopting acetone or oxygen as hydrogen acceptor. The enantioselectivity of C.7 was 79% in entry 110 and 112. Furthermore, using O₂ in the THF reaction system, the activity and enantioselectivity of C.7 was not deteriorated in entry 112, while there was almost no reaction by Ru catalyst by using air as oxidant in entry 107. NEt₃ is unable to activate the catalyst in both C.5 and C.7 catalytic system in entry 109 and 111. It was noticed that the alcohol products obtained by ATH and ADH had different configurations with the catalyst of the same configuration. Therefore, to enrich products of a certain configuration, catalysts with different configurations need to be adopted and they cannot coexist in a system. The immobilized catalyst can be used to tackle this problem.

Table 36 Results of ADH of 1-phenylethanol

Entry ^a	Catalyst	Base ^b	solvent	time(h)	Conversion (%) ^c	ee. (%) ^c
99	C.11	<i>t</i> BuOK	1 mL acetone	24	0	N.A.
100	C. 3	<i>t</i> BuOK	1 mL acetone	24	80	0
101	C. 3	NEt ₃	1 mL acetone	12	95	0
102	C. 3	KOH	1 mL acetone	12	92	0
103 ^d	C. 3	<i>t</i> BuOK	1 mL THF	24	95	0
104 ^d	C. 3	NEt ₃	1 mL THF	24	82	0
105 ^d	C. 3	KOH	1 mL THF	24	95	0
106	C. 5	KOH	1 mL acetone	24	45	79
107 ^d	C. 5	KOH	1 mL THF	24	12	5
108	C. 5	KOH	1 mL acetone	0.5	85	8
109	C. 5	NEt ₃	1 mL acetone	24	0	n.a.
110	C. 7	KOH	1 mL acetone	24	49.5	79
111	C. 7	NEt ₃	1 mL acetone	24	0	n.a.
112	C. 7	KOH	1 mL THF	24	48	79

[a] Entries 99-104 were under room temperature and Entry 108 was heated to 100°C by microwave. [b] 2 mol % base was added. [c] Conversion was measured by ¹H NMR and ee was measured by Chiral GC. [d] Reaction medium use oxygen in the air as oxidant.

The red catalyst had a chloride ligand initially and when KOH was added and stirred for 5 minutes, the reaction medium turned green, which meant that amido form was obtained, Figure 88. After 1-phenylethanol was added, the reaction medium turned red gradually as the amino form resting-state was regenerated. The procedure to carry out the reaction was to pre-mix the catalyst and base in the solvent to generate amido form and then add the substrate to start the oxidation.^[133]

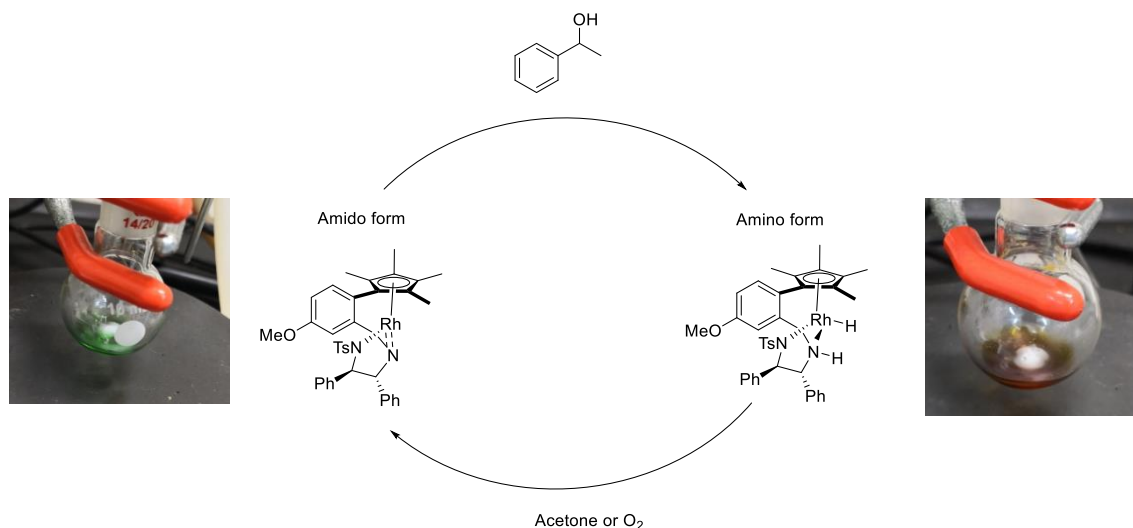
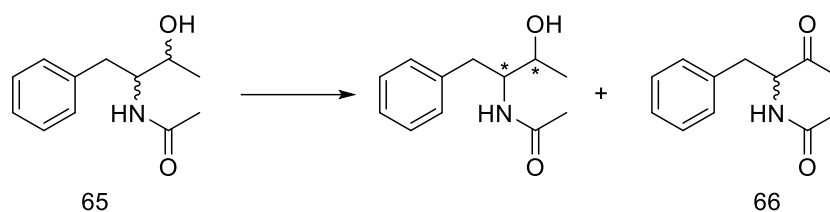


Figure 88 Mechanism of Dehydrogenation

5.4.2 HIV protease inhibitor

The dehydrogenation of substrate 65 did not result in the desired ketone, Table 37. There was no conversion when oxygen was the oxidant in entries 114 and 116. A byproduct was obtained when acetone was used as the oxidant in entries 113 and 115, which may be the condensation product of substrate and acetone.

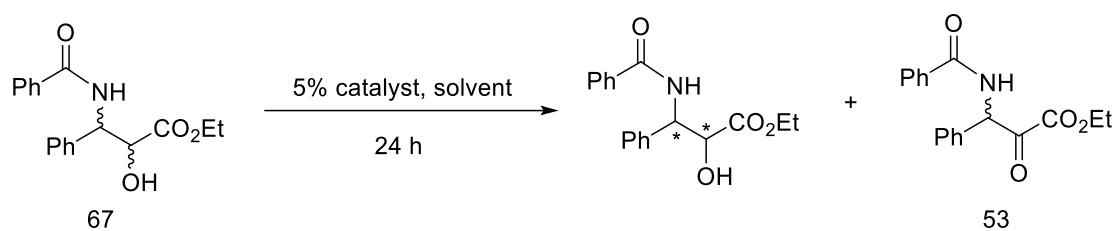
Table 37 ADH of HIV protease mode substrate

Entry ^a	Catalyst	solvent	Time (h)	Conversion (%) ^b	ee. (%)
113	C. 5	1 mL acetone	24	70	n.a.
114	C. 5	1 mL THF	24	0	n.a.
115	C. 7	1 mL acetone	24	65	n.a.
116	C. 7	1 mL THF	24	0	n.a.

[a] S/C/KOH = 100/1/2, room temperature, 24 h. [b] Conversion was monitored by ¹H NMR. Diastereomeric ratio and ee were measured by chiral GC.

5.4.3 Paclitaxel side chain

Table 38 shows the results of asymmetric dehydrogenation of substrate 67. Both rhodium and ruthenium catalysts showed poor activity in this reaction. Increasing temperature could not initiate the reaction.

Table 38 ADH of substrate 67

Entry ^a	Temperature (°C)	base	Catalyst	Oxidant	solvent	Conversion (%) ^b	ee (%)
117	rt	KOH or ^t BuOK or NEt ₃	C. 5	O ₂	Toluene	0	n.a.
118	60	KOH	C. 5	O ₂	Toluene	0	n.a.
119	rt	KOH or ^t BuOK or NEt ₃	C. 5	Acetone	Acetone	0	n.a.
120	60	KOH	C. 5	Acetone	Acetone	0	n.a.
121	rt	KOH or ^t BuOK or NEt ₃	C. 7	O ₂	Toluene	0	n.a.
123	60	KOH	C. 7	O ₂	Toluene	0	n.a.
124	rt	KOH	C. 7	Acetone	Acetone	0	n.a.
125	60	NEt ₃	C. 7	Acetone	Acetone	0	n.a.
126	60	KOH	C. 7	Acetone	Acetone	0	n.a.

[a] S/C/KOH = 100/1/2, room temperature, 24 h. [b] Conversion was monitored by ¹H NMR. Diastereomeric ratio and ee were measured by chiral GC.

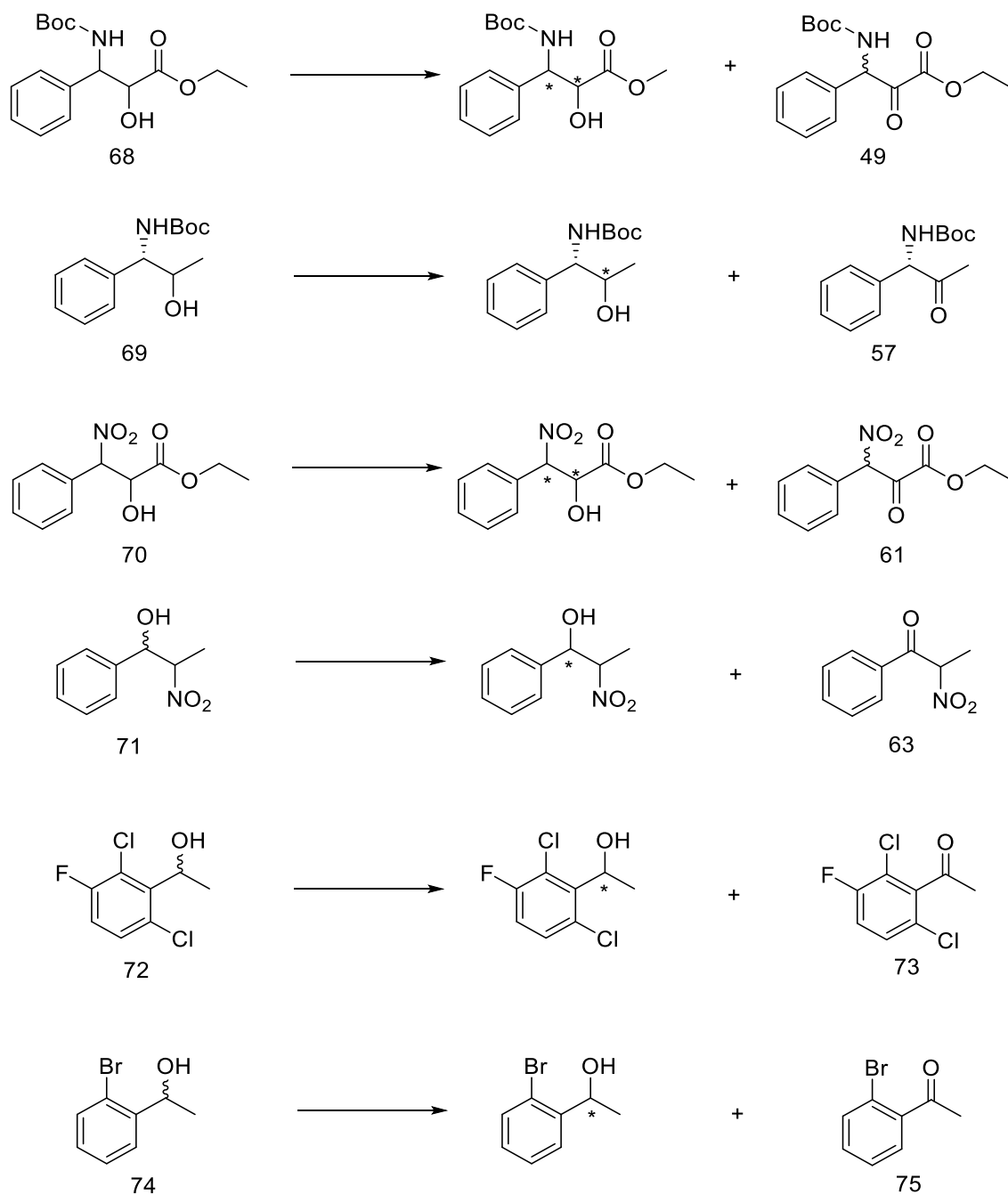
5.4.4 Asymmetric dehydrogenation of challenging substrates

A series of substrates were synthesized to test the asymmetric dehydrogenation reaction. Both rhodium and ruthenium catalysts gave no conversion in the dehydrogenation of substrates 68 and 69, the paclitaxel side chain derived substrates, entry 127 and 128 (Table 39). The amine group was replaced by nitro group for substrates 70 and 71. The presence of NEt_3 base could cause the retro-nitroaldol reaction with decomposition to the corresponding aldehyde and nitro raw materials. Therefore, the desired ketone product could not be obtained, entry 129 and 130. Substrate 72 is a challenging substrate that is an important API building block, because the carbonyl group was hindered by two chloride group in para position. It was found that the raw material remained intact after 24 hours in entry 131.

Substrate 74 can be oxidized by both catalysts C. 5 and C. 7. Dehydrogenation by ruthenium catalyst afforded 53% conversion, but the ee was 3% when acetone was used as the oxidant, entry 133. There was no conversion when O_2 was the oxidant, entry 132. Dehydrogenation by the rhodium catalyst afforded 41% conversion, 31% ee when using O_2 as the oxidant, entry 134, and 44% conversion and 38% ee when acetone was used as the hydrogen acceptor, entry 135.

Since the reaction is reversible, the amido form of the catalyst can also oxidize the isopropanol. The oxidation rate of substrate needs to surpass that of isopropanol to push the equilibrium in the desired direction. To overcome the low reactivity problem, the hydrogen acceptor can be altered by increasing the stability of the corresponding alcohol.

Table 39 ADH of challenging substrates



Entry ^a	Substrate	base	Catalyst	solvent	Conversion (%) ^b	ee (%)
127	68	KOH or ^t BuOK or NEt ₃	C.5 or C.7	Toluene/ Acetone	0	n.a.

128	69	KOH	C.5 or C.7	Toluene/ Acetone	0	n.a.
129	70	KOH or ^t BuOK or NEt ₃	C.5 or C.7	Toluene/ Acetone	>99	n.a.
130	71	KOH	C.5 or C.7	Toluene/ Acetone	>99	n.a.
131	72	KOH or ^t BuOK or NEt ₃	C.5 or C.7	Toluene/ Acetone	0	n.a.
132	74	KOH	C.5	Toluene	0	0
133	74	KOH	C.5	Acetone	53	3
134	74	KOH	C.7	Toluene	41	31
135	74	KOH	C.7	Acetone	44	38

[a] S/C/KOH = 100/1/2, room temperature, 24 h. [b] Conversion was monitored by ¹H NMR. Diastereomeric ratio and ee were measured by chiral HPLC or SFC.

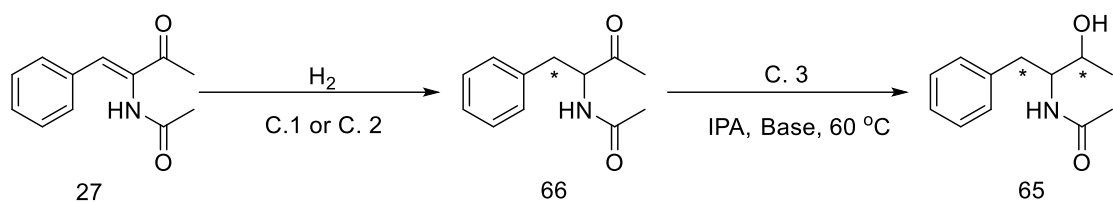
5.5 Results of asymmetric transfer hydrogenation

5.5.1 HIV protease

Substrate 27 was reduced by asymmetric hydrogenation and transfer hydrogenation with results shown in Table 40. The enamide was firstly reduced by AH, then the carbonyl group by isopropanol, catalyzed by C.3. In entry 136, racemic alcohol was produced by Pd/C hydrogenation and sodium borohydride. According to the Felkin-Anh model, the hydride tends to attack the least hindered configuration. The diastereomeric ratio obtained was 3:1, with ee 0%. For the first step, catalyzed by both C.1 and C.2, the product was racemic, whilst in the second step, it was found that by using 5 eq% ^tBuOK in entry 138, the diastereomeric ratio was

5:1. better than by using 3 eq NEt_3 , entry 137, with d.r.= 3:1. In entry 136, 27 was also directly hydrogenated by the chiral iridium catalyst (C.3) and 65 was obtained with diastereomeric ratio = 3:2. Furthermore, the metal catalyst from the first step also had effect in the second step. When C.1 metal catalyst, from the first step was not removed, by using C.1 in entry 137 and C.2 in entry 140, the diastereomeric preference was changed. This can be explained by ligand exchange between the catalysts and the active species is still under study. If catalyst C. 2 was removed after AH, entry 141, the preferred diastereoisomer was the same as entry 138 where Ru-BINAP was used. However, the diastereomeric excess was lower than that in entries 138 and similar to direct transfer hydrogenation, entry 139.

Table 40 AH and ATH of 27



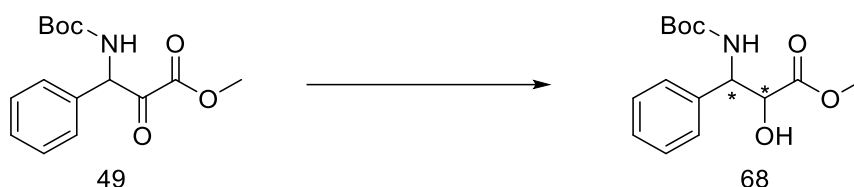
Entry		catalyst	Base	Time (h)	Conversion ^a (%)	ee. (%) ^b	diastereomeric ratio, dr ^b
136	step 1	Pd/C ^c	N.A.	12	100	0	
	step 2	NaBH ₄	N.A.	12	100	0	3:1(by GC); 3:1(by NMR)
137	step1	C.1 ^{c, d}		18	100	0	
	step 2	C.3	3 eq NEt ₃	20	95	97	3.1:1(by GC); 3.1:1(by NMR)
138	step1	C.1 ^{c, d}		18	100	0	
	step 2	C.3	5 eq % ^t BuOK	20	90	98	5:1(by GC); 5:1(by NMR)
139	direct ATH	C.3	3 eq NEt ₃	20	92	98	3:2(by GC)
140	step1	C.2 ^{c, d}		0.5	100	9	
	step 2	C.3	3 eq NEt ₃	20	92	98	1:3(by GC); 1:4(by NMR)
141	step1	C.2 ^{c, e}		18	100	0	
	step 2	C.3	3 eq NEt ₃	20	91	98	2.3:1(by GC)

[a] Conversion was monitored by ¹H NMR. [b] Diastereomeric ratio and ee were measured by chiral GC. [c] The reaction was conducted under room temperature and 5 bars. [d] Metal catalyst from the first step was not removed. [e] Metal catalyst from the first step was removed.

5.5.2 Paclitaxel side chain

Substrate 49 was reduced completely by ATH in 16 hours in Table 41. When C.7 was used, 58% ee and >99:1 de could be obtained, entry 143. When catalyst C. 3 was used, product of 91% ee and 2.8:1 d.r. were obtained in entry 144.

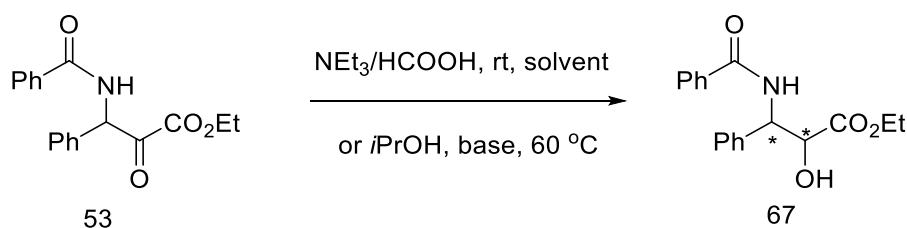
Table 41 ATH of 49



Entry	Catalyst	Reaction	Conversion (%) ^c	dr (%)	ee (%)
142	NaBH ₄		>99	2:1	0
143 ^a	C. 7	ATH (HCO ₂ H/NEt ₃)	>99	>99:1	58
144 ^b	C. 3	ATH (IPA/ ^t BuOK)	>99	2.8:1	91

[a] S/C/TEAF = 20/1/2.7, room temperature, 12 h. [b] S/C/^tBuOK = 20/1/5, 60 °C, 12 h. [c] Conversion was monitored by ¹H NMR. Diastereomeric ratio and ee were measured by chiral HPLC.

High throughput screening machine was used to optimize the ATH of substrate 53. Supercritical carbon dioxide chromatography analysis allows quick analysis of the reaction results. Catalyst C. 3, C. 4, C. 5, C. 6, C. 7 were used for asymmetric transfer hydrogenation. 53 was reduced in TEAF system, while there was no conversion in ⁱPrOH system.



Scheme 12 ATH of 53

Table 42 shows the results of initial screening. The substrate and catalysts were dissolved in MeOH because high throughput screening machine can handle liquid accurately and efficiently, but not solid. It was found that catalyst C. 5 and C. 7 offered good diastereo-control

and conversion.

Table 42 Screening of catalysts for ATH of substrate 53

Reaction scheme showing the asymmetric total hydroxylation (ATH) of substrate 53. The substrate is ethyl 2-phenyl-2-(phenylamino)acetate. The reaction conditions are $\text{NEt}_3/\text{HCOOH}$ (5:2), rt, solvent, 24 h, 1 mol% catalyst. The product is ethyl 2-phenyl-2-(phenylamino)-3-hydroxyacetate, with the newly formed stereocenters marked with asterisks.

Entry ^a	Catalyst	Conversion (%) ^b	ee (%)	de (%)
145	C. 3	96-99	0-37	84-90
146	C. 4	96	19	66
147	C. 5	95-99	50-84	92-98
148	C. 6	95	77	98
149	C. 7	94-99	63-83	8-32

[a] S/C/TEAF = 20/1/2.7, room temperature, 12 h. [b] Conversion was monitored by ^1H NMR. Diastereomeric ratio and ee were measured by chiral SFC.

Table 43 shows the results of screening solvents by using C. 5. It shows in entry 153 that DMSO is the best solvent. It afforded product with 96% yield, 84% ee and 92% de.

Table 43 Solvent effect of catalyst C.5

Entry ^a	solvent	Conversion (%) ^b	ee (%)	de (%)
150	TEAF	95	77	98
151	DCM	99	78	94
152	MeOH	99	50	96
153	DMSO	96	84	92
154	DMF	95	71	98
155	Toluene	99	72	92
156	THF	99	75	92
157	iPrOH	99	72	98

[a] S/C/TEAF = 20/1/2.7, room temperature, 12 h. catalyst: C.5. [b] Conversion was monitored by ¹H NMR. Diastereomeric ratio and ee were measured by chiral SFC.

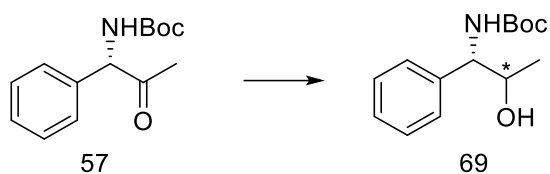
Methanol, added to dissolve the substrate and catalysts, might affect the activity and diastereoselectivity of catalysts. Table 44 shows reactions using solvents without adding methanol. Entries 160 and 164 were carried out with pure DMSO, the ee increased to 91% and 90% for catalysts C.5 and C.6. Entries 161-163 were conducted in water. There was no conversion or low diastereoselectivity. The major configuration of the product was different from the natural product. New methods need to be explored to get the correct configuration.

Table 44 Reactions without MeOH

Entry	Catalyst	solvent	Hydrogen Source	Conversion (%) ^b	ee (%)	de (%)
158	C. 5	TEAF	NEt ₃ /HCOOH	93	81	86
159	C. 5	DCM	NEt ₃ /HCOOH	86	81	92
160	C. 5	DMSO	NEt ₃ /HCOOH	91	91	92
161	C. 5	DMSO/H ₂ O	NEt ₃ /HCOOH	88	41	90
162	C. 5	DMSO/H ₂ O	HCOONH ₄	0	n.a.	n.a.
163	C. 5	H ₂ O	HCOONH ₄	0	n.a.	n.a.
164	C. 6	DMSO	NEt ₃ /HCOOH	95	90	94

[a] S/C/TEAF = 20/1/2.7, room temperature, 12 h. [b] Conversion was monitored by ¹H NMR. Diastereomeric ratio and ee were measured by chiral SFC.

The substrate without ester group that has an amine chiral center was synthesized and tested in Table 45. Ruthenium catalyst (C.5) gave a trace product in 24 hours, entry 166. When the tethered ruthenium catalyst was used, the reactivity of the catalyst increased and afforded >99% conversion for both *R* and *S*-substrate by (*R,R*)-C.6. The diastereoselectivity for (*R*)-57 was 68% ee and 56% de, entry 167, while for *S*-substrate, it was 99% ee and 92% de, entry 168. Rhodium catalyst (C.7) worked for ATH of substrate 57, which gave similar diastereoselectivity for both (*R*)-57 and (*S*)-57, entries 169 and 170. C.6 catalyst that was a tethered Ruthenium catalyst gave the best results. For (*S*)-57, it afforded product with >99% conversion, 99% ee and 92% de, entry 168.

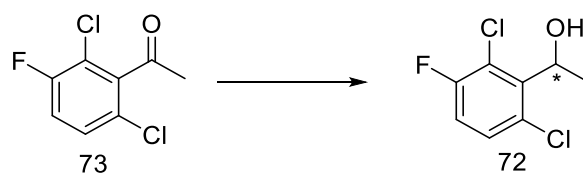
Table 45 ATH of 57

Entry ^a	Catalyst	Configuration of substrate	Conversion (%) ^b	ee (%)	de (%)
165	C.3	<i>R/S</i>	0	N.A.	N.A.
166	C.5	<i>R/S</i>	0	trace	N.A.
167	C.6	<i>R</i>	>99	68	56
168	C.6	<i>S</i>	>99	99	92
169	C.7	<i>R</i>	>99	90	8
170	C.7	<i>S</i>	>99	91	8

[a] S/C/TEAF = 20/1/2.7, room temperature, 12 h. [b] Conversion was monitored by ¹H NMR. Diastereomeric ratio and ee were measured by chiral HPLC.

5.5.3 2,6-dichloro-3-fluoroacetophenone

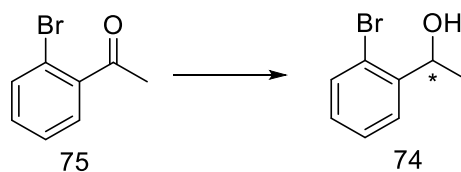
Due to the hindrance of chloride groups in para site, there was no conversion in ATH by both catalysts C.5 and C.7.

**Figure 89** ATH of substrate 73

5.5.4 2-bromoacetophenone

ATH of substrate 75 was achieved using catalysts C. 5 and C. 7. Catalyst C. 5 gave better enantioselectivity of 95% ee, whilst catalysts C. 7 gave 65% ee.

Table 13 ATH of substrate n

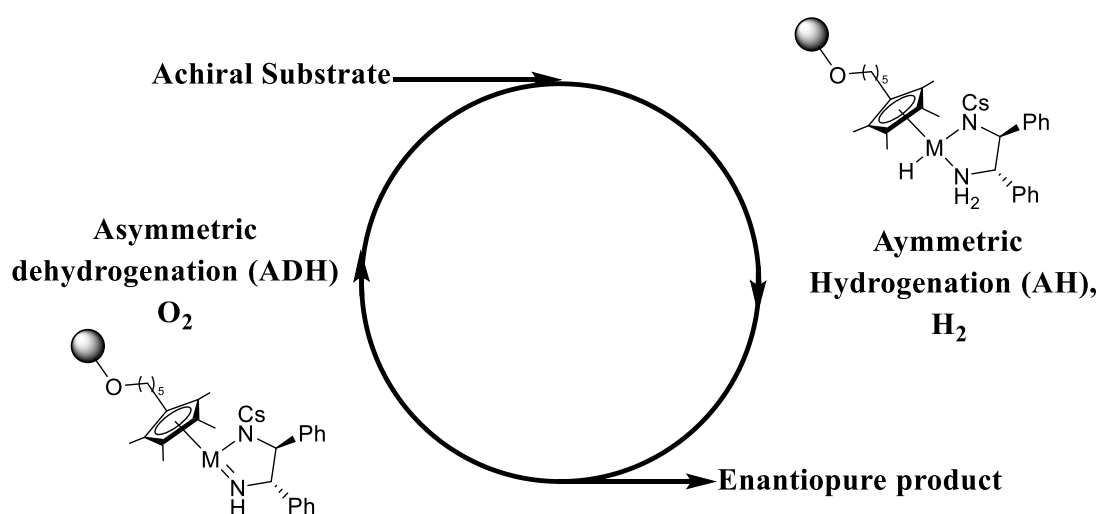


Entry ^a	Catalyst	Conversion (%) ^b	ee (%)
171	C. 5	98	95
172	C. 7	85	65

[a] S/C/TEAF = 20/1/2.7, room temperature, 12 h. [b] Conversion was monitored by ¹H NMR. Diastereomeric ratio and ee were measured by chiral HPLC.

5.6 Process combining AH and ADH

Carrying out a multi catalyst system usually encounters the incompatibility of catalytic systems. By immobilizing catalysts in micro-reactors, they can be compartmentalized to avoid interference. In our case, when using catalyst of the same configuration, the resulting chiral alcohol of a certain configuration by ATH will be oxidized by ADH. To enrich the product of the desired configuration, alcohols with the other configuration needs to be oxidized. Therefore, ADH and ATH catalysts should have different configurations. They cannot be used in one pot, because racemic product will be obtained when catalysts with both configurations coexists. Flow reactor can separate the catalysts with two configurations from each other, which can be the solution to the process. In addition, hydrogen acceptor and donor, such as, acetone and isopropanol, could affect the equilibrium of the reaction, when the concentration of them change during the reaction. A way to overcome the equilibrium is to use irreversible donors such as H₂ and O₂ that are gas can be released after the reactions. The solvent can be THF or toluene rather than an alcohol that are inert in these reactions. The process envisaged is summarized in Scheme 31.



Scheme 31 Process combining ADH and AH

5.7 Conclusion

In conclusion, synthesizing compounds with multiple chiral centres is often a problem. Three strategies are currently adopted, Felkin-Anh rule, dynamic kinetic resolution, and chelated control method. The substrates and configuration scopes are limited. Chelating group and Lewis acid are required for the chelated control method. Thus, we hope to design a continuous reactor system to solve this problem by combining transfer hydrogenation, and transfer dehydrogenation. It was found that iridium catalyst (C.3, C.4 and C.10) showed high reactivity but low enantioselectivity. Both ruthenium catalyst (C.5) and rhodium catalyst (C.7) afforded products with high conversion and high ee value. The reaction was modeled by matlab. It can be concluded that enantiomeric excess can be raised from 60% ee when only using AH to 90% ee by combining ADH and AH with the same catalyst. In terms of substrate, HIV protease inhibitors and paclitaxel side chain were chosen, because they represent a good opportunity to synthesize various compounds with multiple chiral centres, including Felkin-Anh substrates and anti-Felkin-Anh substrates. Eight challenging substrates were synthesized and tested by various catalysts. Phenylethyl alcohol type substrate could be oxidized by asymmetric dehydrogenation, whilst there was no activity for HIV protease inhibitor and paclitaxel side chain derived substrate. The system combining ADH and ATH was not build,

proper substrate for ADH was not found.

Chapter 6: Conclusions and Outlook

6.1 Conclusion

In the past decades, flow chemistry tools have provided a great improvement in efficiency and scope of organic synthesis. However, catalytic asymmetric reactions in flow are still underdeveloped. The project aim is to apply micro-reactor technology in both continuous gas-liquid asymmetric synthesis and mechanism study of pressurized gas liquid reaction.

In Chapter 2, AH was carried out in a customized continuous slug flow reactor able to operate at pressures up to ~ 150 bar and temperature ~ 100 °C and real-time quantitative analysis was performed by *in-situ* IR spectroscopy. A remarkably high TOF of $274,000 \text{ h}^{-1}$ was observed in hydrogenation of acetophenone. Two optically active APIs, ezetimibe and eslicarbazepine acetate, were successfully synthesized by the multi-step flow system with high efficiency (4.8 g/h for ezetimibe and 1.62 g/h for eslicarbazepine acetate) and enantioselectivity (95% de and 98% ee). It was found that changing of flow regime can have a significant effect on the reaction conversion in the slug flow reactor with optimal gas-liquid flow rate and ratio determined. Continuous flow AH is usually quantitative, with no by-product and few impurities, so requires no purification before carrying through to the next reaction. This study demonstrates that continuous flow AH with low catalyst loading will become an important tool in end-to-end enantioselective flow synthesis of chiral compounds. The drawback of slug flow reactor is that the formation of slug flow requires specific flow rate and gas liquid ratio, which limits the range of reaction time and substrate concentration of the reaction.

In Chapter 3, to expand the scope of catalytic gas liquid reactions in flow, the fReactor adopting active mixing was developed for assessing small scale heterogeneous and air-sensitive homogeneous hydrogenations in both batch and continuous flow. The batch experimental design data provided the basis for choosing a residence time for continuous flow

operation; the benefit of using the same reactors and mixing regime is that the mass transfer coefficients are identical. The limitations of most pressure hydrogenators are their size and complexity required to ensure good mixing and safety. Many chemists avoid this by using hydrogen-filled balloons that are restricted to pressures only marginally above atmospheric. The fReactor provides a simple, small-scale, low-cost solution to batch and rapid translation to continuous flow and lab scale-up. The ability to charge hydrogen manually by syringe via a non-return valve up to ~10 bar pressure makes hydrogenations practical, and parallel reactors enable different conditions to be tested. Active mixing gives high gas-liquid mass transfer rates that can be monitored directly using an on-line pressure sensor. In a benchmark Pd/C catalyzed hydrogenation of nitrobenzene, fast reactions and high conversions were achieved using high stirrer speeds and gas to liquid ratios. The fReactor exceeded the mass transfer rates of a 600 mL mechanically stirred Parr hydrogenator. A further benchmark reaction of a homogenous asymmetric hydrogenation showed the use of an air-sensitive catalyst in both batch and flow. Using the fReactor, the hydrogenation of the (*E*)-isomer gave similar conversions and optical activities to those reported in literature. Adopting a standard and easy-to-use hydrogenation platform constructed with good engineering design supports robust batch and flow experimentation and reporting of results.

In Chapter 4, a micro-reactor for acquiring kinetic data with a time scale of second for the pressurized gas liquid reactions was developed. The fast isomerization of 1-octene to 2-octene in hydroformylation was observed. It was found that initially, there was a monohydride rhodium complex without carbon monoxide, that had a higher isomerization rate than that of the active species of hydroformylation. This discovery helps the development of fast isomerization catalyst that can be applied in hydroformylation or other asymmetric synthesis. Vertical fReactor system that decouples gas and liquid flow rate was also developed to prolong the reaction time.

In Chapter 5, asymmetric dehydrogenation of 1-phenylethanol with O₂ and acetone as hydrogen acceptor was firstly studied. It was found that iridium catalyst (C.3, C.4 and C.10) showed high reactivity but low enantioselectivity. Both Ruthenium catalyst (C.5) and Rhodium catalyst (C.7) afforded products with high conversion and high ee value. The reaction was

modeled by matlab. It can be concluded that enantiomeric excess can be raised from 60% ee when only using AH to 90% ee by combining ADH and AH with the same catalyst. Encouraged by the results above, a series of substrates derived from drug intermediates were synthesized and tested for ADH. Only acetophenone-type substrate could be oxidized with good selectivity.

6.2 Outlook

Pipe in series reactor developed by Eli Lilly is one of most widely used reactor for large-scale continuous catalytic biphasic reactions. The enlargement of tubes prolonged the residence time of the liquid but slowed down the mass transfer. Therefore, by integrating active mixing with continuous reactor can leads to the improvement of biphasic reaction reactors used in industry. The identification of catalytic species enabling fast isomerization in hydroformylation could inspire us to design a new and efficient isomerization catalyst.

Catalytic system for ADH with higher activity and wider substrate scope needs to be developed. To achieve this, more catalysts can be tried. Using hydrogen acceptor except oxygen and acetone can be another solution to improve reactivity. In the system combining ADH with AH, inline optical yield analysis can be adopted for inline analysis. Both yield and enantioselectivity can be estimated by this technique. The gas reactant, such as H_2 and O_2 , can be used to avoid solvent switch and ensure the compatibility of ADH and AH.

Asymmetric catalytic reactions often require delicate screening of conditions and additives, due to the complication of reaction mechanism. Micro-reactor technology enables precise and automatic control of conditions, which will accelerate the mechanism study and the development of new reactions. It also can facilitate the scale-up of gas liquid reactions that is often considered as a type of green reaction, because it has good atom economy and is often without the need of purification.

Chapter 7: Experimental

7.1 Chapter 2: High-pressure gas-liquid slug flow reactor and its application in asymmetric hydrogenation.

General Information

Unless otherwise stated, all chemicals were obtained from Sigma-Aldrich, Fisher Scientific, Alfa Aesar or Fluorochem Ltd., and were used without further purification. All the reactions dealing with air- or moisture-sensitive compounds were carried out in a dry reaction vessel under an argon atmosphere or in an argon-filled glovebox. Unless otherwise noted, all reagents were purchased from commercial suppliers without further purification. Acetophenone was purified by distillation under argon. Toluene was distilled over sodium chips and benzophenone under argon. Other anhydrous solvents were purchased from J&K Chemical and degassed by bubbling argon over a period of 30 min. Purification of products was carried out by flash chromatography using silica gel (200-300 mesh). Thin layer chromatography was carried out using silica gel plates from Merck (GF254). $[\text{Ir}(\text{COD})\text{Cl}]_2$ was purchased from Heraeus. Tridentate ligands f-amphox and f-amphol were prepared according to literature.^[40, 105b]

^1H , ^{13}C , ^{19}F and ^{31}P NMR spectra were recorded on a Bruker Avance 400 MHz or on a Bruker Avance 600 MHz spectrometer with tetramethylsilane as the internal standard. Chemical shifts are reported in parts per million (ppm, δ scale) downfield from TMS at 0.00 ppm and referenced to the CDCl_3 at 7.27 ppm for ^1H NMR or 77.0 ppm for ^{13}C NMR. Data are reported as: multiplicity (s = singlet, d = doublet, t = triplet, q = quartet, m = multiplet), coupling constant in hertz (Hz) and signal area integration in natural numbers. ^{13}C NMR and ^{31}P NMR analyses were recorded with ^1H decoupling. Enantiomeric excess values were determined by Agilent 1290 Series HPLC instrument on a chiral stationary phase. Optical rotations were measured using a 1-mL cell with a 1 dm path length on a Rudolph Autopol I polarimeter at 589 nm. ATR TFIR analysis was carried out using Mettler-Toledo ReactIR 15 spectrometer and DST Series 6.3 mm AgX Fiber Conduit probe with a diamond window.

Continuous Asymmetric Hydrogenation of acetophenone

To a 5-mL vial was added the catalyst precursor $[\text{Ir}(\text{COD})\text{Cl}]_2$ (1.4 mg, 0.002 mmol), f-amphox (2.3 mg, 0.0042 mmol) and anhydrous $i\text{PrOH}$ (1.0 mL) in an argon-filled glovebox. This

vial was sealed and mixed for 2 hours at room temperature. ^tBuOK (89.8 mg, 0.8 mmol) was dissolved in 10 mL anhydrous ⁱPrOH. 0.5 mL catalyst solution was firstly mixed with 10 mL base solution and then acetophenone (9.6 g, 9.4 mL, 80 mmol). The resulting mixture was filtered and the filtrate was added into a flask.

The process diagram was shown in Figure 22 and Scheme 1. Figure 23 showed the remote-control app and real time IR analysis. The process was washed by anhydrous and degassed ⁱPrOH at a liquid flow rate of 4 mL/min and gas flow rate of 5 sccm (avoid back flow of liquid to gas flow meter) for 5 minutes and then pressurized the BPR. After the reactor was pressurized to 70 bar and heated to 90 °C, the beforehand reaction medium was pumped instead of solvent. Liquid flow rate was set at 0.23 mL/min and gas flow rate 0.9 mL/min (45 sccm). The reactor system could achieve steady state in 5 reaction volumes. Samples were collected every 15 minutes in an empty vial. The conversion and ee were analyzed by NMR and HPLC. When reaction finished, system was depressurized by releasing the gas of Equilibar BPR slowly and washed the whole system by pumping ⁱPrOH for 10 minutes. Results are shown in Table 5. Due to the high consumption of gas in this case, the gas flow rate dropped from 0.9 mL/min to 0.41 mL/min, which prolonged the residence time. Therefore, the residence time in this case was calculated to be the average of the initial and the final flow rate. When the reaction finished, this system was depressurized by releasing the gas of Equilibar BPR slowly. The whole system was washed by pumping ⁱPrOH for 10 minutes. In 20 minutes at steady state, 2.2 g colorless oil product was obtained after removal of metal and solvent with a yield of >99% and >99 ee. The ee was determined by UPLC.

Synthesis of (3R)-4-(4-(benzyloxy)phenyl)-1-(4-fluorophenyl)-3-((S)-3-(4-fluorophenyl)-3-hydroxypropyl) azetidin-2-one (4) in batch. (S/C = 5000)

To a 20-mL vial was added the catalyst precursor [Ir(COD)Cl]₂ (16.8 mg, 0.025 mmol), f-amphox (31.0 mg, 0.056 mmol) and anhydrous ⁱPrOH (10.0 mL) in an argon-filled glovebox. The mixture was stirred at 25 °C for 2 hours, giving an orange solution. And then substrate **3** (249.0 mg, 0.5 mmol) in 0.5 mL anhydrous toluene were added into a 5-mL hydrogenation vessel. CsOH•H₂O (1.7 mg, 0.01 mmol) in 0.5 mL anhydrous ⁱPrOH was added and a solution

of Ir/f-amphox in anhydrous *i*PrOH (20 μ L) was added via an injection port. Then the vessel was placed in an autoclave, closed it, and moved it out from the glovebox. The autoclave quickly purged with hydrogen gas for three times, then pressurized to 60 bar H₂. The reaction solution was stirred at room temperature (25°C-30°C) for 4 hours, then released pressure carefully. The solution of reaction mixture was purified by a flash chromatography on silica with ethyl acetate and the eluent was removed under reduced pressure to afford the **4** with 199.0 mg as a white solid, 85% conversion, 80% yield, 95% de.

Synthesis of the pair of two diastereomers of (3*R*)-4-(4-(benzyloxy)phenyl)-1-(4-fluorophenyl)-3-((*S*)-3-(4-fluorophenyl)-3-hydroxypropyl)azetidin-2-one (4**).**

NaBH₄ (567 mg, 15 mmol) was added slowly during 20 minutes to the reaction medium consisting of **3** (5.0 g, 10 mmol) in 10 mL MeOH. The reaction medium was kept at room temperature by water bath. The reaction was monitored by TLC. After the completion of reaction, 10.0 mL saturated NH₄Cl was added to quench the reaction. The product was extracted by 20.0 mL DCM for two times. Organic layer was combined and washed by saturated NaCl solution and dried by anhydrous Na₂SO₄. The solvent was removed in vacuo to give 4.6 g **4** (white solid) in 93% yield. The product was analyzed by HPLC and NMR.

Synthesis of (3*R*)-4-(4-(benzyloxy)phenyl)-1-(4-fluorophenyl)-3-((*S*)-3-(4-fluorophenyl)-3-hydroxypropyl)azetidin-2-one (4**) in flow**

To a 20.0-mL vial was added the catalyst precursor [Ir(COD)Cl]₂ (16.8 mg, 0.025 mmol), f-amphox (31.0 mg, 0.055 mmol) and anhydrous *i*PrOH (10.0 mL) in an argon-filled glovebox. The medium was mixed for 2 hours under room temperature. CsOH•H₂O (83.5 mg, 0.5 mmol) was dissolved in 10.0 mL anhydrous *i*PrOH. 10 mL catalyst solution was sequentially mixed with 10 mL base solution and **3** (12.5 g, 25 mmol) in 25.0 mL anhydrous toluene. The resulting mixture was filtered by filter paper and the filtrate was added into a 50 mL volumetric flask. Then, additional *i*PrOH was added to prepare a 50.0 mL reaction solution. For high TON reactions, the concentration of the catalyst was decreased without changing the concentration of the substrate.

The process diagram was shown in Figure 22. The process was washed by anhydrous and degassed *i*PrOH at a liquid flow rate of 4 mL/min and gas flow rate of 5 sccm (avoid back flow of liquid to gas flow meter) for 5 minutes and then pressurized the BPR. After the pressure elevated to desired value. The beforehand reaction solution was pumped instead of solvent. Liquid flow rate and gas flow rate were adjusted to desired flow rates. The reactor system could achieve steady state in 5 reaction volumes. Samples were collected every 15 minutes in an empty vial. The metal catalyst was removed by filtering over a silica pad, and after removing the solvent the conversion and de were analyzed by NMR and HPLC. When the reaction finished, this system was depressurized by releasing the gas of Equilibar BPR slowly. The whole system was washed by pumping *i*PrOH for 10 minutes.

Synthesis of (3*R*)-1-(4-fluorophenyl)-3-((*S*)-3-(4-fluorophenyl)-3-hydroxypropyl)-4-(4-hydroxyphenyl) azetidin-2-one (5) in fReactor

The process is shown in Figure 36. The details could be found in literature.^[79] **4** (125 mg, 0.25 mmol) was dissolved in 0.5 mL mixed solvent (toluene:*i*PrOH = 1:1, v/v) and charged by syringe to a batch fReactor containing a degassed slurry of wet 10% Pd/C (150 mg, 66.2% H₂O). The fReactor was heated to 80 °C. (The mixer was 94.5 °C. Temperature function can be found in <https://freactor.com/index.html>.) Then it was pressurized to 6 bar three times to ensure a completely hydrogen atmosphere and stirred at 1500 rpm for 2.5 minutes. After releasing the pressure, the Pd/C was removed by filtration. ¹H NMR analysis of the crude product showed > 99% removal of the benzyl group. For entry 19, fReactors were used in line for flow reaction. The process is presented in Figure 37 and Scheme 3. 750 mg catalyst was preloaded into the first five fReactors. There was a frit-in-a-ferrule that serves a solid filter installed before the BPR. Then the reactor was pressurized. 0.46 mL/min reaction medium and 45 sccm hydrogen were delivered into the reactor. It afforded a 90% conversion with a residence time of 2.5 mins.

Multi-step flow synthesis of (3*R*)-1-(4-fluorophenyl)-3-((*S*)-3-(4-fluorophenyl)-3-hydroxypropyl)-4-(4-hydroxyphenyl)azetidin-2-one (5)

To a 20-mL vial was added the catalyst precursor [Ir(COD)Cl]₂ (16.8 mg, 0.025 mmol), f-

amphox (31.0 mg, 0.055 mmol) and anhydrous *i*PrOH (10.0 mL) in an argon-filled glovebox. The solution was mixed for 2 hours under room temperature. CsOH•H₂O (83.5 mg, 0.5 mmol) was dissolved in 10.0 mL anhydrous *i*PrOH. 10.0 mL catalyst solution was sequentially mixed with 10.0 mL base solution and **3** (12.5 g, 25 mmol) in 25.0 mL toluene. The resulting mixture was filtered and clear solution was added into a 50-mL volumetric flask. Then, 5.0 mL *i*PrOH was added to prepare a 50.0 mL reaction solution.

The process was shown in Figure 37 and Scheme 4. Deprotection module consisting of 9 fReactors (15.3 mL) were installed after the high-pressure slug flow reactor. The fReactors were filled with 750 mg 10% Pd/C in total. The frit-in-ferrule was installed before the BPR to hold the solid catalyst in the reactor. The hydrogenation module with a residence time of 6.5 minutes was pressurized to 100 bars and heated to 60 °C. After it reached steady state, the gas liquid flow was directed to the deprotection module without separation. The fReactor module was heated to 80 °C. Two step yield of ezetimibe was 84%. 272 mg product was obtained in 15 minutes with 95% de.

Synthesis of 5,11-dihydro-10H-dibenzo[*b,f*]azepin-10-one (6)

10-Methoxy-5H-dibenzo[*b,f*]azepine (15.0 g, 67 mmol) and isopropanol (20.0 mL) were charged into a round bottomed flask and stirred for 5-10 minutes. 37% Aqueous hydrochloride solution (15.0 mL) was then added slowly to the mixture at 25-35 °C and stirred for 15 min. The reaction mixture turned red and was heated to 65 °C and maintained for 6 hours. There was insoluble yellow solid precipitating during the reaction. The progress of the reaction was monitored by TLC, and after completion of the reaction (by TLC), 50.0 mL saturated NaHCO₃ was added dropwise to neutralize the reaction medium. The product was extracted by 30.0 mL DCM for three times. Organic layer was combined and washed by saturated NaCl solution and dried by anhydrous Na₂SO₄. 80 mL solvent was removed *in vacuo* and the product was crystallized from the remained medium under -20 °C for 12 hours. The obtained solid was collected by filtration, washed with 10.0 mL EtOH and dried under vacuum. 11.2 g yellow solid was obtained with a yield of 81%.

Synthesis of racemic 10,11-dihydro-5H-dibenzo[b,f]azepin-10-ol (**7**)

NaBH₄ (567 mg, 15 mmol) was added slowly during 20 minutes to the reaction medium consisting of **6** (2.1 g, 10 mmol) in 10 mL MeOH. The reaction medium was kept at room temperature by water bath. The reaction was monitored by TLC. After the completion of reaction, 10.0 mL saturated NH₄Cl was added to quench the reaction. The product was extracted by 20.0 mL DCM for two times. Organic layer was combined and washed by saturated NaCl solution and dried by anhydrous NaSO₄. The solvent was removed *in vacuo* to give racemic 2.0 g, **7** (white solid) in 93% yield. The product was analyzed by HPLC and NMR.

Asymmetric synthesis of (*R*)-10,11-dihydro-5H-dibenzo[b,f]azepin-10-ol (**7**) in batch (S/C=1000)

To a 5-mL vial was added the catalyst precursor [Ir(COD)Cl]₂ (16.8 mg, 0.025 mmol), f-amphol (38.2 mg, 0.055 mmol) and anhydrous *i*PrOH (10.0 mL) in an argon-filled glovebox. The mixture was stirred for 2.0 hours at 25 °C giving orange solution. And then **6** (105.0 mg, 0.5 mmol) in 0.5 mL anhydrous DCM were added into a 5-mL hydrogenation vessel. ^tBuONa (2.4 mg, 0.025 mmol) in 0.5 mL anhydrous *i*PrOH was added and a solution of Ir/f-amphol in anhydrous *i*PrOH (100 μL) was added via an injection port. Then the vessel was placed in an autoclave. This autoclave was quickly purged with hydrogen gas for three times, then pressurized to 60 atm H₂. The reaction solution was stirred at room temperature (25 °C ~ 30 °C) until for 24 hours, then released pressure carefully. The solution of reaction mixture was purified by a flash chromatography on silica with ethyl acetate and the solvent was removed under reduced pressure to afford the (*R*)-**7** 104.0 mg as a white solid, 99% conversion, 99% yield, 98% ee.

Asymmetric synthesis of (*R*)-10,11-dihydro-5H-dibenzo[b,f]azepin-10-ol (**7**) in flow

To a 20-mL vial was added the catalyst precursor [Ir(COD)Cl]₂ (16.8 mg, 0.025 mmol), f-amphol (38.0 mg, 0.055 mmol) and anhydrous *i*PrOH (10.0 mL) in an argon-filled glovebox. The medium was mixed for 2 hours under room temperature, then, ^tBuONa (120.0 mg, 1.25 mmol) was dissolved in the catalyst solution. To the resulting mixture was added **6** (5.2 g, 25 mmol)

in 25 mL dichloromethane. The resulting solution was filtered and filtrate was transferred into a 50-mL volumetric flask. Then, 10 mL ⁱPrOH was added to prepare a 50 mL reaction solution. For high TON reactions, the concentration of the catalyst was decreased without changing the concentration of the substrate.

The process diagram was shown in Figure 22 and Scheme 1. The process was washed by anhydrous and degassed ⁱPrOH by a liquid flow rate of 4 mL/min and gas flow rate of 5 sccm (avoid back flow of liquid to gas flow meter) for 5 minutes and then pressurized the BPR. After the pressure and temperature were elevated to the level needed, the beforehand reaction medium was pumped instead of solvent. Liquid flow rate and gas flow rate were adjusted to desired flow rates. Reaction was monitored by inline IR. The reactor system could achieve steady state in 5 reaction volumes. Samples were collected every 15 minutes in an empty vial. The metal catalyst was removed by filtering over a silica pad, and after removing the solvent, ee was analyzed by HPLC. When reaction finished, system was depressurized by releasing the gas of Equilibar BPR slowly, and washed by pumping ⁱPrOH for 10 minutes.

Synthesis of (*R*)-eslicarbazepine acetate (9**) in batch**

7 (211.0 mg, 1 mmol), DMAP (6.0 mg, 0.05 mmol) and anhydrous dichloromethane (2.0 mL) were charged into a sealing tube and stirred for 10 min. Triethylamine (0.21 mL, 1.5 mmol) was then added into the reaction mixture at 25 °C and stirred for 5 minutes. Acetic anhydride (0.14 mL, 1.5 mmol) was charged slowly to the reaction mixture at 25 °C and stirred for 5 minutes. The mixture was then heated to 60 °C and maintained for 0.3 h. After completion of the reaction by TLC, chlorosulfonyl isocyanate (0.1 mL, 1.2 mmol) was added to the mixture at 0 °C and stirred for 5 minutes at same temperature. The reaction mixture was allowed to warm to 25 °C. 3.0 mL water was added slowly to quench the reaction. The biphasic medium was left stirring for 1 hour. Organic phase was separated. 5.0 mL DCM was added to wash the aqueous phase for two times. Organic layer was combined and washed with water (5.0 mL). The solvent was evaporated at 40 °C under reduced pressure. The crude product were purified by column chromatography on silica. (60.0 mL 50% ethyl acetate in petroleum ether, then 100.0 mL 80% ethyl acetate in petroleum ether). It afforded 260.5 mg white solid with 88%

yield and 98% ee.

Multi-step flow synthesis of (*R*)-eslicarbazepine acetate (9)

Medium for module 1: To a 20.0 mL vial was added the catalyst precursor $[\text{Ir}(\text{COD})\text{Cl}]_2$ (16.8 mg, 0.025 mmol), f-amphol (38.0 mg, 0.055 mmol) and anhydrous $i\text{PrOH}$ (10.0 mL) in the argon-filled glovebox. The medium was mixed for 2 h under room temperature. $t\text{BuONa}$ (120.0 mg, 1.25 mmol) was dissolved in 5.0 mL catalyst medium. The resulting medium was mixed with **6** (5.2 g, 25 mmol) in anhydrous and degassed 25.0 mL DCM. The resulting medium was filtrated by filter paper and added into a 50 mL volumetric flask. Then, 15.0 mL $i\text{PrOH}$ was added to prepare a 50 mL reaction medium.

Medium for module 2: 37.5 mL acetic anhydride and 12.5 mL NEt_3 were mixed in a 50 mL volumetric flask. 133.0 mg DMAP was dissolved in the medium.

Medium for module 3 was neat ClSO_2NCO .

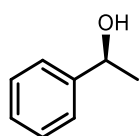
The process was shown in Scheme 6. Details of module 2 and 3 were presented in Figure 38, Figure 39, Figure 40. The module 1 was washed by anhydrous and degassed $i\text{PrOH}$ by a liquid flow rate of 4 mL/min and gas flow rate of 5 sccm (avoid back flow of liquid to gas flow meter) for 5 minutes and then pressurized the BPR. After the pressure and temperature was elevated to 90 bar and 80 °C, the beforehand reaction medium was pumped instead of solvent. Liquid flow rate was 0.46 mL/min and gas flow rate was 44 sccm. The reaction was monitored by TLC analysis. After it reached steady state with full conversion, the product medium was collected in the gas liquid separator (schlenk tube in this process). Module 2 consisting of 5 fReactors (8.5 mL) was installed and filled with dry DCM. The medium for module 2 was taken by a 50 mL syringe that was installed on a PhD Ultra syringe pump. Then it was pumped by a flow rate of 0.26 mL/min. The liquid in gas liquid separator was pumped into module 2 by a flow rate of 0.23 mL/min. The hotplate was heated to 70 °C to have a liquid temperature of 60 °C. The residence time of module 2 was 17 mins. The reaction was monitored by TLC analysis. After it reached steady state with full conversion, the outlet was connected to cooling part of the module 3. Neat ClSO_2NCO was pumped by a flow rate of 0.069 mL/min and mixed with medium from module 2 in a T-junction. Tubes of module 3 were in a room temperature water bath. The final product was connected in a beaker that has 20 mL water to quench the solution.

There was HCl gas generated in module 3. Thus, the calculated residence time was 2.7 minutes that was longer than batch reaction time that was 1 minutes. The biphasic medium was left stirring for 1 h. Organic phase was separated. 5ml DCM was added to wash the aqueous phase for two times. Organic layer was combined and washed with water (5 mL). The solvent was evaporated at 40 °C under reduced pressure. The crude materials were purified by column chromatography. (60 mL 50% ethyl acetate in petroleum ether, then 100 mL 80% ethyl acetate in petroleum ether). In the first run, 320.0 mg eslicabazepine acetate with 76% yield and 98% ee in 13 minutes. In the second run, 2.7g eslicabazepine acetate with 81% yield and 98% ee in 100 minutes. Results can be found in Table 46. Crude ¹H NMR After multi-step process was compared with that of pure product in Figure 41.

Table 46 Results of the telescoped continuous flow synthesis of (*R*)-eslicarbazepine acetate

Collection time	100 mins
Total reaction time	24.5 mins
Isolated yield	81%
Material after purification	2.7 g
Productivity	1.6g/h
ee	98%

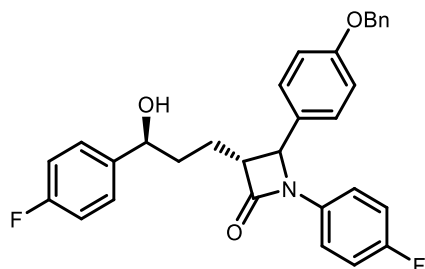
Characterization data of compounds



(S)-1-phenylethanol (2): purified by flash chromatography (on silica, DCM), Colorless oil, 2.2g in 10 minutes; >99% conversion; 98 % yield; 99% ee.

¹H NMR (400 MHz, CDCl₃) δ 7.30 (m, 4H), 7.26 – 7.17 (m, 1H), 4.78 (qd, J = 6.5, 1.4 Hz, 1H), 2.78 (s, 1H), 1.41 (d, J = 6.6 Hz, 3H); ¹³C NMR (101 MHz, CDCl₃) δ 146.0, 128.5, 127.4, 125.5, 70.2, 25.2. In agreement with data in literature.^[40]

The enantiomeric excess was determined by UPLC on Chiralcel OJ-3 column, hexane: isopropanol = 90:10; flow rate = 0.5 mL/min; UV detection at 210 nm; t_R = 3.0 min (minor), 3.5 min (major).

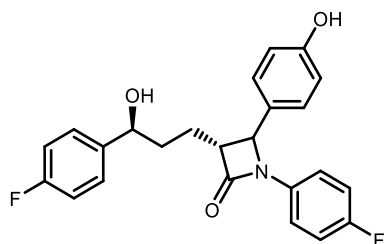


(3R)-4-(4-(benzyloxy)phenyl)-1-(4-fluorophenyl)-3-((S)-3-(4-fluorophenyl)-3-

hydroxypropyl)azetidin-2-one (4): purified by flash chromatography (on silica, petroleum ether/ ethyl acetate = 4/1, v/v), white solid, 199 mg, 85% conversion; 80% yield in batch; 95% de. $[\alpha]_D^{24} = -40.9$ (c = 1.0, CHCl_3).^[134]

^1H NMR (400 MHz, CDCl_3) δ 7.62 – 7.10 (m, 11H), 7.05 – 6.86 (m, 6H), 5.04 (s, 2H), 4.69 (t, J = 6.1 Hz, 1H), 4.56 (dd, J = 5.8, 2.4 Hz, 1H), 3.09 (dtd, J = 12.5, 7.5, 3.8 Hz, 1H), 2.12 – 1.92 (m, 2H), 1.92 – 1.76 (m, 2H). ^{13}C NMR (101 MHz, CDCl_3) δ 167.9, 160.6 (d, J = 240 Hz), 157.5 (d, J = 238.7 Hz), 140.3, 136.8, 133.9, 129.7, 128.7 (d, J = 2.5 Hz), 127.6 (d, J = 2.5 Hz), 118.6, 115.9 (d, J = 7.9 Hz), 73.1, 70.2, 61.1, 60.3, 36.6, 25.0. ^{19}F NMR (376 MHz, CDCl_3) δ -114.9, -117.7. In agreement with data in literature.^[135]

The enantiomeric excess was determined by UPLC on Chiralpak IC-U column, hexane: isopropanol = 80:20; flow rate = 0.5 mL/min; UV detection at 254 nm; t_R = 3.4 min (major), 4.0 min (minor). The reactant **3** was at 6.167 min.

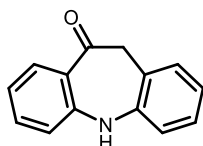


(3R)-1-(4-fluorophenyl)-3-((S)-3-(4-fluorophenyl)-3-hydroxypropyl)-4-(4-

hydroxyphenyl)azetidin-2-one (5): purified by flash chromatography (on silica, petroleum ether/ ethyl acetate = 3/1, v/v), white solid, 204 mg, 100% conversion; 99% yield in batch; 95% de.

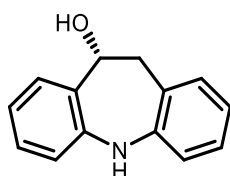
^1H NMR (400 MHz, $\text{DMSO-}d_6$) δ 9.54 (s, 1H), 7.38 (m, 2H), 7.30 – 7.22 (m, 4H), 7.17 (m, 4H), 6.84 – 6.75 (d, $J = 8.4$ Hz, 2H), 5.33 (d, $J = 4.4$ Hz, 1H), 4.84 (d, $J = 2.3$ Hz, 1H), 4.60 (s, 1H), 3.13 (m, 1H), 1.98 – 1.69 (m, 4H). ^{13}C NMR (101 MHz, $\text{DMSO-}d_6$) δ 165.3, 160.3 (d, $J = 240$ Hz), 157.9 (d, $J = 238.7$ Hz), 157.2, 154.8, 155.4, 140.1 (d, $J = 2.8$ Hz), 132.0 (d, $J = 2.5$ Hz), 125.7, 125.6, 116.2 (d, $J = 7.9$ Hz), 113.9, 113.7, 112.7 (d, $J = 20.9$ Hz), 69.1, 57.7, 34.4, 22.5, 18.7, 12.1. ^{19}F NMR (376 MHz, $\text{DMSO-}d_6$) δ -118.9, -121.2. In agreement with data in literature.^[135]

The enantiomeric excess was determined by UPLC on Chiralpak IC-U column, hexane: isopropanol = 80:20; flow rate = 0.5 mL/min; UV detection at 254 nm; $t_R = 2.5$ min (major), 2.8 min (minor).



5,11-dihydro-10H-dibenzo[*b,f*]azepin-10-one (6): purified by recrystallization (DCM/PE), yellow solid, 11.2 g, 100% conversion; 81% yield.

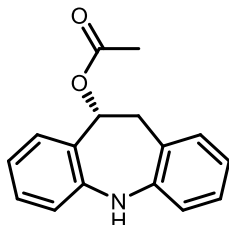
^1H NMR (600 MHz, CDCl_3) δ 8.03 (d, $J = 8.0$ Hz, 1H), 7.41 (d, $J = 8.5$, 1H), 7.31 (d, $J = 7.5$ Hz, 1H), 7.21 (d, $J = 7.7$, 1H), 7.15 (dd, $J = 7.5$, 1.2 Hz, 1H), 7.04 (m, 2H), 6.93 (m, 1H), 3.83 (s, 2H). ^{13}C NMR (101 MHz, CDCl_3) δ 189.7, 146.5, 141.4, 133.6, 130.5, 130.0, 127.6, 124.9, 124.4, 124.0, 119.4, 119.2, 118.9, 49.3. In agreement with data in literature.^[107a]



(*R*)-10,11-dihydro-5H-dibenzo[*b,f*]azepin-10-ol (7): purified by flash chromatography (on silica, petroleum ether/ ethyl acetate = 4/1, v/v), white solid, 104 mg, 100% conversion; 99% yield in batch; 98% ee.

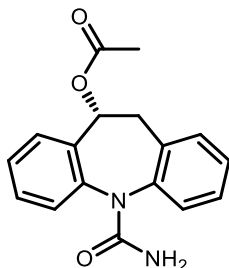
^1H NMR (400 MHz, CDCl_3) δ 7.33 (d, $J = 7.7$ Hz, 1H), 7.22 – 7.10 (m, 3H), 6.91 (m, 1H), 6.88 – 6.74 (m, 3H), 6.09 (s, 1H), 5.12 (dd, $J = 8.2$, 6.5, 1H), 3.31 – 3.18 (m, 2H), 1.76 (s, 1H). ^{13}C NMR (151 MHz, CDCl_3) δ 12.9, 141.8, 132.5, 131.6, 128.7, 128.5, 127.6, 124.2, 121.3, 119.4, 118.6, 118.3, 71.7, 40.9. In agreement with data in literature.^[107a]

The enantiomeric excess was determined by HPLC on Chiralpak OD-H column, hexane: isopropanol = 90:10; flow rate = 0.8 mL/min; UV detection at 210 nm; t_R = 33.5 min (minor), 36.7 min (major).



(R)-10,11-dihydro-5H-dibenzo[*b,f*]azepin-10-yl acetate (8): purified by flash chromatography (on silica, petroleum ether/ ethyl acetate = 4/1, v/v), white solid, 240 mg, 100% conversion; 95% yield in batch;

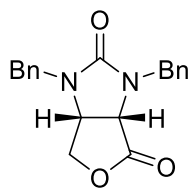
^1H NMR (400 MHz, CDCl_3) δ 7.27 – 7.20 (m, 1H), 7.20 – 7.15 (m, 1H), 7.12 (m, 1H), 7.06 – 7.00 (m, 1H), 6.87 (m, 1H), 6.79 (m, 3H), 6.23 (s, 1H), 6.15 (dd, J = 7.5, 1.2 Hz, 1H), 3.42 (d, J = 14.2, 1H), 3.18 (d, J = 14.2 Hz, 1H), 1.85 (s, 3H). ^{13}C NMR (151 MHz, CDCl_3) δ 170.6, 142.7, 142.3, 132.2, 131.4, 129.3, 127.3, 124.6, 123.6, 121.2, 119.0, 118.6, 118.0, 74.4, 37.8, 21.1. In agreement with data in literature.^[107a]



(R)-eslicarbazepine acetate (9): purified by flash chromatography (on silica, petroleum ether/ ethyl acetate = 1/1, v/v), white solid, 259 mg, 100% conversion; 85% yield in batch;

^1H NMR (600 MHz, CDCl_3) δ 7.44-7.22 (m, 8H), 6.42 – 5.99 (m, 1H), 5.21 (s, 2H), 3.59 (d, J = 14.9 Hz, 1H), 3.20-3.06 (m, 1H), 2.09 (s, 3H). ^{13}C NMR (151 MHz, CDCl_3) δ 170.4, 157.1, 140.7, 139.1, 133.5, 131.1, 131.0, 129.3, 129.2, 128.9, 128.8, 128.5, 128.3, 128.2, 128.0, 127.8, 72.3, 70.1, 35.9, 21.2. In agreement with data in literature.^[107a]

The enantiomeric excess was determined by UPLC on Chiralpak ID-3 column, hexane: isopropanol = 80:20; flow rate = 0.5 mL/min; UV detection at 210 nm; t_R = 18.5 min (major), 20.7 min (minor)



(3aS,6aR)-1,3-dibenzyltetrahydro-1H-furo[3,4-d]imidazole-2,4-dione (11). purified by flash chromatography (on silica, ethyl acetate), white solid, 320 mg, 100% conversion; 99% yield and 97% ee in batch;

^1H NMR (400 MHz, $\text{DMSO-}d_6$) δ 7.37 (m, 5H), 7.29 (m, 5H), 4.81 (dd, $J = 15.6, 4.0$ Hz, 1H), 4.54 (dd, $J = 15.9, 3.9$ Hz, 1H), 4.40 – 4.26 (m, 4H), 4.20 (d, $J = 11.9$, 2H).

^{13}C NMR (101 MHz, $\text{DMSO-}d_6$) δ 174.7, 158.7, 137.6, 137.1, 129.2, 129.1, 128.3, 128.2, 128.2, 128.0, 70.7, 55.4, 53.6, 46.0, 45.2.

The enantiomeric excess was determined by HPLC on Chiralpak OD-H column, hexane: isopropanol = 70:30; flow rate = 0.5 mL/min; UV detection at 210 nm; $t_R = 24.7$ min (major), 30.7 min (minor)

7.2 Chapter 3: Horizontal micro-fluidics CSTR and its application in heterogeneous and homogeneous hydrogenation

General Consideration

Unless otherwise stated, all chemicals were obtained from Sigma-Aldrich, Fisher Scientific, Alfa Aesar or Fluorochem Ltd., and were used without further purification. All reaction solvents were of HPLC grade. Solvents for the AH were dried and degassed by Freeze-pump thaw cycling. Deuterated CDCl_3 was used as supplied and ^1H and ^{13}C NMR spectra were recorded on a Bruker DPX300 (300/75 MHz) spectrometer, a Bruker AV3-400 (400/100 MHz) spectrometer or a Bruker Avance 500 (500/126 MHz) spectrometer using the residual solvent as an internal standard. Chemical shifts are reported in ppm with the multiplicities of the spectra reported as follows: singlet (s), doublet (d), triplet (t), quartet (q), multiplet (m) and broad (br), values for coupling constants (J) are assigned in Hz. GC measurement were performed on a HP 6890 Series GC system, 7693 injector, 7693 autosampler and 5973 mass-selective detector. Two columns were employed:

- Agilent HP-5 achiral column (30 m × 0.32 mm × 0.25 μm); H₂ (3 mL/min); injection temp, 300°C; initial column temperature, 50°C; progress rate, 30°C /min; final column temperature, 280°C.
- Agilent CP-ChirasilDex CB (25 m × 0.25 mm × 0.25 μm); H₂ (3 mL/min); injection temp, 290°C; initial column temperature, 90°C; progress rate, 10°C /min; final column temperature, 195°C.

The pumps used were Jasco PU980 Intelligent HPLC pumps and Knauer K-1800. Pumps were connected to the flow reactors using PTFE tubing (1 /8" or 1 /16" O.D.) and flangeless male HPLC nuts (1 /8") with flangeless ferrules (1 /8")

General procedure for batch fReactor heterogeneous hydrogenation of nitrobenzene by Pd/C.

A gas inlet check valve and 6.3 bar BPR were screwed into the fReactor. 5.3 mg of water wet (~ 50%) 10 wt. % Pd/C (2.5 μmol Pd) catalyst paste was weighed into the fReactor; the viton O-ring was seated uniformly in the groove and the reactor assembled making sure the nuts were hand-tight. The liquid medium, consisting of a nitrogen degassed solution of nitrobenzene (200 μmol) in methanol (1 mL, 0.2 M), was charged by syringe. N₂ was charged by syringe to purge the reactor three times, and released via the sealing screw. Hydrogen was charged by syringe via the check valve to 4.5 bar. Since the gas inlet check valve requires an excess pressure to let gas in, a 0.4 bar excess was used, to be certain of the desired pressure in the reactor. The reactor was placed on the mixer with a stirring frequency of 1500 rpm to start the reaction. The progress of the reaction could be monitored by taking a sample via the liquid inlet septum by a syringe. At the end of the reaction, the pressure was released by the sealed screw and the reactor disassembled. The conversion was analyzed by NMR or GC.

Optimisation of batch nitrobenzene hydrogenation conditions.

The conditions required to operate continuous flow were identified using the fReactor in batch-mode. Five individual reactors were set-up with different conditions defined using design of experiment methodology (DoE). The data was processed by Modde to generate an optimization model. Variable limits for entries 1-11 were defined as: pressure 1 to 4.5 bar; reaction time 10 to 30 minutes; substrate to catalyst ratio (S/C) from 200 to 2000. The results are shown in Table 47.

Table 47 Screening of Reaction Conditions.

#	Pressure (bar)	Reaction time (min)	S/C	Phenylhydroxyamine (%)	Yield ^a (%)
173	1	10	200	<1	22
174	4.5	10	200	<1	>99
175	1	30	200	2	25
176	4.5	30	200	<1	>99
177	1	10	2000	<1	1
178	4.5	10	2000	2	14
179	1	30	2000	<1	3
180	4.5	30	2000	1	27
181	2.75	20	1100	1	35
182	2.75	20	1100	<1	34
183	2.75	20	1100	1	31
184	6.3	2	400	2	41
185	6.3	10	400	1	99
186	6.3	2	800	3	18
187	6.3	10	800	2	70
188	6.3	2	600	4	19
189	6.3	10	600	1	97
190	6.3	6	400	1	75
191	6.3	6	800	4	36
192	6.3	6	600	3	49
193	6.3	2	400	2	41
194	6.3	10	400	1	99

[a] Yield is defined as the mole percentage of aniline formed and determined by ¹H NMR. Phenylhydroxyamine was the only intermediate observed.

The results of the experimental design are presented in the Figure 90.

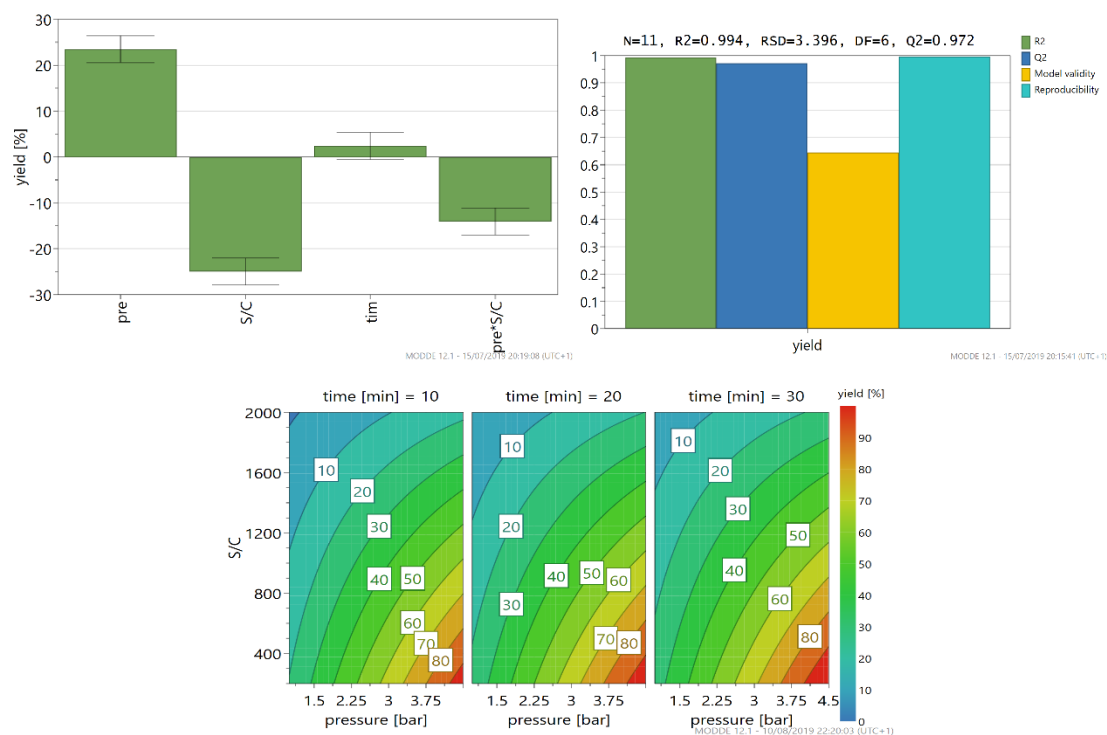


Figure 90 Results of Screening by DoE

From the coefficient plots, the variables of pressure, substrate to catalyst (S/C) loading, and the interaction between pressure and S/C were all significant terms in the model. However, the reaction time was identified as an insignificant model term, which meant that conversion did not increase significantly as the reaction time was prolonged from 10-30 minutes. As DoE builds an empirical model, it can give a prediction of how the reaction is likely to progress. This can be used to build predicted kinetic profiles of the reaction constituents. When S/C was 2000 at 4.5 bar (Figure 91 left), the reaction rate was so low that the yield increased only slightly during this period. When the S/C was 200 at 4.5 bar (Figure 91 right), the conversions were all above 90% from 10 to 30 minutes. To obtain the optimal zero order condition, the reaction was screened in a narrower area (Table 47 Entry 150 to 160). The reaction time was reduced to 2-10 minutes and catalyst loading from 400-800 to reach the target conversion. Since a 6.9 bar back pressure regulator was used for both the batch and flow reactions, the actual pressure used for the optimization was 6.3 bar.

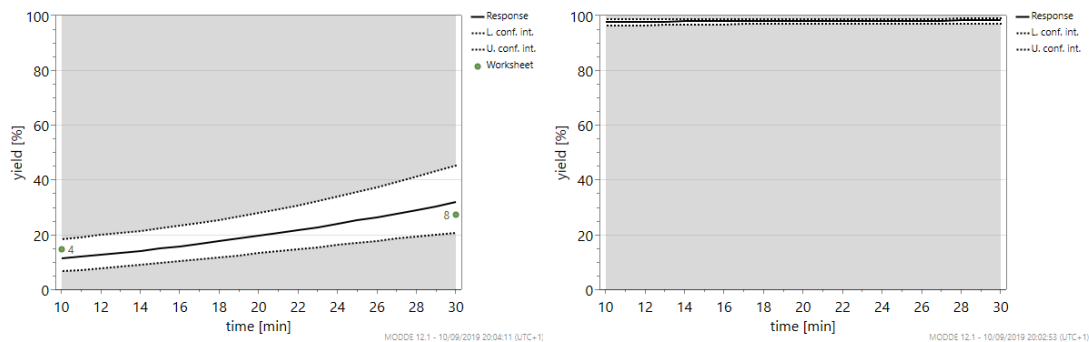


Figure 91 Predicted kinetic profiles of the reaction constituents of S/C = 2000 (left) and S/C = 200 (right) in 4.5 bar

The coefficient plot, summary of fit and response surface plot from optimizing 11 reactions is presented in Figure 92. It shows that reaction time and catalyst loading are both significant factors. According to the model, the yield increased proportionally with the catalyst loading and time. Figure 92 (lower right) is the predicted kinetic profiles when S/C was 600. The yield increased linearly from 23% to 87%, as the reaction time increased from 2 minutes to 10 minutes. The R^2 value is 0.95 and the Q^2 value is 0.92 with model viability is 0.64 and reproducibility of 0.95. Thus, the model is reliable for prediction. It is predicted that when the catalyst loading was 400 and reaction time was 9.2 min, the yield could achieve 95% under 6.3 bar. This condition was chosen for transferring reaction to flow mode.

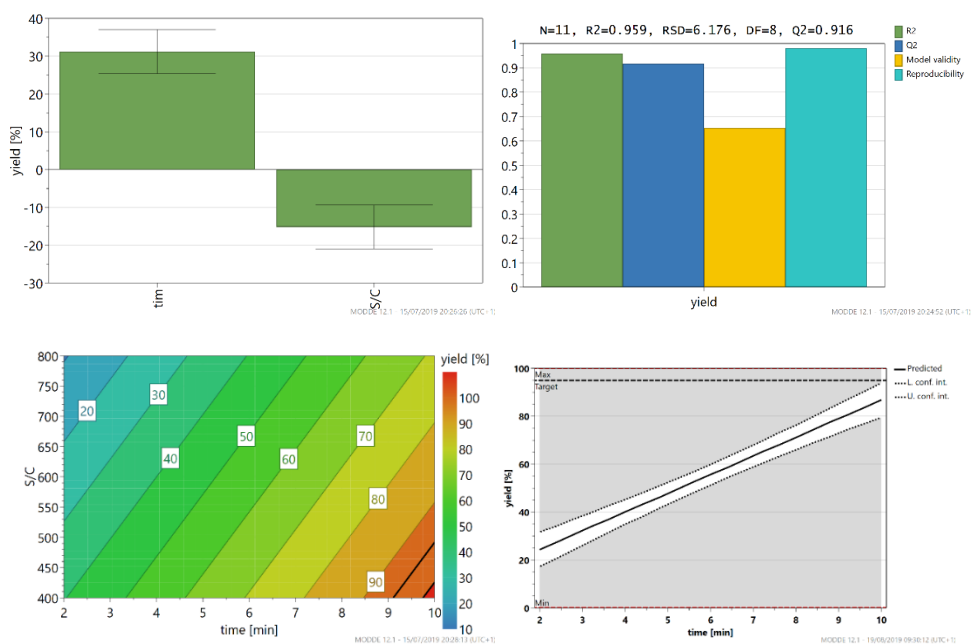


Figure 92 Results of Optimization by DoE

Procedure for Continuous Hydrogenation of Nitrobenzene by Pd/C

The reactor system was assembled and a sealing test was conducted by pressurizing the reactor. A frit-in-a-ferrule was added to each end of connecting tubes instead of normal ferrule. When the S/C = 400, nitrobenzene (6.15g, 0.05 mol) was dissolved in methanol to prepare 100 mL of a 0.5 M solution. The concentration was lowered when the S/C was 80 or 200. Then 1.4 mg catalyst (0.66 μ mol) and 0.5 mL reaction medium were added to each reactor. The reactor system was pressurized to 6.5 bar, with a 6.9 bar BPR and released three times to degas the medium and purging the reactor. Hydrogen and liquid were pumped with the desired flow rate at the same time. The stirring rate was 1500 rpm. Samples were collected every 15 minutes by a vial and analyzed by GC or ^1H NMR. The reaction medium was collected and aniline was isolated after column chromatography, allowing calculation of the production rate and catalyst turnover. Pressure data was collected by an on line pressure sensor.

Synthesis of (E) and (Z)-methyl-3-acetamido-2-butenate.

A 250 mL round-bottomed flask was charged with methyl 3-aminocrotonate (5 g, 0.043 mol) and 43 mL THF. Acetic anhydride (22.3mL, 0.24 mol) and pyridine (5.7 mL, 0.0714 mol) were added. The reaction mixture was stirred under reflux at 75 °C for 15 h. The reaction was quenched with 100 mL saturated K_2CO_3 solution and extracted with ethyl acetate for three times. The combined organic phases were washed with 100 mL K_2CO_3 , thrice with 50 mL K_2HPO_4 , then 50mL brine, dried over Na_2SO_4 and concentrated *in vacuo*. The crude materials were purified by biotage column (60 mL 10-90% ethyl acetate in petroleum ether, then 120 mL 20-80% ethyl acetate and 240 mL 60-40% ethyl acetate) to afford methyl-(E)-3-acetamido-2-butenate (light yellow solid) 6.7% yield, and methyl-(Z)-3-acetamido-2-butenate (white solid) 37% yield.

Synthesis of racemic methyl 3-acetamidobutanoate

A Parr hydrogenator was used for the reaction. All manifold valves, cylinder regulator and isolation valves were checked. The process controller and computer were turned on and the

temperature and pressure alarms were tested. The reaction medium consisting of methyl-3-acetamido-2-butenate (1 g, 6.4 mmol) in methanol (40 mL) were added into vessel along with 10% Pd/C (50% water content) (640 mg, 0.3 mmol) and purged, by filling under pressure and emptying, with nitrogen 5 times then hydrogen 5 times. The agitator was set at 1000 rpm and temperature at 25 °C. The bypass hydrogen valve was closed, and pressure was set to 4 bar. The reaction was monitored by hydrogen uptake for 8 hours, the agitator stopped, and the reactor depressurized and purged with nitrogen 5 times. The reaction medium was collected and catalyst separated over a plug of silica, washed with methanol and the solvent removed *in vacuo* to give 0.97 g racemic methyl 3-acetamidobutanoate (white solid) in 96% yield. The product was analysed by chiral GC and NMR.

Procedure for batch mode homogeneous asymmetric hydrogenation:

The reaction medium was prepared, and reactor was assembled in a glovebox. The solvent was degassed using the freeze-pump-thaw method. (+)-1,2-Bis[(2*R*,5*R*)-2,5-diethylphospholano]benzene (duphos, 1.5 mg, 0.0041 mmol), and Bis(1,5-cyclooctadiene)rhodium(I) tetrafluoroborate catalyst precursor (1.6 mg, 0.004 mmol) were dissolved in 1 mL dry DCM. The mixture was stirred for 30 minutes, then, the substrate (62.8 mg, 0.4 mmol) was added into 1 mL catalyst medium with S/C of 100. 0.5 mL reaction medium was charged to the reactor. The reactor was sealed and then taken out of the glove box. It was pressurized to the desired level with hydrogen supplied from a syringe or a cylinder. The stirring rate was 1500 rpm. Samples were taken from the septum port to monitor reaction. When reaction was finished, gas was released from one port slowly and a sample was collected by pipette from reactor. The metal catalyst was removed by filtering over a silica pad, and after removing the solvent the conversion and ee were analyzed by NMR and GC.

Procedure for flow mode homogeneous asymmetric hydrogenation:

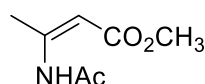
(+)-1,2-Bis[(2*R*,5*R*)-2,5-diethylphospholano]benzene (58 mg, 0.164 mmol), and Bis(1,5-cyclooctadiene)rhodium(I) tetrafluoroborate catalyst precursor (64 mg, 0.16 mmol) were dissolved in 40 mL dry and degassed DCM. The medium was mixed for 30 minutes, then, the

substrate (1256 mg, 8 mmol) was added into 1 mL catalyst medium with S/C of 50. The fReactor flow system was assembled and a sealing test conducted. The reactor was purged by pressurising with N₂ 5 times. The empty reactor system was then pressurized to 6.5 bar (6.9 bar BPR) with H₂ supplied from a regulated cylinder and mass flow controller, and the liquid was pumped simultaneously. The stirring rate was 1500 rpm. Samples were collected every 15 minutes in an empty vial. The metal catalyst was removed by filtering over a silica pad, and after removing the solvent the conversion and ee were analyzed by NMR and GC. When reaction finished, system was depressurized by disassembling the BPR slowly, and washed by pumping DCM.

Avoidance of leaking:

Leaks can be identified using a pressure sensor attached to the fReactor, or after pressurizing the fReactor, with a bubble solution (snoop). PTFE pipe tape is recommended to improve sealing performance if leaks are found at screw fittings. It is critical to sit the Viton O-ring correctly in the groove to achieve a gas-tight condition. Make sure it is clean and seated uniformly; checked by gently pressing the glass window against the O-ring. If it is observed that the O-ring is deformed uniformly, this means it can hold pressure. If there is part that is not pressed by the window, the O-ring need to be cleaned and placed properly. The Viton O-ring can swell considerably in contact with THF, slightly with MeOH, and not in contact with DCM. If it does swell, it is recommended to change it for a new one. Other materials are available that offer different resistance to solvents. Old seals can recover to normal state after the solvent evaporates. When assembling the fReactor, it is important to tighten the screws in turn to keep the gap between the top and base plate even.

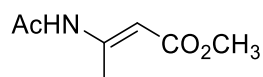
Characterization data for compounds



methyl-(Z)-3-acetamido-2-butenoate. The crude materials were purified by biotage column (60 mL 10-90% ethyl acetate in petroleum ether, then 120 mL 20-80% ethyl acetate and 240 mL 60-40% ethyl acetate) to afford methyl-(Z)-3-acetamido-2-butenoate (white solid) 37%

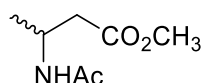
yield.

^1H NMR (500 MHz, CDCl_3) δ 11.10 (s, 1H), 4.91 (d, $J = 1.1$ Hz, 1H), 3.70 (s, 3H), 2.38 (d, $J = 1.1$ Hz, 3H), 2.15 (s, 3H). ^{13}C NMR (126 MHz, CDCl_3) δ 169.6, 169.0, 155.3, 96.0, 77.3, 76.8, 51.1, 25.3, 21.9. Same as literature.^[119a]



methyl-(E)-3-acetamido-2-butenoate. The crude materials were purified by biotage column (60 mL 10-90% ethyl acetate in petroleum ether, then 120 mL 20-80% ethyl acetate and 240 mL 60-40% ethyl acetate) to afford methyl-(E)-3-acetamido-2-butenoate (yellow solid) 6.7% yield.

^1H NMR (500 MHz, CDCl_3) δ 6.76 (d, $J = 0.6$ Hz, 1H), 6.71 (s, 1H), 3.68 (s, 3H), 2.36 (d, $J = 0.8$ Hz, 3H), 2.12 (s, 3H). ^{13}C NMR (126 MHz, CDCl_3) δ 168.7, 148.5, 102.3, 50.9, 25.1, 18.7. Same as literature.^[119a]



racemic methyl 3-acetamidobutanoate (white solid) in 96% yield. The product was analysed by chiral GC and NMR.

^1H NMR (500 MHz, CDCl_3) δ 6.11 (s, 1H), 4.41 – 4.28 (m, 1H), 3.70 (s, 3H), 2.62 – 2.46 (m, 2H), 1.96 (s, 3H), 1.22 (d, $J = 6.8$ Hz, 3H). ^{13}C NMR (126 MHz, CDCl_3) δ 172.3, 169.3, 51.7, 41.9, 39.7, 23.5, 20.0. Same as the literature.^[119a]

The enantiomeric excess was determined by GC on CP-Chirasil Dex CB, injection temperature, 290 °C; initial column temperature, 90 °C; progress rate, 10 °C/min; final column temperature, 195 °C; $t_R = 11.8$ min, 11.9 min.

7.3 Chapter 4: Continuous hydroformylation in microreactor

General consideration

All the reactions dealing with air- or moisture-sensitive compounds were carried out in a dry reaction vessel under an argon atmosphere or in an argon-filled glovebox. Unless otherwise noted, all reagents were purchased from commercial suppliers without further

purification. Toluene was distilled over sodium chips. Other anhydrous solvents were purchased from J&K Chemical and degassed by bubbling argon over a period of 30 min. Purification of products was carried out by flash chromatography using silica gel (200-300 mesh). Thin layer chromatography was carried out using silica gel plates from Merck (GF254). An achiral column is employed: Agilent HP-5 achiral column (30 m × 0.25 mm × 0.12 μm); H₂ (3 mL/min); temperature range: -60 °C-280 °C.

General procedure for hydroformylation in batch

To a 5-mL vial was added the catalyst precursor Rh(acac)(CO)₂ (5.2 mg, 0.02 mmol), tetrakisphosphite (104 mg, 0.08 mmol) and anhydrous Toluene (2.0 mL) in an argon-filled glovebox. The mixture was stirred at 25 °C for 2 hours, giving a light-yellow solution. And then 1-octene (112 mg, 1 mmol) in 1 mL anhydrous toluene were added into a 5-mL hydrogenation vessel. 100 μL catalyst solution and 100 μL tridecane were added. Then the vessel was placed in an autoclave, closed it and moved it out from the glovebox. The autoclave quickly purged with hydrogen gas for three times, then pressurized to 10 bar H₂ and then additional 10 bar of CO. The pressure was released to 10 bar. The reaction solution was stirred at 100 °C for 24 hours, then it was cooled down to room temperature and the pressure was released carefully. The solution of reaction mixture was taken directly for analysis.

For kinetic study in Batch, a Mettler Toledo Chemical Synthesis Reactor was used. The reactor enabled inline sampling without releasing pressure.

General procedure for hydroformylation in slug flow reactor

To a 5-mL vial was added the catalyst precursor Rh(acac)(CO)₂ (8 mg, 0.031 mmol), tetrakisphosphate (160 mg, 0.13 mmol) and anhydrous Toluene (5.0 mL) in an argon-filled glovebox. The mixture was stirred at 25 °C for 2 hours, giving a light-yellow solution. And then 1-octene (14 g, 125 mmol) and 5 mL catalyst solution and 250 mg tridecane were added into a 50 mL volumetric flask. Anhydrous toluene was added to have the 50 mL reaction medium. Then the solution was filtrated through filter paper to a 50 mL flask that was sealed with septum afterwards.

The process diagram was shown in Figure 22 and Scheme 1. The process was washed by

anhydrous and degassed toluene at a liquid flow rate of 4 mL/min and gas flow rate of 5 sccm (avoid back flow of liquid to gas flow meter) for 5 minutes and then pressurized the BPR. After the reactor was pressurized to 10 bar and heated to 100 °C, the beforehand reaction medium was pumped instead of solvent. Liquid flow rate was set at 0.23 mL/min and gas flow rate 0.9 mL/min (6.6 sccm). The reactor system could achieve steady state in 5 reaction volumes. Samples were collected every 15 minutes in an empty vial. The product distribution was analyzed by GC. When the reaction was finished, system was depressurized by releasing the gas of Equilibar BPR slowly and washed the whole system by pumping toluene for 10 minutes.

General procedure for hydroformylation in flashstop reactor

The procedure was the same as above. The valve was adjusted to the desired part for each condition. The process is shown in Scheme 16 and Figure 70. The time to reach the steady state was 5 times residence time and the sample was collected every 5 minutes.

HP-5, Length: 30 m, Diameter: 0.25 mm, film thickness: 0.12 μ m, N₂ (3 mL/min); injection temp, 250 °C; initial column temperature, 75 °C with a holding time of 2 minutes; progress rate, 0.7 °C /min to 87 °C; Then 25 °C/min to final column temperature, 240 °C; $t_{1\text{-octene}} = 7.42$ min; $t_{3\text{-octene}} = 16.407$ min; $t_{\text{octane}} = 16.407$ min; $t_{(Z),(E)\text{-2-octene}} = 16.407$ min; $t_{\text{b-aldehyde}} = 16.407$ min; $t_{\text{i-aldehyde}} = 16.407$ min; $t_{\text{tridecane}} = 16.407$ min.

Figure 93, Figure 94 and Figure 95 show kinetic data under different pressure in flashstop reactor. The reaction conditions are shown below:

Entry	Temperature (°C)	Pressure (bar)	Liquid flow rate (mL/min)	Gas flow rate (sccm)
140	90	20	0.23	13
141	90	15	0.23	9.9
142	90	5	0.23	3.3

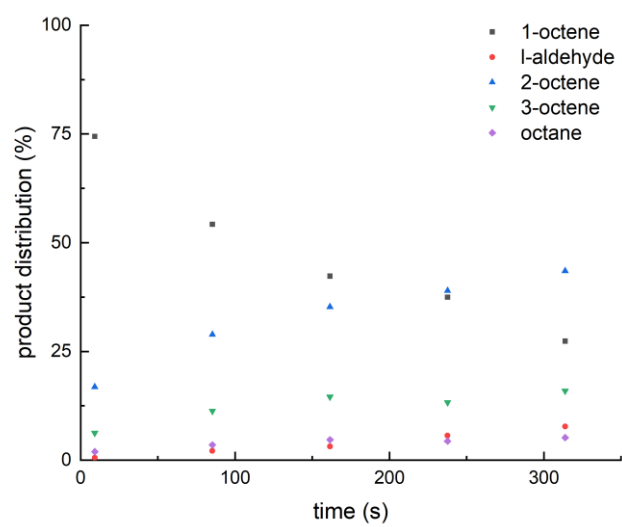


Figure 93 Kinetic data of hydroformylation in flow under 20 bars.

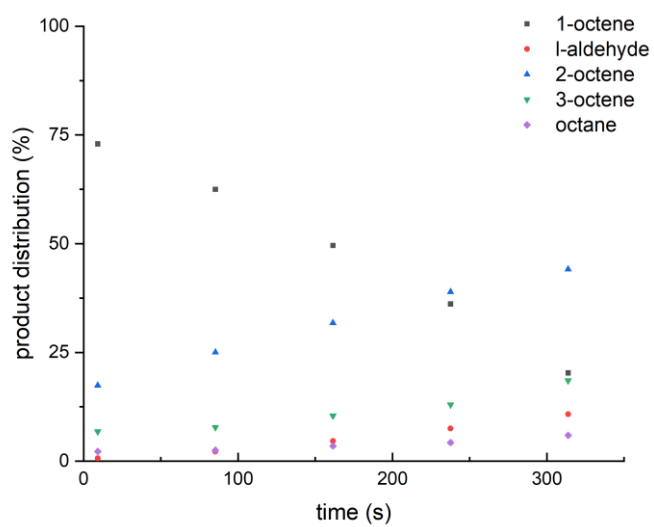


Figure 94 Kinetic data of hydroformylation in flow under 15 bars.

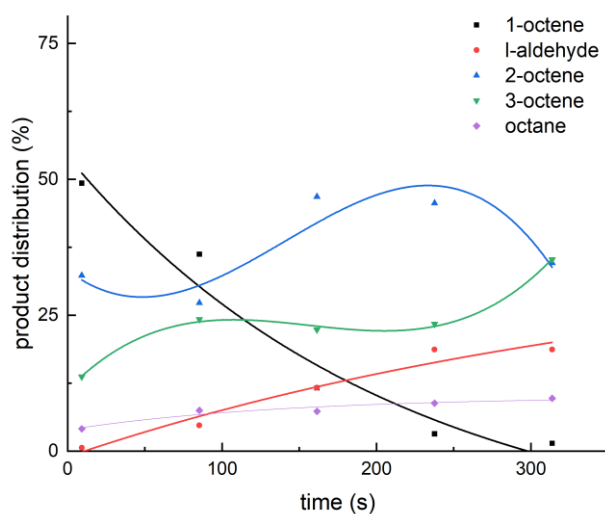


Figure 95 Kinetic data of hydroformylation in flow under 5 bars.

7.4 Chapter 5: Controlling diastereoselectivity: Integrating asymmetric hydrogenation and transfer dehydrogenation.

General Consideration

Unless otherwise stated, all chemicals reported in the manuscript were obtained from Sigma-Aldrich, Fisher Scientific, Alfa Aesar or Fluorochem Ltd. and were used without further purification. All reaction solvents employed were of HPLC grade. Deuterated CDCl_3 was used as supplied. ^1H and ^{13}C NMR spectra were recorded on a Bruker DPX300 (300/75 MHz) spectrometer, a Bruker AV3-400 (400/100 MHz) spectrometer or a Bruker Avance 500 (500/126 MHz) spectrometer using the residual solvent as an internal standard. The values of chemical shifts are reported in parts per million (ppm) with the multiplicities of the spectra reported as follows: singlet (s), doublet (d), triplet (t), quartet (q), multiplet (m) and broad (br), values for coupling constants (J) are assigned in Hz. GC measurements were performed on a HP 6890 Series GC system, 7693 injector, 7693 autosampler and 5973 mass-selective detector. The method employed two columns. One achiral column is a HP-5 column (30 m \times 0.32 mm \times 0.25 μm). Temperature range of oven is -60 $^\circ\text{C}$ to 325 $^\circ\text{C}$. Another is CP-Chirasil Dex CB (25 m \times 0.25 mm \times 0.25 μm). Temperature range of oven is 20 - 200 $^\circ\text{C}$. Pumps were Jasco PU980 Intelligent HPLC pumps and Knauer K-1800 Pump. They were connected to the flow reactors

using PTFE tubing (1 /8" or 1 /16" O.D.) and flangeless male HPLC nuts (1 /8") with flangeless ferrules (1 /8").

Synthesis of N-(3-oxo-1-phenylbut-1-en-2-yl) acetamide (27)

A 50 mL round-bottomed flask was charged with N-acetamidoacetone (500 mg, 4.35 mmol) and 5 mL toluene then benzaldehyde (0.55mL, 5.23 mmol), piperidine (21.5 μ L, 0.22 mmol) and propionic acid (8.5 μ L, 0.12 mmol) were added. The reaction mixture was stirred at 120 °C under reflux by Dean Stark Apparatus for 3 h. TLC plate was used to monitor the reaction. When reaction finished, the solvent was evaporated in vacuo. The crude materials were purified by biotage column (20 mL 10-90% ethyl acetate in petroleum ether, then 60 mL 50-50% ethyl acetate and 20 mL 80-20% ethyl acetate) to afford N-(3-oxo-1-phenylbut-1-en-2-yl)acetamide (412 mg, white solid, yield = 46%).

Synthesis of racemic 3-acetylamino-4-phenyl-2-butanone (66)

Racemic 3-acetylamino-4-phenyl-2-butanone was synthesized by hydrogenation of 10% Pd/C. Procedure is the same as synthesis of racemic methyl 3-acetamidobutaboate in Chapter 3. 381 mg white solid was obtained and yield was 92%.

Synthesis of racemic acetamido-3-phenyl-4-butan-2-ol (65)

3-acetylamino-4-phenyl-2-butanone (100 mg, 0.5 mmol) was dissolved in 0.5 ml MeOH. Then NaBH₄ (20 mg, 0.5 mmol) was added into reaction medium. The reaction was monitored by TLC plate. The reaction was quenched by saturated NH₄Cl. The product was extracted by 5 mL DCM for three times. The organic layer was combined, washed by brine, and dried by Na₂SO₄. 100 mg white solid was obtained by the yield of 95%. de. value was 3:1.

General procedure of homogeneous asymmetric transfer hydrogenation by isopropanol

0.1 mmol substrate and IrCp*₂C₁₄OHCsDPEN (4.1 mg, 0.005 mmol) or immobilized IrCp*₂C₁₄OHCsDPEN (35.7 mg, 0.005 mmol) was dissolved in 1 ml isopropanol. Then NEt₃ (105 μ L, 0.75 mmol) or ^tBuOK (1.4 mg, 0.0125 mmol) was added into reaction medium. The reaction

was stirred under 60 °C for 24 h and monitored by TLC plate. Isopropanol and NEt₃ were removed by evaporation in vacuo. The residue was dissolved in dichloromethane and purified by flash column chromatography to remove metal catalyst.

General procedure of homogeneous asymmetric transfer hydrogenation by TEAF.

IrCp*C₁₄OHCsDPEN (4.1 mg, 0.005 mmol) or immobilized IrCp*C₁₄OHCsDPEN (35.7 mg, 0.005 mmol) was dissolved in 1 ml isopropanol. 40 µL TEAF and 1 mL solvent was added. 0.1 mmol substrate was then added. The reaction was monitored by TLC analysis. TEAF and solvent were removed by evaporation in vacuo. The residue was dissolved in dichloromethane and purified by flash column chromatography to remove metal catalyst.

General procedure of asymmetric dehydrogenation

A 10 mL Schlenk tube was charged with RuCl[(*R,R*)-TsPEN](*p*-cymene) (6.4 mg, 0.01 mmol) and KOH (1.1 mg, 0.02 mmol). Then it is flushed with nitrogen. Acetone (1 mL) was added into the flask and the reaction medium was stirred for 15 minutes until the color changed. Then phenylethanol (122 mg, 1 mmol) was added. The solution was stirred for 22 hours. The reaction was monitored by GC. The solution was purified by flash chromatography to remove metal. 55 mg colourless oil was obtained and yield was 45%. ee was 79%.

Synthesis of 1-chloro-3-phthalimido-propan-2-ol

A 250 mL round bottom flask was charged with epichlorohydrin (2.78g, 30 mmols) and phthalimide (3.97g, 27 mmols) in isopropanol (60 mL). Pyridine (119 mg, 1.5 mmol) was added. The solution stirred under reflux at 85 °C. The solvent was removed *in vacuo*. The residue was dissolved in dichloromethane and washed by 10% NaOH solution and brine. The solution was dried by anhydrous Na₂SO₄. After removing solvent, 5.5 g white solid was obtained with the yield of 85%.

Synthesis of 2-(3-chloro-2-oxopropyl)-1H-isoindole-1,3-dione (29)

1-chloro-3-phthalimido-propan-2-ol (3.6 g, 15 mmols) was dissolved in dichloromethane.

Dess-Martin Reagent (7.35 g, 17 mmols) was added. The reaction was monitored by TLC and finished in 2 hours. The reaction medium was firstly washed by saturated NaHCO₃, washed by water, and dried by anhydrous Na₂SO₄. The solvent was removed *in vacuo*. The resulting product was purified by flash chromatography. 3.4 g yellow solid was obtained with a yield of 95%.

Synthesis of 1-(5-hydroxypentyl)-2,3,4,5-tetramethylcyclopentadiene.

Under a nitrogen atmosphere, lithium wire (7.84 g, 1.13 mol) was added to anhydrous diethyl ether (250 mL) and the lithium suspension was vigorously stirred. 2-bromo-2-butene (80 g, 0.59 mol) in diethyl ether (150 mL) was added to a dropping funnel and a small portion added to the reaction mixture to initiate the reaction. Diethyl ether was also added to the remaining 2-bromo-2-butene, which was then added at a rate that maintained a gentle reflux. After completing addition of 2-bromo-2-butene the reaction was stirred at room temperature for 2 hours. ϵ -Caprolactone (30.7 g, 0.27 mol) in diethyl ether (100 mL) was then added dropwise and the mixture stirred for 1 hour. The resulting mixture was poured into saturated NH₄Cl (300 mL) and after separating the ether layer, the aqueous layer was extracted with *tert*-butyl methyl ether (3*100 mL). The combined ether layers were washed with brine, dried over magnesium sulfate and concentrated to 100 mL. 150 mL 10% aqueous HCl was added to the resulting concentrate and biphasic layers was stirred for 3 h at r.t. After separating the ether layer, the aqueous layer with *tert*-butyl methyl ether (3*50 mL). The combined organic layer was washed with water (2*100 mL), dried over Na₂SO₄, and the solvent evaporated to leave a brown oil, which was purified through a large plug of silica (1:10 ethyl acetate in hexane). Light 19.7 g yellow oil liquid was obtained, and the yield was 35%.

Synthesis of [Ir { η^5 -C₅(CH₃)₄C₅H₁₀OH}Cl₂]₂.

Under nitrogen atmosphere, iridium trichloride hydrate (0.339 g, 1 mmol) and sodium bicarbonate (0.08 g, 1 mmol) were added to degassed methanol (10 mL) in a 30 mL capacity microwave tube and the suspension was purged with nitrogen for 10 minutes. After adding 1-(5-hydroxypentyl)-2,3,4,5-tetramethylcyclopentadiene (0.4 g, 1.9 mmol), the suspension was

purged for a further 5 minutes. The tube was then sealed, and microwave heating was applied at 150 °C for 10 minutes. After effervescence from the solution had subsided, the tube was opened and the solution was diluted with dichloromethane (20 mL), washed with water (3*20 mL), brine (20 mL), dried over Na₂SO₄ and the solvent evaporated. The resulting red oil was purified by column chromatography (1:15 methanol in dichloromethane) to yield an orange powder (0.2 g, 23%).

Synthesis of IrCl{η⁵-C₅(CH₃)₄C₅H₁₀OH}-(S,S,S)-CsDPEN (C.3)

[Ir {η⁵-C₅(CH₃)₄C₅H₁₀OH} Cl₂]₂. (0.8 g, 0.85 mmol) and (S) – (+) – Camphorsulphonyl – (S,S) – DPEN (0.732 g, 1.72 mmol) were dissolved in 12 mL anhydrous dichloromethane. NEt₃ (0.486 mL, 4.45 mmol) was added into the solution. The solution stirred for 24 hours. It was evaporated in vacuo and afford to deep red solid (1.6 g, 98%) without further purification.

Immobilization of IrCl{η⁵-C₅(CH₃)₄C₅H₁₀OH}-(S,S,S)-CsDPEN (C.10)

Under an anhydrous nitrogen atmosphere, a solution of 2,6-di-*tert*-butylpyridine (0.725 g, 3.79 mmol) in dichloromethane (4 mL) was added to trifluoromethanesulfonic anhydride (0.548 g, 1.94 mmol) in dichloromethane (4 mL) at -10 °C. A solution of C. 3 (0.8 g, 0.971 mmol) in dichloromethane (4 mL) was slowly added over an hour. After stirring for an hour, the solution was evaporated to dryness to remove excess trifluoromethanesulfonic anhydride, leaving a brown residue. The resulting residue was dissolved in dichloromethane (4 mL) and Wang resin (0.676 g, 0.947 mmol) was added. The suspension stirred for 24 hours. The resin was washed with dichloromethane until the filtrate was colourless. Then it is washed by water, 1M hydrochloric acid, water and methanol respectively. The resulting dark red resin was repeatedly washed with dichloromethane/propan-2-ol (1:1, 10 mL) at 60 °C for 1 hour until no colour was seen in solution, followed by washing with acetone. The solid is dried in the oven overnight.

Synthesis of 3-phenyloxirane-2-carbonitrile (42)

To a solution of tetrabutylammonium bromide (77 mg, 0.24 mmol), benzaldehyde (0.21 mL,

2.0 mmols) and chloroacetonitrile (0.25 mL, 4.0 mmols) in 10 mL THF, KOH (269 mg, 4.8 mmols) was added slowly. The solution turned from colorless to orange. The reaction was monitored by TLC analysis. The reaction was left stirred for 24 hours under room temperature. The product was extracted by 20 mL DCM for three times. The organic layer was combined, washed by 30 mL brine and 30 mL water and dried by Na₂SO₄. The solvent was evaporated and the crude product was purified by column chromatography (PE:EA, 9:1), which afforded 263 mg product of light yellow oil with a yield of 85 %.

Synthesis of methyl 3-phenyloxirane-2-carboxylate (43)

42 (145 mg, 1 mmol) and K₂CO₃ (138 mg, 1 mmol) were dissolved in 5 mL MeOH. The reaction was monitored by TLC analysis. The reaction was stirred for 3 hours at room temperature. Then the reaction medium was acidified to PH = 6 by 10 mL 0.24 M HCl aqueous solution. The reaction was stirred for another 3 hours. The reaction was quenched by 10 mL saturated NaHCO₃. The product was extracted by 20 mL DCM for three times. The organic layer was combined, washed by 30 mL brine and 30 mL water and dried by Na₂SO₄. The solvent was evaporated and the crude product was purified by column chromatography (PE:EA, 9:1), which afforded 120 mg product of yellow oil with a yield of 67%.

Synthesis of *tert*-butyl (phenyl(phenylsulfonyl)methyl)carbamate (47)

A 50 mL round-bottomed flask equipped with a magnetic stir bar was charged with benzaldehyde (2.1 mL, 20 mmols) and *tert*-butyl carbamate (2.34 g, 20 mmols) in 7 mL THF. To this solution was added 20 mL H₂O, benzene sulfinic acid-sodium salt (3.28 g, 20 mmols) and formic acid (3.8 mL, 100 mmols). The reaction was monitored by TLC analysis. There was white solid precipitating. After 48 hours, the reaction medium was diluted with 20 mL DCM and 50 mL water. The organic layer was separated, and the aqueous layer was extracted with DCM (2*40 mL). The combined organic extracts were dried over Na₂SO₄, filtered and concentrated in vacuo. The crude residue was crystallized by DCM/PE. It afforded 4.3 g white solid with a yield of 62%.

Synthesis of ethyl 3-((*tert*-butoxycarbonyl)amino)-2-diazo-3-phenylpropanoate (48)

A 50 mL round-bottomed flask equipped with a magnetic stir bar and a reflux condenser was charged with CsF (905 mg, 6 mmols) and heated under vacuum for 2 minutes to remove water. 47 (695 mg, 2 mmols) was then added and the flask was sealed with rubber septum and purged with N₂. THF was then added and heated at 60 °C for 12 hours. The reaction was monitored by TLC analysis. The medium was filtrated through celite and concentrated in vacuum. The crude residue was dissolved in 16 mL acetonitrile. The bottle was pured by N₂. Then ethyl diazoacetate (0.3 mL, 2.6 mmols) and DBU (0.1 mL, 0.6 mmol) was added. The reaction was stirred for another 12 hours. The reaction was monitored by TLC analysis. Then the reaction medium was diluted with 20 mL EtOAc and 40 mL water. The organic layer was combined, washed by 30 mL brine and 30 mL water and dried by Na₂SO₄. The solvent was evaporated and the crude product was purified by column chromatography (PE:EA, 19:1), which afforded 359 mg product of yellow oil with a yield of 56%.

Synthesis of ethyl 3-((*tert*-butoxycarbonyl)amino)-2-oxo-3-phenylpropanoate (49)

To a 500 mL round-bottomed flask equipped with a magnetic bar, NaHCO₃ (1.5 g, 17.8 mmols) and 26.7 mL acetone/water (1:1) were added. The reaction medium was cooled down to 0 °C by ice batch and the oxone (2.73 g, 4.45 mmols) was added in three portions. Then the reaction medium was stirred under room temperature for 30 minutes. The reaction medium was recooled to 0 °C. 48 (359 mg, 0.89 mmol) was dissolved in 17.8 mL DCM and was added dropwise into oxone solution. There were bubble generating when it was added. The reaction was stirred under room temperature for another one hour. The reaction was monitored by TLC analysis. Then the reaction medium was diluted with 40 mL DCM and 40 mL water. The organic layer was combined, washed by 30 mL brine and 30 mL water and dried by Na₂SO₄. The solvent was evaporated and the crude product was purified by column chromatography (PE:EA, 14:1), which afforded 351 mg product of colorless oil with a yield of 92%.

Synthesis of 2-benzamido-2-phenylacetic acid (51)

To a 500 mL round-bottomed flask, phenylglycine (9g, 60 mmols) was added and dissolved

in 180 mL NaOH (1 M). The reaction medium was cooled down to 0 °C. Benzoyl chloride (7.73 mL, 66 mmols) was added dropwise and stirred for 8 hours. The reaction was monitored by TLC analysis. When the reactant was all consumed, concentrated H₂SO₄ was added dropwise till the Ph = 7. The product was precipitated during this process. The crude product was crystallized again by MeOH/DCM to afford 8.5 g white solid with a yield of 56%.

Synthesis of ethyl 3-benzamido-2-oxo-3-phenylpropanoate (53)

To a 100 mL round-bottomed flask, 51 (6.12 g, 24 mmols) and DMAP (100 mg, 0.82 mmol) were added. The flask was purged with N₂. 24 mL anhydrous THF and pyridine (6 mL, 72 mmols) were added to dissolve the substrate. To the above solution, ethyl oxalyl chloride was added dropwise to initiate gentle refluxing. The reaction medium turned yellow with white precipitation generated. The mixture was refluxed for 3.5 hours. The reaction was monitored by TLC analysis. Then the reaction medium was cooled down and 48 mL was added. The solution was stirred for half an hour before it is extracted by 20 mL EA for three times. The organic layer was combined, washed by 30 mL brine and 30 mL water and dried by Na₂SO₄. The solvent was evaporated, and the crude product was purified by crystallization (EA/PE). The white solid was redissolved in 50 mL ethanol and 6 g NaHCO₃ was added. The reaction medium was heated to reflux for 0.5 hour. The substrate was not soluble in the beginning and dissolved gradually. The reaction was monitored by TLC analysis. The reaction medium was diluted by 100 mL DCM and 100 mL water. The aqueous layer was washed by 30 mL DCM for three times. The organic layer was combined, washed by 50 mL brine and 50 mL water and dried by Na₂SO₄. The solvent was evaporated and the crude product was purified by column chromatography (PE: EA, 4:1), which afforded 1.9 g product of colorless oil with a yield of 25% by two steps reaction.

Synthesis of *tert*-butyl (S)-2-(2-(methoxy(methyl)amino)-2-oxo-1-phenylethyl)carbamate (56)

To the solution of (S)-2-((*tert*-butoxycarbonyl)amino)-2-phenylacetic acid (5 g, 20 mmols) in dichloromethane (50 mL) was added N,O-dimethylhydroxylamine (3.9 g, 40 mmols). To the resulting mixture was then added HOBT (0.25 g, 2 mmol), EDCI•HCl (6 g, 30 mmol) and NEt₃

(4 g, 40 mmol). The reaction mixture was stirred at ambient temperature for 3 h. TLC analysis indicated complete consumption of the starting material. The reaction mixture was bi-phased with dichloromethane (125 mL) and water (60 mL). The aqueous layer was extracted with dichloromethane (2 x 50 mL). The combined organic layers were washed with 50 mL brine, dried (Na_2SO_4) and concentrated under reduced pressure. The crude product was purified by a flash column chromatography to afford 2.8 g white solid with a yield of 48%.

Synthesis of *tert*-butyl (S)-(2-oxo-1-phenylpropyl)carbamate (57)

At 0°C, to a solution of (S)-*tert*-butyl (2-(methoxy(methyl)amino)-2-oxo-1-phenylethyl)carbamate (0.9 g, 3.06 mmol) in anhydrous THF (15 mL), was added MeMgBr (3M solution in Et_2O , 2.0 mL, 6.1 mmol) and resulting mixture was allowed to warm and stirred at ambient temperature. After 2 hours, the reaction was carefully quenched with saturated aqueous NH_4Cl solution (10 mL), and the organic contents were extracted with CH_2Cl_2 (3 x 25 mL). The solvent was removed under reduced pressure. The compound obtained is purified by recrystallization to afford 700 mg white solid with a yield of 92%.

Synthesis of (nitromethyl)benzene (59)

Benzyl bromide (171 mg, 1 mmol) in diethyl ether (2.6 mL) was added dropwise to a slurry of powdered silver nitrite (230 mg, 1.3 mmol) in diethyl ether (2.6 mL) placed in an ice bath and wrapped with aluminum foil, while maintaining the temperature below 0 °C. The mixture was then stirred at room temperature in the dark until completion, was then filtered on a Celite plug and washed with 20 mL of diethyl ether. The combined organic layers were washed with 50 mL brine, dried by anhydrous Na_2SO_4 and concentrated under reduced pressure. The crude product was purified by a column chromatography (PE:EA, 1:1) to afford 69 mg light yellow oil with a yield of 50%.

Synthesis of methyl 2-hydroxy-3-nitro-3-phenylpropanoate (61)

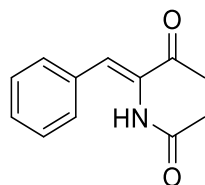
To a solution of 59 (411 mg, 3 mmols) and 3-oxo-propionic acid ethyl ester (357 mg, 3.5 mmols) in 2.5 mL $t\text{BuOH/THF}$ (1:1), $t\text{BuOK}$ (28 mg, 0.25 mmol) was added slowly. Then the

reaction medium was stirred under room temperature for 24 hours. The reaction was monitored by TLC analysis. The reaction mixture was bi-phased with dichloromethane (20 mL) and water (40 mL). The aqueous layer was extracted with dichloromethane (2 x 20 mL). The combined organic layers were washed with 30 mL brine, dried by anhydrous Na₂SO₄ and concentrated under reduced pressure. The crude product was purified by column chromatography (PE/EA, 95:5) to afford 322 mg light yellow oil with a yield of 45%.

Synthesis of 2-nitro-1-phenylpropan-1-ol (63)

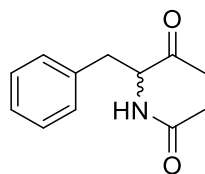
To a stirred solution of benzaldehyde (3.18 g, 30 mmol) in nitroethane (11 mL, 150 mmol) and 30 mL DCM at rt was added dropwise triethylamine (420 μ L, 3 mmol). The resulting mixture was stirred under N₂ for 16 h. The reaction was monitored by TLC analysis. Excess solvent was evaporated in vacuo. The crude product was purified by column chromatography (PE/EA, 90:10) to afford 4.6 g light yellow oil with a yield of 85%.

Characterization data for compounds



N-(3-oxo-1-phenylbut-1-en-2-yl) acetamide (27) purified by biotage column (20 mL 10-90% ethyl acetate in petroleum ether, then 60 mL 50-50% ethyl acetate and 20 mL 80-20% ethyl acetate) to afford N-(3-oxo-1-phenylbut-1-en-2-yl)acetamide (white solid, yield = 46%).

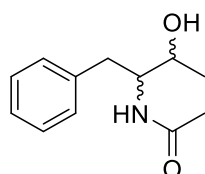
¹H NMR (501 MHz, CDCl₃) δ 7.45 (d, J = 6.1 Hz, 2H), 7.36 (m, 3H), 7.20 (s, 1H), 2.47 (s, 3H), 2.13 (s, 3H). ¹³C NMR (126 MHz, CDCl₃) δ 196.1, 168.2, 134.2, 131.8, 131.0, 129.7, 129.6, 128.6, 25.2, 23.7.



N-(3-oxo-1-phenylbutan-2-yl) acetamide (66) White solid was obtained and yield was 92%.

^1H NMR (400 MHz, CDCl_3) δ 7.44 – 7.18 (m, 3H), 7.18 – 6.96 (m, 3H), 6.14 (s, 1H), 4.89 (dd, J = 12.8, 6.9 Hz, 1H), 3.11 (ddd, J = 19.7, 14.0, 6.2 Hz, 2H), 2.17 (s, 3H), 2.00 (s, 3H). ^{13}C NMR (101 MHz, CDCl_3) 206.3, 169.7, 135.8, 129.2, 128.7, 127.2, 59.5, 37.2, 28.1, 23.1.

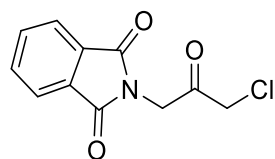
CP-Chirasil Dex Cb, Length: 25 m, Diameter: 0.25 mm, film thickness: 0.25 μm , H_2 (3 mL/min); injection temp, 290 $^\circ\text{C}$; initial column temperature, 80 $^\circ\text{C}$; progress rate, 15 $^\circ\text{C}/\text{min}$ to 135 $^\circ\text{C}$; Then 0.5 $^\circ\text{C}/\text{min}$ to final column temperature, 150 $^\circ\text{C}$; t_{R} = 16.05 min, 16.41 min.



N-(3-hydroxy-1-phenylbutan-2-yl) acetamide (65) White solid was obtained by the yield of 95%. de. value was 3:1.

^1H NMR (501 MHz, CDCl_3) δ 7.27 – 7.20 (m, 2H), 7.18 – 7.08 (m, 3H), 5.82 – 5.33 (m, 1H), 4.15 – 3.92 (m, 1H), 3.92 – 3.59 (m, 1H), 3.36 – 3.01 (m, 1H), 2.96 – 2.61 (m, 2H), 1.87 (d, J = 34.3 Hz, 3H), 1.18 – 1.07 (m, 3H). ^{13}C NMR (126 MHz, CDCl_3) δ 171.3, 137.8, 129.2, 129.0, 128.7, 128.7, 128.6, 126.6, 69.8, 67.4, 56.9, 55.7, 38.3, 35.4, 23.3, 21.0, 18.8.

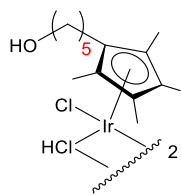
CP-Chirasil Dex Cb, Length: 25 m, Diameter: 0.25 mm, film thickness: 0.25 μm , H_2 (3 mL/min); injection temp, 290 $^\circ\text{C}$ initial column temperature, 80 $^\circ\text{C}$; progress rate, 15 $^\circ\text{C}/\text{min}$ to 135 $^\circ\text{C}$; Then 0.5 $^\circ\text{C}/\text{min}$ to final column temperature, 150 $^\circ\text{C}$; t_{R} = 28.63 min, 29.0 min, 30.16 min, 30.79 min.



2-(3-chloro-2-oxopropyl) isoindoline-1,3-dione (29) Purified by flash chromatography. Yellow solid was obtained with a yield of 95%.

^1H NMR (400 MHz, CDCl_3) δ 7.92 – 7.76 (m, 2H), 7.75 – 7.55 (m, 2H), 4.70 (s, 2H), 4.15 (s, 2H).

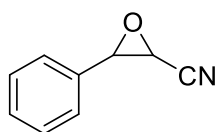
It is the same as results in the literature.^[125]



[Ir { η^5 -C5(CH₃)₄C₅H₁₀OH}Cl₂]₂ Purified by column chromatography (1:15 methanol in dichloromethane) to yield an orange powder (0.2 g, 23%).

¹H NMR (400 MHz, CDCl₃) δ 3.56 (t, *J* = 6.3 Hz, 2H), 2.15 – 1.97 (m, 2H), 1.60 – 1.43 (m, 12H), 0.81 (m, 6H).

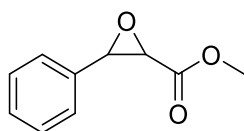
It is the same as results in the literature.^[51f]



3-phenyloxirane-2-carbonitrile (42) The crude product was purified by column chromatography (PE:EA, 9:1), which afforded 263 mg product of light yellow oil with a yield of 85 %.

¹H NMR (600 MHz, CDCl₃) δ 7.35 – 7.28 (m, 5H), 4.10 (d, *J* = 3.8 Hz, 1H), 3.62 (d, *J* = 3.8 Hz, 1H).

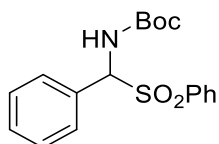
It is the same as results in the literature.^[136]



methyl 3-phenyloxirane-2-carboxylate (43) The solvent was evaporated and the crude product was purified by column chromatography (PE:EA, 9:1), which afforded 120 mg product of yellow oil with a yield of 67%.

¹H NMR (600 MHz, CDCl₃) δ 7.38 – 7.29 (m, 5H), 4.10 (d, *J* = 1.8 Hz, 1H), 3.86 – 3.79 (s, 3H), 3.52 (d, *J* = 1.8 Hz, 1H).

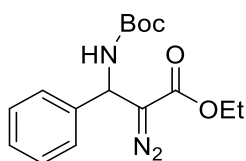
It is the same as results in the literature.^[137]



tert-butyl (phenyl(phenylsulfonyl)methyl) carbamate (47) purified by crystallization (DCM/PE). It afforded 4.3 g white solid with a yield of 62%.

^1H NMR (600 MHz, CDCl_3) δ 7.92 (d, $J = 7.7$ Hz, 2H), 7.64 (t, $J = 7.5$ Hz, 1H), 7.54 (d, $J = 7.7$ Hz, 2H), 7.49 – 7.37 (m, 5H), 5.92 (d, $J = 10.8$ Hz, 1H), 5.73 (d, $J = 10.9$ Hz, 1H), 1.26 (s, 9H).

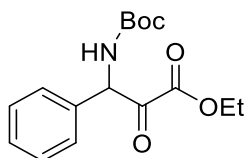
It is the same as results in the literature.^[127]



ethyl 3-((tert-butoxycarbonyl)amino)-2-diazo-3-phenylpropanoate (48) purified by column chromatography (PE:EA, 19:1), which afforded 359 mg product of yellow oil with a yield of 56%.

^1H NMR (400 MHz, CDCl_3) δ 7.35 – 7.06 (m, 5H), 5.86 – 5.64 (m, 1H), 5.59 (d, $J = 8.0$ Hz, 1H), 4.09 (q, $J = 7.1$ Hz, 2H), 1.33 (s, 9H), 1.12 (t, $J = 7.2$ Hz, 3H). ^{13}C NMR (101 MHz, CDCl_3) δ 165.9, 155.1, 139.0, 128.8, 127.9, 126.2, 80.1, 77.6, 77.3, 77.0, 61.0, 51.0, 28.3, 14.4.

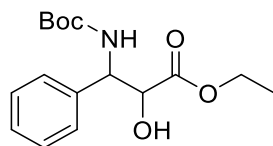
It is the same as results in the literature.^[127]



ethyl 3-((tert-butoxycarbonyl)amino)-2-oxo-3-phenylpropanoate (49) purified by column chromatography (PE:EA, 14:1), which afforded 351 mg product of colorless oil with a yield of 92%.

^1H NMR (400 MHz, CDCl_3): δ 7.37-7.30 (m, 5H), 6.05-6.03 (d, $J = 6.8$ Hz, 1H), 5.62-5.61 (d, $J = 5.6$ Hz, 1H), 4.23-4.16 (m, 2H), 1.41 (s, 9H), 1.23-1.20 (t, $J = 7.2$ Hz, 3H); ^{13}C NMR (100 MHz, CDCl_3): δ 189.4, 159.6, 154.7, 133.7, 129.2, 128.9, 128.5, 80.3, 76.7, 62.7, 61.0, 28.2, 13.7

It is the same as results in the literature.^[127]

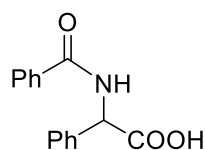


ethyl 3-((tert-butoxycarbonyl)amino)-2-hydroxy-3-phenylpropanoate (68) purified by a flash column chromatography to afford 294 mg white solid with a yield of 95%.

^1H NMR (400 MHz, CDCl_3) δ 7.28-7.26 (m, 5H), 5.64-5.62 (d, $J = 7.6$ Hz, 1H), 5.12-5.10 (d, $J = 7.2$ Hz, 1H), 4.57 (bs, 1H), 4.16-4.08 (m, 2H), 2.94-2.93 (d, $J = 6.4$ Hz, 1H), 1.42 (s, 9H), 1.25-1.22 (t, $J = 7.2$ Hz, 3H); ^{13}C NMR (100 MHz, CDCl_3) δ 171.8, 154.9, 128.3, 128.1, 127.4, 79.8, 73.2, 62.0, 56.5, 28.3, 14.0;

The enantiomeric excess was determined by HPLC on Chiralpak OD-H column, hexane: isopropanol = 90:10; flow rate = 1 mL/min; UV detection at 220 nm; $t_R = 8.7$ min, 9.9 min, 10.6 min, 11.1 min.

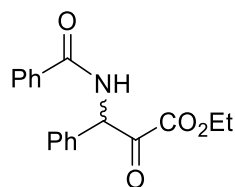
It is the same as results in the literature.^[127]



2-benzamido-2-phenylacetic acid (51) purified by crystallization (MeOH/DCM) to afford 8.5 g white solid with a yield of 56%.

^1H NMR (600 MHz, $\text{DMSO}-d_6$) δ 13.50 (s, 1H), 9.60 (dd, $J = 7.5, 3.5$ Hz, 1H), 8.55 – 8.35 (m, 2H), 8.16 – 7.99 (m, 5H), 7.98 – 7.84 (m, 3H), 6.16 (ddt, $J = 7.6, 5.1, 2.0$ Hz, 1H). ^{13}C NMR (151 MHz, $\text{DMSO}-d_6$) δ 173.0, 167.3, 138.1, 134.8, 132.5, 129.4, 129.2, 129.2, 129.0, 128.7, 57.8, 40.9, 40.8, 40.7, 40.5, 40.4, 40.3, 40.1.

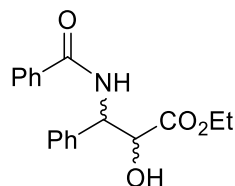
It is the same as results in the literature.^[129]



ethyl 3-benzamido-2-oxo-3-phenylpropanoate (53) purified by column chromatography (PE:EA, 4:1), which afforded 1.9 g product of colorless oil with a yield of 25% by two steps reaction.

^1H NMR (400 MHz, CDCl_3) δ 7.90 – 7.78 (m, 2H), 7.66 – 7.33 (m, 8H), 7.18 (d, J = 6.5 Hz, 1H), 6.48 (d, J = 6.4 Hz, 1H), 4.26 (m, 2H), 1.26 (t, J = 7.2 Hz, 3H).

It is the same as results in the literature.^[129]

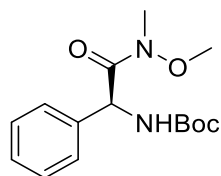


ethyl 3-benzamido-2-hydroxy-3-phenylpropanoate (67) purified by a flash column chromatography to afford 306 mg white solid with a yield of 98%.

^1H NMR (600 MHz, CDCl_3) δ 7.74 (m, 2H), 7.50 – 7.20 (m, 8H), 7.13 (d, J = 8.6 Hz, 1H), 5.56 (dd, J = 8.6, 3.6 Hz, 1H), 4.62 (d, J = 3.6 Hz, 1H), 4.09 (m, 2H), 1.18 (t, J = 7.1 Hz, 3H). ^{13}C NMR (151 MHz, CDCl_3) δ 170.8, 165.6, 135.6, 133.1, 131.0, 130.7, 127.7, 127.6, 127.6, 127.5, 127.3, 127.2, 126.6, 126.3, 126.1, 76.2, 76.1, 75.8, 71.9, 61.3, 54.5, 13.1.

ee was determined by SFC analysis. Column: Trefoil AMY1 2.1 \times 50 mm, 2.5 μm ; CO_2 :MeOH,93:7; 0.6 mL/min; 120 bar; 35 $^\circ\text{C}$; t_{R} = 7.0 min, 9.1 min, 9.8 min, 11.9 min.

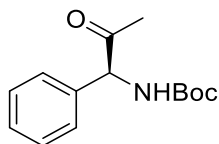
It is the same as results in the literature.^[129]



tert-butyl (S)-(2-(methoxy(methyl)amino)-2-oxo-1-phenylethyl)carbamate (56) The crude product was purified by a flash column chromatography to afford 2.8 g white solid with a yield of 48%.

^1H NMR (400 MHz, CDCl_3) δ 7.47 – 7.08 (m, 5H), 5.83 (d, J = 8.3 Hz, 1H), 5.77 – 5.62 (m, 1H), 3.58 – 3.37 (m, 3H), 3.23 – 3.07 (m, 3H), 1.40 (dd, J = 6.4, 3.5 Hz, 9H).

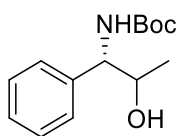
It is the same as results in the literature.^[138]



tert-butyl (S)-(2-oxo-1-phenylpropyl)carbamate (57) purified by recrystallization to afford 700 mg white solid with a yield of 92%.

^1H NMR (400 MHz, CDCl_3) δ 7.42 – 7.27 (m, 5H), 5.89 (d, J = 6.5 Hz, 1H), 5.28 (d, J = 6.4 Hz, 1H), 2.09 (s, 3H), 1.41 (s, 9H). ^{13}C NMR (101 MHz, CDCl_3) δ 203.6, 154.9, 136.9, 129.2, 128.5, 127.8, 79.9, 77.4, 77.5, 76.7, 64.8, 28.3, 27.1.

It is the same as results in the literature.^[139]

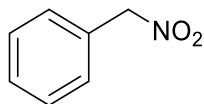


tert-butyl ((1S)-2-hydroxy-1-phenylpropyl)carbamate (69) purified by a flash column chromatography to afford 238 mg white solid with a yield of 95%.

^1H NMR (400 MHz, CDCl_3) δ 7.41 – 7.16 (m, 5H), 5.39 (d, J = 8.1 Hz, 1H), 4.61 (s, 1H), 4.19 – 3.90 (m, 1H), 1.42 (s, 10H), 1.22 (d, J = 6.3 Hz, 1H), 1.08 (d, J = 6.4 Hz, 2H). ^{13}C NMR (151 MHz, CDCl_3) δ 155.6, 128.8, 128.5, 127.7, 127.7, 127.6, 126.6, 79.8, 77.2, 77.0, 76.8, 70.4, 60.1, 28.4, 20.3, 19.7.

The enantiomeric excess was determined by HPLC on Chiralpak IA column, hexane: isopropanol = 97:3; flow rate = 0.8 mL/min; UV detection at 210 nm; t_R = 27.3 min, 32.2 min, 33.5 min, 39.0 min.

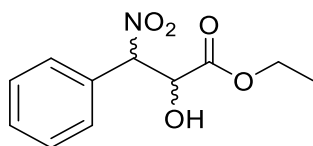
It is the same as results in the literature.^[139]



(nitromethyl)benzene (59) purified by a column chromatography (PE:EA, 1:1) to afford 69 mg light yellow oil with a yield of 50%.

^1H NMR (600 MHz, CDCl_3) δ 7.35 (d, J = 12.3 Hz, 5H), 5.33 (s, 2H). ^{13}C NMR (151 MHz, CDCl_3) δ 130.0, 129.8, 129.1, 80.1, 77.3, 77.1, 76.9.

It is the same as results in the literature.^[140]

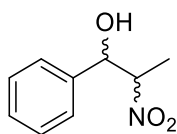


ethyl 2-hydroxy-3-nitro-3-phenylpropanoate (61) The crude product was purified by column chromatography (PE/EA, 95:5) to afford 322 mg light yellow oil with a yield of 45%.

^1H NMR (600 MHz, CDCl_3) δ 7.52 (d, $J = 7.2$ Hz, 2H), 7.44 (m, 3H), 5.81 – 5.63 (m, 1H), 4.84 (m, 1H), 4.28 – 4.14 (m, 2H), 3.39 (dd, $J = 12.9, 6.4$ Hz, 1H), 1.23 (t, $J = 7.2$, 1H), 1.13 (t, $J = 7.2$ Hz, 2H). ^{13}C NMR (151 MHz, CDCl_3) δ 170.5, 170.4, 131.0, 130.3, 130.2, 129.4, 129.0, 128.9, 128.8, 91.8, 90.4, 77.2, 77.0, 76.8, 72.4, 71.5, 63.0, 62.8, 14.0, 13.8.

The enantiomeric excess was determined by HPLC on Chiralpak OD-H column, hexane: isopropanol = 90:10; flow rate = 0.8 mL/min; UV detection at 220 nm; $t_1 = 10.2$ min, $t_2 = 10.8$ min, $t_3 = 12.1$ min, $t_4 = 18.7$ min.

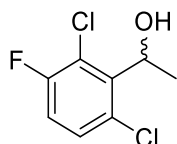
It is the same as results in the literature.^[131]



2-nitro-1-phenylpropan-1-ol (63) The crude product was purified by column chromatography (PE/EA, 90:10) to afford 4.6 g light yellow oil with a yield of 85%.

^1H NMR (400 MHz, CDCl_3) δ 7.41 – 7.21 (m, 5H), 4.96 (dd, $J = 9.1, 3.9$ Hz, 1H), 4.73 (dq, $J = 9.0, 6.8$ Hz, 1H), 3.16 (dd, $J = 7.3, 4.0$ Hz, 1H), 1.45 (d, $J = 6.8$ Hz, 1H), 1.26 (d, $J = 6.9$ Hz, 2H). ^{13}C NMR (101 MHz, CDCl_3) δ 138.7, 138.5, 129.1, 129.0, 128.7, 128.5, 127.0, 126.0, 88.5, 87.5, 77.5, 77.2, 76.9, 76.2, 74.0, 16.4, 12.1.

It is the same as results in the literature.^[132]

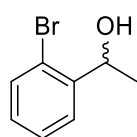


1-(2,6-dichloro-3-fluorophenyl)ethan-1-ol (72) The compound was obtained by asymmetric transfer hydrogenation. The crude product was purified by a flash column chromatography to afford 208 mg colourless oil with a yield of 99%.

^1H NMR (600 MHz, CDCl_3) δ 7.35 – 7.16 (m, 1H), 7.02 (dd, $J = 8.9, 8.0$ Hz, 1H), 5.57 (q, $J = 9.7$ Hz, 1H), 2.99 (d, $J = 9.7$ Hz, 1H), 1.64 (d, $J = 6.9$ Hz, 3H). ^{13}C NMR (151 MHz, CDCl_3) δ 157.3 ($^1J_{\text{C-F}} = 248$ Hz), 140.6, 129.6 ($^3J_{\text{C-F}} = 7$ Hz), 115.6 ($^2J_{\text{C-F}} = 23$ Hz), 68.4, 21.3. ^{19}F NMR (565 MHz, CDCl_3) δ -113.3.

The enantiomeric excess was determined by HPLC on Chiralpak OD-H column, hexane: isopropanol = 99:1; flow rate = 0.5 mL/min; UV detection at 254 nm; $t_{\text{R}} = 17.9$ min (major), 19.1 min (minor)

It is the same as results in the literature.^[141]



1-(2-bromophenyl) ethan-1-ol (74) The compound was obtained by asymmetric transfer hydrogenation. The crude product was purified by a flash column chromatography to afford 200 mg colourless oil with a yield of 99%.

^1H NMR (600 MHz, CDCl_3) δ 7.50 (dd, $J = 7.8, 1.7$ Hz, 1H), 7.46 – 7.39 (dd, $J = 8.0, 1.1$ Hz, 1H), 7.25 (t, $J = 7.5$ Hz, 1H), 7.04 (td, $J = 7.7, 1.7$ Hz, 1H), 5.14 (q, $J = 6.4$ Hz, 1H), 1.39 (d, $J = 6.4$ Hz, 3H). ^{13}C NMR (151 MHz, CDCl_3) δ 144.7, 132.7, 128.8, 127.9, 126.7, 121.7, 77.3, 77.1, 76.9, 69.2, 23.6, 1.1.

The enantiomeric excess was determined by HPLC on Chiralpak OD-H column, hexane: isopropanol = 99:1; flow rate = 1 mL/min; UV detection at 254 nm; $t_{\text{R}} = 15.9$ min (major), 17.7 min (minor)

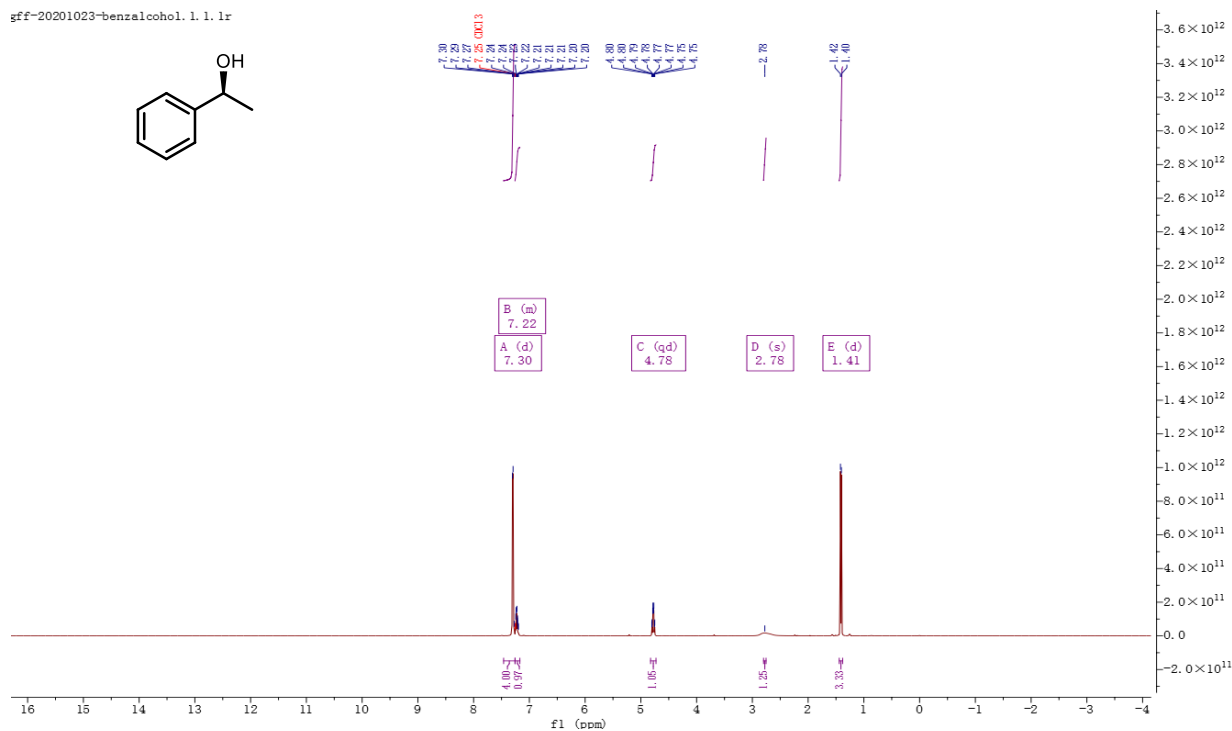
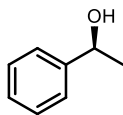
It is the same as results in the literature.^[142]

7.5 NMR, HPLC and GC spectrum

(S)-1-phenylethan-1-ol (2):

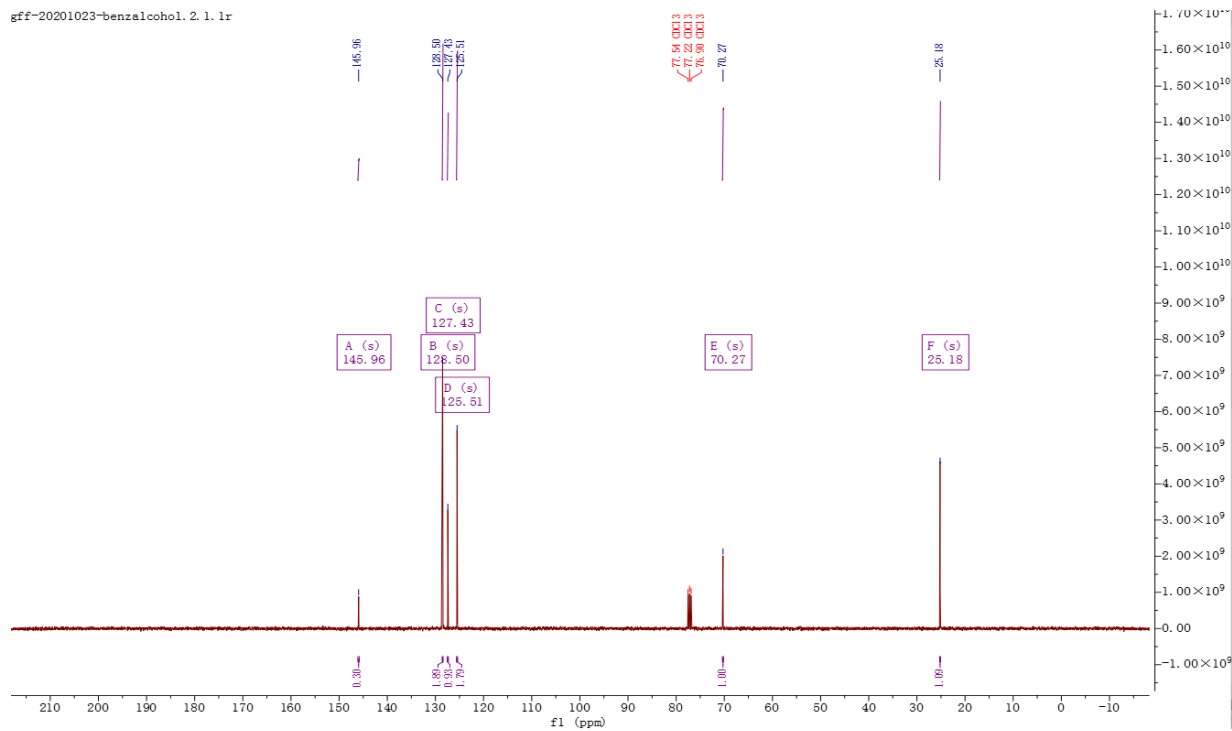
¹H NMR (400 MHz, CDCl₃)

gff-20201023-benzalcohol.1.1.1r



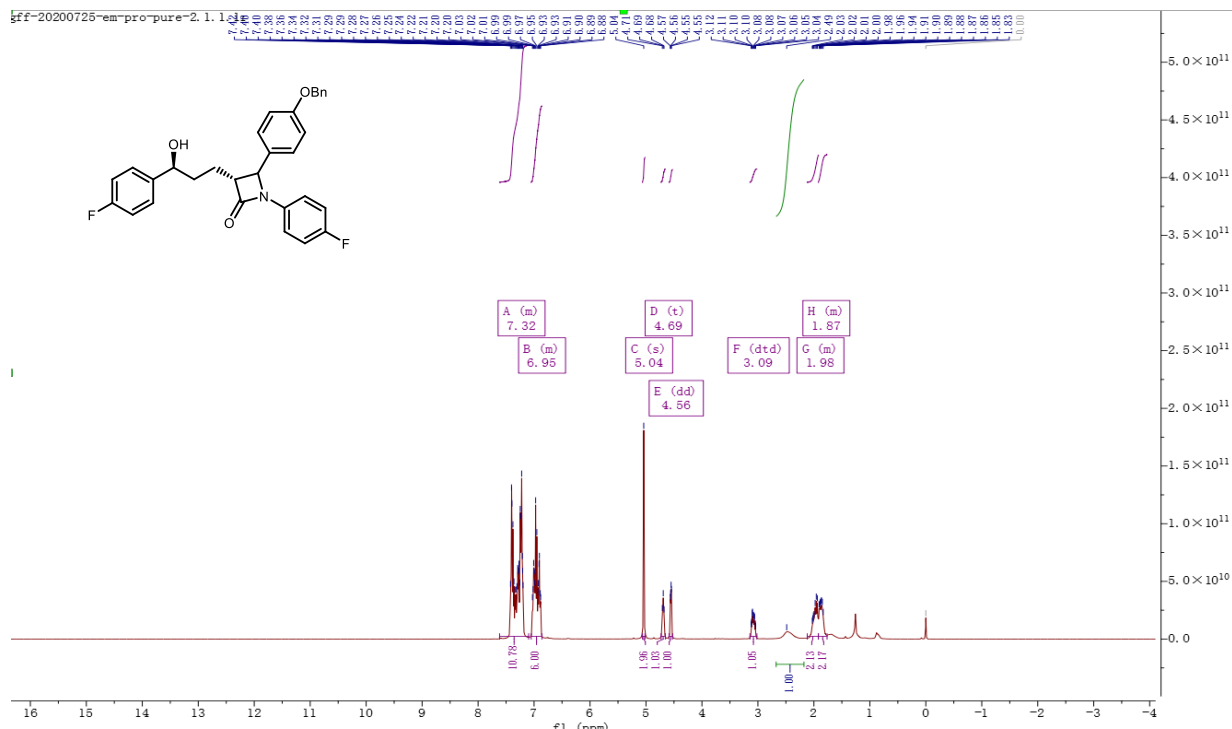
¹³C NMR (101 MHz, CDCl₃)

gff-20201023-benzalcohol.2.1.1r

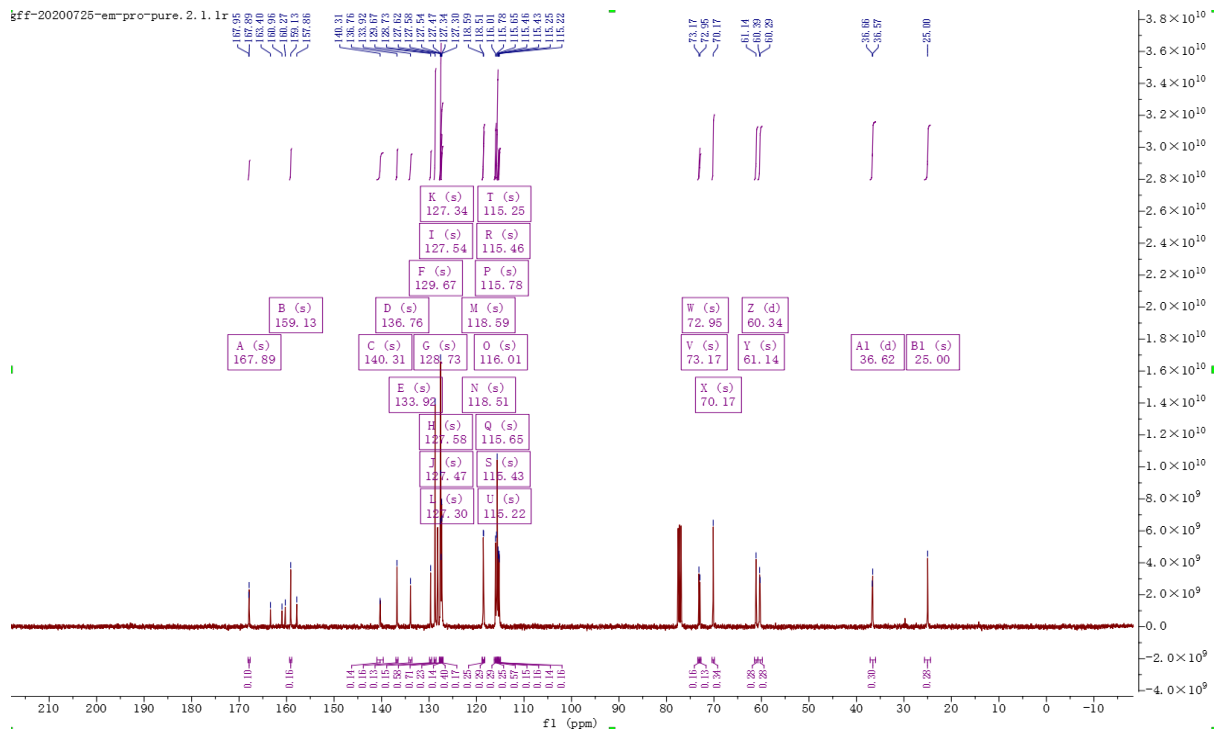


(3*R*)-4-(4-(benzyloxy)phenyl)-1-(4-fluorophenyl)-3-((*S*)-3-(4-fluorophenyl)-3-hydroxypropyl)azetidin-2-one (4):

¹H NMR (400 MHz, CDCl₃)

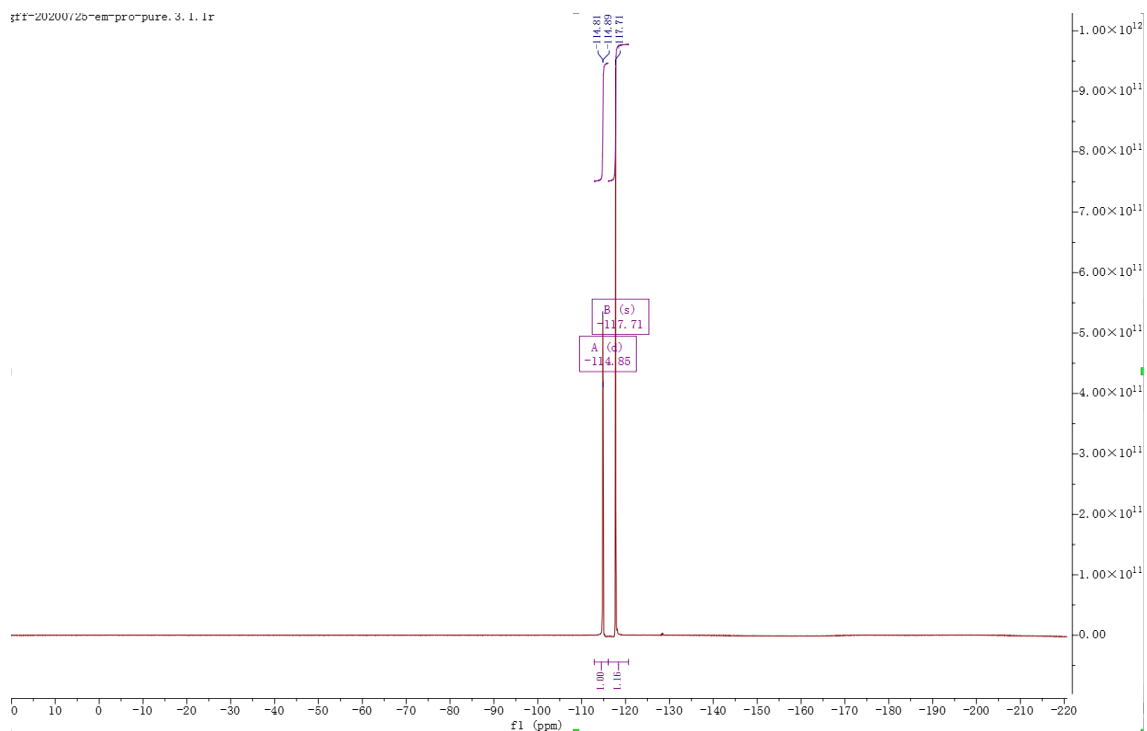


¹³C NMR (101 MHz, CDCl₃)



¹⁹F NMR (376 MHz, CDCl₃)

fff-20200720-em-pure. 3. 1. 1r



(3R)-1-(4-fluorophenyl)-3-((S)-3-(4-fluorophenyl)-3-hydroxypropyl)-4-(4-hydroxyphenyl)azetidin-2-one (5):

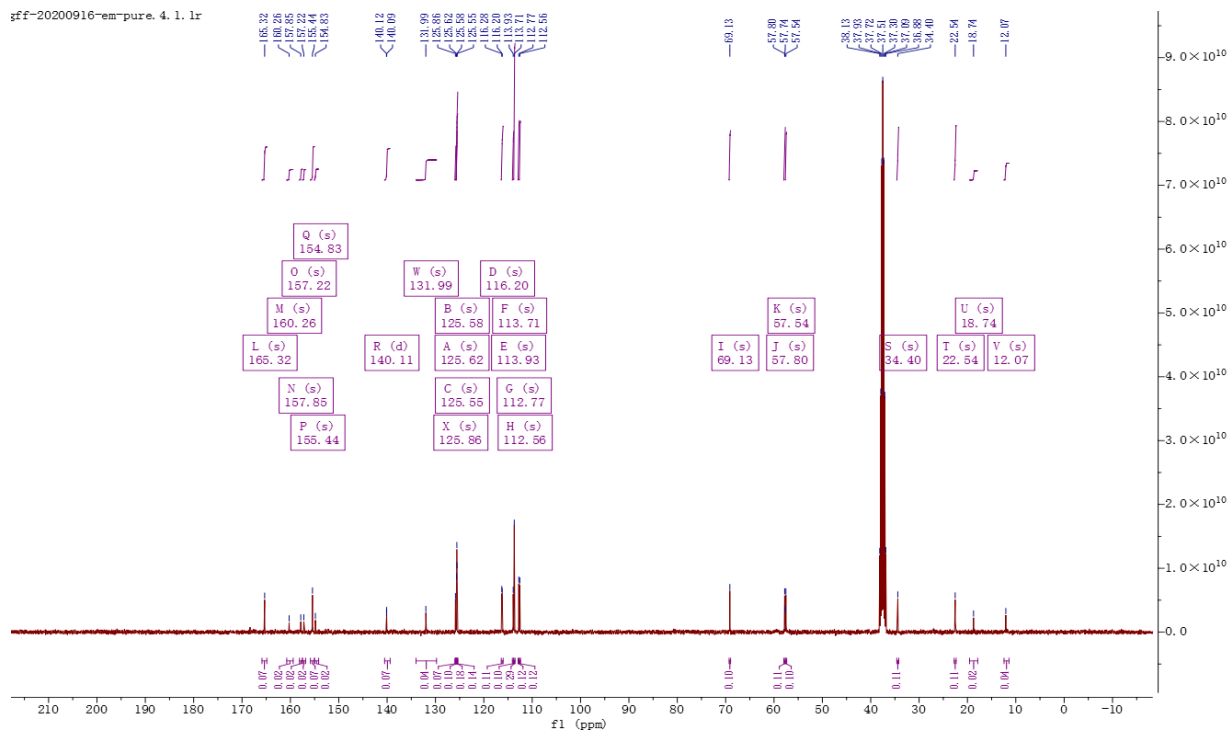
¹H NMR (400 MHz, DMSO-d₆)

fff-20200916-em-pure. 1. 1. 1r



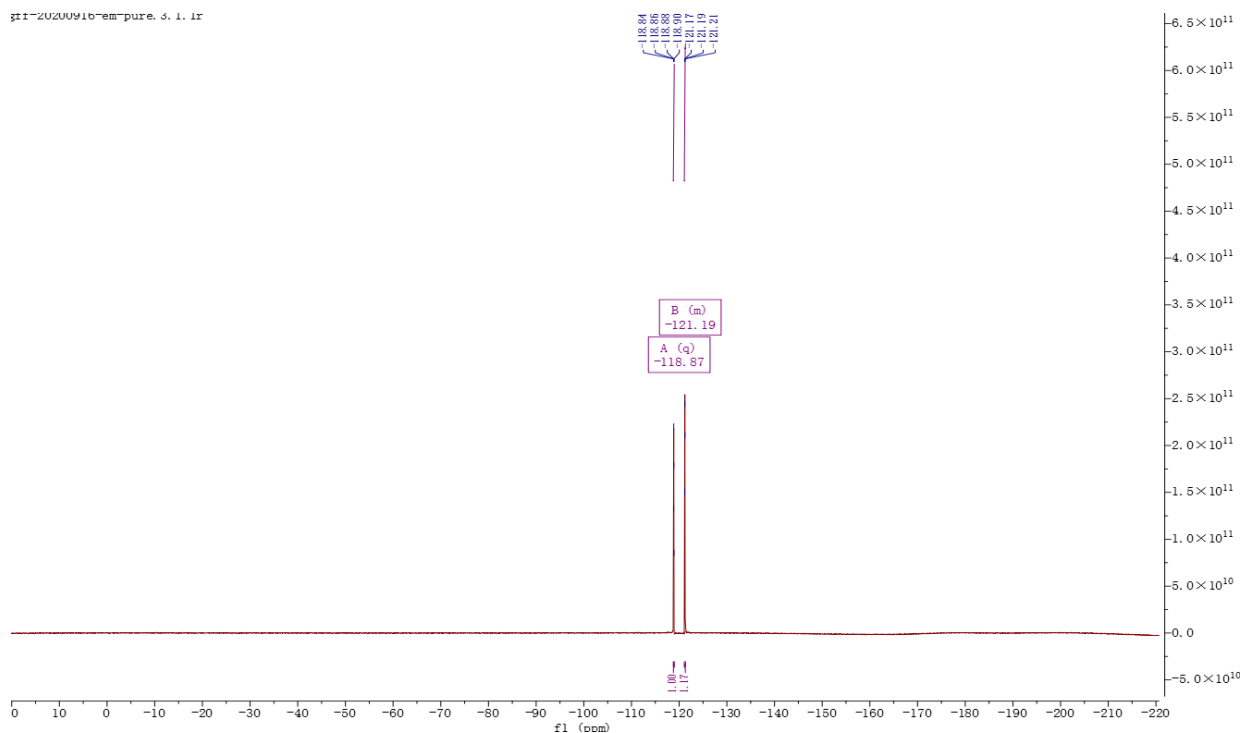
¹³C NMR (400 MHz, DMSO-d⁶)

iff-20200916-em-pure. 4. 1. 1r



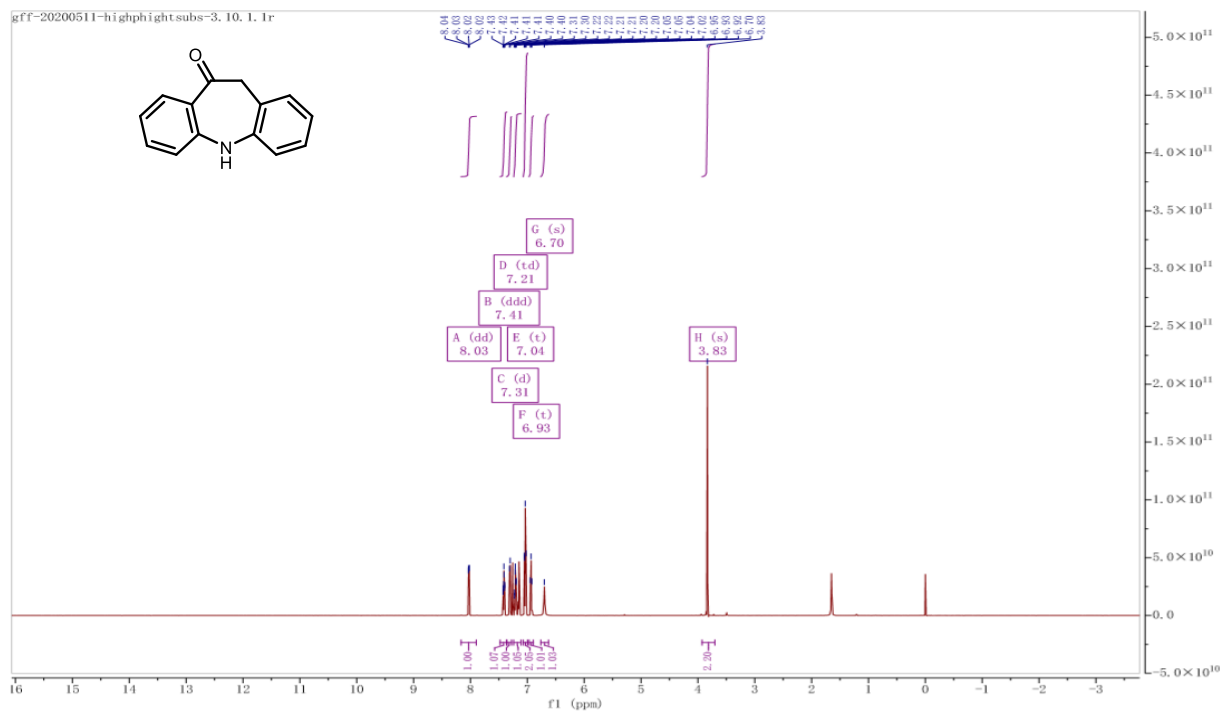
¹⁹F NMR (376 MHz, DMSO-d⁶)

gti-20200916-em-pure. 3. 1. 1r

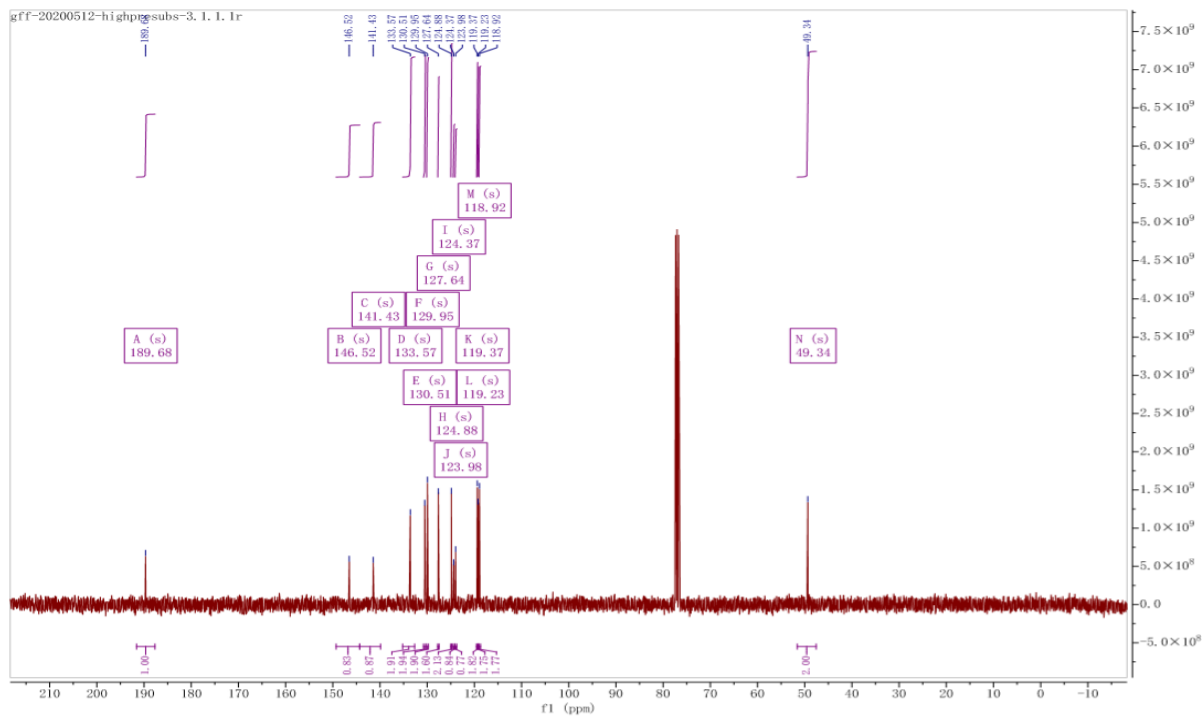


5,11-dihydro-10H-dibenzo[b,f]azepin-10-one (6):

^1H NMR (600 MHz, CDCl_3)

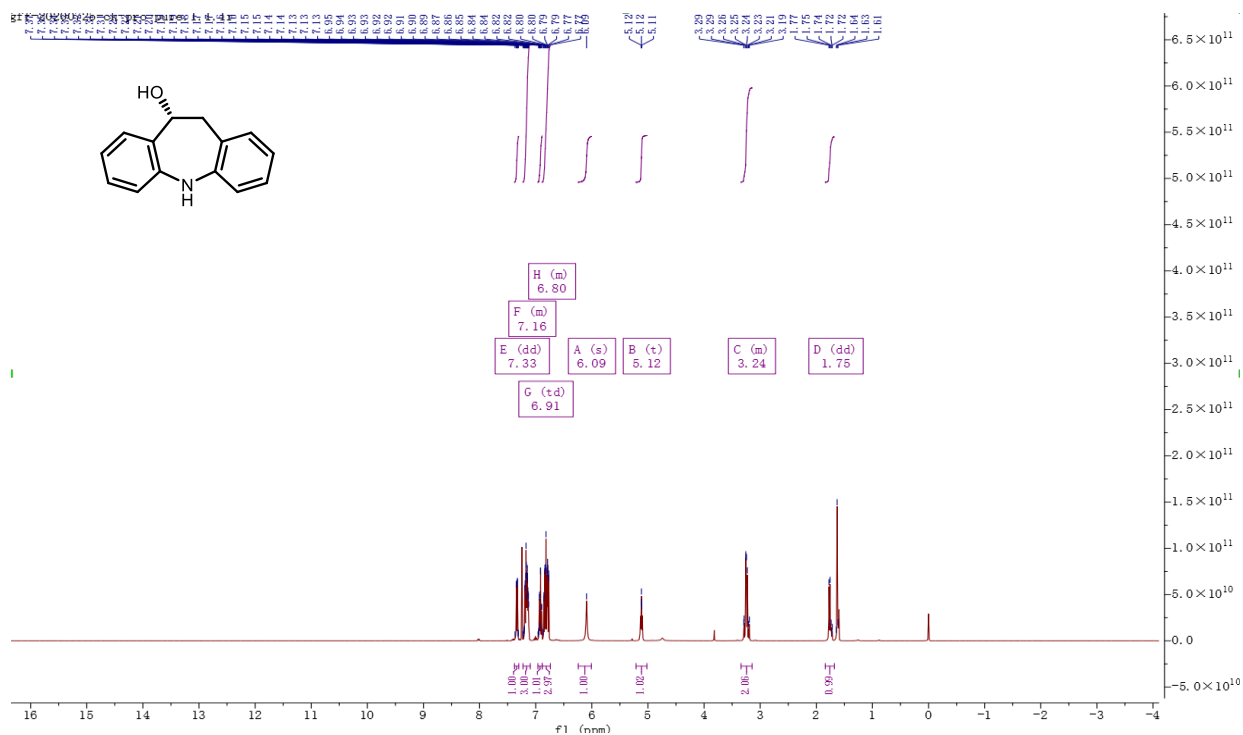


^{13}C NMR (101 MHz, CDCl_3)

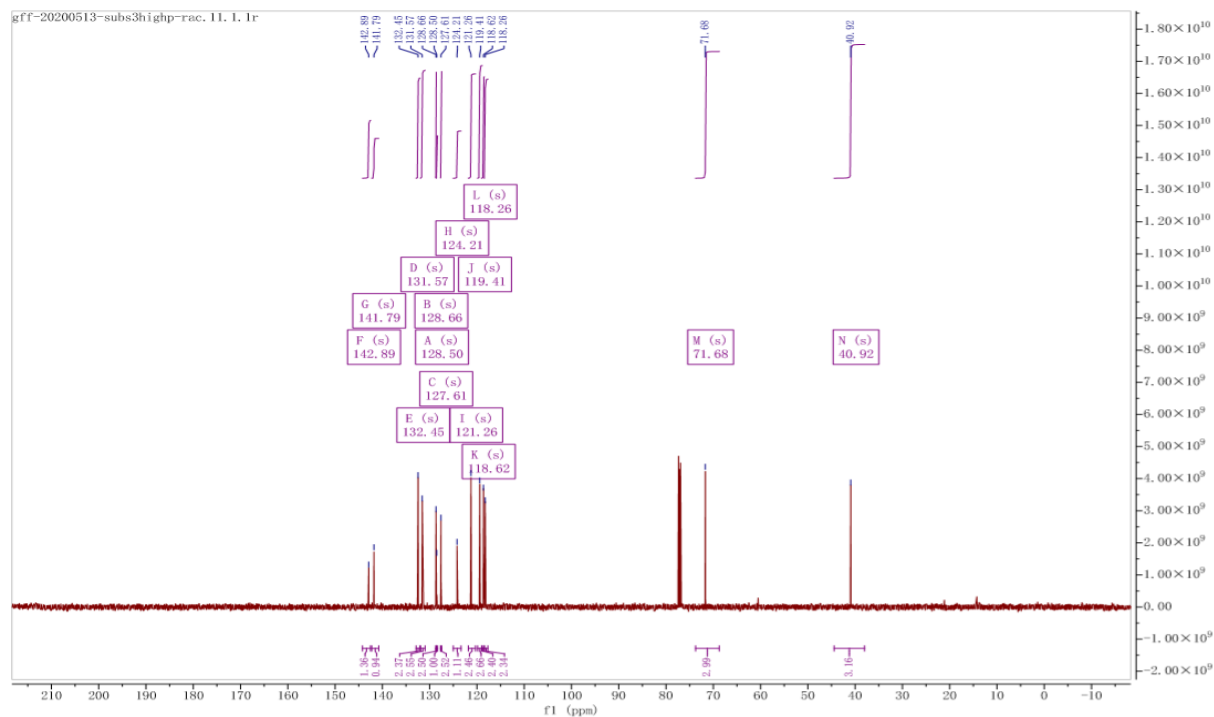


(R)-10,11-dihydro-5H-dibenzo[b,f]azepin-10-ol (7):

¹H NMR (400 MHz, CDCl₃)

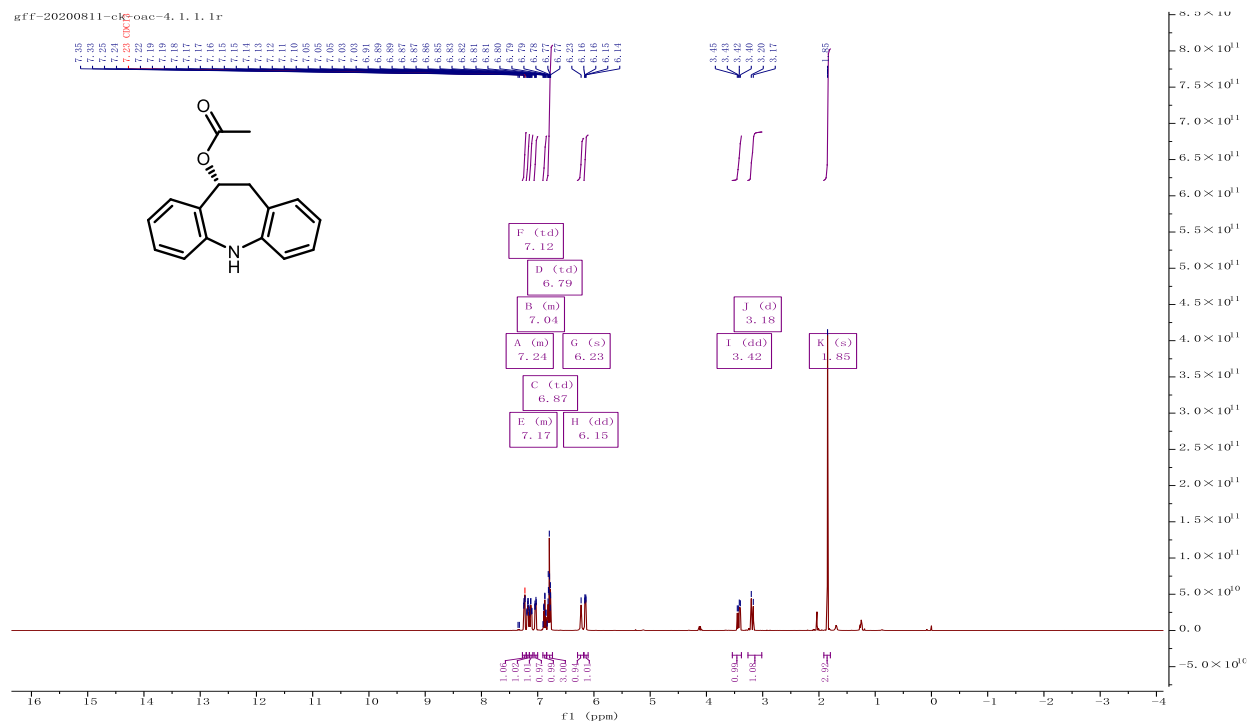


¹³C NMR (101 MHz, CDCl₃)

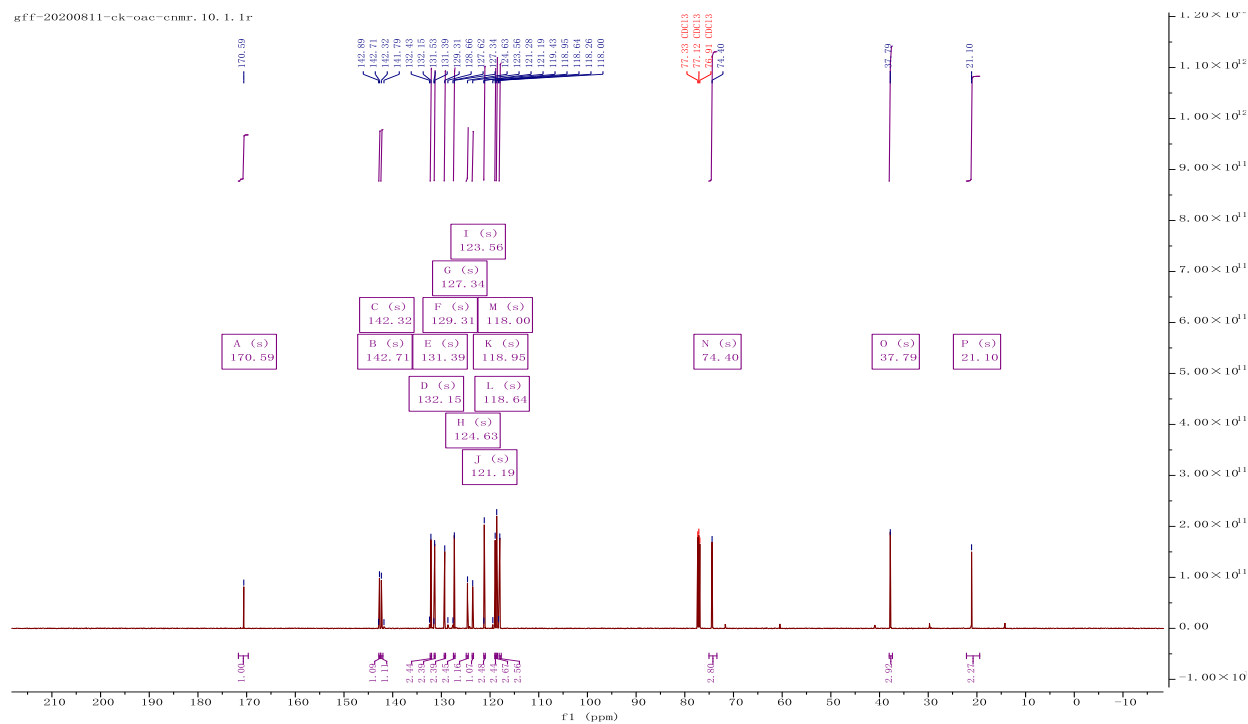


(R)-10,11-dihydro-5H-dibenzo[b,f]azepin-10-yl acetate (8):

¹H NMR (400 MHz, CDCl₃)

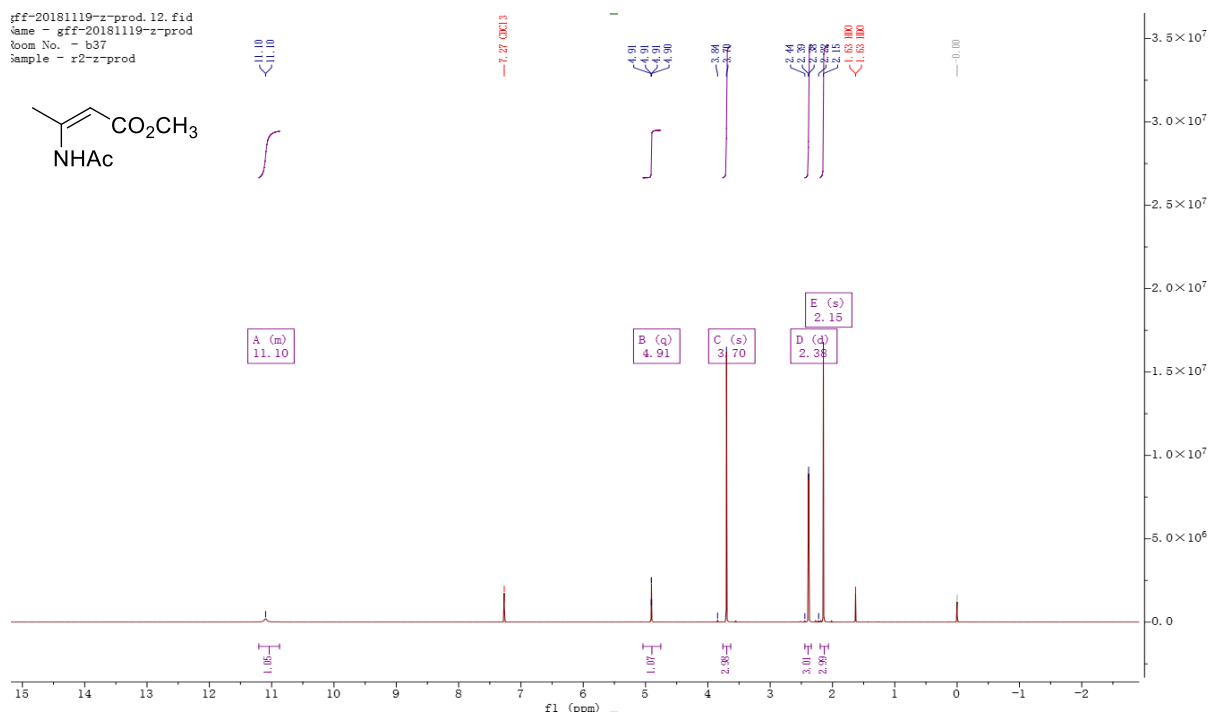


¹³C NMR (101 MHz, CDCl₃)

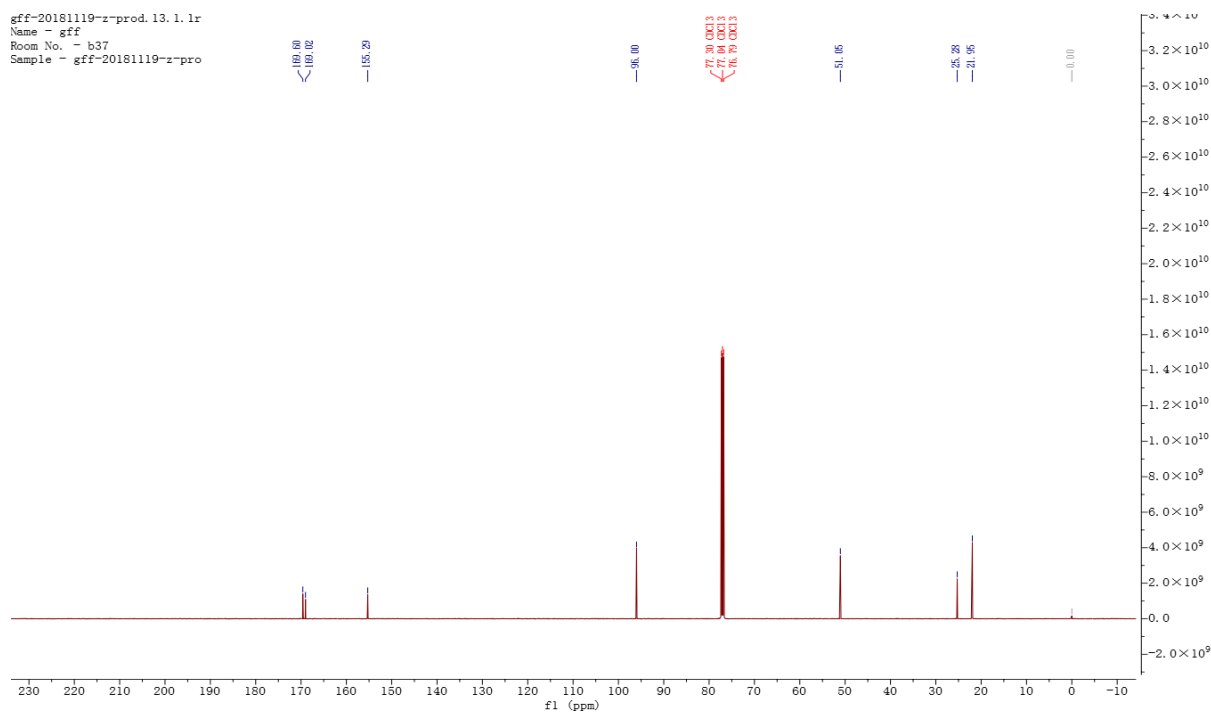


(Z)-methyl 3-acetamidobutanoate

¹H-NMR (600 MHz, CDCl₃)



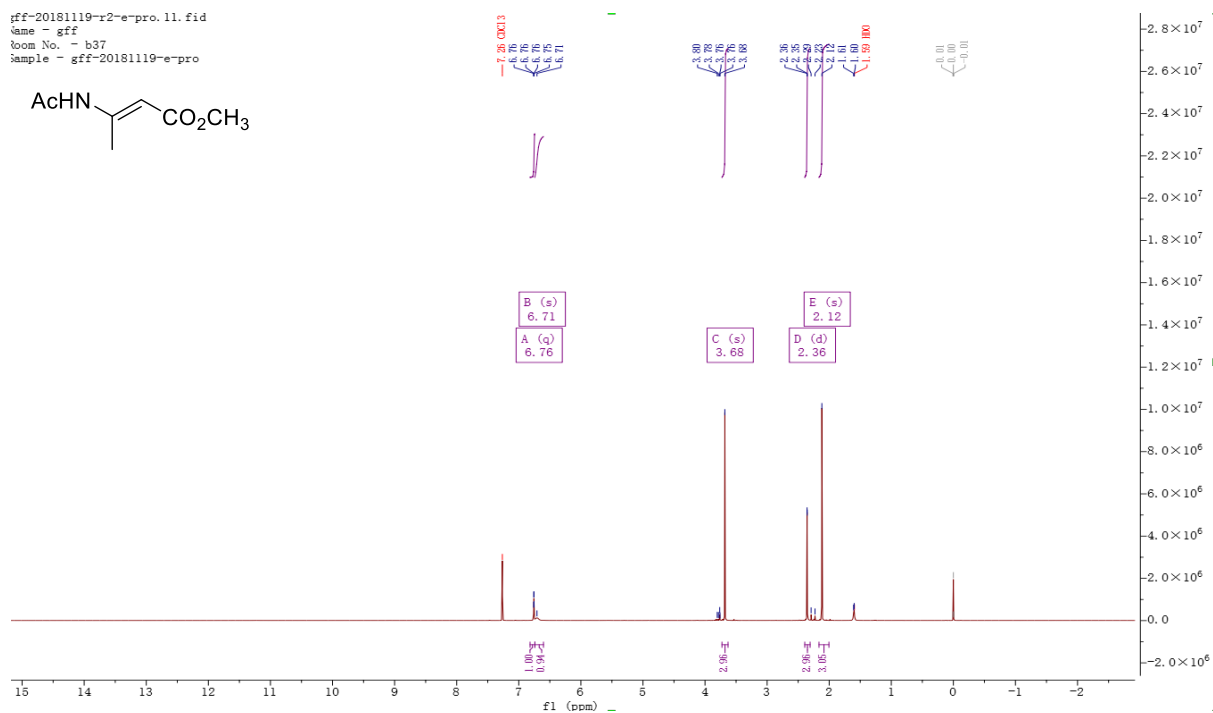
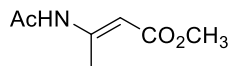
¹³C-NMR (101 MHz, CDCl₃)



(E)-methyl 3-acetamidobutanoate

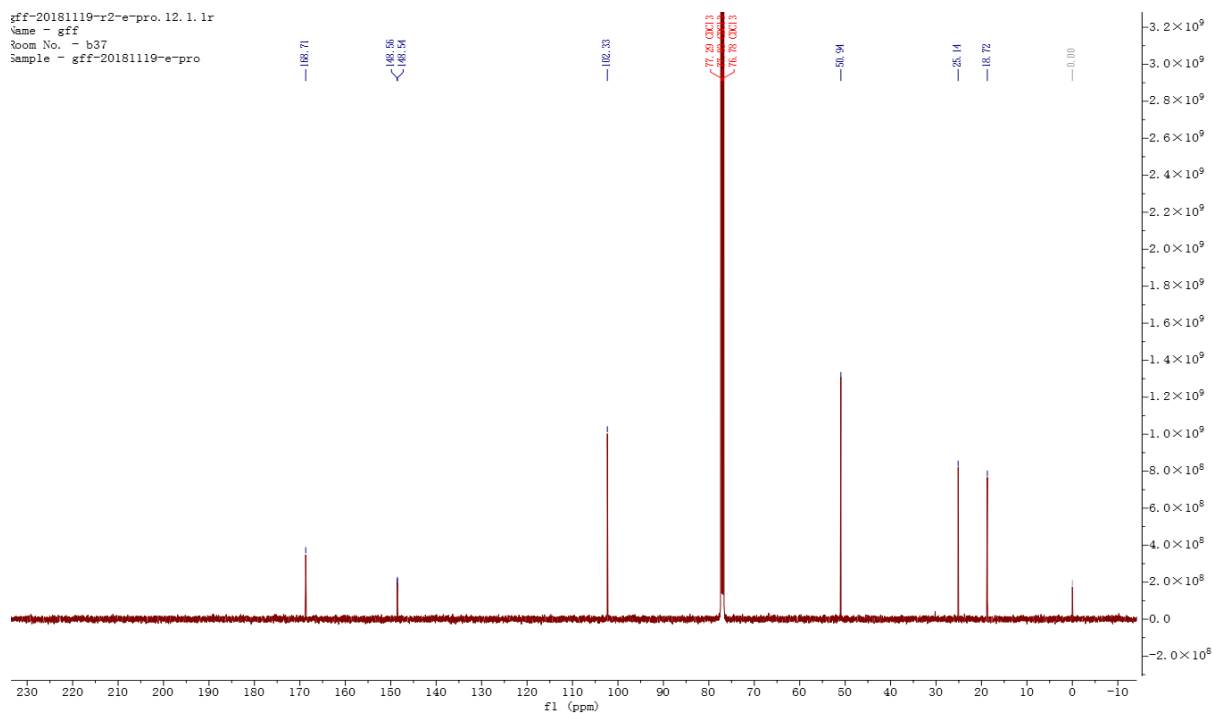
¹H-NMR (600 MHz, CDCl₃)

fff-20181119-r2-e-pro.11.fid
Name - gff
Room No. - b37
Sample - gff-20181119-e-pro



¹³C-NMR (101 MHz, CDCl₃)

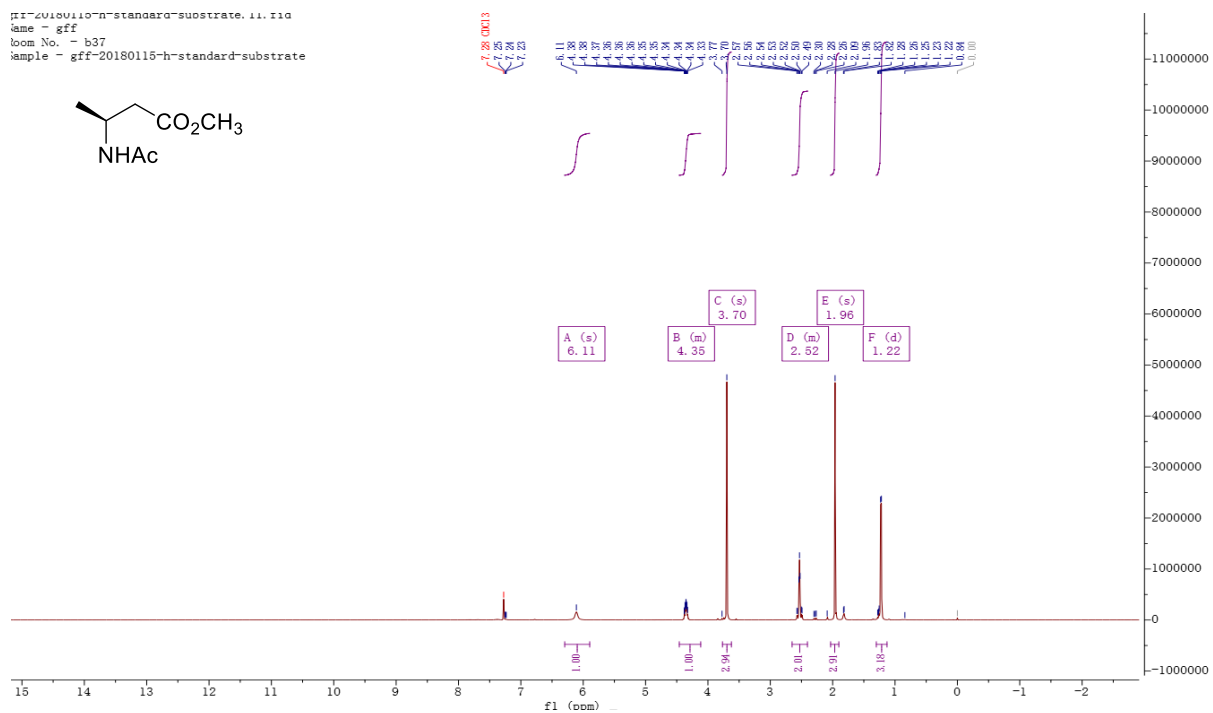
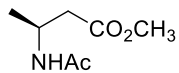
fff-20181119-r2-e-pro.12.1.lr
Name - gff
Room No. - b37
Sample - gff-20181119-e-pro



(S)-methyl 3-acetamidobutanoate

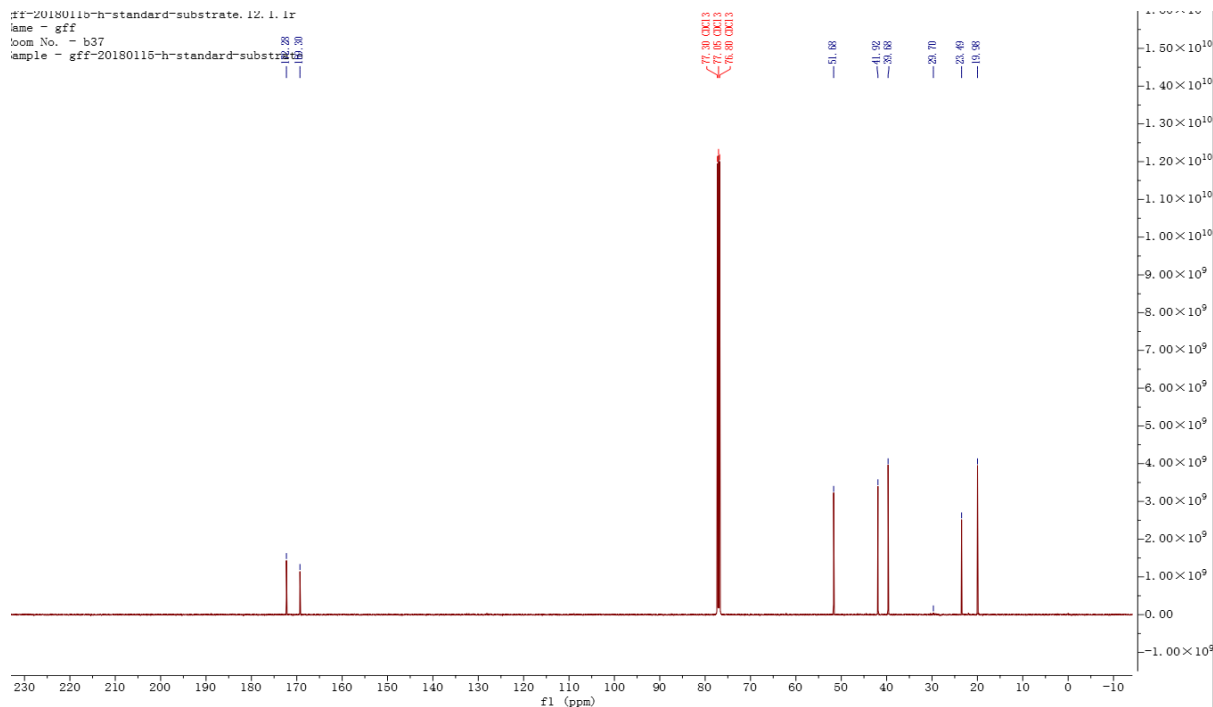
$^1\text{H-NMR}$ (600 MHz, CDCl_3)

```
#1-20180110-h-standard-substrate.11.f1d  
name - gff  
loom No. - b37  
sample - gff-20180115-h-standard-substrate
```



$^{13}\text{C-NMR}$ (101 MHz, CDCl_3)

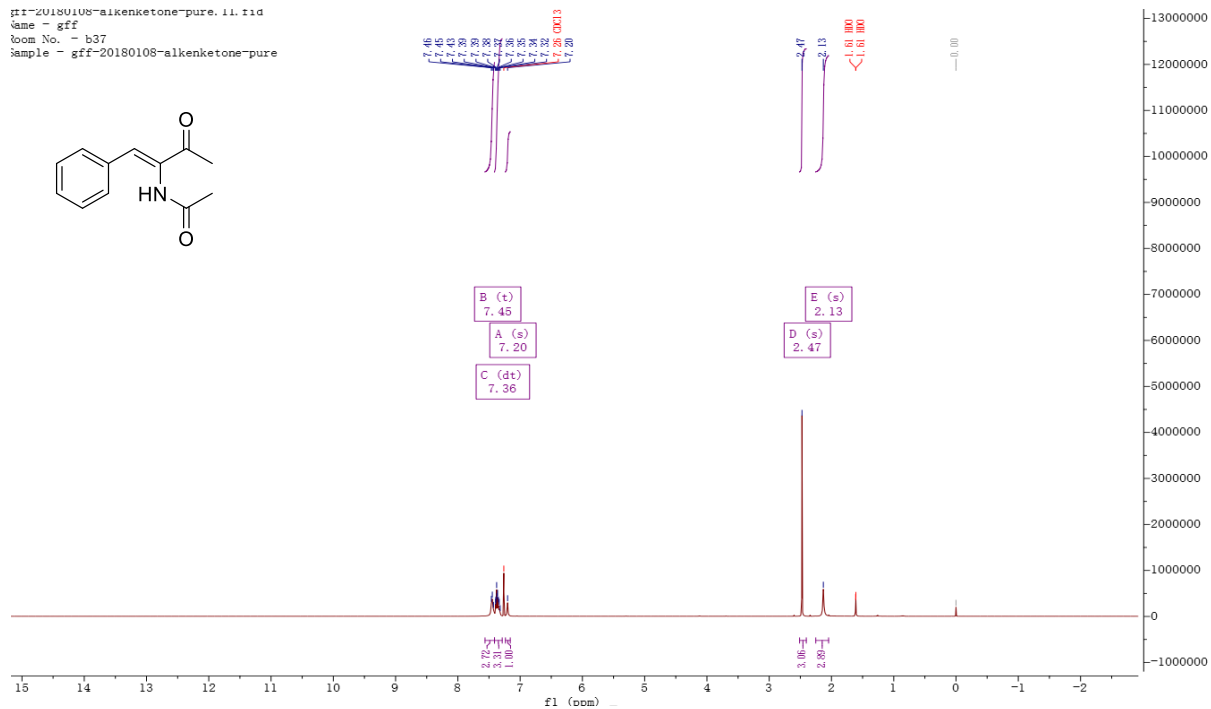
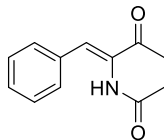
```
#1-20180110-h-standard-substrate.12.1.f1r  
name - gff  
loom No. - b37  
sample - gff-20180115-h-standard-substrate
```



N-(3-oxo-1-phenylbut-1-en-2-yl) acetamide (27)

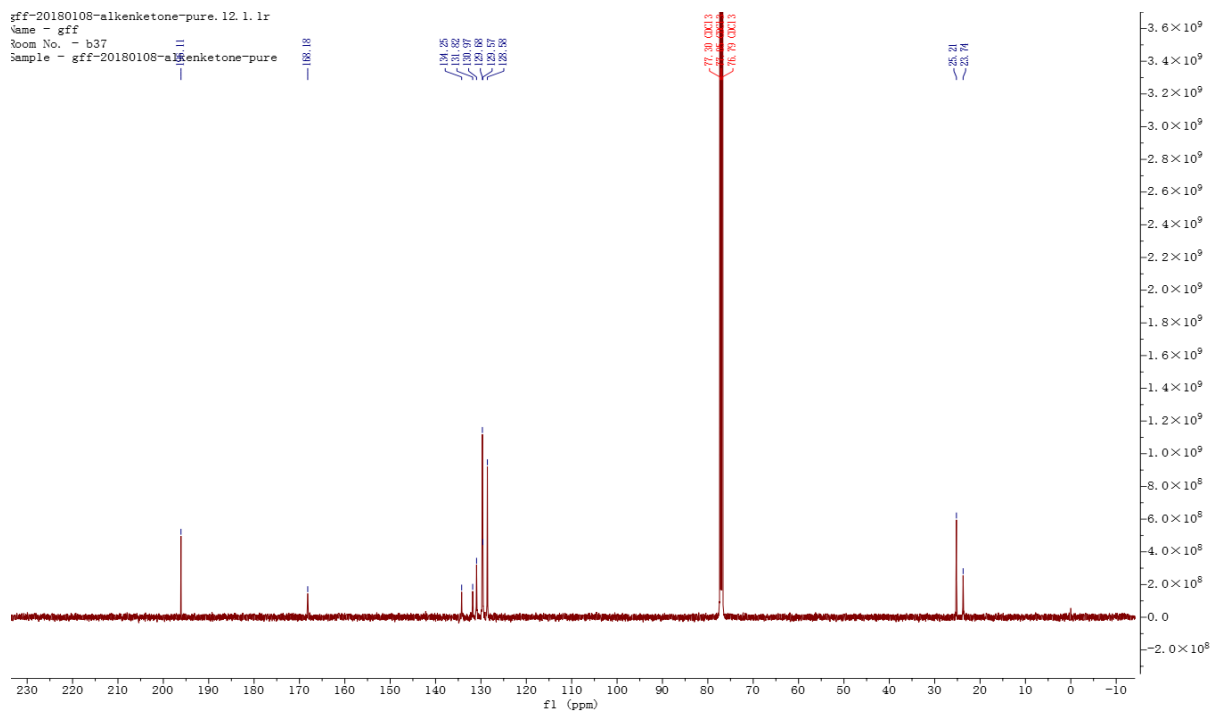
¹H-NMR (600 MHz, CDCl₃)

fff-20180108-alkenketone-pure. 11. r1d
Name - gff
Room No. - b37
Sample - gff-20180108-alkenketone-pure



¹³C-NMR (101 MHz, CDCl₃)

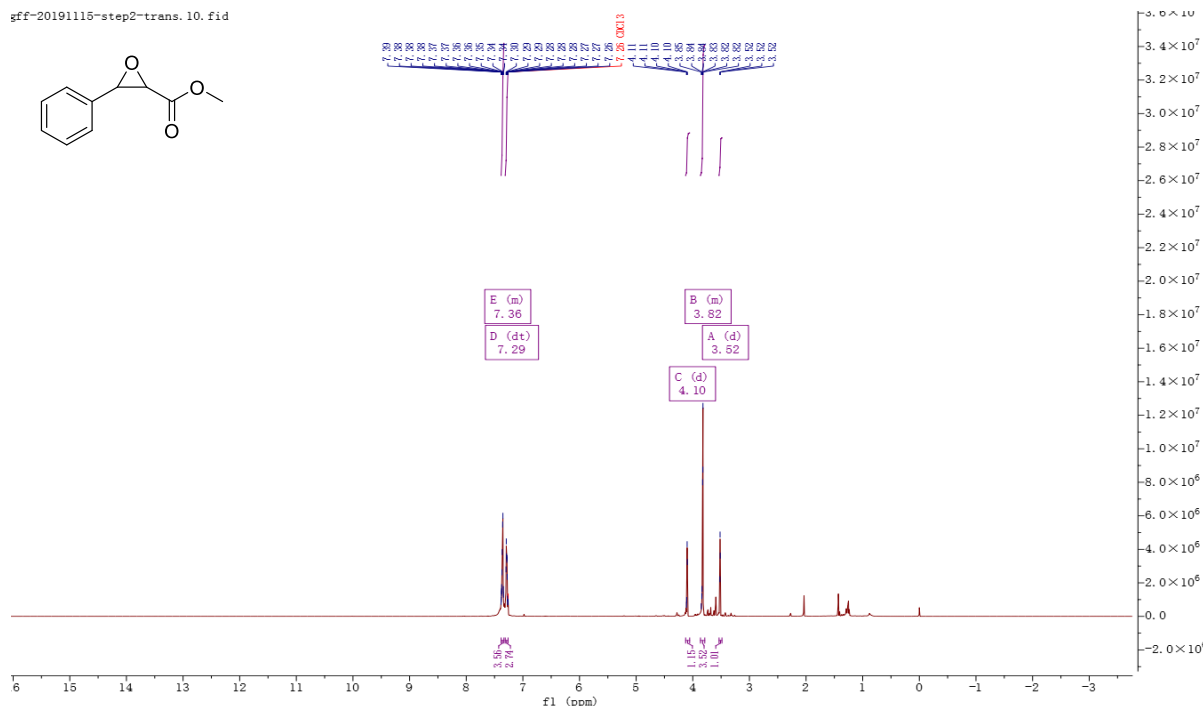
fff-20180108-alkenketone-pure. 12. 1. 1r
Name - gff
Room No. - b37
Sample - gff-20180108-alkenketone-pure



Methyl 3-phenyloxirane-2-carboxylate (43)

¹H-NMR (600 MHz, CDCl₃)

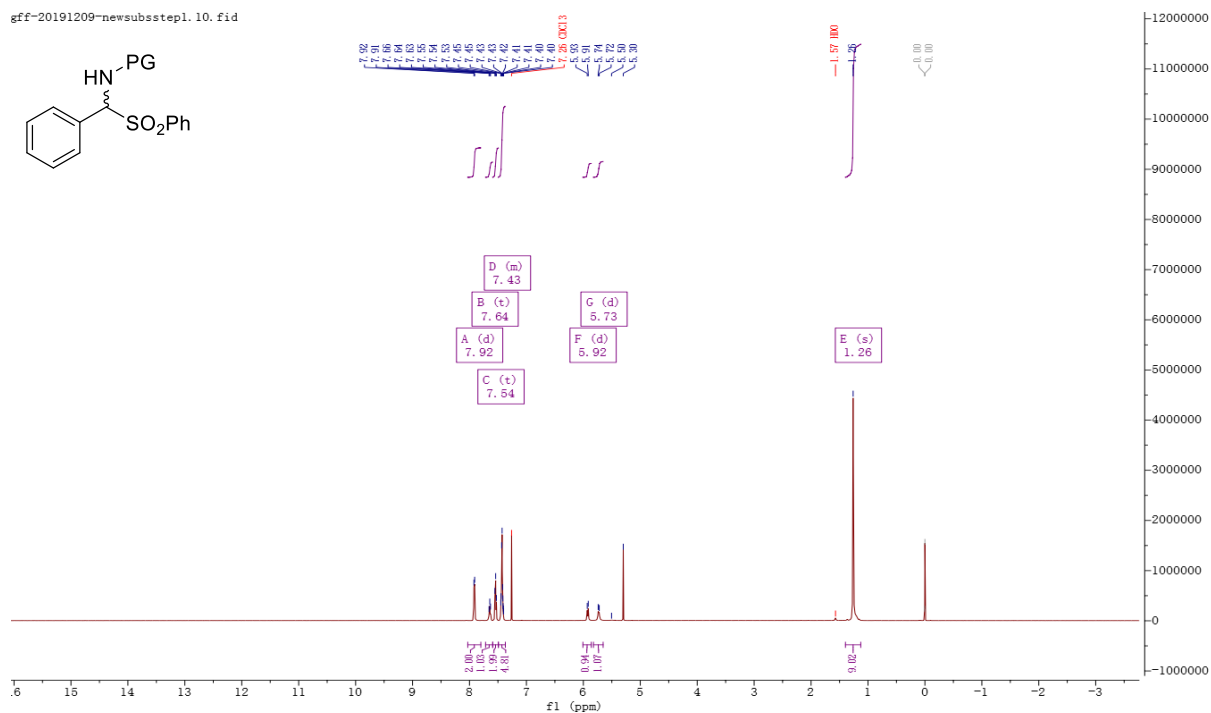
gff-20191115-step2-trans.10.fid



tert-butyl (phenyl(phenylsulfonyl)methyl) carbamate (47)

¹H-NMR (600 MHz, CDCl₃)

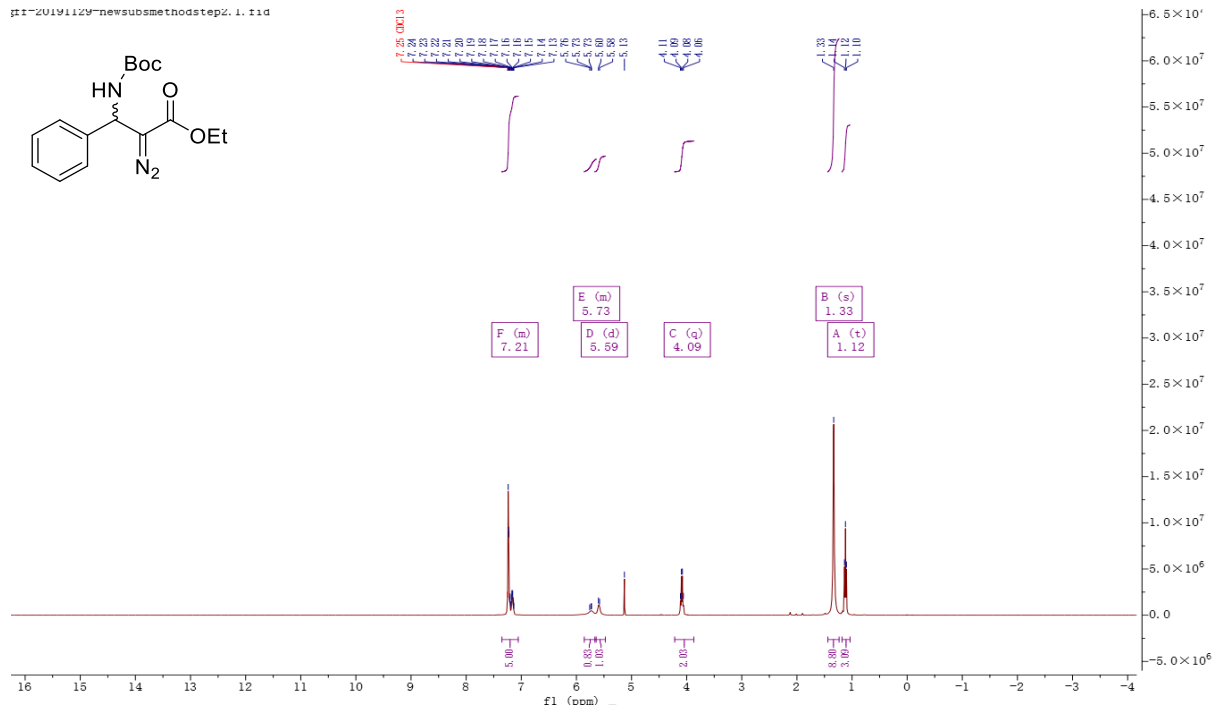
gff-20191209-newsubsstep1.10.fid



ethyl 3-((tert-butoxycarbonyl)amino)-2-diazo-3-phenylpropanoate (48)

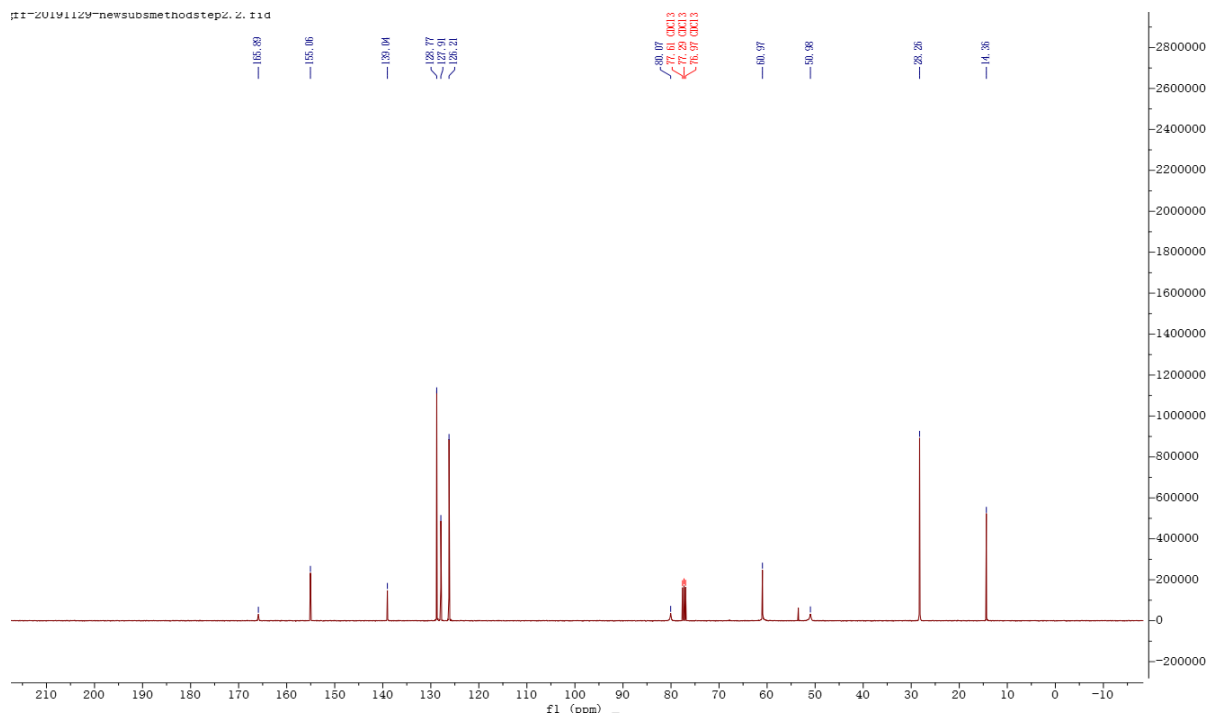
¹H-NMR (600 MHz, CDCl₃)

ff-20191129-newsubsmethodstep2.1.f1d



¹³C-NMR (101 MHz, CDCl₃)

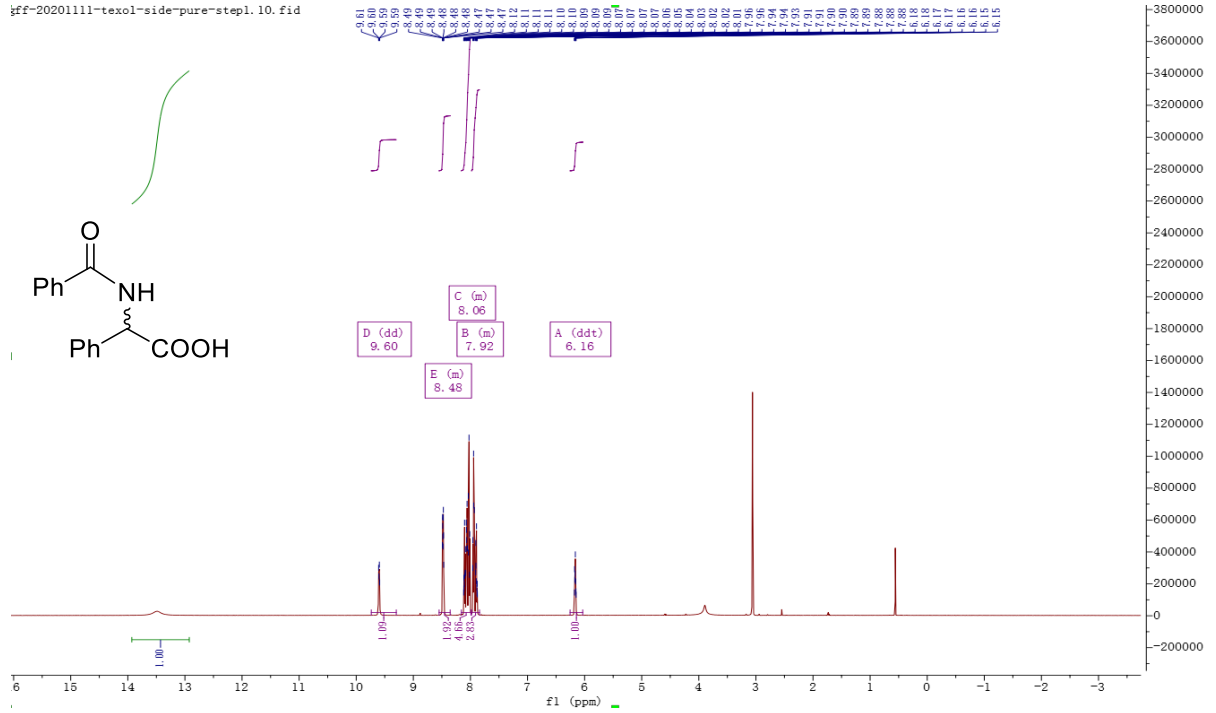
ff-20191129-newsubsmethodstep2.2.f1d



2-benzamido-2-phenylacetic acid (51)

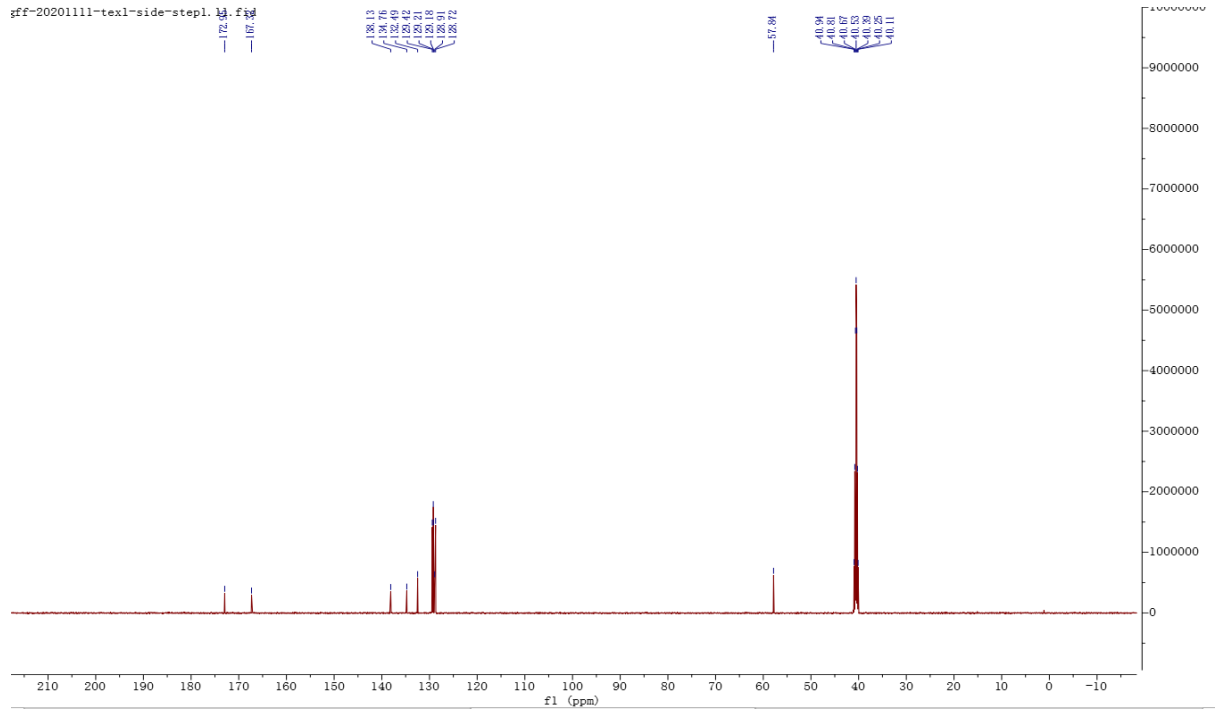
¹H-NMR (600 MHz, CDCl₃)

fff-20201111-texol-side-pure-step1.10.fid



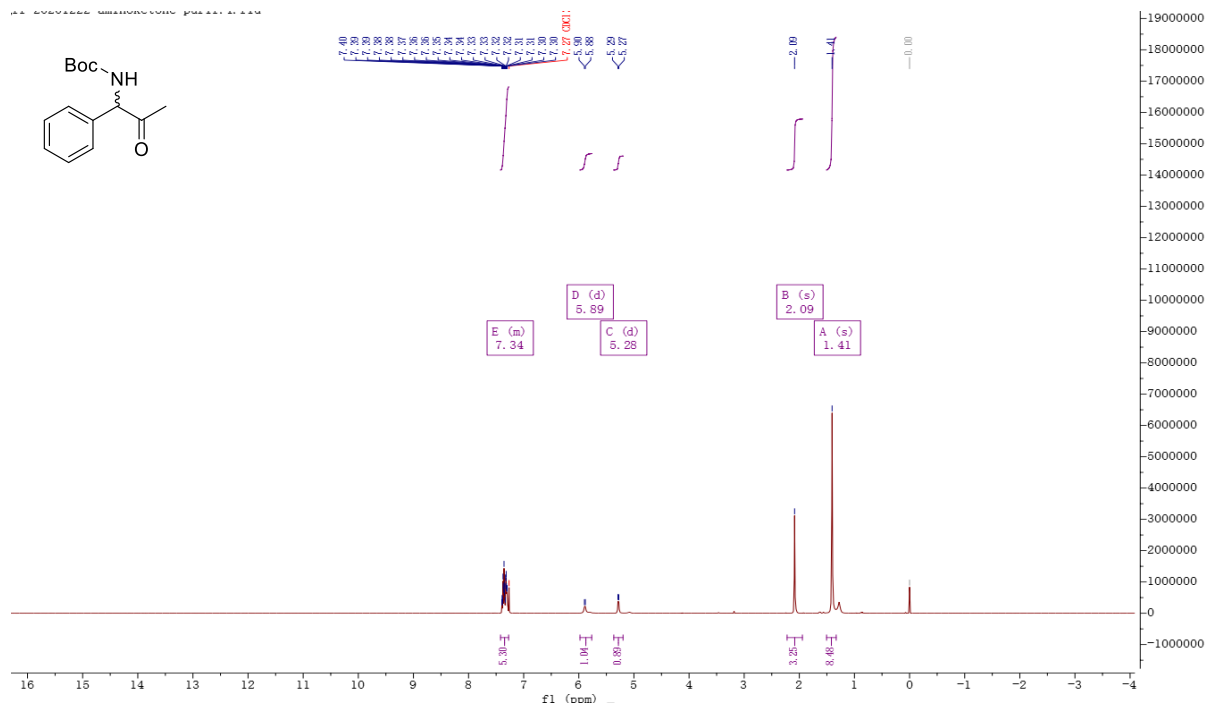
¹³C-NMR (101 MHz, CDCl₃)

fff-20201111-texol-side-step1.10.fid

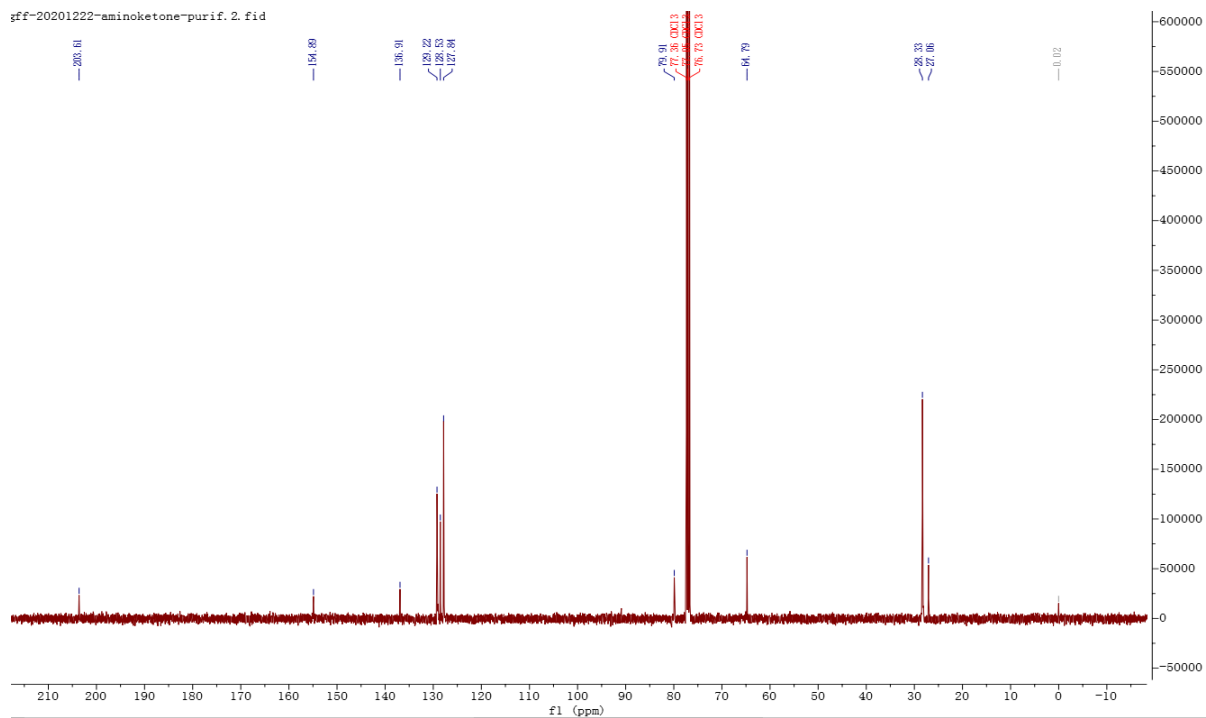


tert-butyl (2-oxo-1-phenylpropyl)carbamate (57)

¹H-NMR (600 MHz, CDCl₃)



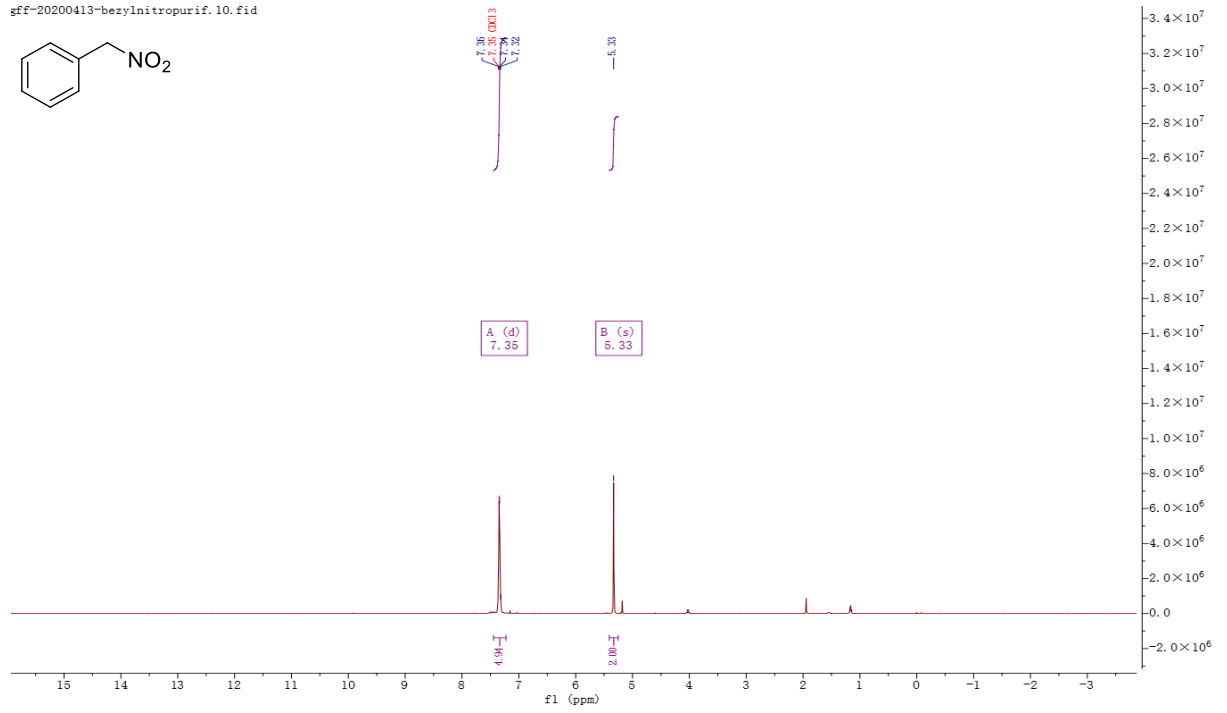
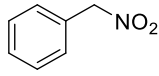
¹³C-NMR (101 MHz, CDCl₃)



(nitromethyl)benzene (59)

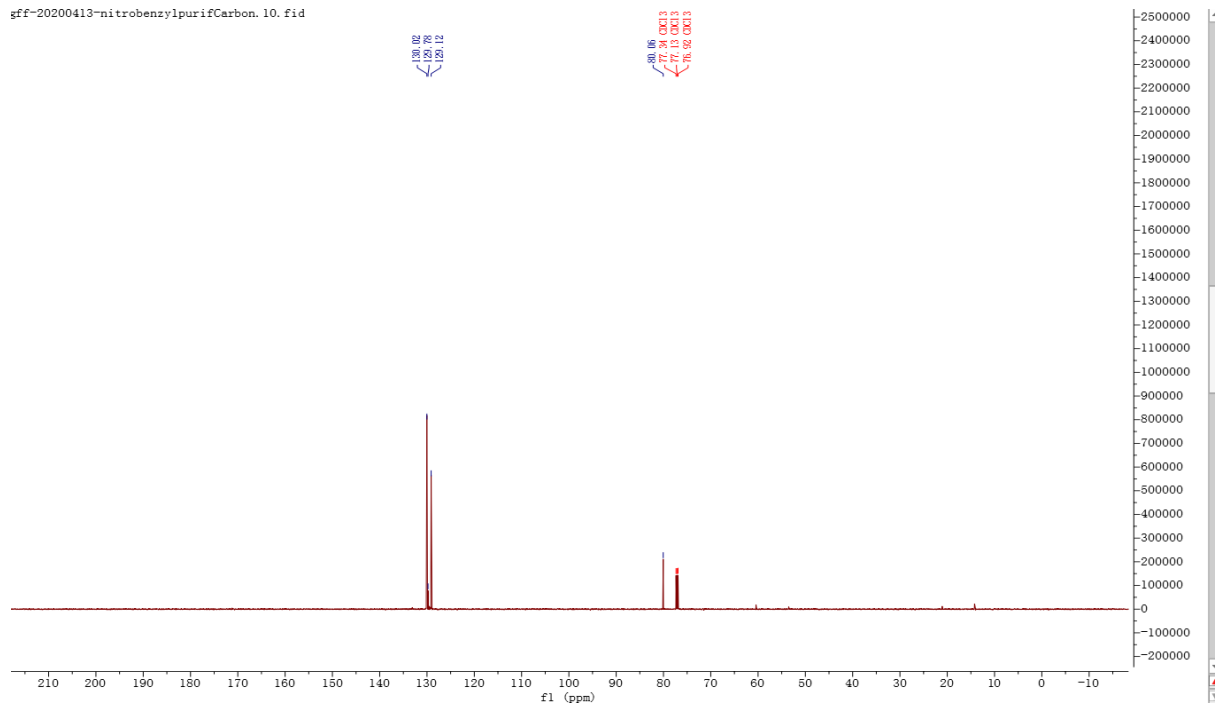
$^1\text{H-NMR}$ (600 MHz, CDCl_3)

gff-20200413-bezylNitropurif. 10. fid



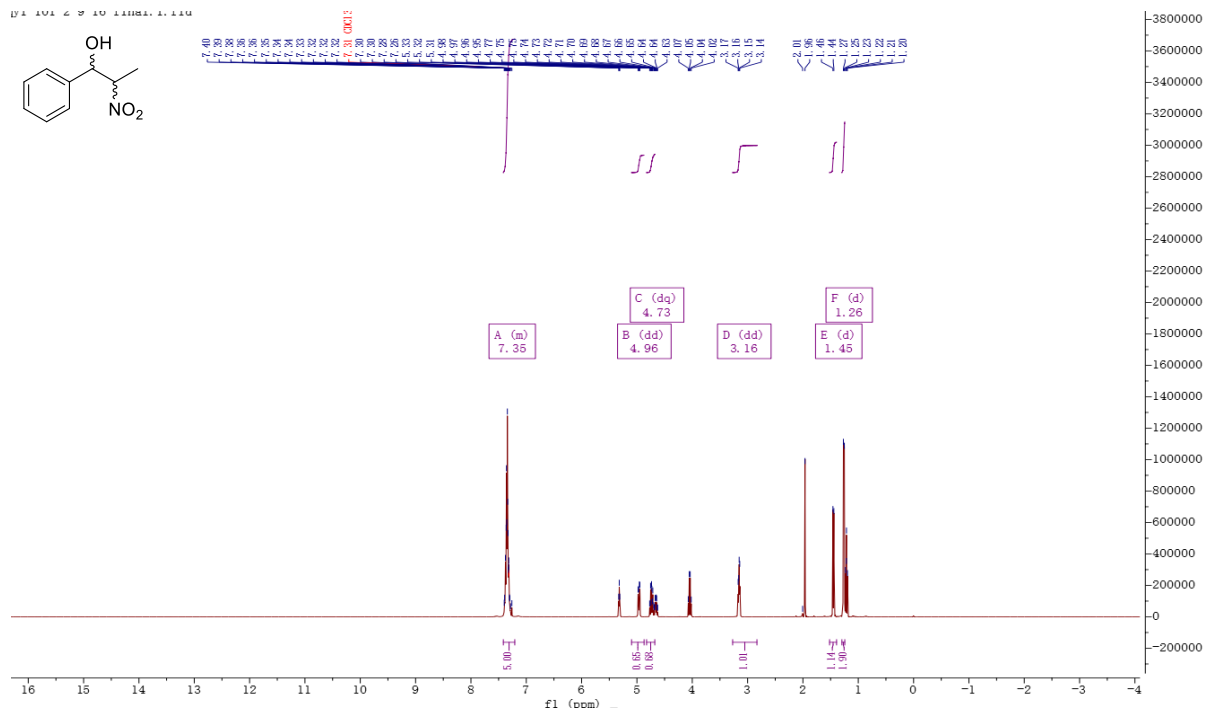
$^{13}\text{C-NMR}$ (101 MHz, CDCl_3)

gff-20200413-nitrobenzylpurifCarbon. 10. fid

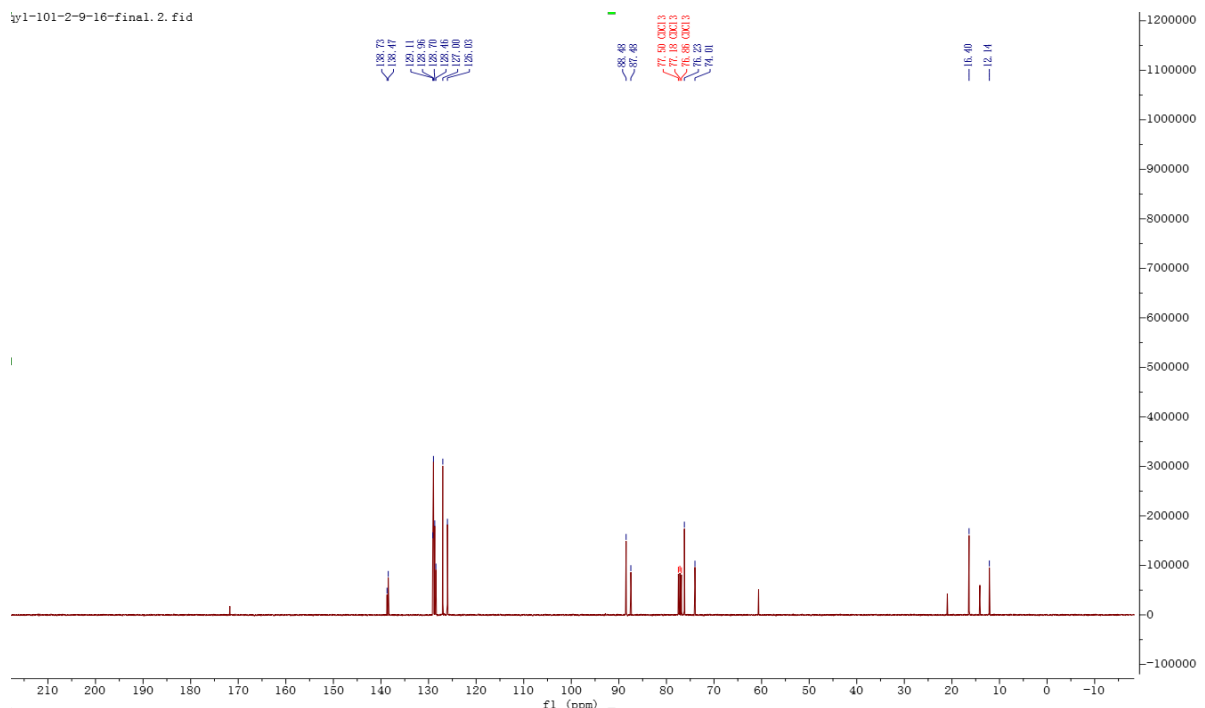


2-nitro-1-phenylpropan-1-ol (63)

$^1\text{H-NMR}$ (600 MHz, CDCl_3)

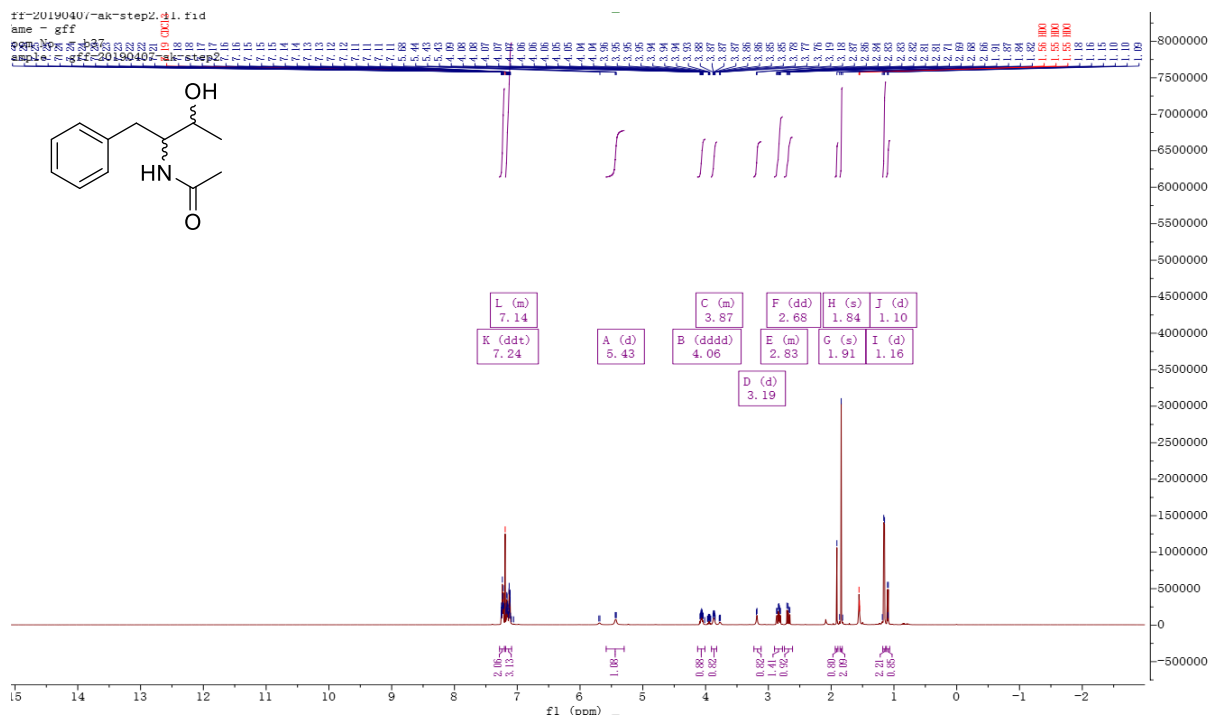


$^{13}\text{C-NMR}$ (101 MHz, CDCl_3)

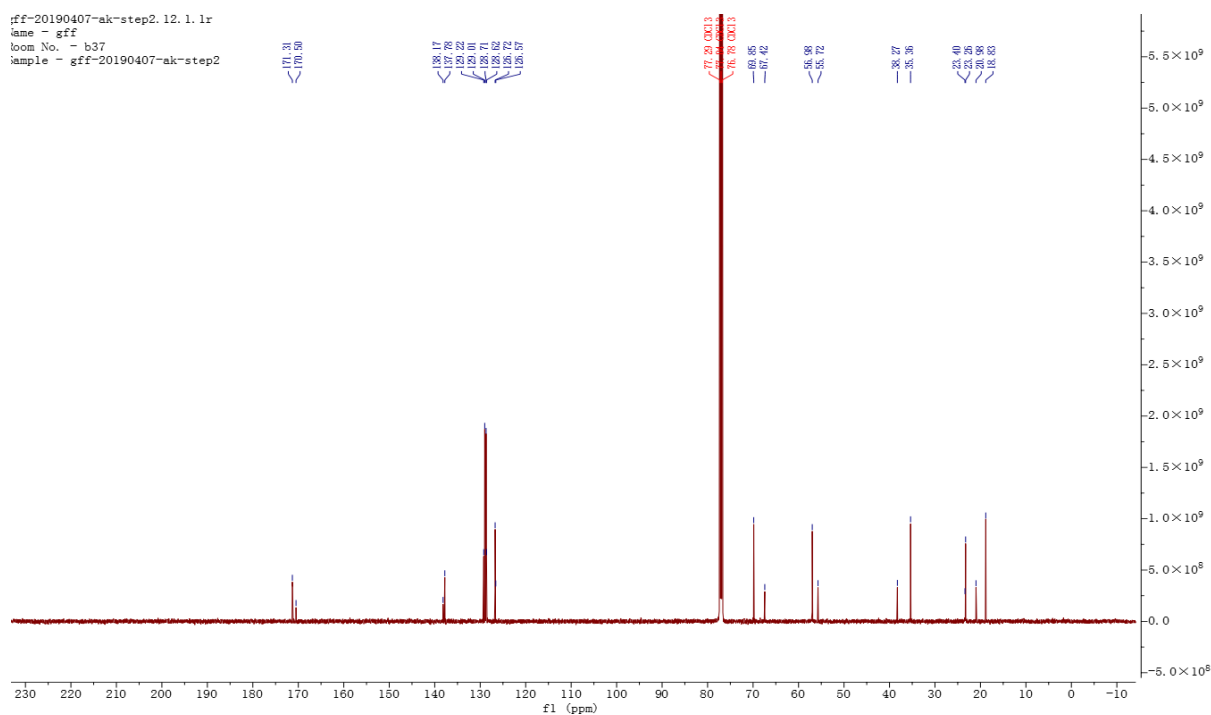


N-(3-hydroxy-1-phenylbutan-2-yl) acetamide (65)

¹H-NMR (600 MHz, CDCl₃)

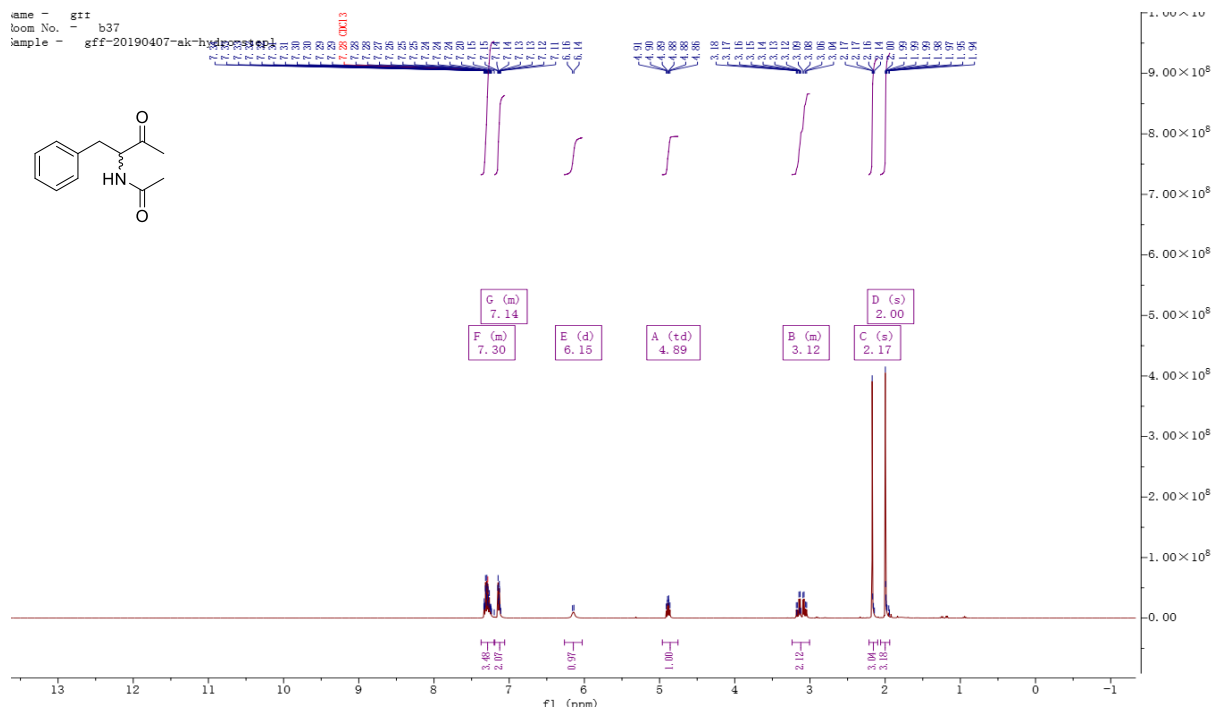


¹³C-NMR (101 MHz, CDCl₃)

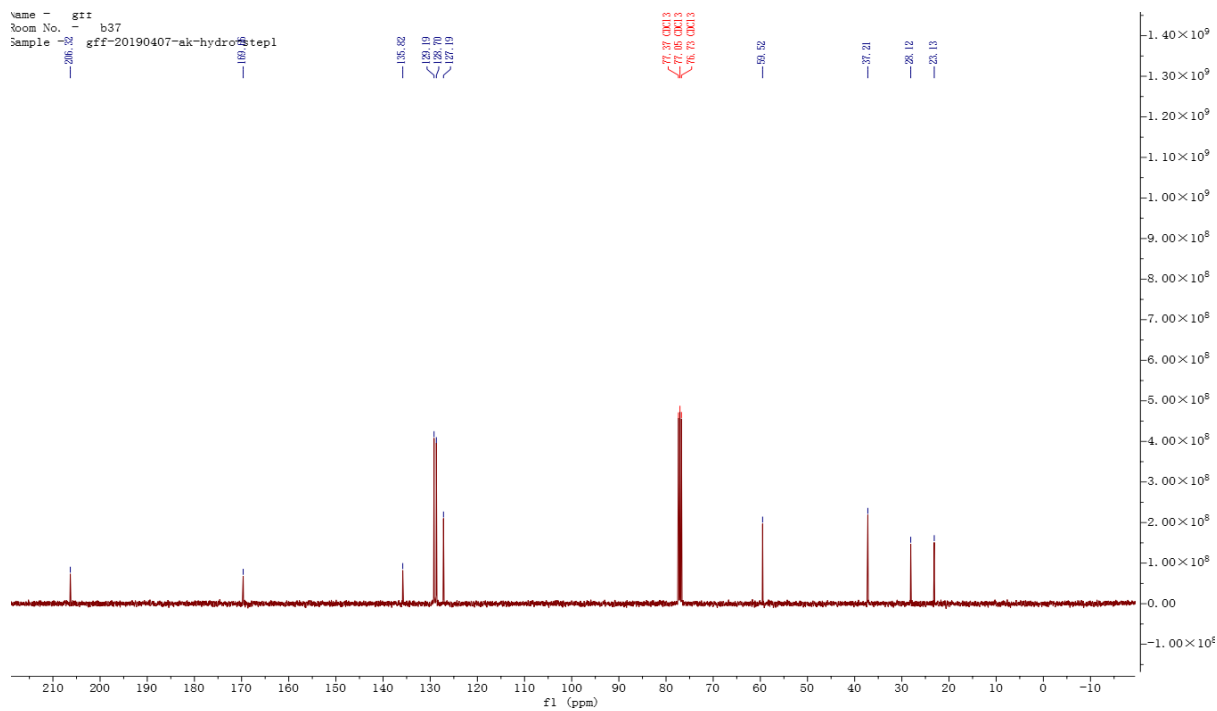


N-(3-oxo-1-phenylbutan-2-yl) acetamide (66)

¹H-NMR (600 MHz, CDCl₃)



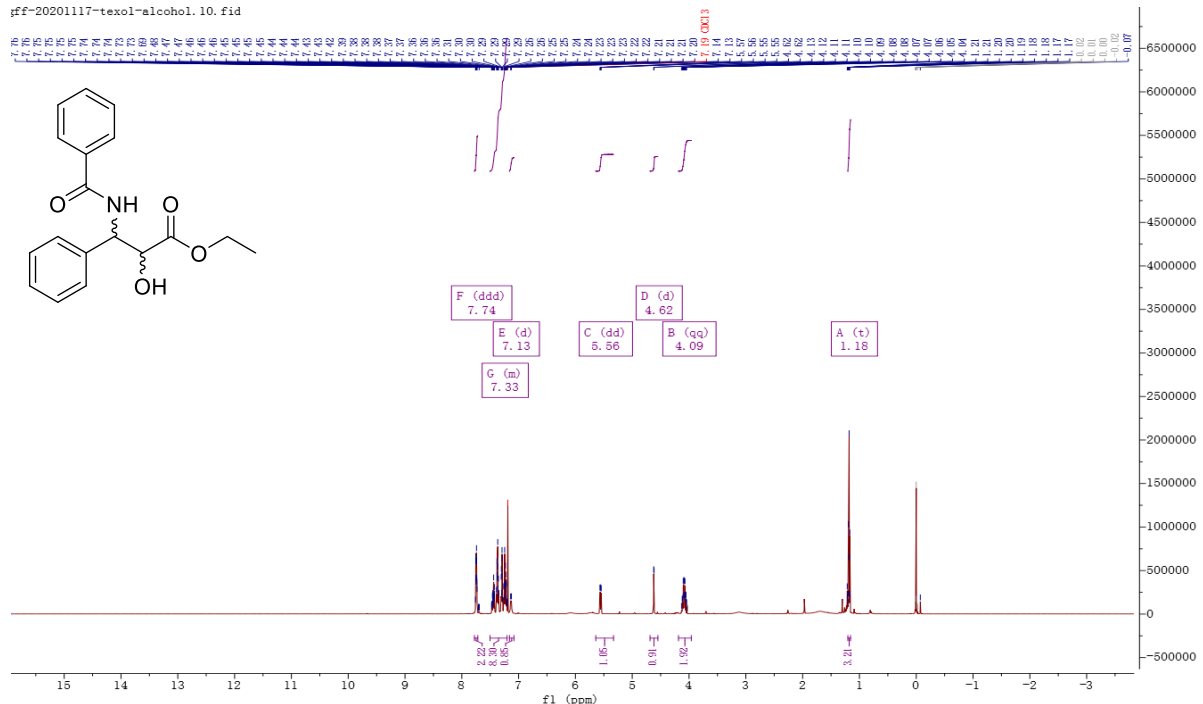
¹³C-NMR (101 MHz, CDCl₃)



ethyl 3-benzamido-2-hydroxy-3-phenylpropanoate (67)

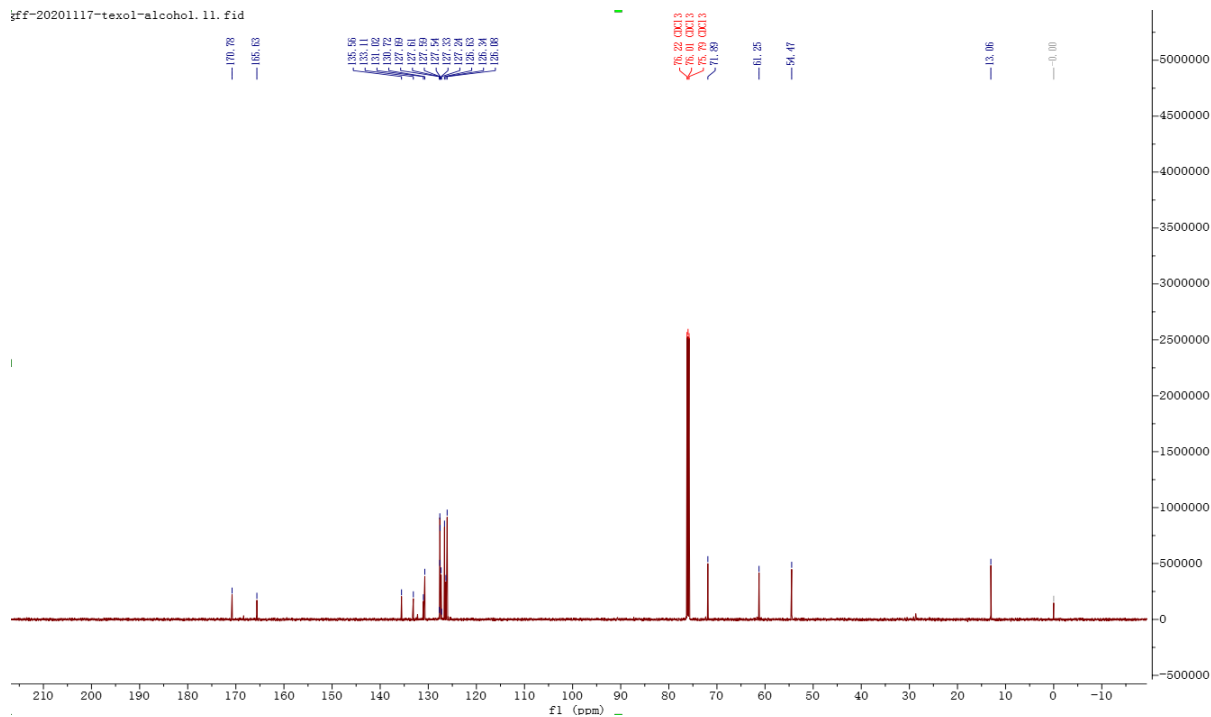
¹H-NMR (600 MHz, CDCl₃)

ff-20201117-texol-alcohol.10.fid



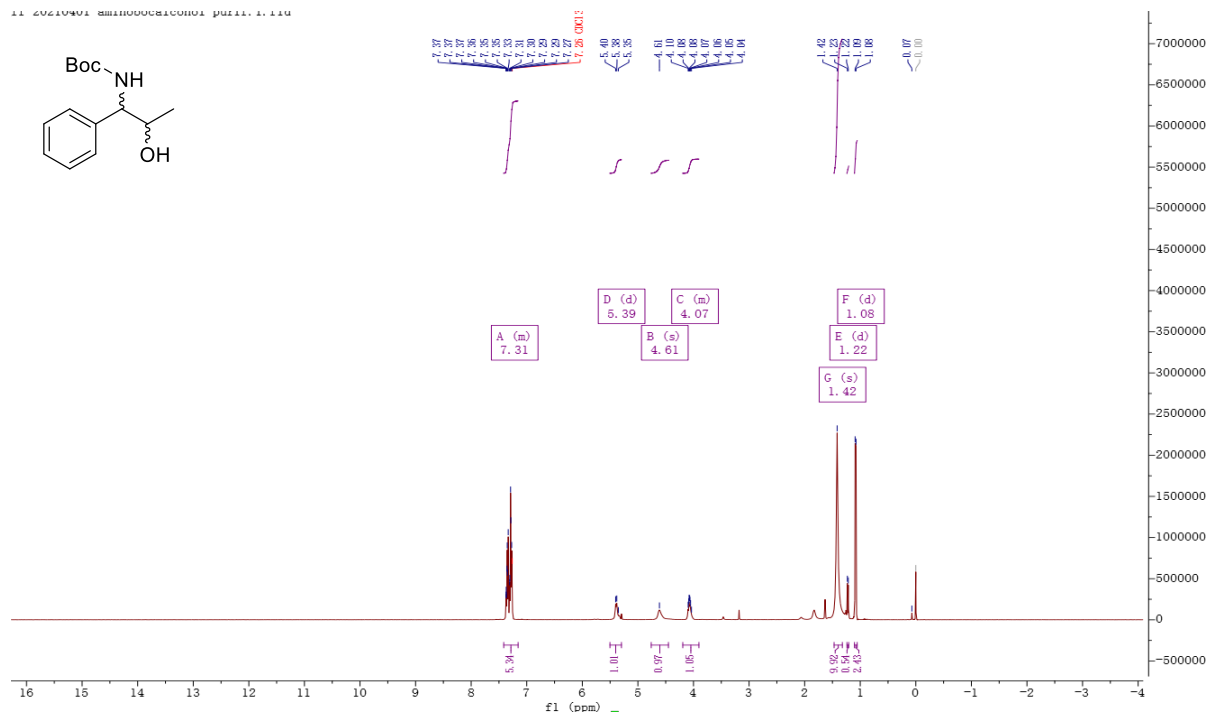
¹³C-NMR (101 MHz, CDCl₃)

ff-20201117-texol-alcohol.11.fid

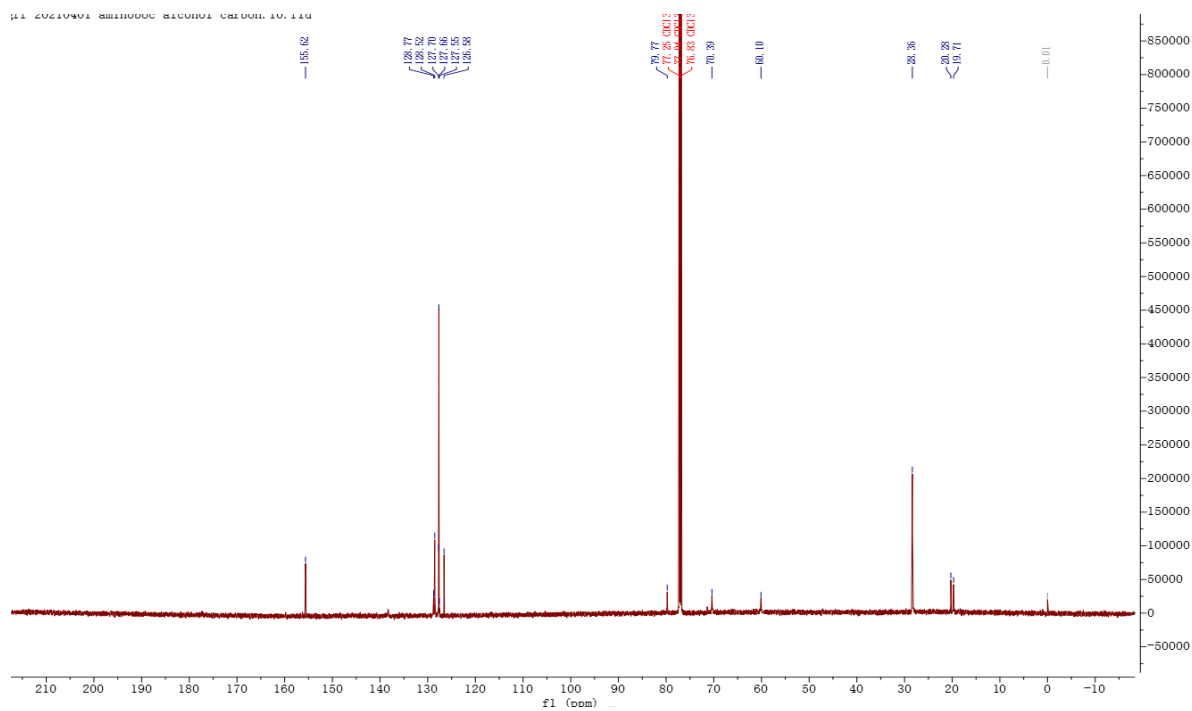


tert-butyl (2-hydroxy-1-phenylpropyl)carbamate (69)

¹H-NMR (600 MHz, CDCl₃)

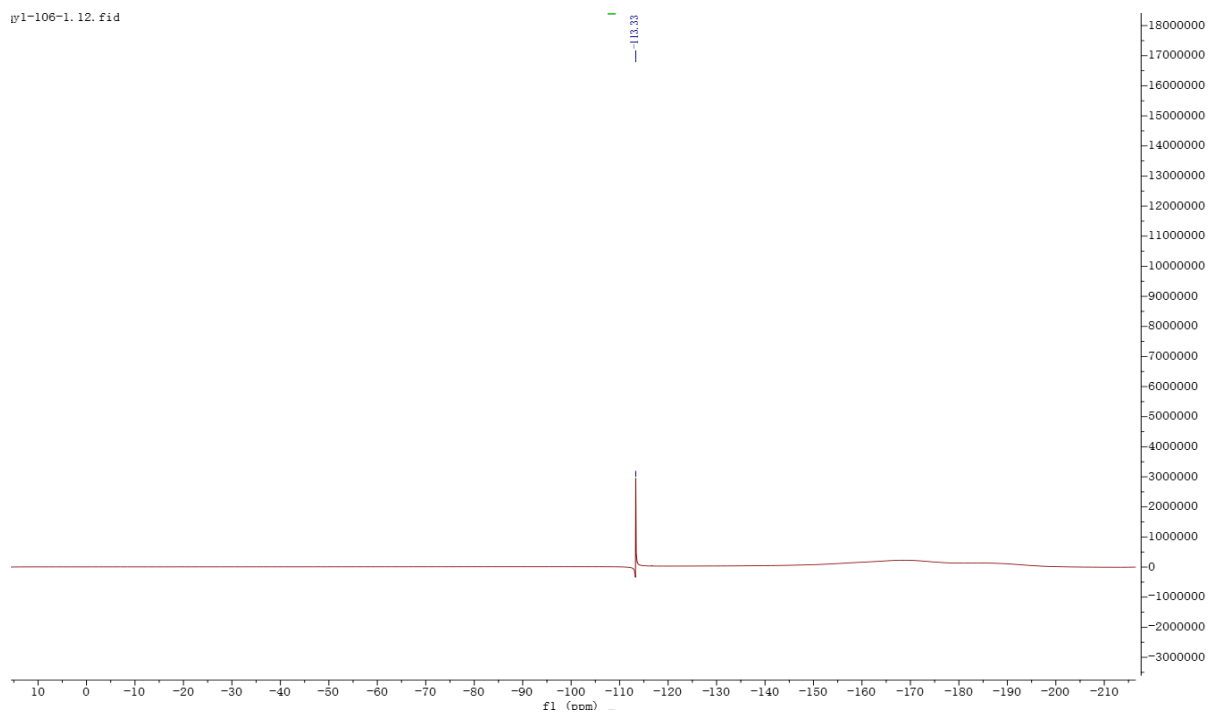


¹³C-NMR (101 MHz, CDCl₃)



^{19}F NMR (376 MHz, CDCl_3)

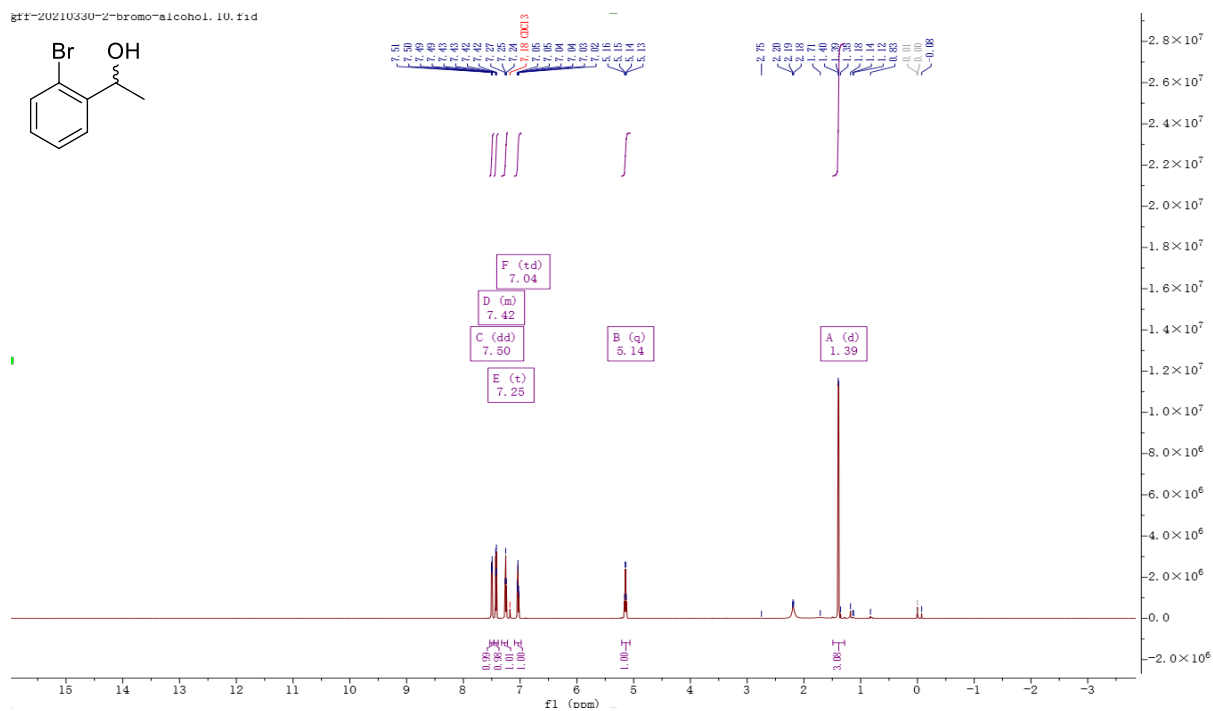
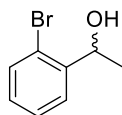
py1-106-1.12.fid



1-(2-bromophenyl) ethan-1-ol (74)

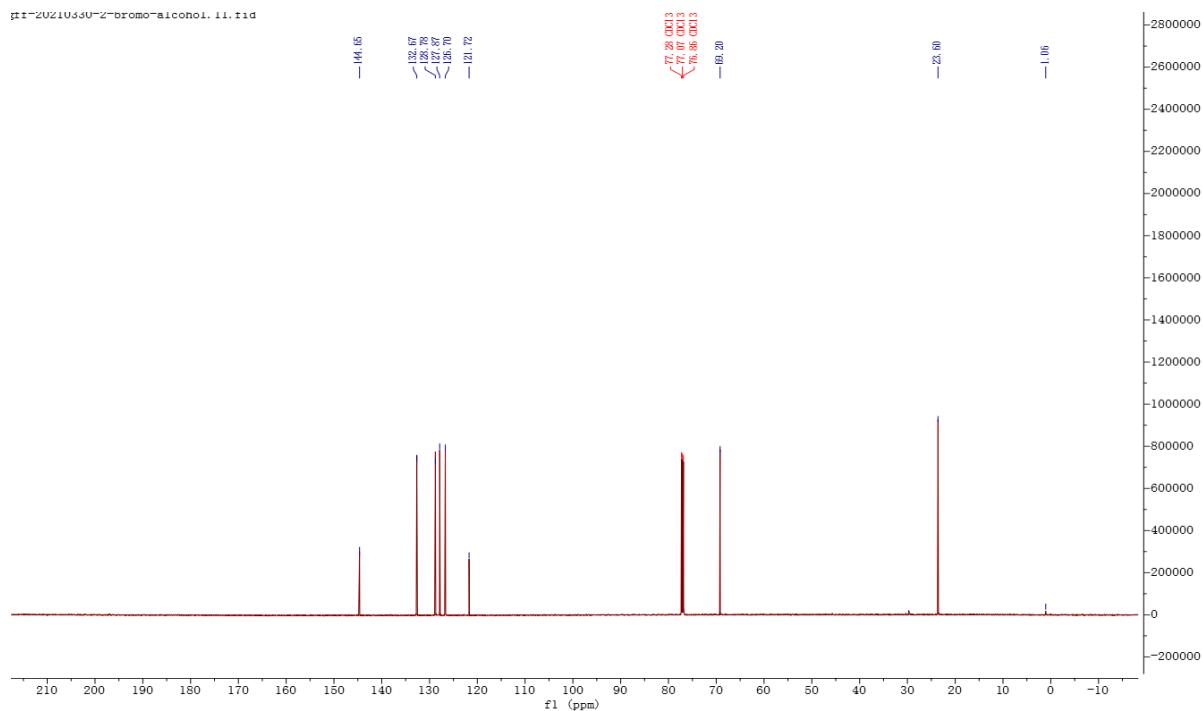
^1H -NMR (600 MHz, CDCl_3)

g1t-2U21U33U-2-bromo-alcohol.10.fid

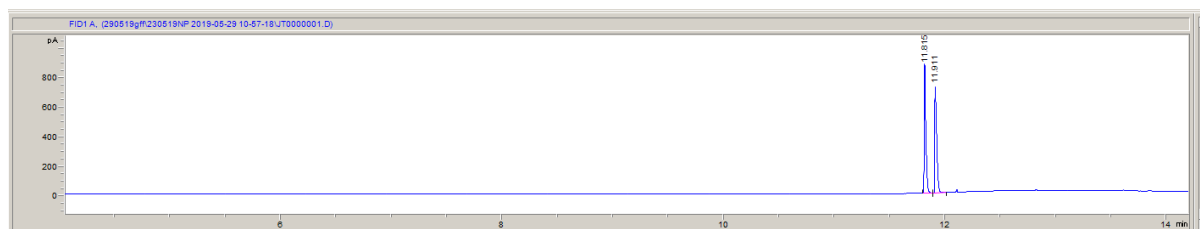
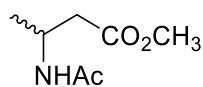


¹³C-NMR (101 MHz, CDCl₃)

ft-2U21U33U-2-bromo-alcohol. 11. 11d

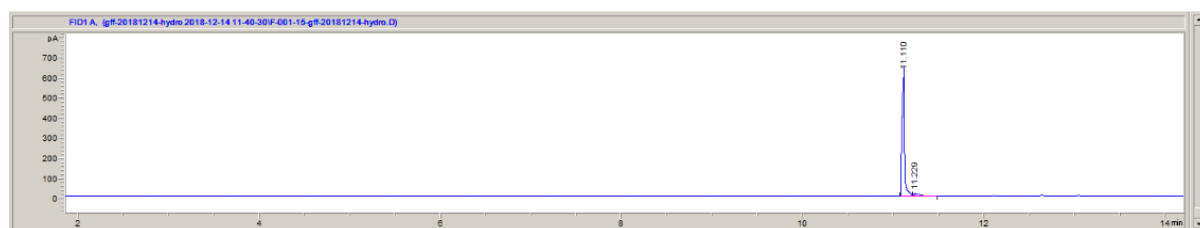
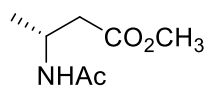


Racemic methyl 3-acetamidobutanoate



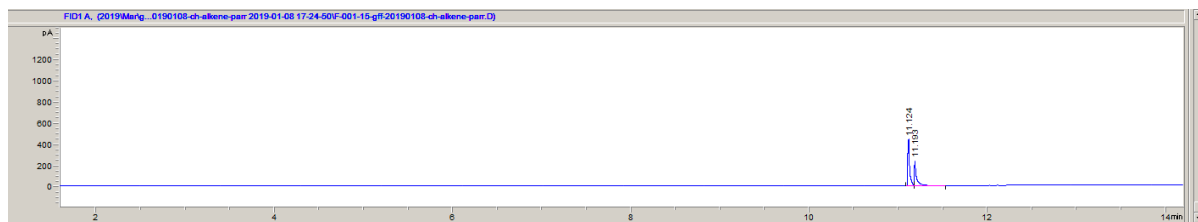
Peak #	RetTime [min]	Type	Width [min]	Area [pA*s]	Height [pA]	Area %
1	11.815	BB	0.0152	898.97290	874.37762	49.94991
2	11.911	BB	0.0186	900.77576	718.89716	50.05009

(R)-Ethyl 3-acetamidobutanoate(Hydrogenation of (E)-a by C.1)⁶⁸



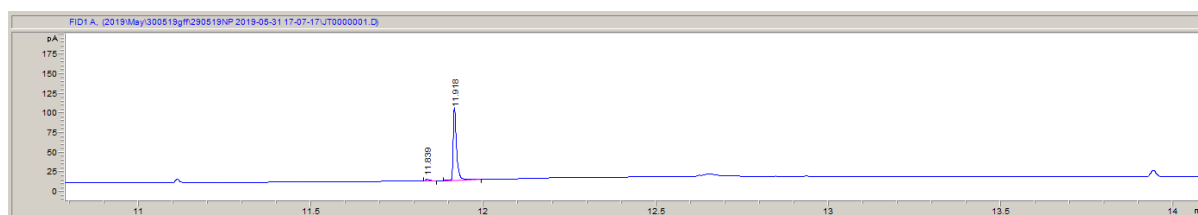
Peak #	RetTime [min]	Type	Width [min]	Area [pA*s]	Height [pA]	Area %
1	11.110	BV R	0.0267	1229.21887	611.27228	96.57493
2	11.229	VB E	0.0489	43.59472	11.75371	3.42507

(R)-Ethyl 3-acetamidobutanoate(Hydrogenation of (Z)-a by C.1)⁶⁸



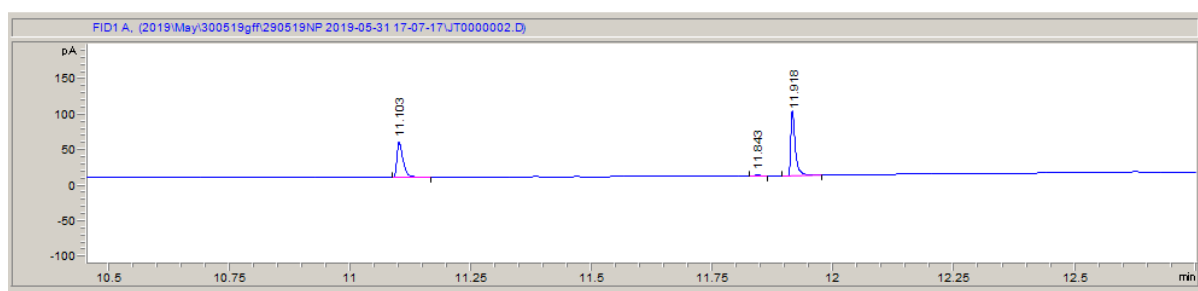
Peak #	RetTime [min]	Type	Width [min]	Area [pA*s]	Height [pA]	Area %
1	11.124	BV	0.0211	667.09583	435.02521	64.32362
2	11.193	VB	0.0213	369.99722	228.97014	35.67638

(S)-Ethyl 3-acetamidobutanoate(Hydrogenation of (E)-a by C.2 under 9 bar)⁷⁰



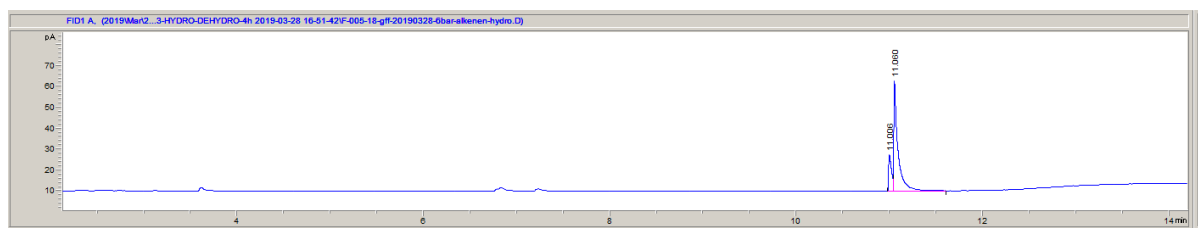
Peak #	RetTime [min]	Type	Width [min]	Area [pA*s]	Height [pA]	Area %
1	11.839	BB	0.0126	1.43343	1.77222	2.22764
2	11.918	BB	0.0107	62.91411	88.16644	97.77236

(S)-Ethyl 3-acetamidobutanoate(Hydrogenation of (E)-a by C.2 under 6.3 bar)⁷⁰



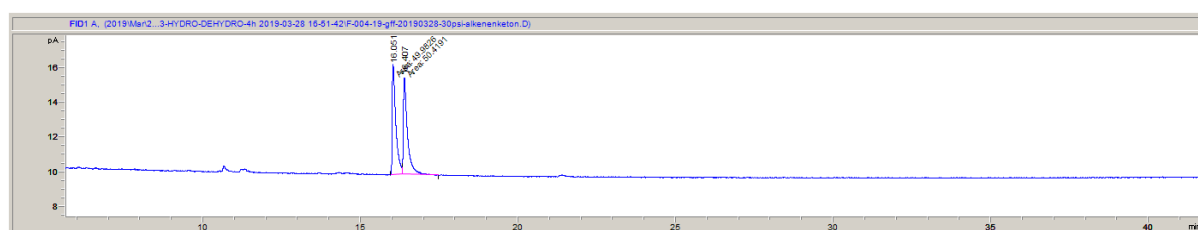
Peak #	RetTime [min]	Type	Width [min]	Area [pA*s]	Height [pA]	Area %
1	11.103	BB	0.0135	42.95728	48.46906	41.89994
2	11.843	BB	0.0122	1.08861	1.40795	1.06181
3	11.918	BB	0.0103	58.47760	86.17917	57.03825

(S)-Ethyl 3-acetamidobutanoate(Hydrogenation of (Z)-a by C.2 under 9 bar)⁷⁰



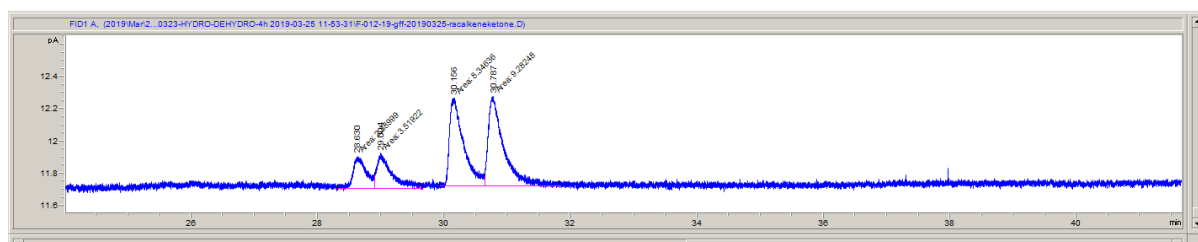
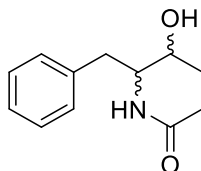
Peak #	RetTime [min]	Type	Width [min]	Area [pA*s]	Height [pA]	Area %
1	11.006	BV	0.0306	36.17657	17.41931	18.29789
2	11.060	VB	0.0397	161.53238	52.80730	81.70211

Racemic 3-acetylamino-4-phenyl-2-butanone



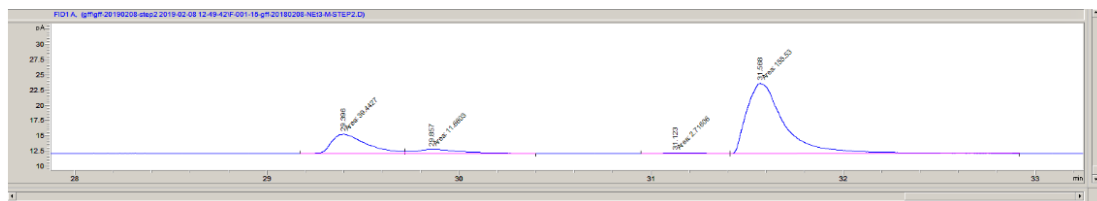
Peak #	RetTime [min]	Type	Width [min]	Area [pA*s]	Height [pA]	Area %
1	16.051	MM	0.1303	49.98259	6.39134	49.78263
2	16.407	MM	0.1512	50.41908	5.55815	50.21737

Racemic acetamido-3-phenyl-4-butan-2-ol



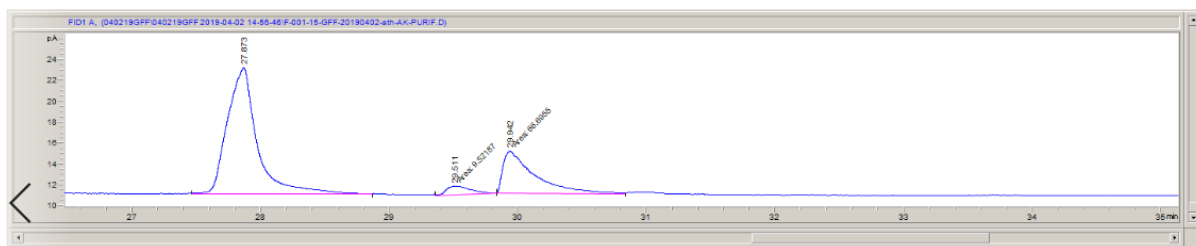
Peak #	RetTime [min]	Type	Width [min]	Area [pA*s]	Height [pA]	Area %
1	28.630	MM	0.2412	2.88999	1.99662e-1	12.02256
2	29.004	MM	0.2691	3.51922	2.17991e-1	14.64020
3	30.156	MM	0.2557	8.34636	5.44005e-1	34.72144
4	30.787	MM	0.2793	9.28248	5.53815e-1	38.61580

Acetamido-3-phenyl-4-butan-2-ol (Hydrogenated by C. 1 and C. 3 without removing metal of step1 by using tert-butyl potassium as base)



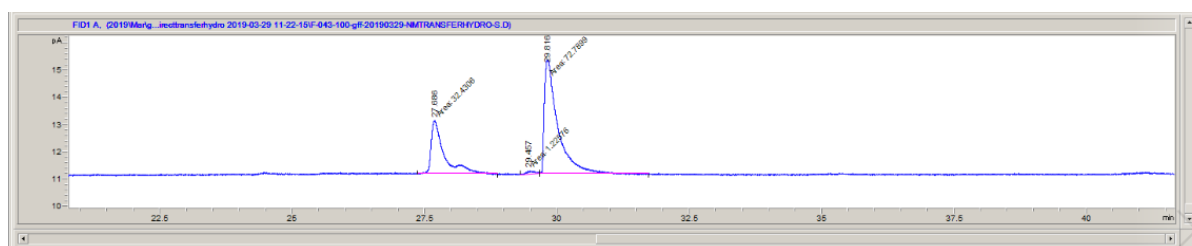
Peak #	RetTime [min]	Type	Width [min]	Area [pA*s]	Height [pA]	Area %
1	29.411	MM	0.2088	27.53411	2.19808	9.13064
2	29.807	MM	0.2334	22.32329	1.59373	7.40267
3	31.113	MM	0.1793	2.38452	2.21663e-1	0.79074
4	31.632	MM	0.2352	249.31529	17.66408	82.67595

Acetamido-3-phenyl-4-butan-2-ol (Hydrogenated by C. 2 and C. 3 without removing metal of step1 by using triethylamine as base)



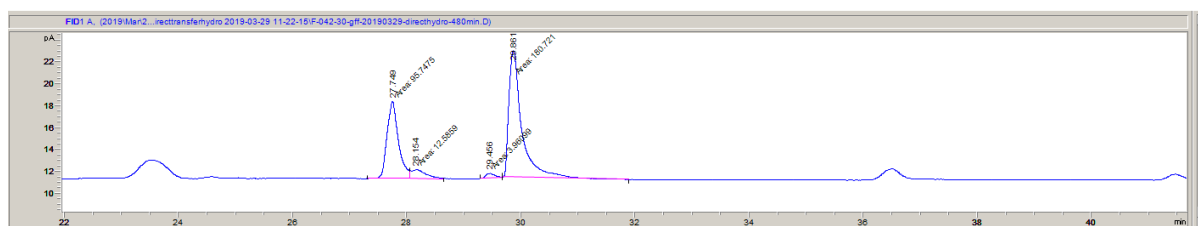
Peak #	RetTime [min]	Type	Width [min]	Area [pA*s]	Height [pA]	Area %
1	27.873	BB	0.1996	193.92799	12.05705	71.78652
2	29.511	MM	0.2023	9.52187	7.84364e-1	3.52472
3	29.942	MM	0.2776	66.69555	4.00464	24.68876

Acetamido-3-phenyl-4-butan-2-ol (Hydrogenated by C. 2 and C. 3 and metal of step 1 was removed)



Peak #	RetTime [min]	Type	Width [min]	Area [pA*s]	Height [pA]	Area %
1	27.686	MM	0.2783	32.43060	1.94238	30.46664
2	29.457	MM	0.1630	1.22576	1.25307e-1	1.15153
3	29.816	MM	0.2911	72.78990	4.16718	68.38183

Acetamido-3-phenyl-4-butan-2-ol (Transfer hydrogenated by C. 3)



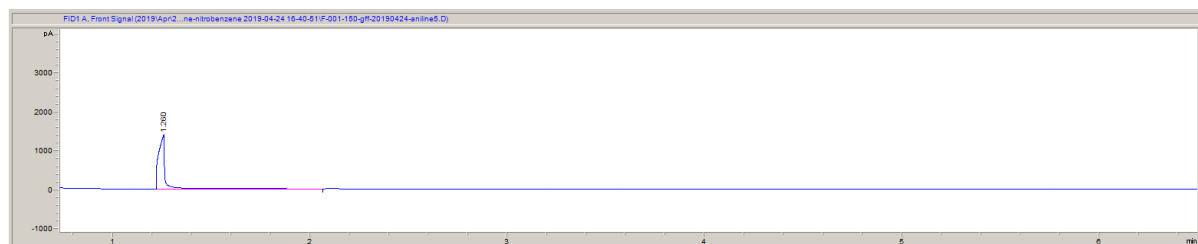
Peak #	RetTime [min]	Type	Width [min]	Area [pA*s]	Height [pA]	Area %
1	27.749	MM	0.2288	95.74754	6.97362	32.67667
2	28.154	MM	0.2748	12.58588	7.63247e-1	4.29530
3	29.456	MM	0.1687	3.96099	3.91311e-1	1.35180
4	29.861	MM	0.2615	180.72063	11.52037	61.67623

Nitrobenzene



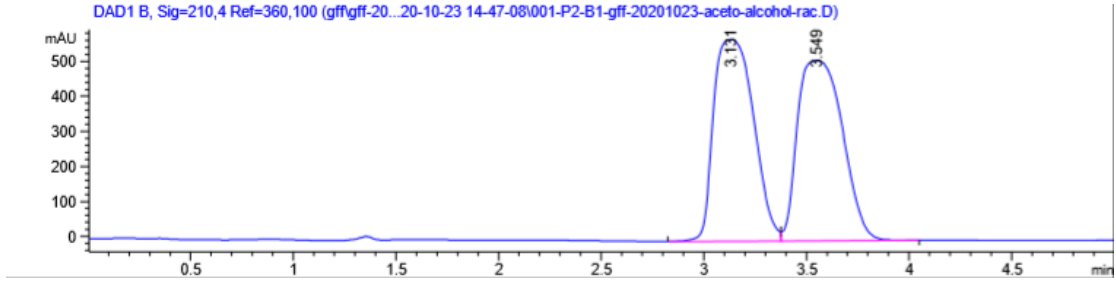
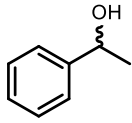
Peak #	RetTime [min]	Type	Width [min]	Area [pA*s]	Height [pA]	Area %
1	1.970	BB	0.0271	449.82852	212.42920	1.000e2

Aniline



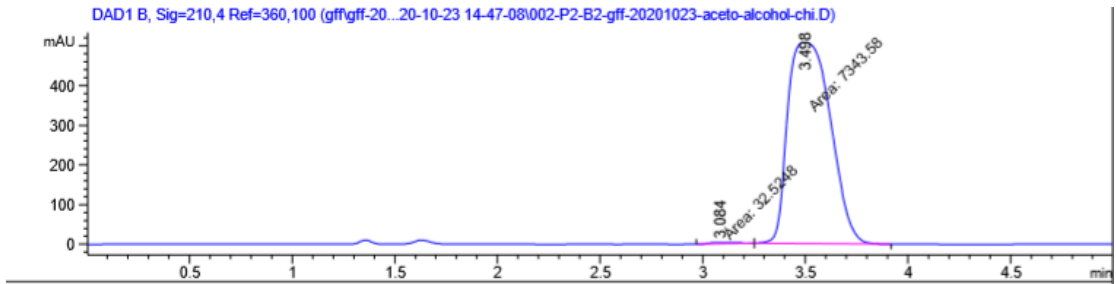
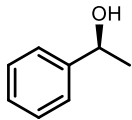
Peak #	RetTime [min]	Type	Width [min]	Area [pA*s]	Height [pA]	Area %
1	1.260	BB	0.0386	3079.35083	1350.05786	1.000e2

(S)-1-phenylethan-1-ol (2):



Signal 2: DAD1 B, Sig=210,4 Ref=360,100

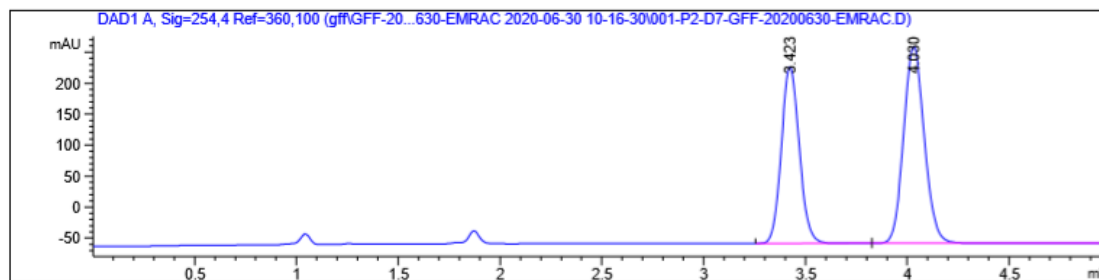
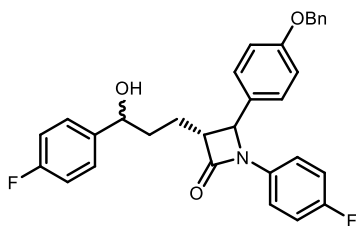
Peak #	RetTime [min]	Type	Width [min]	Area [mAU*s]	Height [mAU]	Area %
1	3.131	BV	0.2239	7795.02490	575.89935	49.8477
2	3.549	VB	0.2519	7842.66455	514.45782	50.1523



Signal 2: DAD1 B, Sig=210,4 Ref=360,100

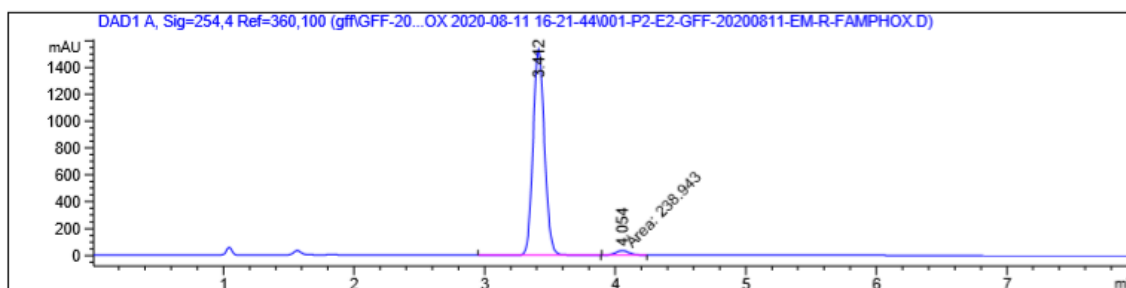
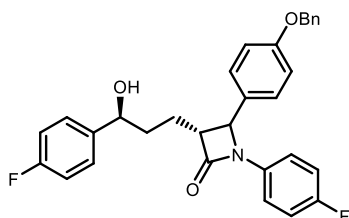
Peak #	RetTime [min]	Type	Width [min]	Area [mAU*s]	Height [mAU]	Area %
1	3.084	MM	0.1585	32.52481	3.41916	0.4409
2	3.498	MM	0.2413	7343.58252	507.12729	99.5591

(3R)-4-(4-(benzyloxy)phenyl)-1-(4-fluorophenyl)-3-((S)-3-(4-fluorophenyl)-3-hydroxypropyl)azetidin-2-one (4):



Signal 1: DAD1 A, Sig=254,4 Ref=360,100

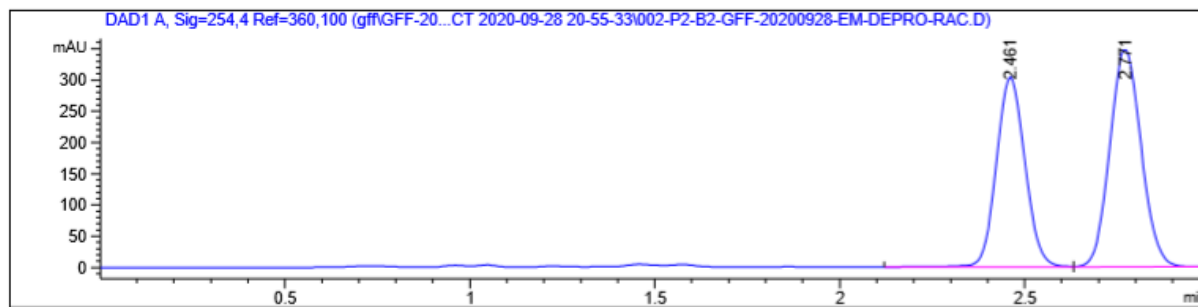
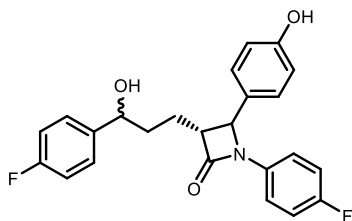
Peak #	RetTime [min]	Type	Width [min]	Area [mAU*s]	Height [mAU]	Area %
1	3.423	BB	0.0954	1743.24963	284.80435	43.6504
2	4.030	BBA	0.1105	2250.41016	318.34717	56.3496



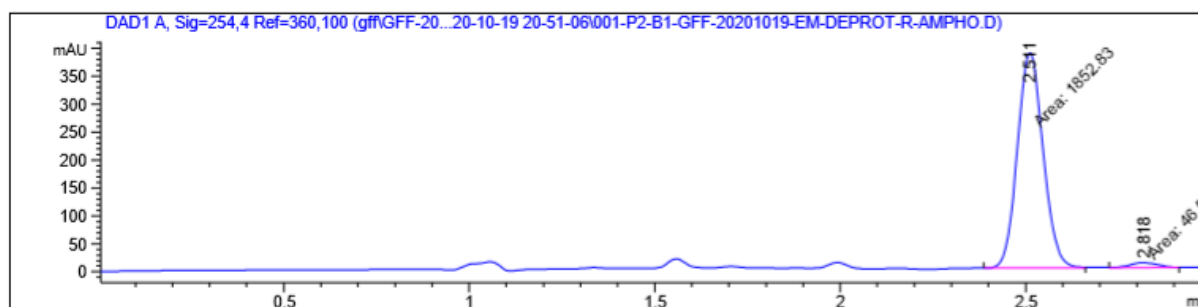
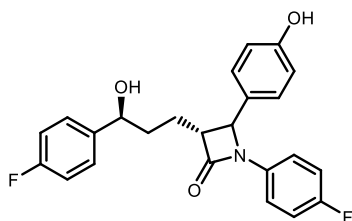
Signal 1: DAD1 A, Sig=254,4 Ref=360,100

Peak #	RetTime [min]	Type	Width [min]	Area [mAU*s]	Height [mAU]	Area %
1	3.412	VV R	0.0949	9330.31445	1533.70544	97.5030
2	4.054	MM	0.1174	238.94305	33.93001	2.4970

(3R)-1-(4-fluorophenyl)-3-((S)-3-(4-fluorophenyl)-3-hydroxypropyl)-4-(4-hydroxyphenyl)azetidin-2-one (5):



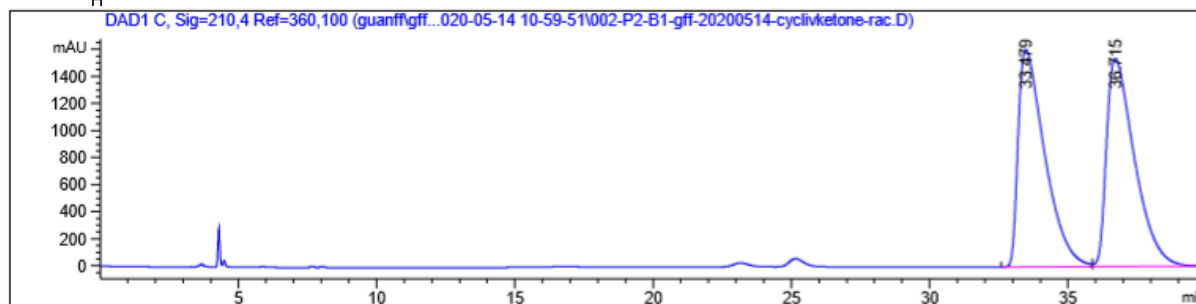
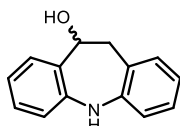
Peak #	RetTime [min]	Type	Width [min]	Area [mAU*s]	Height [mAU]	Area %
1	2.461	VV R	0.0848	1637.42712	304.16727	44.4132
2	2.771	VBA	0.0925	2049.37476	349.18344	55.5868



Signal 1: DAD1 A, Sig=254,4 Ref=360,100

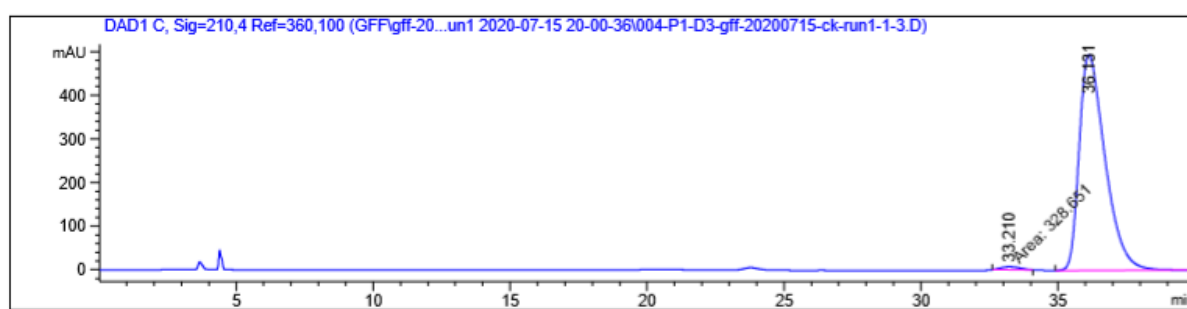
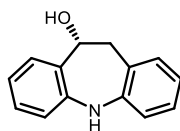
Peak #	RetTime [min]	Type	Width [min]	Area [mAU*s]	Height [mAU]	Area %
1	2.511	MM	0.0799	1852.83325	386.58603	97.5477
2	2.818	MM	0.0873	46.57941	8.89634	2.4523

(R)-10,11-dihydro-5H-dibenzo[b,f]azepin-10-ol (7):



Signal 1: DAD1 C, Sig=210,4 Ref=360,100

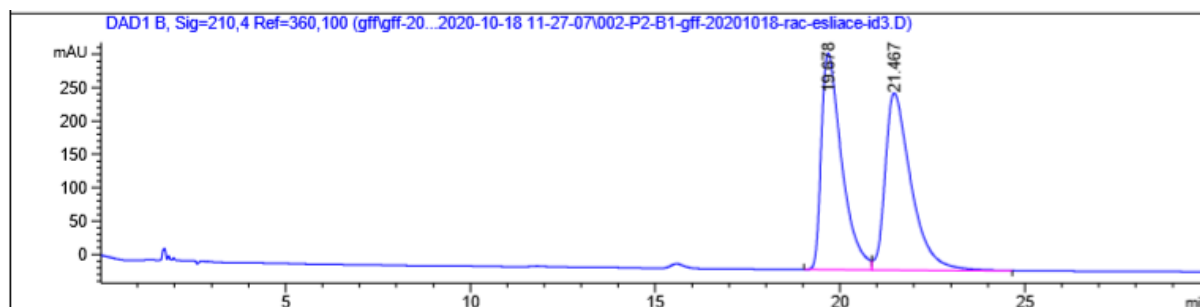
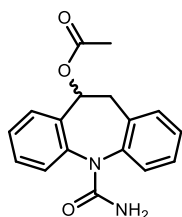
Peak #	RetTime [min]	Type	Width [min]	Area [mAU*s]	Height [mAU]	Area %
1	33.479	BV	0.9428	1.07428e5	1605.27478	49.8240
2	36.715	VBA	1.0211	1.08186e5	1537.24329	50.1760



Signal 1: DAD1 C, Sig=210,4 Ref=360,100

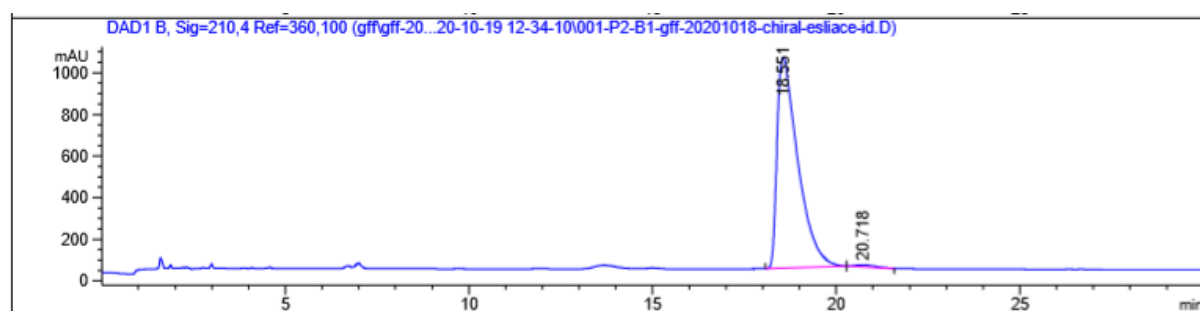
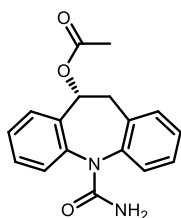
Peak #	RetTime [min]	Type	Width [min]	Area [mAU*s]	Height [mAU]	Area %
1	33.210	MM	0.7853	328.65112	6.97466	1.0037
2	36.131	BBA	0.9878	3.24158e4	493.85522	98.9963

(R)-eslicarbazepine acetate (9):



Signal 2: DAD1 B, Sig=210,4 Ref=360,100

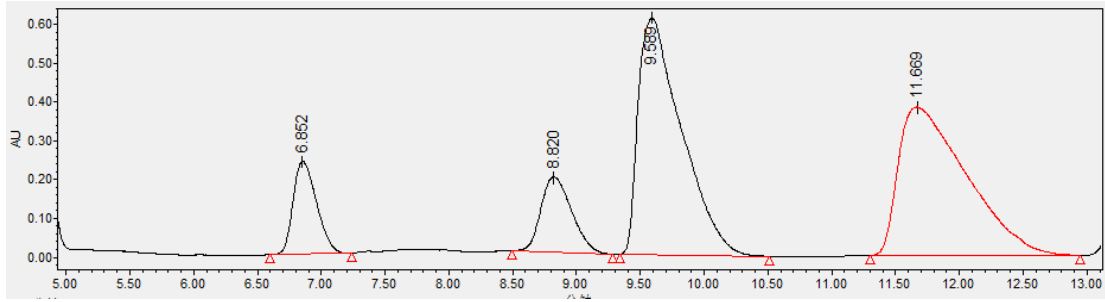
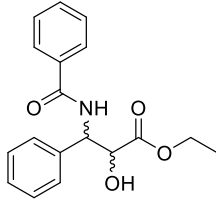
Peak #	RetTime [min]	Type	Width [min]	Area [mAU*s]	Height [mAU]	Area %
1	19.678	BV	0.5737	1.24475e4	324.40259	49.0643
2	21.467	VB	0.7267	1.29223e4	265.11630	50.9357



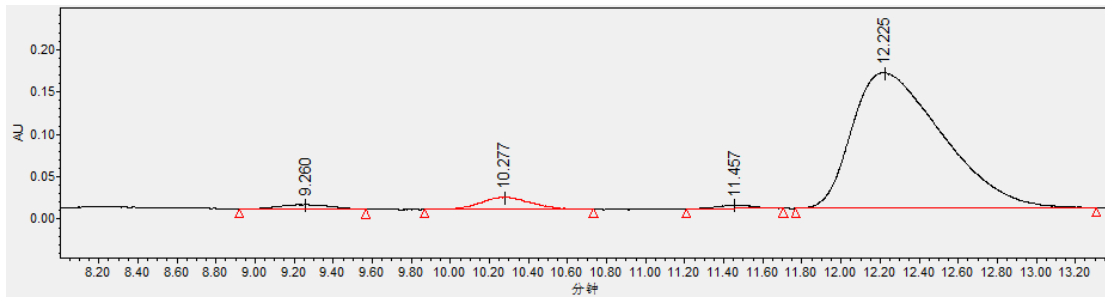
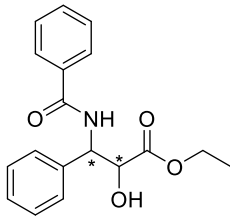
Signal 2: DAD1 B, Sig=210,4 Ref=360,100

Peak #	RetTime [min]	Type	Width [min]	Area [mAU*s]	Height [mAU]	Area %
1	18.551	BB	0.5834	3.99156e4	1013.66193	99.1415
2	20.718	BB	0.5625	345.65854	9.28059	0.8585

ethyl 3-benzamido-2-hydroxy-3-phenylpropanoate (53)

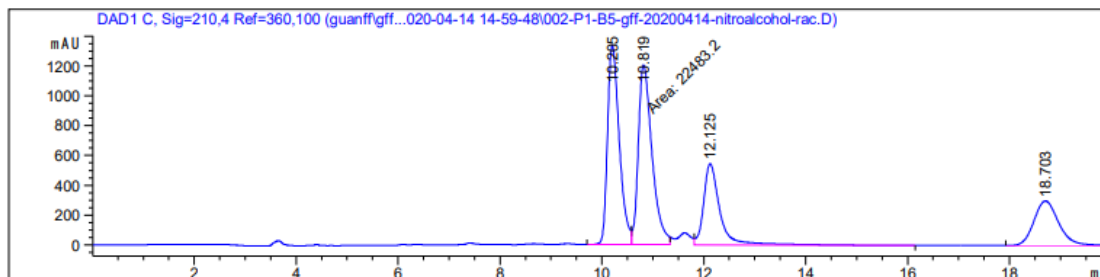
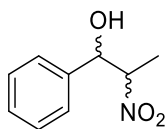


序号	名称	保留时间 (分钟)	纯度1 角度	纯度1 阈值	PDA/FLR 匹配1 光谱名	PDA/FLR 匹配1 角度	PDA/FLR 匹配2 阈值	PDA/FLR 匹配1 库名	面积 (微伏·秒)	% 面积	高度 (微伏)	积分类型	含量	单位	峰类型	峰代码
1		6.852							3038073	8.72	238847	bb			未知	
2		8.820							3249376	9.32	193924	bb			未知	
3		9.589							14379578	41.26	608801	bb			未知	
4		11.669							14187197	40.70	383288	bb			未知	



序号	名称	保留时间 (分钟)	纯度1 角度	纯度1 阈值	PDA/FLR 匹配1 光谱名	PDA/FLR 匹配1 角度	PDA/FLR 匹配2 阈值	PDA/FLR 匹配1 库名	面积 (微伏·秒)	% 面积	高度 (微伏)	积分类型	含量	单位	峰类型	峰代码
1		9.260							105671	1.91	5633	bb			未知	
2		10.277							252246	4.56	14011	bb			未知	
3		11.457							57013	1.03	4324	bb			未知	
4		12.225							5114533	92.50	159630	bb			未知	

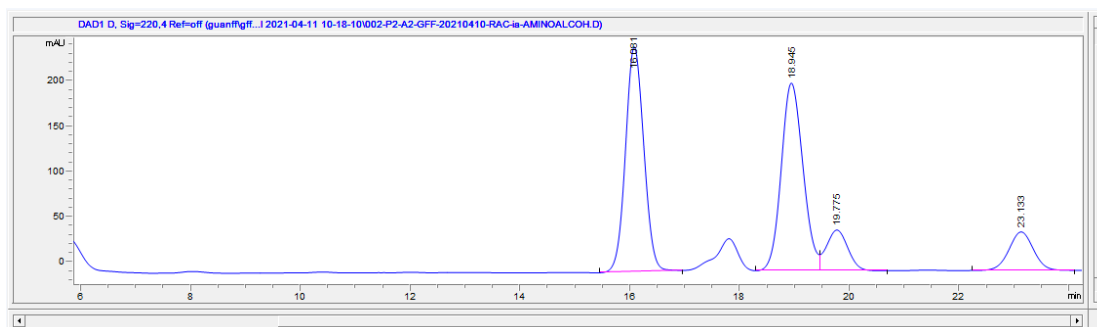
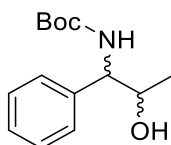
2-nitro-1-phenylpropan-1-ol (63)



Signal 1: DAD1 C, Sig=210,4 Ref=360,100

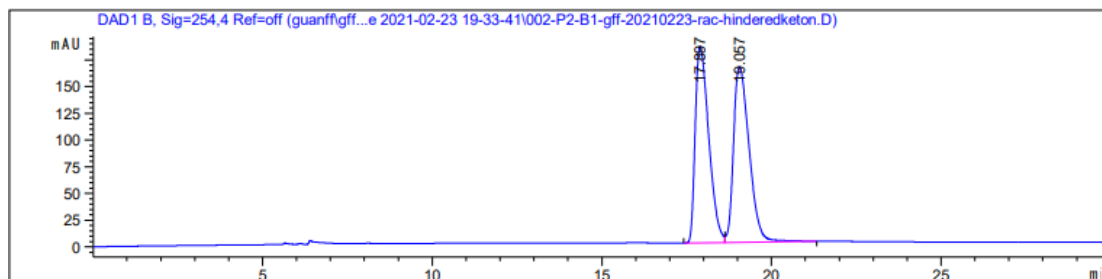
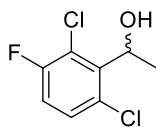
Peak #	RetTime [min]	Type	Width [min]	Area [mAU*s]	Height [mAU]	Area %
1	10.205	BV	0.2466	2.13519e4	1334.77600	32.3913
2	10.819	MF	0.3109	2.24832e4	1205.23511	34.1075
3	12.125	VB	0.3288	1.20872e4	544.84399	18.3365
4	18.703	BBA	0.5169	9996.46582	298.33673	15.1648

tert-butyl (2-hydroxy-1-phenylpropyl)carbamate (69)



#	Time	Type	Area	Height	Width	Area%	Symmetry
1	16.081	BB	5739.1	247.3	0.3627	41.083	0.886
2	18.945	BV	5693.7	206.5	0.4297	40.759	0.844
3	19.775	VB	1221.9	44.8	0.4182	8.747	0.916
4	23.133	BB	1314.7	42.4	0.4839	9.411	0.978

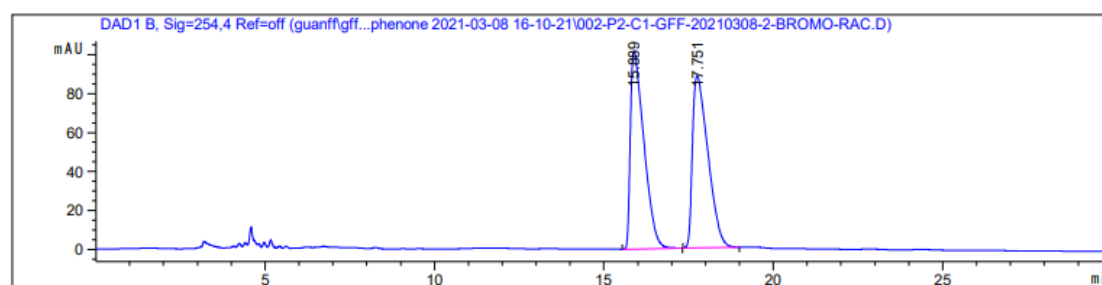
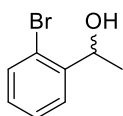
1-(2,6-dichloro-3-fluorophenyl)ethan-1-ol (72)



Signal 1: DAD1 B, Sig=254,4 Ref=off

Peak #	RetTime [min]	Type	Width [min]	Area [mAU*s]	Height [mAU]	Area %
1	17.897	BV	0.4329	5079.56738	183.53676	49.1504
2	19.057	VB	0.5021	5255.17285	163.87875	50.8496

1-(2-bromophenyl)ethan-1-ol (74)



Signal 1: DAD1 B, Sig=254,4 Ref=off

Peak #	RetTime [min]	Type	Width [min]	Area [mAU*s]	Height [mAU]	Area %
1	15.889	BB	0.4210	2818.71021	101.79534	50.1664
2	17.751	BB	0.4837	2800.00659	88.35082	49.8336

7.6 Analytical protocol

Analytical protocol of 5,11-dihydro-10H-dibenzo[b,f]azepin-10-one (6)

The carbonyl absorption at 1661 cm^{-1} was selected to reflect the concentration of **6** in Figure 96. To eliminate the background, the data was obtained by substrate absorption of 1704 cm^{-1} by 1661 cm^{-1} . Then the conversion was calculated by Lamber-Beer Law.

$$c = A/\varepsilon l \quad \text{Equation 9}$$

where c is concentration of the medium (M), A is the absorbance, ε is the molar extinction coefficient and l is the length of light pathway. l and ε are constant. Concentration is proportional to absorbance. Calibration curve was shown in Figure 97.

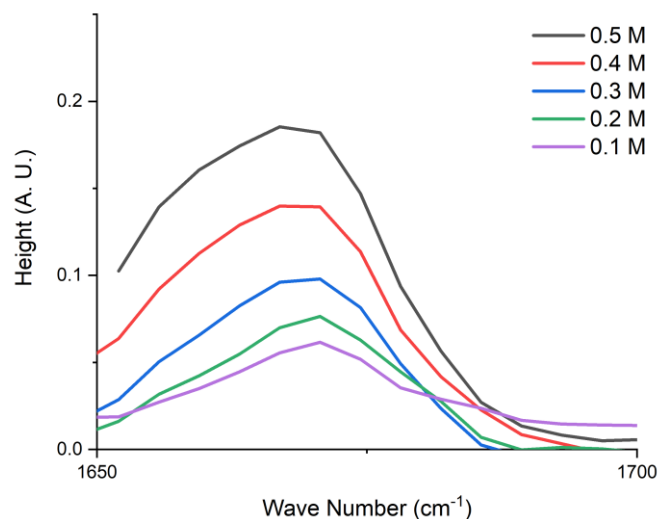


Figure 96 Target Peak of **6** in IR spectrum

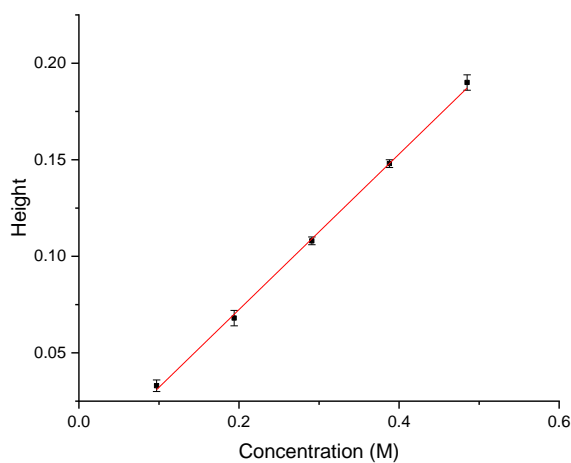


Figure 97 Calibration Curve of **6**

Analytical protocol of nitrobenzene and aniline

Conversion was monitored direct injection of reaction samples. The nitrobenzene and aniline calibration curve is shown in Figure 98 and Figure 99.

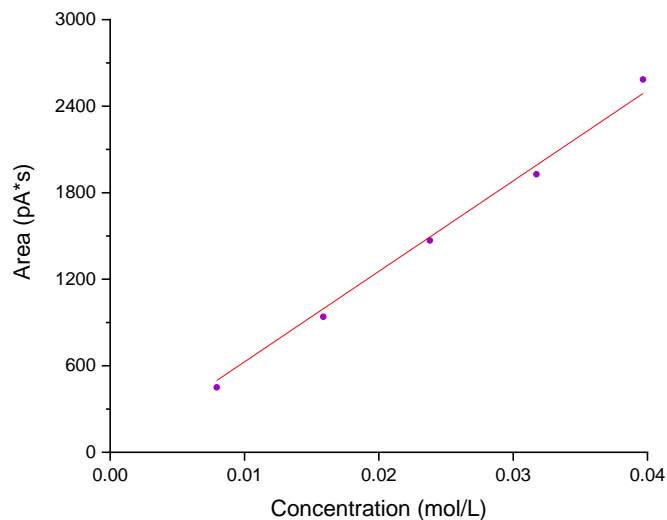


Figure 98 Nitrobenzene calibration curve

$$\text{Area (pA*s)} = 62724 * \text{Concentration (mmol/mL)}; R^2 = 0.998$$

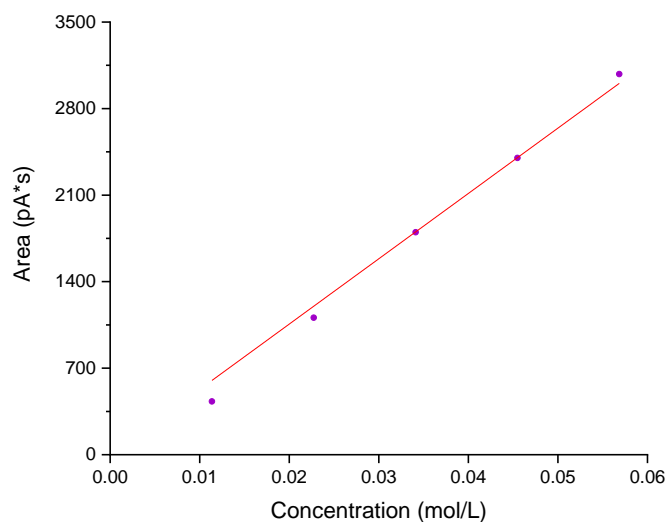


Figure 99 Aniline calibration curve

$$\text{Area (pA*s)} = 52839 * \text{Concentration (mmol/mL)}; R^2 = 0.998$$

Analytical protocol of (E) and (Z)-methyl-3-acetamido-2-butenate and racemic methyl 3-

acetamidobutanoate.

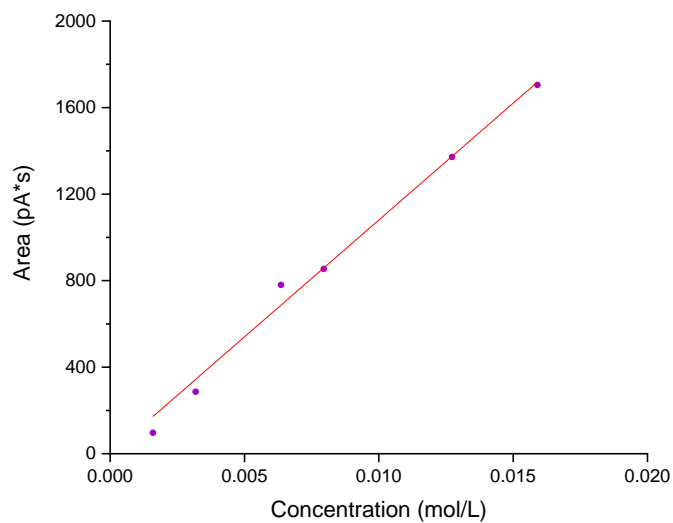


Figure 100 (Z)-methyl-3-acetamido-2-butenate calibration curve

Area (pA*s) = 108027*Concentration (mmol/mL); $R^2 = 0.990$

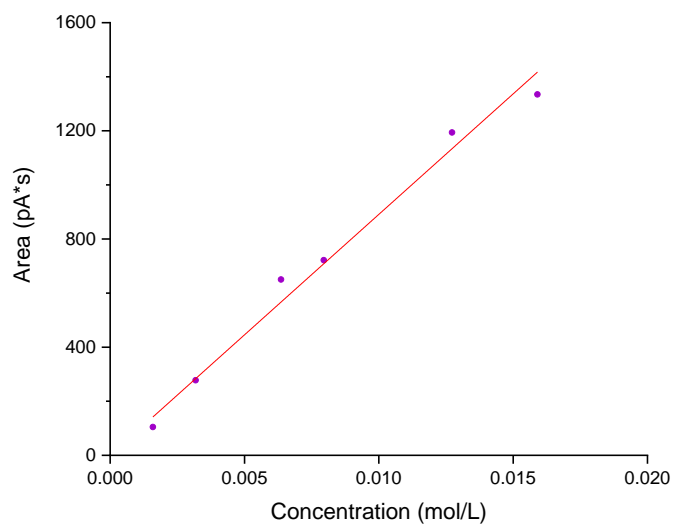


Figure 101 (E)-methyl-3-acetamido-2-butenate calibration curve

Area (pA*s) = 89104*Concentration (mmol/mL); $R^2 = 0.995$

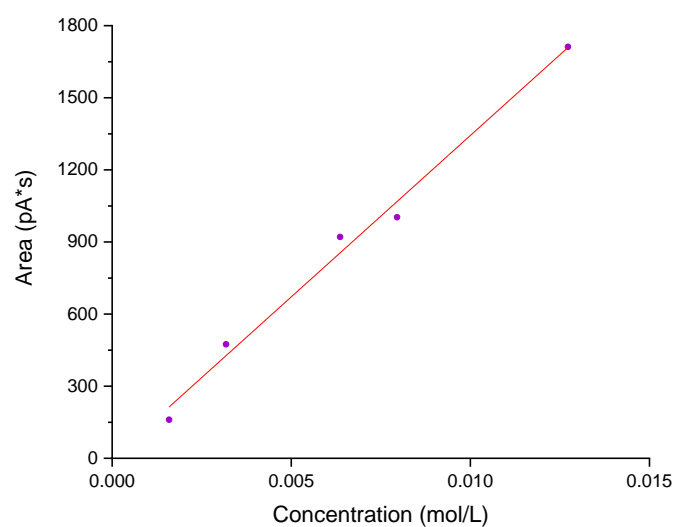


Figure 102 racemic methyl 3-acetamidobutanoate calibration curve

Area (pA*s) = 134312*Concentration (mmol/mL); $R^2 = 0.997$

Analytical protocol for hydroformylation of 1-octene

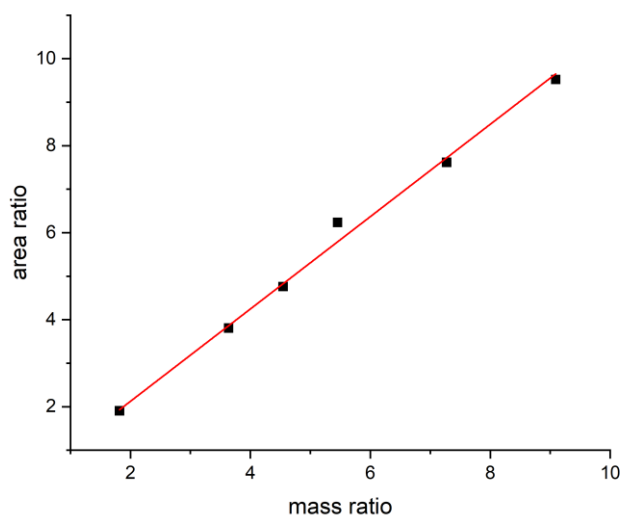


Figure 103 Calibration curve of 1-octene with tridecane as internal standard

Area ratio = 1.062*mass ratio; $R^2 = 0.99$

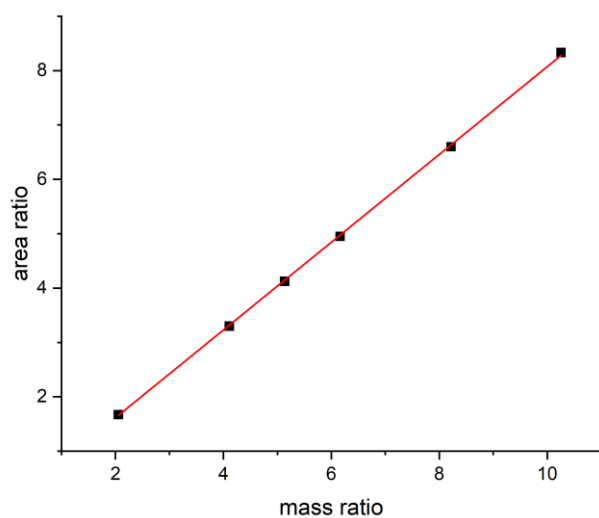


Figure 104 Calibration curve of aldehyde with tridecane as internal standard

Area ratio=0.81*mass ratio; $R^2 = 0.99$

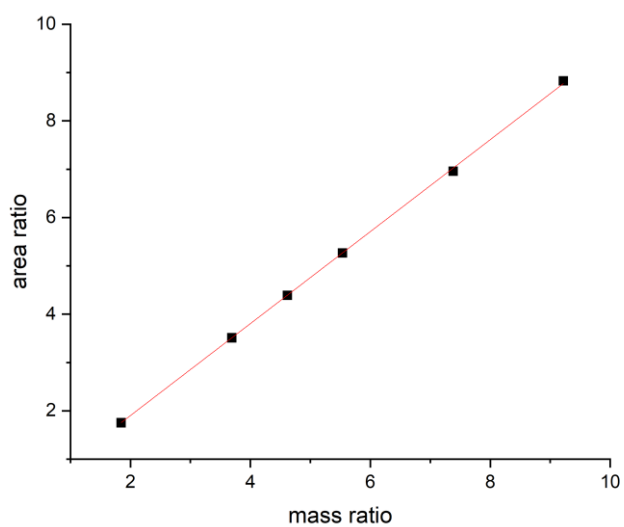


Figure 105 Calibration curve of octane with tridecane as internal standard

Area ratio = 0.95*mass ratio; $R^2 = 0.99$

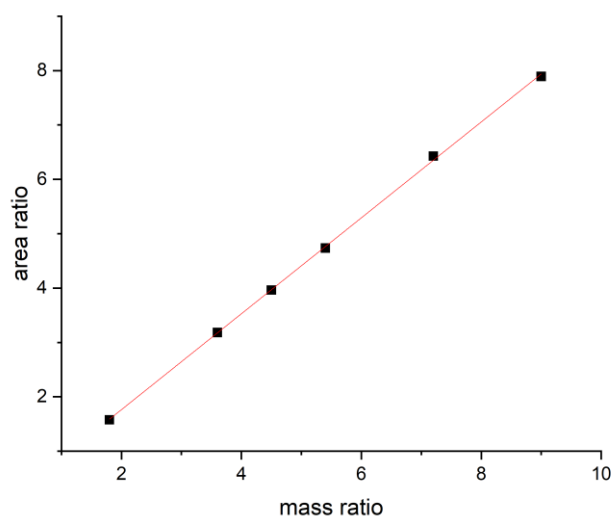


Figure 106 Calibration curve of 2-octene with tridecane as internal standard

Area ratio = $0.88 \cdot \text{mass ratio}$; $R^2 = 0.99$

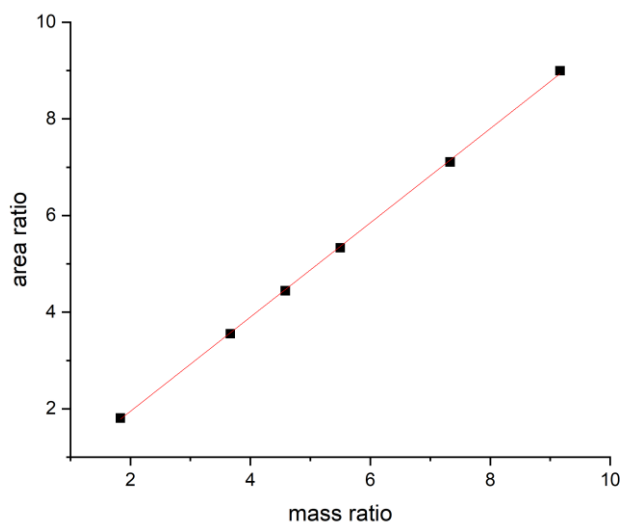


Figure 107 Calibration curve of 3-octene with tridecane as internal standard

Area ratio = $0.97 \cdot \text{mass ratio}$; $R^2 = 0.99$

8. References

- [1] a) T. Tsubogo, H. Oyamada, S. Kobayashi, *Nature* **2015**, *520*, 329-332; b) S. Rossi, R. Porta, D. Brenna, A. Puglisi, M. Benaglia, *Angewandte Chemie International Edition*

- 2017, 56, 4290-4294; c) S. B. Ötvös, M. A. Pericàs, C. O. Kappe, *Chemical Science* **2019**, 10, 11141-11146; d) Y. Saito, S. Kobayashi, *Journal of the American Chemical Society* **2020**, 142, 16546-16551; e) S. B. Ötvös, P. Llanes, M. A. Pericàs, C. O. Kappe, *Organic Letters* **2020**, 22, 8122-8126.
- [2] a) P. Rylander, in *The Catalytic Hydrogenation in Organic Syntheses* (Ed.: P. Rylander), Academic Press, **1979**, pp. 1-12; b) C. Jäkel, R. Paciello, *Chemical Reviews* **2006**, 106, 2912-2942.
- [3] a) T. Yu, J. Jiao, P. Song, W. Nie, C. Yi, Q. Zhang, P. Li, *ChemSusChem* **2020**, 13, 2876-2893; b) T. Yu, Z. Ding, W. Nie, J. Jiao, H. Zhang, Q. Zhang, C. Xue, X. Duan, Y. M. A. Yamada, P. Li, *Chemistry – A European Journal* **2020**, 26, 5729-5747.
- [4] G. Roos, C. Roos, in *Organic Chemistry Concepts* (Eds.: G. Roos, C. Roos), Academic Press, Boston, **2015**, pp. 43-54.
- [5] a) P. G. Mezey, in *Progress in Biological Chirality* (Eds.: G. Pályi, C. Zucchi, L. Caglioti), Elsevier Science Ltd, Oxford, **2004**, pp. 209-219; b) W. D. Lubell, K. S. Beauregard, F. Polyak, in *Comprehensive Chirality* (Eds.: E. M. Carreira, H. Yamamoto), Elsevier, Amsterdam, **2012**, pp. 86-104.
- [6] a) V. Goldanskii, V. V. Kuzmin, *Nature* **1991**, 352, 114-114; b) K. P. Bryliakov, *Research* **2020**, 2020, 5689246; cE. P. Talsi, A. A. Bryliakova, R. V. Ottenbacher, T. V. Rybalova, K. P. Bryliakov, *Research* **2019**, 2019, 4756025.
- [7] a) K. Geyer, J. D. C. Codée, P. H. Seeberger, *Chemistry – A European Journal* **2006**, 12, 8434-8442; b) W. C. Fu, T. F. Jamison, *Angewandte Chemie International Edition* **2020**, 59, 13885-13890.
- [8] M. B. Plutschack, B. Pieber, K. Gilmore, P. H. Seeberger, *Chemical Reviews* **2017**, 117, 11796-11893.
- [9] L. A. Oro, D. Carmona, in *The Handbook of Homogeneous Hydrogenation*, **2006**, 2-30.
- [10] a) D. Evans, G. Yagupsky, G. Wilkinson, *Journal of the Chemical Society A: Inorganic, Physical, Theoretical* **1968**, 2660-2665; b) M. Yagupsky, C. K. Brown, G. Yagupsky, G. Wilkinson, *Journal of the Chemical Society A: Inorganic, Physical, Theoretical* **1970**, 937-941.
- [11] a) R. R. Schrock, J. A. Osborn, *Journal of the American Chemical Society* **1976**, 98, 2134-2143; b) R. R. Schrock, J. A. Osborn, *Journal of the American Chemical Society* **1976**, 98, 4450-4455; c) R. R. Schrock, J. A. Osborn, *Journal of the American Chemical Society* **1976**, 98, 2143-2147.
- [12] J. R. Shapley, R. R. Schrock, J. A. Osborn, *Journal of the American Chemical Society* **1969**, 91, 2816-2817.
- [13] R. Crabtree, *Accounts of Chemical Research* **1979**, 12, 331-337.
- [14] a) R. Noyori, *Angewandte Chemie International Edition* **2002**, 41, 2008-2022; b) R. Noyori, *Advanced Synthesis & Catalysis* **2003**, 345, 15-32.
- [15] P. G. Jessop, R. H. Morris, *Coordination Chemistry Reviews* **1992**, 121, 155-284.
- [16] J. Wen, F. Wang, X. Zhang, *Chemical Society Reviews* **2021**, 50, 3211-3237.
- [17] H. U. Blaser, F. Spindler, M. Studer, *Applied Catalysis A: General* **2001**, 221, 119-143.
- [18] W. S. Knowles, *Accounts of Chemical Research* **1983**, 16, 106-112.
- [19] T. Saito, T. Yokozawa, T. Ishizaki, T. Moroi, N. Sayo, T. Miura, H. Kumobayashi, *Advanced Synthesis & Catalysis* **2001**, 343, 264-267.

- [20] I. C. Lennon, C. J. Pilkington, *SYNTHESIS -STUTT GART-* **2003**, *1*, 1639-1642.
- [21] K. Fukatsu, O. Uchikawa, M. Kawada, T. Yamano, M. Yamashita, K. Kato, K. Hirai, S. Hinuma, M. Miyamoto, S. Ohkawa, *Journal of Medicinal Chemistry* **2002**, *45*, 4212-4221.
- [22] Y. Hsiao, N. R. Rivera, T. Rosner, S. W. Krska, E. Njolito, F. Wang, Y. Sun, J. D. Armstrong, E. J. J. Grabowski, R. D. Tillyer, F. Spindler, C. Malan, *Journal of the American Chemical Society* **2004**, *126*, 9918-9919.
- [23] J. A. F. Boogers, U. Felfer, M. Kotthaus, L. Lefort, G. Steinbauer, A. H. M. de Vries, J. G. de Vries, *Organic Process Research & Development* **2007**, *11*, 585-591.
- [24] W. Tang, X. Zhang, *Chemical Reviews* **2003**, *103*, 3029-3070.
- [25] B. D. Vineyard, W. S. Knowles, M. J. Sabacky, G. L. Bachman, D. J. Weinkauff, *Journal of the American Chemical Society* **1977**, *99*, 5946-5952.
- [26] H. B. Kagan, T.-P. Dang, *Journal of the American Chemical Society* **1972**, *94*, 6429-6433.
- [27] a) A. Miyashita, H. Takaya, T. Souchi, R. Noyori, *Tetrahedron* **1984**, *40*, 1245-1253; b) R. Noyori, H. Takaya, *Accounts of Chemical Research* **1990**, *23*, 345-350; c) H. Takaya, K. Mashima, K. Koyano, M. Yagi, H. Kumobayashi, T. Taketomi, S. Akutagawa, R. Noyori, *The Journal of Organic Chemistry* **1986**, *51*, 629-635.
- [28] M. Kitamura, M. Tokunaga, T. Ohkuma, R. Noyori, *Organic Syntheses*, **1993**, *71*, 1.
- [29] T. Ohkuma, H. Ooka, S. Hashiguchi, T. Ikariya, R. Noyori, *Journal of the American Chemical Society* **1995**, *117*, 2675-2676.
- [30] T. Ohkuma, T. Hattori, H. Ooka, T. Inoue, R. Noyori, *Organic Letters* **2004**, *6*, 2681-2683.
- [31] a) M. J. Burk, *Journal of the American Chemical Society* **1991**, *113*, 8518-8519; b) M. J. Burk, J. E. Feaster, R. L. Harlow, *Organometallics* **1990**, *9*, 2653-2655; c) M. J. Burk, T. G. P. Harper, C. S. Kalberg, *Journal of the American Chemical Society* **1995**, *117*, 4423-4424.
- [32] W. Tang, X. Zhang, *Angewandte Chemie International Edition* **2002**, *41*, 1612-1614.
- [33] a) D. Liu, W. Gao, C. Wang, X. Zhang, *Angewandte Chemie International Edition* **2005**, *44*, 1687-1689; b) D. Liu, X. Zhang, *European Journal of Organic Chemistry*, **2005**, *2005*, 646-649.
- [34] X. Zhang, K. Huang, G. Hou, B. Cao, X. Zhang, *Angewandte Chemie International Edition* **2010**, *49*, 6421-6424.
- [35] W. Tang, W. Wang, Y. Chi, X. Zhang, *Angewandte Chemie International Edition* **2003**, *42*, 3509-3511.
- [36] a) C.-J. Wang, X. Sun, X. Zhang, *Angewandte Chemie International Edition* **2005**, *44*, 4933-4935; b) W. Tang, S. Wu, X. Zhang, *Journal of the American Chemical Society* **2003**, *125*, 9570-9571; c) S. Wu, W. Wang, W. Tang, M. Lin, X. Zhang, *Organic Letters* **2002**, *4*, 4495-4497; d) Z. Zhang, H. Qian, J. Longmire, X. Zhang, *The Journal of Organic Chemistry* **2000**, *65*, 6223-6226.
- [37] H. Nishiyama, H. Sakaguchi, T. Nakamura, M. Horihata, M. Kondo, K. Itoh, *Organometallics* **1989**, *8*, 846-848.
- [38] Y. Jiang, Q. Jiang, X. Zhang, *Journal of the American Chemical Society* **1998**, *120*, 3817-3818.

- [39] J.-H. Xie, X.-Y. Liu, J.-B. Xie, L.-X. Wang, Q.-L. Zhou, *Angewandte Chemie International Edition* **2011**, *50*, 7329-7332.
- [40] W. Wu, S. Liu, M. Duan, X. Tan, C. Chen, Y. Xie, Y. Lan, X.-Q. Dong, X. Zhang, *Organic Letters* **2016**, *18*, 2938-2941.
- [41] J. Yu, M. Duan, W. Wu, X. Qi, P. Xue, Y. Lan, X.-Q. Dong, X. Zhang, *Chemistry – A European Journal* **2017**, *23*, 970-975.
- [42] J. Yu, J. Long, Y. Yang, W. Wu, P. Xue, L. W. Chung, X.-Q. Dong, X. Zhang, *Organic Letters* **2017**, *19*, 690-693.
- [43] Z. Liang, T. Yang, G. Gu, L. Dang, X. Zhang, *Chinese Journal of Chemistry* **2018**, *36*, 851-856.
- [44] X. Lin, F. Guan, W. Jialin, S. Pan-Lin, Z. Xumu, *Progress in Chemistry* **2020**, *32*, 1680-1696.
- [45] a) M. J. Palmer, M. Wills, *Tetrahedron: Asymmetry* **1999**, *10*, 2045-2061; b) T. Ikariya, A. J. Blacker, *Accounts of Chemical Research* **2007**, *40*, 1300-1308.
- [46] J. Blacker, J. Martin, in *Asymmetric Catalysis on Industrial Scale*, **2003**, pp. 201-216.
- [47] J. Blacker Andrew, J. Mellor Ben, AVECIA LIMITED, **1998**.
- [48] K.-J. Haack, S. Hashiguchi, A. Fujii, T. Ikariya, R. Noyori, *Angewandte Chemie International Edition in English* **1997**, *36*, 285-288.
- [49] a) K. Murata, T. Ikariya, R. Noyori, *The Journal of Organic Chemistry* **1999**, *64*, 2186-2187; b) L.-S. Zheng, Q. Llopis, P.-G. Echeverria, C. Féraud, G. Guillaumot, P. Phansavath, V. Ratovelomanana-Vidal, *The Journal of Organic Chemistry* **2017**, *82*, 5607-5615; c) T. Thorpe, J. Blacker, S. M. Brown, C. Bubert, J. Crosby, S. Fitzjohn, J. P. Muxworthy, J. M. J. Williams, *Tetrahedron Letters* **2001**, *42*, 4041-4043.
- [50] H. G. Nedden, A. Zanotti-Gerosa, M. Wills, *The Chemical Record* **2016**, *16*, 2623-2643.
- [51] a) N. Künzle, T. Mallat, A. Baiker, *Applied Catalysis A: General* **2003**, *238*, 251-257; b) E. J. O'Neal, C. H. Lee, J. Brathwaite, K. F. Jensen, *ACS Catalysis* **2015**, *5*, 2615-2622; c) Z. Amara, M. Poliakoff, R. Duque, D. Geier, G. Franciò, C. M. Gordon, R. E. Meadows, R. Woodward, W. Leitner, *Organic Process Research & Development* **2016**, *20*, 1321-1327; d) J. Madarász, B. Nánási, J. Kovács, S. Balogh, G. Farkas, J. Bakos, *Monatshefte für Chemie - Chemical Monthly* **2018**, *149*, 19-25; e) T. Yasukawa, R. Masuda, S. Kobayashi, *Nature Catalysis* **2019**, *2*, 1088-1092; f) Y. Kawakami, A. Borissova, M. R. Chapman, G. Goltz, E. Koltsova, I. Mitrichev, A. J. Blacker, *European Journal of Organic Chemistry* **2019**, *2019*, 7499-7505.
- [52] a) S. Newton, C. F. Carter, C. M. Pearson, L. de C. Alves, H. Lange, P. Thansandote, S. V. Ley, *Angewandte Chemie International Edition* **2014**, *53*, 4915-4920; b) M. O'Brien, N. Taylor, A. Polyzos, I. R. Baxendale, S. V. Ley, *Chemical Science* **2011**, *2*, 1250-1257; c) S. Newton, S. V. Ley, E. C. Arcé, D. M. Grainger, *Advanced Synthesis & Catalysis* **2012**, *354*, 1805-1812.
- [53] T. F. Jamison, G. Koch, *Science of Synthesis: Flow Chemistry in Organic synthesis*. Thieme, New York, **2018**.
- [54] a) G. Luo, C. Lv, K. Wang, *Micro Chemical Engineering and Technology*, Chemical Industry Press, **2020**; b) F. E. Valera, M. Quaranta, A. Moran, J. Blacker, A. Armstrong,

- J. T. Cabral, D. G. Blackmond, *Angewandte Chemie International Edition* **2010**, *49*, 2478-2485.
- [55] Y. Mo, H. Lin, K. F. Jensen, *Chemical Engineering Journal* **2018**, *335*, 936-944.
- [56] M. R. Chapman, M. H. T. Kwan, G. King, K. E. Jolley, M. Hussain, S. Hussain, I. E. Salama, C. González Niño, L. A. Thompson, M. E. Bayana, A. D. Clayton, B. N. Nguyen, N. J. Turner, N. Kapur, A. J. Blacker, *Organic Process Research & Development* **2017**, *21*, 1294-1301.
- [57] a) F. Reichmann, K. Vennemann, T. A. Frede, N. Kockmann, *Chemie Ingenieur Technik* **2019**, *91*, 622-631; b) Z. Dong, S. Zhao, Y. Zhang, C. Yao, Q. Yuan, G. Chen, *AIChE Journal* **2017**, *63*, 1404-1418.
- [58] A. J. Blacker, J. R. Breen, R. A. Bourne, C. A. Hone, in *Green and Sustainable Medicinal Chemistry: Methods, Tools and Strategies for the 21st Century Pharmaceutical Industry*, The Royal Society of Chemistry, **2016**, pp. 140-155.
- [59] F. M. Akwi, P. Watts, *Chemical Communications* **2018**, *54*, 13894-13928.
- [60] A. D. Clayton, J. A. Manson, C. J. Taylor, T. W. Chamberlain, B. A. Taylor, G. Clemens, R. A. Bourne, *Reaction Chemistry & Engineering* **2019**, *4*, 1545-1554.
- [61] J.-i. Yoshida, Y. Takahashi, A. Nagaki, *Chemical Communications* **2013**, *49*, 9896-9904.
- [62] R. Radjagobalou, J.-F. Blanco, O. Dechy-Cabaret, M. Oelgemöller, K. Loubière, *Chemical Engineering and Processing - Process Intensification* **2018**, *130*, 214-228.
- [63] M. Elsherbini, T. Wirth, *Accounts of Chemical Research* **2019**, *52*, 3287-3296.
- [64] S. Nanda, M. Chauhan, *Reactors and Fundamentals of Reactors Design for Chemical Reaction*, **2008**.
- [65] T. Abadie, C. Xuereb, D. Legendre, J. Aubin, *Chemical Engineering Research and Design* **2013**, *91*, 2225-2234.
- [66] H. S. Fogler, *Elements of Chemical Reaction Engineering (Fourth Edition) Vol. 13*, Pearson, **2008**.
- [67] R. Abdallah, V. Meille, J. Shaw, D. Wenn, C. de Bellefon, *Chemical Communications* **2004**, 372-373.
- [68] a) P. J. Cossar, L. Hizartzidis, M. I. Simone, A. McCluskey, C. P. Gordon, *Organic & Biomolecular Chemistry* **2015**, *13*, 7119-7130; b) R. V. Jones, L. Godorhazy, N. Varga, D. Szalay, L. Urge, F. Darvas, *Journal of Combinatorial Chemistry* **2006**, *8*, 110-116; c) S. Balogh, G. Farkas, J. Madarász, Á. Szöllösy, J. Kovács, F. Darvas, L. Üрге, J. Bakos, *Green Chemistry* **2012**, *14*, 1146-1151.
- [69] C. de Bellefon, T. Lamouille, N. Pestre, F. Bornette, H. Pennemann, F. Neumann, V. Hessel, *Catalysis Today* **2005**, *110*, 179-187.
- [70] L. Shi, X. Wang, C. A. Sandoval, Z. Wang, H. Li, J. Wu, L. Yu, K. Ding, *Chemistry – A European Journal* **2009**, *15*, 9855-9867.
- [71] T. Ouchi, C. Battilocchio, J. M. Hawkins, S. V. Ley, *Organic Process Research & Development* **2014**, *18*, 1560-1566.
- [72] a) M. L. Abrams, J. Y. Buser, J. R. Calvin, M. D. Johnson, B. R. Jones, G. Lambertus, C. R. Landis, J. R. Martinelli, S. A. May, A. D. McFarland, J. R. Stout, *Organic Process Research & Development* **2016**, *20*, 901-910; b) S. A. May, M. D. Johnson, J. Y. Buser, A. N. Campbell, S. A. Frank, B. D. Haeberle, P. C. Hoffman, G. R. Lambertus, A. D. McFarland, E. D. Moher, T. D. White, D. D. Hurley, A. P. Corrigan, O. Gowran, N. G.

- Kerrigan, M. G. Kissane, R. R. Lynch, P. Sheehan, R. D. Spencer, S. R. Pulley, J. R. Stout, *Organic Process Research & Development* **2016**, *20*, 1870-1898.
- [73] M. D. Johnson, S. A. May, J. R. Calvin, J. Remacle, J. R. Stout, W. D. Diserod, N. Zaborenko, B. D. Haeberle, W.-M. Sun, M. T. Miller, J. Brennan, *Organic Process Research & Development* **2012**, *16*, 1017-1038.
- [74] M. D. Johnson, S. A. May, J. R. Calvin, G. R. Lambertus, P. B. Kokitkar, C. R. Landis, B. R. Jones, M. L. Abrams, J. R. Stout, *Organic Process Research & Development* **2016**, *20*, 888-900.
- [75] M. O. Frederick, M. A. Pietz, D. P. Kjell, R. N. Richey, G. A. Tharp, T. Touge, N. Yokoyama, M. Kida, T. Matsuo, *Organic Process Research & Development* **2017**, *21*, 1447-1451.
- [76] S. V. Tsukanov, M. D. Johnson, S. A. May, S. P. Kolis, M. H. Yates, J. N. Johnston, *Organic Process Research & Development* **2018**, *22*, 971-977.
- [77] T. Touge, M. Kuwana, Y. Komatsuki, S. Tanaka, H. Nara, K. Matsumura, N. Sayo, Y. Kashibuchi, T. Saito, *Organic Process Research & Development* **2019**, *23*, 452-461.
- [78] A. Campbell Brewer, P. C. Hoffman, J. R. Martinelli, M. E. Kobierski, N. Mullane, D. Robbins, *Organic Process Research & Development* **2019**, *23*, 1484-1498.
- [79] F. Guan, N. Kapur, L. Sim, C. J. Taylor, J. Wen, X. Zhang, A. J. Blacker, *Reaction Chemistry & Engineering* **2020**, *5*, 1903-1908.
- [80] C. A. Challener, *Chiral Drug*, Routledge, **2017**.
- [81] a) I. Ojima, *Catalytic Asymmetric Synthesis, Third Edition*, John Wiley & Sons, Inc; b) T.-L. Liu, C.-J. Wang, X. Zhang, *Angewandte Chemie International Edition* **2013**, *52*, 8416-8419; c) L. Wei, Z. Xumu, *Stereoselective Formation of Amines*, Springer-Verlag Berlin Heidelberg, **2014**; d) W. Zhang, Y. Chi, X. Zhang, *Accounts of Chemical Research* **2007**, *40*, 1278-1290.
- [82] M. Besson, C. Pinel, *Topics in Catalysis* **1998**, *5*, 25-38.
- [83] a) M. Akashi, N. Arai, T. Inoue, T. Ohkuma, *Advanced Synthesis & Catalysis* **2011**, *353*, 1955-1960; b) P. Kukula, R. Prins, *Journal of Catalysis* **2002**, *208*, 404-411.
- [84] a) V. Ratovelomanana-Vidal, J.-P. Genêt, *Canadian Journal of Chemistry* **2000**, *78*, 846-851; b) X. Fan, P. J. Walsh, *Accounts of Chemical Research* **2017**, *50*, 2389-2400; c) E. Vedejs, M. Jure, *Angewandte Chemie International Edition* **2005**, *44*, 3974-4001; d) F. F. Huerta, A. B. E. Minidis, J.-E. Bäckvall, *Chemical Society Reviews* **2001**, *30*, 321-331.
- [85] a) S. Caddick, K. Jenkins, *Chemical Society Reviews* **1996**, *25*, 447-456; b) R. Stürmer, *Angewandte Chemie International Edition in English* **1997**, *36*, 1173-1174; c) R. S. Ward, *Tetrahedron: Asymmetry* **1995**, *6*, 1475-1490.
- [86] H. E. Zimmerman, M. D. Traxler, *Journal of the American Chemical Society* **1957**, *79*, 1920-1923.
- [87] a) L. Raffier, O. Gutierrez, G. R. Stanton, M. C. Kozlowski, P. J. Walsh, *Organometallics* **2014**, *33*, 5371-5377; b) I. Fleming, D. A. Hrovat, W. T. Borden, *Journal of the Chemical Society, Perkin Transactions 2* **2001**, 331-338.
- [88] Z. Ke, Y. Li, C. Hou, Y. Liu, *Physical Sciences Reviews* **2018**, *3*, 1-28.
- [89] a) R. Carr, M. Alexeeva, M. J. Dawson, V. Gotor-Fernández, C. E. Humphrey, N. J. Turner, *ChemBioChem* **2005**, *6*, 637-639; b) Y. Cao, C. Soares, N. Padoin, T. Noël, *Chemical Engineering Journal* **2021**, *406*, 126811.

- [90] a) H. Pellissier, *Tetrahedron* **2018**, *74*, 3459-3468; b) J. W. Faller, A. R. Lavoie, *Organic Letters* **2001**, *3*, 3703-3706.
- [91] a) A. J. Blacker, M. J. Stirling, M. I. Page, *Organic Process Research & Development* **2007**, *11*, 642-648; b) X. Sun, G. Manos, J. Blacker, J. Martin, A. Gavriilidis, *Organic Process Research & Development* **2004**, *8*, 909-914.
- [92] a) Q.-J. Liang, Y.-H. Xu, T.-P. Loh, *Organic Chemistry Frontiers* **2018**, *5*, 2765-2768; b) L. M. Ambrosini, T. H. Lambert, *ChemCatChem* **2010**, *2*, 1373-1380.
- [93] a) A. J. Blacker, M. Roy, S. Hariharan, C. Headley, A. Upare, A. Jagtap, K. Wankhede, S. K. Mishra, D. Dube, S. Bhise, S. Vishwasrao, N. Kadam, *Organic Process Research & Development* **2011**, *15*, 331-338; b) K. Izawa, T. Onishi, *Chemical Reviews* **2006**, *106*, 2811-2827.
- [94] a) H.-J. Ha, G.-S. Park, Y.-G. Ahn, G. S. Lee, *Bioorganic & Medicinal Chemistry Letters* **1998**, *8*, 1619-1622; b) K. C. Nicolaou, W.-M. Dai, R. K. Guy, *Angewandte Chemie International Edition in English* **1994**, *33*, 15-44.
- [95] a) A. Adamo, R. L. Beingessner, M. Behnam, J. Chen, T. F. Jamison, K. F. Jensen, J.-C. M. Monbaliu, A. S. Myerson, E. M. Revalor, D. R. Snead, T. Stelzer, N. Weeranoppanant, S. Y. Wong, P. Zhang, *Science* **2016**, *352*, 61; b) K. P. Cole, J. M. Groh, M. D. Johnson, C. L. Burcham, B. M. Campbell, W. D. Diseroad, M. R. Heller, J. R. Howell, N. J. Kallman, T. M. Koenig, S. A. May, R. D. Miller, D. Mitchell, D. P. Myers, S. S. Myers, J. L. Phillips, C. S. Polster, T. D. White, J. Cashman, D. Hurley, R. Moylan, P. Sheehan, R. D. Spencer, K. Desmond, P. Desmond, O. Gowran, *Science* **2017**, *356*, 1144; c) M. G. Russell, T. F. Jamison, *Angewandte Chemie International Edition* **2019**, *58*, 7678-7681; d) S. Steiner, J. Wolf, S. Glatzel, A. Andreou, J. M. Granda, G. Keenan, T. Hinkley, G. Aragon-Camarasa, P. J. Kitson, D. Angelone, L. Cronin, *Science* **2019**, *363*, 2211; e) Z. Fülöp, P. Szemesi, P. Bana, J. Éles, I. Greiner, *Reaction Chemistry & Engineering* **2020**, *5*, 1527-1555; f) S. Chatterjee, M. Guidi, P. H. Seeberger, K. Gilmore, *Nature* **2020**, *579*, 379-384; g) L. Rogers, N. Briggs, R. Achermann, A. Adamo, M. Azad, D. Brancazio, G. Capellades, G. Hammersmith, T. Hart, J. Imbrogno, L. P. Kelly, G. Liang, C. Neurohr, K. Rapp, M. G. Russell, C. Salz, D. A. Thomas, L. Weimann, T. F. Jamison, A. S. Myerson, K. F. Jensen, *Organic Process Research & Development* **2020**, *24*, 2183-2196.
- [96] Knauer APG20FG.
- [97] Bronhorst In-Flow F-230MI.
- [98] Equilibar Zero flow BPR.
- [99] Zaiput laboratory scale liquid-liquid separator.
- [100] a) K. A. Triplett, S. M. Ghiaasiaan, S. I. Abdel-Khalik, D. L. Sadowski, *International Journal of Multiphase Flow* **1999**, *25*, 377-394; b) N. Shao, A. Gavriilidis, P. Angeli, *Chemical Engineering Science* **2009**, *64*, 2749-2761; c) M. Mei, F. Felis, G. Hébrard, N. Dietrich, K. Loubière, *Theoretical Foundations of Chemical Engineering* **2020**, *54*, 25-47; d) G. I. Taylor, *Journal of Fluid Mechanics* **1961**, *10*, 161-165.
- [101] J. Bobers, J. Grün, S. Höving, T. Pyka, N. Kockmann, *Organic Process Research & Development* **2020**, *24*, 2094-2104.
- [102] a) M. T. Kreutzer, F. Kapteijn, J. A. Moulijn, J. J. Heiszwolf, *Chemical Engineering Science* **2005**, *60*, 5895-5916; b) A. Günther, K. F. Jensen, *Lab on a Chip* **2006**, *6*, 1487-1503.

- [103] T. Kraus, A. Günther, N. de Mas, M. A. Schmidt, K. F. Jensen, *Experiments in Fluids* **2004**, *36*, 819-832.
- [104] T. Kosoglou, P. Statkevich, A. Johnson-Levonas, J. F. Paolini, A. J. Bergman, K. B. Alton, *Clinical Pharmacokinetics* **2005**, *44*, 467-494.
- [105] a) L. Almeida, P. Soares-da-Silva, *Neurotherapeutics* **2007**, *4*, 88-96; b) C. Yin, X.-Q. Dong, X. Zhang, *Advanced Synthesis & Catalysis* **2018**, *360*, 4319-4324.
- [106] F. Guan, A. J. Blacker, B. Hall, N. Kapur, J. Wen, X. Zhang, *Journal of Flow Chemistry* **2021**.
- [107] a) B. Ravinder, S. Rajeshwar Reddy, M. Sridhar, M. Murali Mohan, K. Srinivas, A. Panasa Reddy, R. Bandichhor, *Tetrahedron Letters* **2013**, *54*, 2841-2844; b) P. C. Fuenfschilling, W. Zaugg, U. Beutler, D. Kaufmann, O. Lohse, J.-P. Mutz, U. Onken, J.-L. Reber, D. Shenton, *Organic Process Research & Development* **2005**, *9*, 272-277.
- [108] I. Atodiresei, I. Schiffers, C. Bolm, *Chemical Reviews* **2007**, *107*, 5683-5712.
- [109] M. Ito, T. Ootsuka, R. Watari, A. Shiibashi, A. Himizu, T. Ikariya, *Journal of the American Chemical Society* **2011**, *133*, 4240-4242.
- [110] T.-L. Liu, W. Li, H. Geng, C.-J. Wang, X. Zhang, *Org Lett* **2013**, *15*, 1740-1743.
- [111] F. Pukelsheim, *Optimal Design of Experiments*, Society for Industrial and Applied Mathematics.
- [112] C. Nunn, A. DiPietro, N. Hodnett, P. Sun, K. M. Wells, *Organic Process Research & Development* **2018**, *22*, 54-61.
- [113] R. A. Ockuly, M. L. Weese, B. J. Smucker, D. J. Edwards, L. Chang, *Chemometrics and Intelligent Laboratory Systems* **2017**, *164*, 64-75.
- [114] U. K. Singh, M. A. Vannice, *Applied Catalysis A: General* **2001**, *213*, 1-24.
- [115] a) E. Dietrich, C. Mathieu, H. Delmas, J. Jenck, *Chemical Engineering Science* **1992**, *47*, 3597-3604; b) M. D. Johnson, S. A. May, B. Haeberle, G. R. Lambertus, S. R. Pulley, J. R. Stout, *Organic Process Research & Development* **2016**, *20*, 1305-1320; c) I. K. Stamatiou, F. L. Muller, *AIChE Journal* **2017**, *63*, 273-282.
- [116] E. A. Gelder, S. D. Jackson, C. M. Lok, *Catalysis Letters* **2002**, *84*, 205-208.
- [117] M. Viviano, C. Milite, D. Rescigno, S. Castellano, G. Sbardella, *RSC Advances* **2015**, *5*, 1268-1273.
- [118] M. K. Abdel-Hamid, K. A. Macgregor, L. R. Odell, N. Chau, A. Mariana, A. Whiting, P. J. Robinson, A. McCluskey, *Organic & Biomolecular Chemistry* **2015**, *13*, 8016-8028.
- [119] a) W. D. Lubell, M. Kitamura, R. Noyori, *Tetrahedron: Asymmetry* **1991**, *2*, 543-554; b) D. Heller, J. Holz, H.-J. Drexler, J. Lang, K. Drauz, H.-P. Krimmer, A. Börner, *The Journal of Organic Chemistry* **2001**, *66*, 6816-6817.
- [120] M. Kitamura, M. Tokunaga, R. Noyori, *The Journal of Organic Chemistry* **1992**, *57*, 4053-4054.
- [121] B. Breit, W. Seiche, *Synthesis* **2001**, *2001*, 0001-0036.
- [122] A. Jörke, T. Gaide, A. Behr, A. Vorholt, A. Seidel-Morgenstern, C. Hamel, *Chemical Engineering Journal* **2017**, *313*, 382-397.
- [123] E. J. P.-F. U. J. JÁUREGUI-HAZA, A. M. WILHELM and H. DELMAS, *Latin American Applied Research* **2004**, *34*, 71-74.
- [124] M. Robinson, M. Ahmed, N. Alaniz, T. Boyles, C. Brasher, K. Floyd, P. Holland, L. Maruffo, T. McMahan, S. Middleton, K. O'Hara, M. Pack, B. Reynolds, R. Rodriguez, D.

- Sawyer, E. Sharp, S. Simpson, C. Vanlandingham, R. Velasquez, C. Wright, *Journal of Heterocyclic Chemistry* **1998**, *35*, 65-69.
- [125] R. J. Chew, M. Wills, *Journal of Catalysis* **2018**, *361*, 40-44.
- [126] a) C. A. Merlic, M. F. Semmelhack, *Journal of Organometallic Chemistry* **1990**, *391*, 23-27; b) T. Onishi, Y. Otake, N. Hirose, T. Nakano, T. Torii, M. Nakazawa, K. Izawa, *Tetrahedron Letters* **2001**, *42*, 6337-6340.
- [127] C. G. Goodman, D. T. Do, J. S. Johnson, *Org Lett* **2013**, *15*, 2446-2449.
- [128] J. Kearns, M. M. Kayser, *Tetrahedron Letters* **1994**, *35*, 2845-2848.
- [129] R. N. Patel, A. Banerjee, J. M. Howell, C. G. McNamee, D. Brozozowski, D. Mirfakhrae, V. Nanduri, J. K. Thottathil, L. J. Szarka, *Tetrahedron: Asymmetry* **1993**, *4*, 2069-2084.
- [130] L. De Luca, G. Giacomelli, M. Taddei, *The Journal of Organic Chemistry* **2001**, *66*, 2534-2537.
- [131] T. Devi, P. Saikia, N. Barua, *Letters in Organic Chemistry - LETT ORG CHEM* **2009**, *6*, 616-618.
- [132] H. Hu, Y. Huang, Y. Guo, *Journal of Fluorine Chemistry* **2012**, *133*, 108-114.
- [133] A. J. Blacker, E. Clot, S. B. Duckett, O. Eisenstein, J. Grace, A. Nova, R. N. Perutz, D. J. Taylor, A. C. Whitwood, *Chemical Communications* **2009**, 6801-6803.
- [134] M. Sova, J. Mravljak, A. Kovač, S. Pečar, Z. Časar, S. Gobec, *Synthesis* **2010**, *2010*, 3433-3438.
- [135] C. H. V. A. Sasikala, P. Reddy Padi, V. Sunkara, P. Ramayya, P. K. Dubey, V. Bhaskar Rao Uppala, C. Praveen, *Organic Process Research & Development* **2009**, *13*, 907-910.
- [136] C. Xu, J. Xu, *Organic & Biomolecular Chemistry* **2020**, *18*, 127-134.
- [137] D. Shen, C. Miao, S. Wang, C. Xia, W. Sun, *European Journal of Inorganic Chemistry* **2014**, *2014*, 5777-5782.
- [138] M. K. Ghorai, A. Kumar, D. P. Tiwari, *The Journal of Organic Chemistry* **2010**, *75*, 137-151.
- [139] S. K. Gediya, G. J. Clarkson, M. Wills, *The Journal of Organic Chemistry* **2020**, *85*, 11309-11330.
- [140] S. Cai, S. Zhang, Y. Zhao, D. Z. Wang, *Org Lett* **2013**, *15*, 2660-2663.
- [141] M. B. Widegren, G. J. Harkness, A. M. Z. Slawin, D. B. Cordes, M. L. Clarke, *Angewandte Chemie International Edition* **2017**, *56*, 5825-5828.
- [142] F. Puls, H.-J. Knölker, *Angewandte Chemie International Edition* **2018**, *57*, 1222-1226.

9. Appendix

9.1 Calculations involved in the study

Gas-liquid volume ratio calculation

Dividing gas flow rate by liquid flow rate is gas-liquid volume ratio.

$$r = g/l \quad \text{Equation 10}$$

r: gas-liquid volume ratio

g: gas flow rate (mL/min) that is calculated by non-ideal gas law.

l: liquid flow rate (mL/min)

Non-ideal gas volume calculation

Non ideal gas law is used to calculate the pressure, because conditions adopted were all more than 20 bars. Ideal gas law is used for reactions under 20 bars.

$$\left[P + e * \left(\frac{n}{V} \right)^2 \right] * \left(\frac{V}{n} - b \right) = RT \quad \text{Equation 11}$$

P: Pressure in reactor (bar)

e: correction for the intermolecular forces, $0.2453 \text{ bar} * \text{mL}^2/\text{mmol}^2$ for hydrogen

b: correction for the volume occupied by the gas particles, $0.02651 \text{ mL}/\text{mmol}$

n: the number of moles of hydrogen (mmol)

V: Volume (mL)

T: absolute temperature (K)

R: idea gas constant, $0.0821 \text{ bar} * \text{mL}/(\text{mmol} * \text{K})$

Residence time calculation for slug flow reactor

Assume that the gas flow rate was not changing in the case of synthesis of ezetimibe and eslicarbazepine acetate, because the consumption of hydrogen is much less than hydrogen supply. Residence time is calculated by dividing sum of gas and liquid flow rate into volume of reactor.

$$t = \frac{V_R}{(g + l)} \quad \text{Equation 12}$$

V_R : Volume of Reactor (mL)

t: Residence Time (min)

Surface-area-to-volume ratio calculation

Gas bubble is surrounded by liquid film in Figure 108. Therefore gas liquid contact area is

the surface area of gas bubble and volume is the volume of liquid slug.^[102]

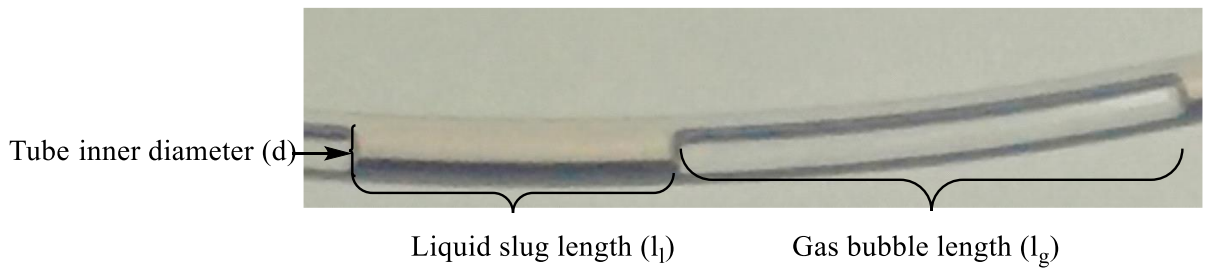


Figure 108 Slug flow parameters

$$S = \pi * d * l_g + 2\pi * \left(\frac{d}{2}\right)^2 \quad \text{Equation 13}$$

$$V_l = l_l * \pi * \left(\frac{d}{2}\right)^2 \quad \text{Equation 14}$$

$$r = \frac{g}{l} = \frac{l_g}{l_l} \quad \text{Equation 15}$$

$$a = \frac{S}{V_l} = \frac{4r}{d} + \frac{2}{l_l} \quad \text{Equation 16}$$

a: surface-area-to-volume ratio (cm⁻¹)

S: surface area (cm²)

d: tube inner diameter, 0.057 cm.

V_l: liquid slug volume (cm³)

Since r equals 0.5 ~ 3 cm and the tube inner diameter is 0.057 cm that is much smaller than $l_l = 1 \sim 3$ cm, $\frac{2}{l_l}$ is much smaller than $\frac{4r}{d}$, the term of $\frac{2}{l_l}$ is neglected. Thus, equation 7 is the final equation to calculate surface-area-to volume ratio.

$$a = \frac{4r}{d} \quad \text{Equation 17}$$

Pressure Increasing by Hydrogen Syringe

Pressing the plunger down fully to the bottom of the syringe, the gas will be compressed into the reactor and filling the deadspace at the base of the syringe. Releasing the syringe plunger, the residual gas in the deadspace will partially expand into the filling syringe.

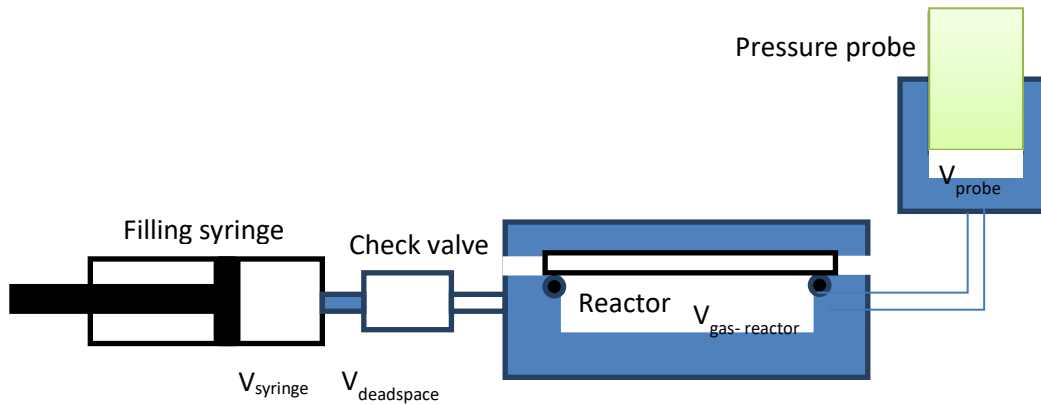


Figure 109 Schematic showing addition of gas to pressurise a reactor using a check valve

The pressure within the reactor is given by

$$P'_{reactor} = \frac{P_{syringe}V_{syringe} + P_{reactor}(V_{reactor} + V_{probe}) - P_{crack}V_{deadspace}}{V_{deadspace} + V_{reactor} + V_{probe}} \quad \text{Equation 18}$$

$P'_{reactor}$: final pressure within the reactor

$P_{syringe}$: initial pressure within the syringe

$P_{reactor}$: initial pressure within the reactor

P_{crack} : cracking pressure of the check valve

$V_{syringe}$: initial volume of the gas within the syringe

$V_{gas_reactor}$: gas volume within the reactor (ie reactor volume – liquid volume present)

V_{probe} : any additional volume e.g. in the probe adapter

$V_{deadspace}$: deadspace at the base of the syringe when the plunger is pushed fully down (0.23ml for a typical plastic syringe)

Example Calculation (no probe adapter present)

Charging 5ml of gas from syringe ($V_{syringe} = 5ml$) from atmospheric pressure: $P_{reactor} = 1\ bar$; $P_{syringe} = 1bar$ into a fReactor that has 0.5ml of liquid in it (ie $V_{gas_reactor} = 1.7 - 0.5 = 1.2ml$) using a check valve with $P_{crack} = 1bar$ (e.g. component CV-3301). A typical deadspace is 0.23ml ($V_{deadspace} = 0.23ml$). Final pressure after injection is 4.17 bar.

To achieve higher pressure, you refill the syringe with gas and repeat. All figures remain as above except the starting pressure of the reactor is higher: $P_{reactor} = 4.17\ bar$. Final pressure after injection is 6.8 bar.

Heating the reactor will increase the pressure. Our experience shows it is best to ensure that the final pressure is below that of the back pressure regulator that should be fitted for safety reasons. Due to the design of spring based BPRs, on opening at the regulating pressure, the pressure will fall to below the stated value, due to the hysteresis in operation.

Heating from T1 (pressure reactor is charged at) to T2 will give a rise in pressure of

$$P'_{heated\ reactor} = P'_{reactor} \frac{T_{heated}}{T_{charged}} \quad \text{Equation 19}$$

Continuing the example, on heating the reactor from the temperature at which it was charged 20 °C (293K) to 60 °C (333K) will give a final pressure of 7.72bar.

Note: when using a pressure probe, the additional gas within this fixture will not be heated. In this case the pressure upon heating can be calculated as:

$$P'_{heated\ reactor} = P'_{reactor} T_{heated} \left(\frac{V_{gas_reactor} + V_{probe}}{V_{gas_reactor} T_{charged} + V_{probe} T_{heated}} \right) \quad \text{Equation 20}$$

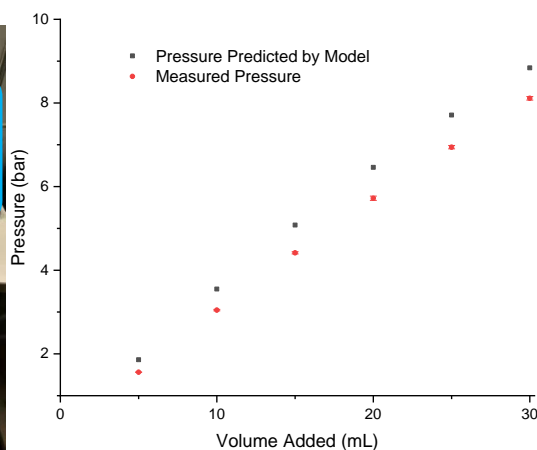
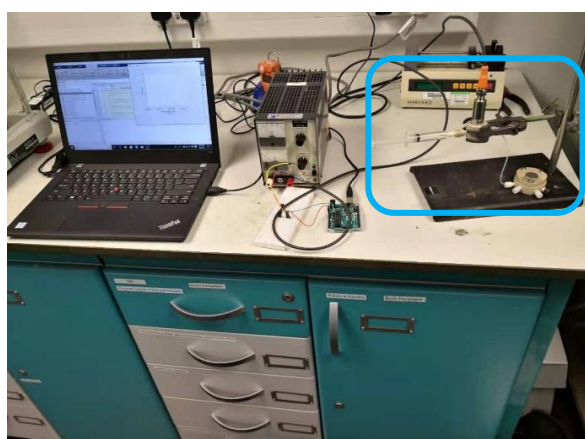


Figure 110 Left (a) Adding pressure by a 5 mL syringe pump; Right (b) prediction and measured value.

To evaluate the model, a syringe is charged with 5ml of gas, injected into the reactor and the pressure measured. Subsequent additions are made (ie volume added is nominal gas in syringe). Each subsequent addition increases the pressure of a fReactor system in blue frame of Figure 110a. The total volume is 3 mL, which includes an empty reactor (no stirring bar) and a pressure sensor holder. The syringe was pulled to 5 mL and pushed to add pressure each time. Less gas can be added due to the existence of dead volume in the head of syringe. Figure 110b shows the comparison of measured pressure and pressure predicted by model. It can be

used to predict pressure when the gas is added by syringe. The discrepancy is thought to be due to the valve opening dynamics.

Residence Time Calculation for fReactor system

$$F_{gA} = \frac{T}{273\text{ K}} \frac{1.01\text{ bar}}{P} F_g \quad \text{Equation 21}$$

$$F_A = F_l + F_{gA} \quad \text{Equation 22}$$

$$t = \frac{V}{F_A} \quad \text{Equation 23}$$

F_g : Gas Flow Rate (sccm: mL/min at 273 K and atmospheric pressure)

F_l : Liquid Flow Rate (mL/min)

T: Operating Temperature

P: Absolute Pressure (the pressure of back pressure regulator plus atmospheric pressure)

F_{gA} : Gas Flow Rate under Pressure

F_A : Total Volumetric Flow Rate (mL/min)

V: Total volume including volume of fReactor and connecting tubes (mL)

t: Residence Time (min)

$k_L a$ calculations

$$C_{Lsat} = \left[\frac{(P-P_E)(P_M-P_E)}{(P_F-P_E)} \right] \cdot \left(\frac{V_g}{V_l} \right) \left(\frac{1}{RT} \right) t \quad \text{Equation 24}$$

$$\ln \left[\frac{P_m - P_0}{(1+K)(P-P_0) - K(P_M-P_0)} \right] = k_L a \left(1 + \frac{1}{K} \right) t \quad \text{Equation 25}$$

$$\text{with } K = \frac{P_f - P_0}{P_m - P_f} = \frac{HeV_g}{V_l RT}$$

$$\alpha = \frac{P_m - P_0}{(1+K)(P-P_0) - K(P_M-P_0)} \quad \text{Equation 26}$$

C_{Lsat} = saturation solubility of gas in the liquid phase (mol/L)

P = pressure measured in the vessel (bar)

P_m = maximum pressure after the reactor is charged with gas (bar), prior to saturation of the liquid

P_f = final pressure after gas has saturated the liquid phase (bar)

P_0 = equilibrium pressure of the liquid with its vapour(bar)

V_g = volume of the gas phase (L)

V_l = volume of the liquid phase (L)

R = ideal gas constant, 0.08134 (bar·L/mole·K)

T =temperature (K)

$k_L a$ = mass transfer coefficient (s^{-1})

t = time from the onset of agitation (s)

The key assumptions of this methods are as follows: The gas follows the ideal gas law, the value of $k_L a$ is constant during the experiment and the volume of the liquid and gas phases does not change during the experiment. The data presented in Figure 111 is the pressure change of the fReactor vessel with 1 mL solvent and is then plotted according to Equation 25. The value of $k_L a$ can be calculated by identifying the gradients of the lines in Figure 111. The effect of gas-liquid volume ratio (r) and comparison between Parr Reactor and fReactor were also studied. The detailed calculation procedure of $k_L a$ is shown in Figure 112.

$$r = \frac{\text{Volume of gas in a reactor}}{\text{Volume of liquid in a reactor}} \quad \text{Equation 27}$$

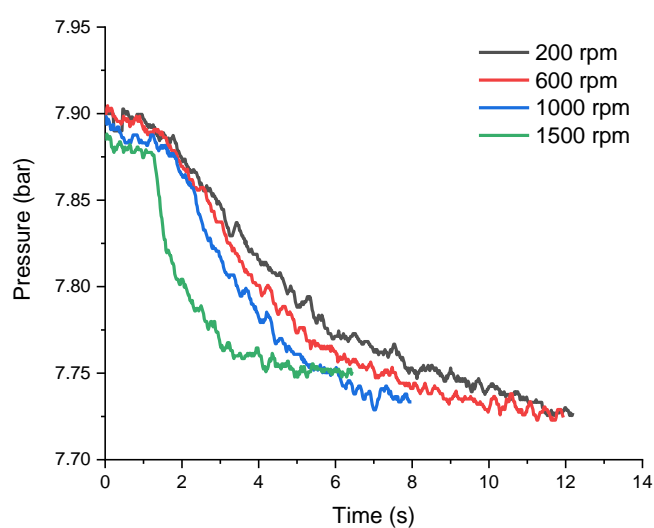


Figure 111 The pressure changing under different stirring rates with 1 mL MeOH ($r =$

0.7) in the reactor

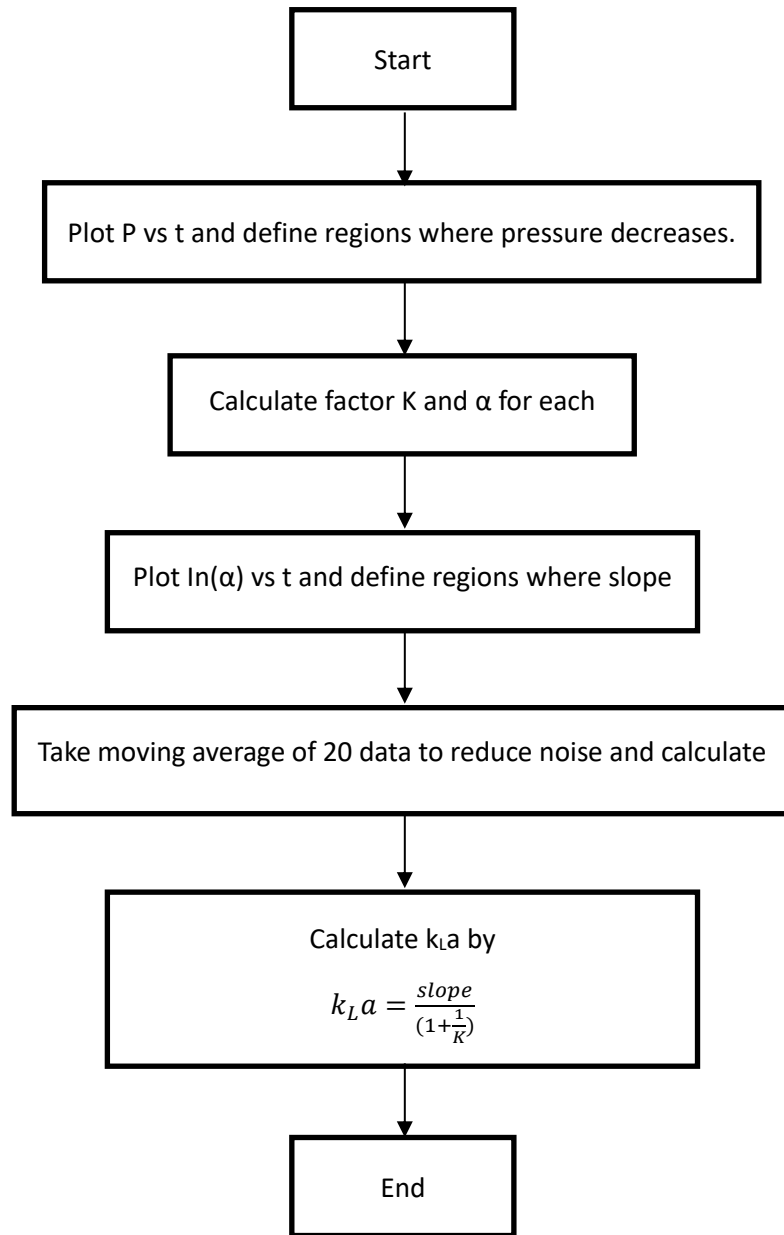


Figure 112 Steps of calculation of k_La

9.2 Components details of reactor system.

All process parts, including fittings, tubes, valves, and junctions that hold pressure were purchased from Swagelok. PTFE tubing (1/8" or 1/16" O.D.) and flangeless male HPLC nuts (1/8") with flangeless ferrules (1/8") were purchased from IDEX Health & Science. The information of other main components is summarized in Table 48.

Table 48 Components details of reactor system

Reaction IR	Mettler Toledo ReactIR 15
Pump	Knauer high pressure HPLC pump APG90FA (0.01-50 mL/min; Pressure rate: 150 bar); PhD Ultra Syringe Pump;
Gas flow meter	Bronkhorst In-flow mass flow meters (0.1-50 sccm H ₂ ; inlet pressure: 300 bar; outlet pressure: 400 bar)
Back pressure regulator for high pressure module	Equilibar Research Series Precision Back Pressure Regulator (Temperature Rate: 150 °C; Pressure Rate: 172 bar)
Gas liquid separator	Zaiput Lab Scale Separator
Reactor	Swagelok 1/16 inch tube and fittings (pressure rate: 757 bar)
Mixer	Swagelok 1/16 inch Tee SS-100-3 (pressure rate: 757 bar)
RS232 Concentrator	Z-Tek RS232 Concentrator
Miniature CSTR	fReactor System (https://www.freactor.com/) Available from Asynt
Gas inlet	Standard Inline 1/4-28 Check Valves https://www.idex-hs.com/store/fluidics/valves/flow-regulating-valves/check-valves/standard-inline-1-4-28-check-valves.html . e.g. Part CV-3301
Back pressure regulator (BPR) for fReactor system	Back Pressure Regulator Assemblies https://www.idex-hs.com/store/fluidics/valves/back-pressure-regulators/back-pressure-regulator-assemblies.html .
Frit in a ferrule	https://www.idex-hs.com/store/fluidics/fluidic-connections/filters-frits/frits/frit-in-a-ferrule.html 
PTFE tube	

9.3 Code for inline pressure sensor

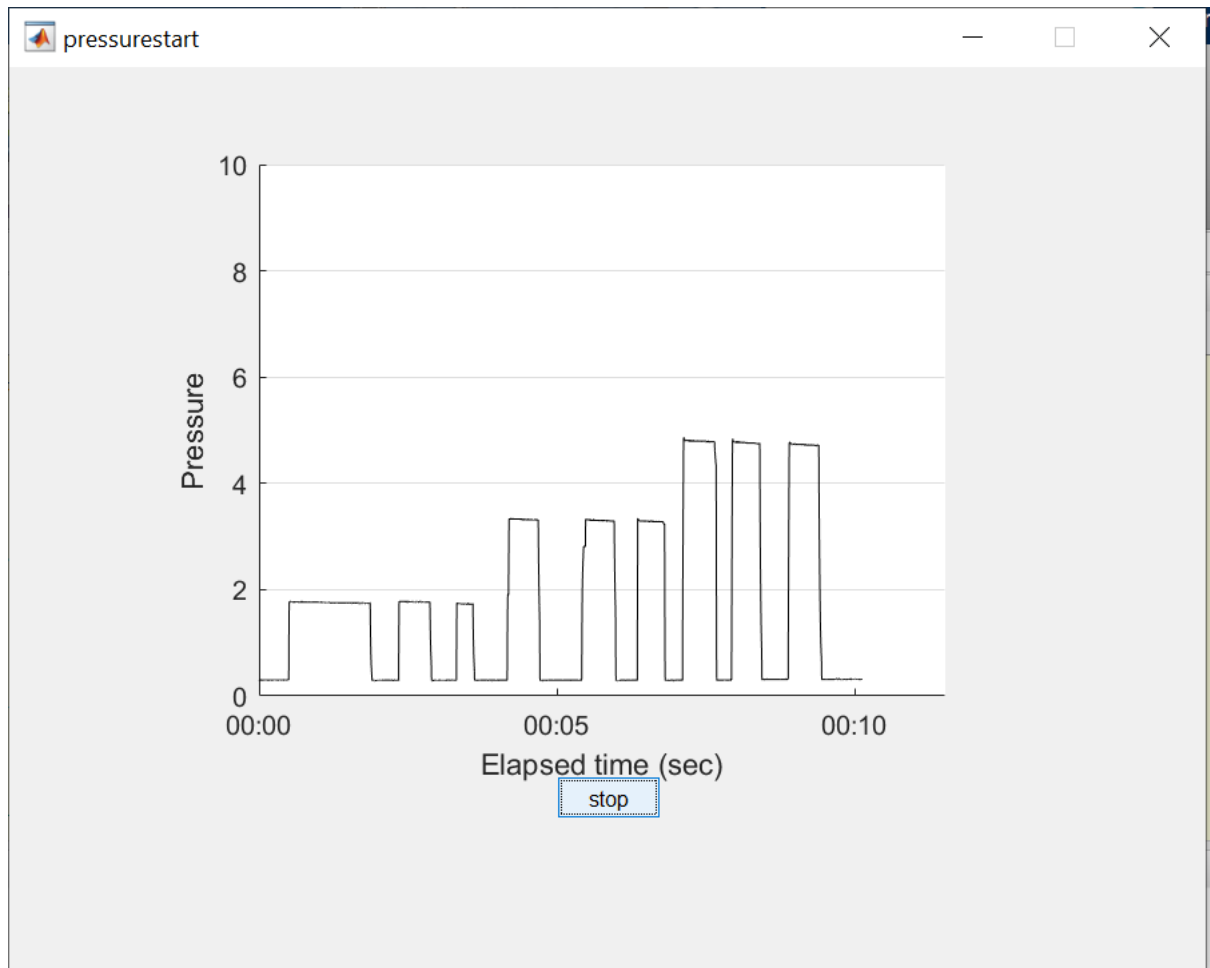


Figure 113 Matlab interface of Pressure Measurement



Figure 114 Pressure sensor and pressure sensor holder

```

function varargout = pressurestart(varargin)

% PRESSURESTART MATLAB code for pressurestart.fig

%     PRESSURESTART, by itself, creates a new PRESSURESTART or raises the existing
%     singleton*.

%
%     H = PRESSURESTART returns the handle to a new PRESSURESTART or the handle to
%     the existing singleton*.

%
%     PRESSURESTART('CALLBACK',hObject,eventData,handles,...) calls the local
%     function named CALLBACK in PRESSURESTART.M with the given input arguments.

%
%     PRESSURESTART('Property','Value',...) creates a new PRESSURESTART or raises the
%     existing singleton*. Starting from the left, property value pairs are
%     applied to the GUI before pressurestart_OpeningFcn gets called. An
%     unrecognized property name or invalid value makes property application
%     stop. All inputs are passed to pressurestart_OpeningFcn via varargin.

%
%     *See GUI Options on GUIDE's Tools menu. Choose "GUI allows only one
%     instance to run (singleton)".

%
% See also: GUIDE, GUIDATA, GUIHANDLES

% Edit the above text to modify the response to help pressurestart

% Last Modified by GUIDE v2.5 29-May-2019 23:11:23

% Begin initialization code - DO NOT EDIT
gui_Singleton = 1;
gui_State = struct('gui_Name',      mfilename, ...

```

```

        'gui_Singleton',  gui_Singleton, ...
        'gui_OpeningFcn', @pressurestart_OpeningFcn, ...
        'gui_OutputFcn',  @pressurestart_OutputFcn, ...
        'gui_LayoutFcn',  [], ...
        'gui_Callback',   []);

    nargin && ischar(varargin)
)
    gui_State.gui_Callback = str2func(varargin);
end

if nargin
    [varargout] = gui_mainfcn(gui_State, varargin);
else
    gui_mainfcn(gui_State, varargin);
end

% End initialization code - DO NOT EDIT

% --- Executes just before pressurestart is made visible.
function pressurestart_OpeningFcn(hObject, eventdata, handles, varargin)
% This function has no output args, see OutputFcn.
% hObject    handle to figure
% eventdata  reserved - to be defined in a future version of MATLAB
% handles    structure with handles and user data (see GUIDATA)
% varargin   command line arguments to pressurestart (see VARARGIN)

% Choose default command line output for pressurestart
handles.output = hObject;

% Update handles structure

```

```

guidata(hObject, handles);

% UIWAIT makes pressurestart wait for user response (see UIRESUME)
% uiwait(handles.figure1);

% --- Outputs from this function are returned to the command line.
function varargout = pressurestart_OutputFcn(hObject, eventdata, handles)
% varargout    cell array for returning output args (see VARARGOUT);
% hObject     handle to figure
% eventdata   reserved - to be defined in a future version of MATLAB
% handles     structure with handles and user data (see GUIDATA)

% Get default command line output from handles structure
varargout = handles.output;

% --- Executes on button press in stop.
function stop_Callback(hObject, eventdata, handles)
% hObject     handle to stop (see GCBO)
% eventdata   reserved - to be defined in a future version of MATLAB
% handles     structure with handles and user data (see GUIDATA)

% Hint: get(hObject,'Value') returns toggle state of stop

stop = get(hObject,'Value')

% --- Executes on button press in togglebutton1.
function togglebutton1_Callback(hObject, eventdata, handles)
% hObject     handle to togglebutton1 (see GCBO)

```

```

% eventdata reserved - to be defined in a future version of MATLAB
% handles structure with handles and user data (see GUIDATA)

% Hint: get(hObject,'Value') returns toggle state of togglebutton1

% Use the arduino command to connect to an Arduino device.

clear a

a = arduino;

%% Take a single temperature measurement

% The datasheet for the TMP36 temperature sensor tells us that the voltage
% reading is directly proportional to temperature in Celsius with an
% offset of 0.5V and a scale factor of 10 mV/°C (equivalent to 100 °C/V).

% Therefore the conversion can be represented as
%
%  $T_C = (V - 0.5) * 100$ 
% We can read the output voltage, convert it to Celsius and convert the
% result to Fahrenheit as follows:

v = readVoltage(a,'A1');
sv = (v*5.0)/1024.0;
pressure_bar = (sv-1.0)/(4.0)*(10.0-0.0);
fprintf('Pressure Reading',pressure_bar)

h = animatedline;

stop = false

ax = gca;

ax.YGrid = 'on';

ax.YLim = [0 10];

startTime = datetime('now');

```

```

while ~stop

    % Read current voltage value

    v = readVoltage(a,'A1');

    sv = (v*5.0)/1024.0;

    % Calculate temperature from voltage (based on data sheet)

    pressure_bar = (sv-1.0)/(4.0)*(10.0-0.0);

    [timeLogs,ECGLogs] = getpoints(h);

    f = [timeLogs,ECGLogs];

    % Get current time

    t = datetime('now') - startTime;

    % Add points to animation

    addpoints(h,datenum(t),pressure_bar)

    datetick('x','keplimits')

    drawnow;

    stop = get(hObject,'Value')

end

%% Plot the recorded data

plot(timeLogs,ECGLogs)

xlabel('Elapsed time (sec)')

ylabel('Pressure')

%% Save results to a file

T = table(timeLogs,ECGLogs,'VariableNames');

filename = 'pressure_Data.xlsx';

% Write table to file

writetable(T,filename)

```

9.4 Code for gas liquid reaction system interface

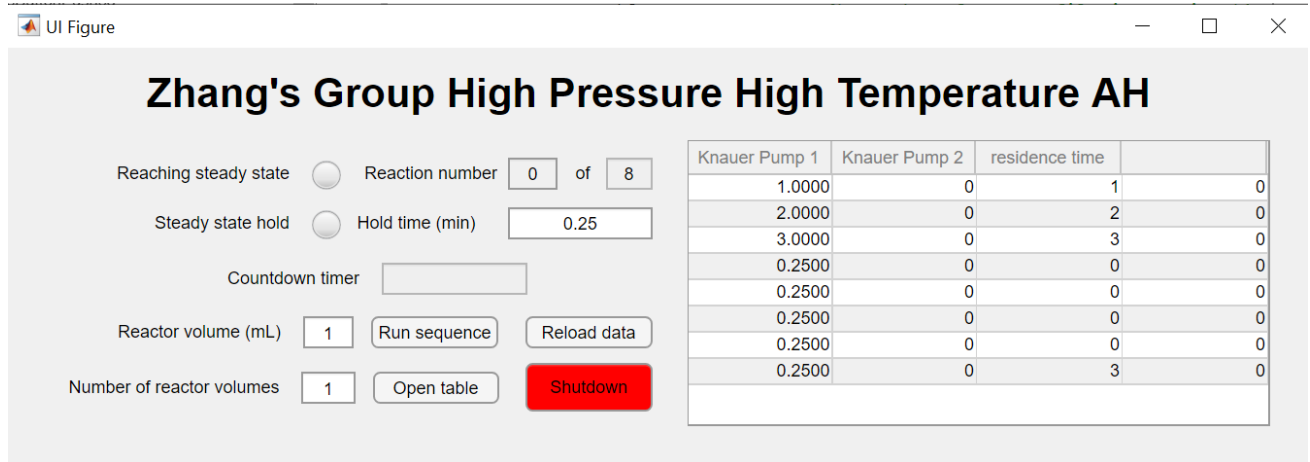


Figure S21. Interface of automatic control app.

```

classdef DoEguiFanfu < matlab.apps.AppBase
    % Properties that correspond to app components
    properties (Access = public)
        UIFigure                matlab.ui.Figure
        RunSequenceButton       matlab.ui.control.Button
        ShutdownButton          matlab.ui.control.Button
        OpenTableButton         matlab.ui.control.Button
        ReactorvolumemLEditFieldLabel  matlab.ui.control.Label
        ReactorVolumemLEditField
        matlab.ui.control.NumericEditField
        NumberofreactorvolumesLabel  matlab.ui.control.Label
        NumberOfReactorVolumesEditField
        matlab.ui.control.NumericEditField
        ReloadDataButton       matlab.ui.control.Button
        UITable                 matlab.ui.control.Table
        ofLabel                 matlab.ui.control.Label
        ofEditField
        matlab.ui.control.NumericEditField
        ReachingsteadystateLampLabel  matlab.ui.control.Label
        ReachingsteadystateLamp      matlab.ui.control.Lamp
        ReactionnumberEditFieldLabel  matlab.ui.control.Label
        ReactionnumberEditField
        matlab.ui.control.NumericEditField
        CountdowntimerLabel        matlab.ui.control.Label
        ResidenceTimeEditField     matlab.ui.control.EditField
        SteadystateholdLampLabel    matlab.ui.control.Label
    end
end

```

```

        SteadystateholdLamp          matlab.ui.control.Lamp
        HoldtimeminEditFieldLabel    matlab.ui.control.Label
        HoldtimeminEditField
matlab.ui.control.NumericEditField
        ZhangsGroupHighPressureHighTemperatureAHLLabel
matlab.ui.control.Label
    end
    %Eurotherm = SyrDos

    %These properties are the ones not autogenerated by app designer
    properties (Access = public);

        syr;
        R;          %Red
        W;          %White
        G;          %Green
        B;          %Blue
        shutdown;   %Flag for shutdown button
        t;          %table object
        NoOfRxns;   %counts the number of reactions in an array
        P1;         %Pump Knauer 1
        P2;         %Pump Knauer 2
        P3;         %residence time

    end

    methods (Access = public);

        %This function is executed in the event of a loop interupt it
        %checks state of shutdown flag (if 0 run, if 1 shutdown)
        function shutdownfunction(app);
%
            knauerpumpobjwriteflow(app.P1, 0); %Red
            knauerpumpobjwriteflow(app.P2, 0); %White

        end

    end

    methods (Access = private)
        % Code that executes after component creation
        function startupFcn(app)
            instrreset;

```

```

app.t = readtable('LED.csv'); %Gets data from csv file
app.UITable.Data = app.t; %Puts data from csv file into
gui table

app.NoOfRxns = height(app.t); %Checks the number of rows
in the table and sets NoOfRxns to that number
app.ofEditField.Value = app.NoOfRxns; %Displays number of
reactions to be executed in the gui

app.P1 = knaerpumpobj(9);
knaerpumpobjconnect(app.P1);
app.P2 = knaerpumpobj(10);
knaerpumpobjconnect(app.P2);

end
% Button pushed function: RunSequenceButton
function RunSequenceButtonPushed(app, event)
    app.shutdown = 0; %Sets shutdown flag to zero;

    knaerpumpobjwriteflow(app.P1, 0);
    knaerpumpobjwriteflow(app.P2, 0);
%     fprintf(app.T1, sprintf('%01;OUT_MODE_00 1'));
%     fprintf(app.B1, sprintf('%01;OUT_MODE_00 1'));
%
%     fprintf(app.P1, sprintf('% pump set'));
%     fprintf(app.P2, sprintf('% pump set'));

    %fprintf(app.B1, 'RUN');
    knaerpumpobjcomm(app.P1, 'write', 'ON');
    knaerpumpobjcomm(app.P2, 'write', 'ON');
    app.t = app.UITable.Data; %acquires table data for gui

    %table data from the csv file is converted to an array,
matlab seems to prefer working with data arays
    app.R = table2array(app.t(:,1)); %Knauer Pump 1
    app.W = table2array(app.t(:,2)); %Knauer Pump 2
    app.G = table2array(app.t(:,3)); %residencetime
    app.B = table2array(app.t(:,4)); %Bronhorst

    counter = 0; %counter sets to zero, this is used to count
the number of reactions which have been run

    for i = 1:length(app.R); %i represents the values in each
row

```

```

        if app.shutdown; %calls shutdown function if shutdown
flag is set to 1
            shutdownfunction(app); %executes shutdown function
(see above)
            break %stops the matlab from returning to the loop
        end

        counter = counter+1;

        app.ReactionnumberEditField.Value = counter; %This
displays the reaction number currently in progress, it is *30+1
because it is divided by 30 later on for the servo.

        % Defines collum values from table
        r = app.R(i);
        w = app.W(i);
        b = app.B(i);
        g = app.G(i);
        %sets device settings
        knaerpumpobjwriteflow(app.P1, r)
        knaerpumpobjwriteflow(app.P2, w)

        app.ReachingsteadystateLamp.Color = [0.9 0.9
0.9]; %turns the lamp off so that the user knows the reactor has
reached steady state and it's time to begin taking a sample

        app.SteadystateholdLamp.Color = 'green';

        steadystateholdtime = g*60;

        while steadystateholdtime > -0.1; %until timer goes
below -0.1 it will run the loop below

            if app.shutdown; %calls shutdown function if
shutdown flag is set to 1
                shutdownfunction(app); %executes shutdown
helper function
            break %stops the matlab from returning to the
loop
        end

```

```

        app.ResidenceTimeEditField.Value =
string(duration(0,0,steadystateholdtime)); %sets display time for
residence time remaining in the gui
        pause(1); %waits one second before going to the
next line of code and returning to the loop.
        steadystateholdtime = steadystateholdtime -
1; %sets a new display value in the gui and takes 1 second off the
time remaing
    end

    app.SteadystateholdLamp.Color = [0.9 0.9 0.9];
    if app.shutdown; %shuts down the reactor and returns
all values to zero if the shutdown button is pushed
        shutdownfunction(app); %executes shutdown helper
function
            break %stops the matlab from returning to the loop
        end

    end
    shutdownfunction(app);

end
% Button pushed function: ShutdownButton
function ShutdownButtonPushed(app, event)
    app.shutdown = 1;
    shutdownfunction(app);
end
% Button pushed function: OpenTableButton
function OpenTableButtonPushed(app, event)
    winopen('LED.csv');
end
% Close request function: UIFigure
function UIFigureCloseRequest(app, event)
    shutdownfunction(app);
    instrreset;
    delete(app);
end
% Button pushed function: ReloadDataButton
function ReloadDataButtonPushed(app, event)
    app.t = readtable('LED.csv');
    app.UITable.Data = app.t;
    app.NoOfRxns = height(app.t);
    app.ofEditField.Value = app.NoOfRxns;
end

```

```

% Callback function
function ButtonPushed(app, event)

    fprintf(app.B1, 'RUN');
end
end
% App initialization and construction
methods (Access = private)
    % Create UIFigure and components
    function createComponents(app)
        % Create UIFigure
        app.UIFigure = uifigure;
        app.UIFigure.Position = [100 100 896 287];
        app.UIFigure.Name = 'UI Figure';
        app.UIFigure.CloseRequestFcn = createCallbackFcn(app,
@UIFigureCloseRequest, true);
        % Create RunSequenceButton
        app.RunSequenceButton = uibutton(app.UIFigure, 'push');
        app.RunSequenceButton.ButtonPushedFcn =
createCallbackFcn(app, @RunSequenceButtonPushed, true);
        app.RunSequenceButton.Position = [251 83 87 22];
        app.RunSequenceButton.Text = 'Run sequence';
        % Create ShutdownButton
        app.ShutdownButton = uibutton(app.UIFigure, 'push');
        app.ShutdownButton.ButtonPushedFcn =
createCallbackFcn(app, @ShutdownButtonPushed, true);
        app.ShutdownButton.BackgroundColor = [1 0 0];
        app.ShutdownButton.Position = [357 40 87 33];
        app.ShutdownButton.Text = 'Shutdown';
        % Create OpenTableButton
        app.OpenTableButton = uibutton(app.UIFigure, 'push');
        app.OpenTableButton.ButtonPushedFcn =
createCallbackFcn(app, @OpenTableButtonPushed, true);
        app.OpenTableButton.Position = [252 45 87 22];
        app.OpenTableButton.Text = 'Open table';
        % Create ReactorvolumemLEditFieldLabel
        app.ReactorvolumemLEditFieldLabel =
uilabel(app.UIFigure);
        app.ReactorvolumemLEditFieldLabel.HorizontalAlignment =
'right';
        app.ReactorvolumemLEditFieldLabel.Position = [71 83 118
22];
        app.ReactorvolumemLEditFieldLabel.Text = 'Reactor volume
(mL)';
    end
end

```

```

    % Create ReactorVolumemLEditField
    app.ReactorVolumemLEditField = uieditfield(app.UIFigure,
'numeric');
    app.ReactorVolumemLEditField.HorizontalAlignment =
'center';
    app.ReactorVolumemLEditField.Position = [204 83 35 22];
    app.ReactorVolumemLEditField.Value = 1;
    % Create NumberofreactorvolumesLabel
    app.NumberofreactorvolumesLabel = uilabel(app.UIFigure);
    app.NumberofreactorvolumesLabel.HorizontalAlignment =
'right';
    app.NumberofreactorvolumesLabel.Position = [38 45 150
22];
    app.NumberofreactorvolumesLabel.Text = 'Number of reactor
volumes';
    % Create NumberOfReactorVolumesEditField
    app.NumberOfReactorVolumesEditField =
uieditfield(app.UIFigure, 'numeric');
    app.NumberOfReactorVolumesEditField.HorizontalAlignment =
'center';
    app.NumberOfReactorVolumesEditField.Position = [203 45 37
22];
    app.NumberOfReactorVolumesEditField.Value = 1;
    % Create ReloadDataButton
    app.ReloadDataButton = uibutton(app.UIFigure, 'push');
    app.ReloadDataButton.ButtonPushedFcn =
createCallbackFcn(app, @ReloadDataButtonPushed, true);
    app.ReloadDataButton.Position = [357 83 87 22];
    app.ReloadDataButton.Text = 'Reload data';
    % Create UITable
    app.UITable = uitable(app.UIFigure);
    app.UITable.ColumnName = {'Knauer Pump 1'};
    app.UITable.RowName = {};
    app.UITable.ColumnEditable = true;
    app.UITable.Position = [468 30 400 196];
    % Create ofLabel
    app.ofLabel = uilabel(app.UIFigure);
    app.ofLabel.BackgroundColor = [0.9412 0.9412 0.9412];
    app.ofLabel.Position = [388 192 25 22];
    app.ofLabel.Text = ' of';
    % Create ofEditField
    app.ofEditField = uieditfield(app.UIFigure, 'numeric');
    app.ofEditField.Editable = 'off';
    app.ofEditField.HorizontalAlignment = 'center';

```

```

app.ofEditField.BackgroundColor = [0.9412 0.9412 0.9412];
app.ofEditField.Position = [412 192 32 22];
% Create ReachingsteadystateLampLabel
app.ReachingsteadystateLampLabel = uilabel(app.UIFigure);
app.ReachingsteadystateLampLabel.HorizontalAlignment =
'right';
app.ReachingsteadystateLampLabel.Position = [71 192 124
22];
app.ReachingsteadystateLampLabel.Text = 'Reaching steady
state';
% Create ReachingsteadystateLamp
app.ReachingsteadystateLamp = uilamp(app.UIFigure);
app.ReachingsteadystateLamp.Position = [210 192 20 20];
app.ReachingsteadystateLamp.Color = [0.902 0.902 0.902];
% Create ReactionnumberEditFieldLabel
app.ReactionnumberEditFieldLabel = uilabel(app.UIFigure);
app.ReactionnumberEditFieldLabel.BackgroundColor =
[0.9412 0.9412 0.9412];
app.ReactionnumberEditFieldLabel.HorizontalAlignment =
'right';
app.ReactionnumberEditFieldLabel.Position = [241 192 97
22];
app.ReactionnumberEditFieldLabel.Text = 'Reaction
number';
% Create ReactionnumberEditField
app.ReactionnumberEditField = uieditfield(app.UIFigure,
'numeric');
app.ReactionnumberEditField.HorizontalAlignment =
'center';
app.ReactionnumberEditField.BackgroundColor = [0.9412
0.9412 0.9412];
app.ReactionnumberEditField.Position = [345 192 34 22];
% Create CountdowntimerLabel
app.CountdowntimerLabel = uilabel(app.UIFigure);
app.CountdowntimerLabel.BackgroundColor = [0.9412 0.9412
0.9412];
app.CountdowntimerLabel.HorizontalAlignment = 'right';
app.CountdowntimerLabel.Position = [147 120 96 22];
app.CountdowntimerLabel.Text = 'Countdown timer';
% Create ResidenceTimeEditField
app.ResidenceTimeEditField = uieditfield(app.UIFigure,
'text');
app.ResidenceTimeEditField.Editable = 'off';

```

```

        app.ResidenceTimeEditField.HorizontalAlignment =
'center';
        app.ResidenceTimeEditField.BackgroundColor = [0.9412
0.9412 0.9412];
        app.ResidenceTimeEditField.Position = [258 120 100 22];
        % Create SteadystateholdLampLabel
        app.SteadystateholdLampLabel = uilabel(app.UIFigure);
        app.SteadystateholdLampLabel.HorizontalAlignment =
'right';
        app.SteadystateholdLampLabel.Position = [97 158 98 22];
        app.SteadystateholdLampLabel.Text = 'Steady state hold';
        % Create SteadystateholdLamp
        app.SteadystateholdLamp = uilamp(app.UIFigure);
        app.SteadystateholdLamp.Position = [210 158 20 20];
        app.SteadystateholdLamp.Color = [0.902 0.902 0.902];
        % Create HoldtimeminEditFieldLabel
        app.HoldtimeminEditFieldLabel = uilabel(app.UIFigure);
        app.HoldtimeminEditFieldLabel.HorizontalAlignment =
'right';
        app.HoldtimeminEditFieldLabel.Position = [236 158 87 22];
        app.HoldtimeminEditFieldLabel.Text = 'Hold time (min)';
        % Create HoldtimeminEditField
        app.HoldtimeminEditField = uieditfield(app.UIFigure,
'numeric');
        app.HoldtimeminEditField.HorizontalAlignment = 'center';
        app.HoldtimeminEditField.Position = [345 158 99 22];
        app.HoldtimeminEditField.Value = 0.25;
        % Create ZhangsGroupHighPressureHighTemperatureAHLLabel
        app.ZhangsGroupHighPressureHighTemperatureAHLLabel =
uilabel(app.UIFigure);

app.ZhangsGroupHighPressureHighTemperatureAHLLabel.FontSize = 28;

app.ZhangsGroupHighPressureHighTemperatureAHLLabel.FontWeight =
'bold';

app.ZhangsGroupHighPressureHighTemperatureAHLLabel.Position = [97 242
711 34];
        app.ZhangsGroupHighPressureHighTemperatureAHLLabel.Text =
'Zhang''s Group High Pressure High Temperature AH';
        end
    end
    methods (Access = public)
        % Construct app

```

```

function app = DoEguiFanfu
    % Create and configure components
    createComponents(app)
    % Register the app with App Designer
    registerApp(app, app.UIFigure)
    % Execute the startup function
    runStartupFcn(app, @startupFcn)
    if nargin == 0
        clear app
    end
end
% Code that executes before app deletion
function delete(app)
    % Delete UIFigure when app is deleted
    delete(app.UIFigure)
end
end
end

```

9.5 Code for modelling diastereoselectivity

Dehydrogenation reaction code:

```

clc;
clear;
%concentration of catalyst was not changing and all catalyst are in
%oxidation form during the whole process
kr = 0.01;%kinetic constant for R configuration (mmol mL-1 min-1)
ks= 0.2;%kinetic constant for S configuration (mmol mL-1 min-1)
cs=0.05; %concentration of S configuration (mmol/mL)
cr = 0.05;%concentration of R configuration (mmol/mL)
V = 1;% Volume (mL)
b = [];
ms = [];
mr = [];
ns = [];
nr = [];
for t=1:36; % time(min)
    rs = ks*cs % reaction rate of S configuration
    cs = V*cs-rs/2 %new concentration of S configuration
    rr = kr*cr % reaction rate of R configuration
    cr = V*cr-rr/2 %new concentration of R configuration

```

```

    ee = (cr-cs)/(cr+cs) %ee value
    b = [b,ee]
    ms =[ms,rs]
    mr = [mr, rr]
    ns = [ns;cs]
    nr = [nr;cr]
end
plot(b)
% plot(ms);
% hold on;
% plot (mr);
% plot (ns);
% hold on;
% plot (nr);

```

Dehydrogenation reaction with hydrogenation catalyst code:

```

clc;
clear;
%concentration of catalyst was not changing and all catalyst are in
%oxidation form during the whole process
kr = 0.01;%kinetic constant for R configuration (mmol-1 s-1)
ks= 0.2;%kinetic constant for S configuration (mmol-1 s-1)
cs=0.05; %concentration of S configuration (mmol/mL)
cr = 0.05;%concentration of R configuration (mmol/mL)
V = 1;% Volume (mL)
b = [];
ms = [];
mr = [];
ns = [];
nr = [];
for t=1:1000;
    rs = ks*cs % reaction rate of S configuration
    cs = V*cs-rs/2 %new concentration of S configuration
    rr = kr*cr % reaction rate of R configuration
    cr = V*cr-rr/2 %new concentration of R configuration
    cs = cs+(rs/2+rr/2)*0.2
    cr = cr+(rs/2+rr/2)*0.8
    ee = (cr-cs)/(cr+cs) %ee value
    b = [b,ee]
    ms =[ms,rs]
    mr = [mr, rr]
    ns = [ns;cs]

```

```
    nr = [nr;cr]
end
plot(b)
% plot(ms);
% hold on;
% plot (mr);
% plot (ns);
% hold on;
% plot (nr);
```